Development of a Multi-Hour Ahead Wind Power Forecasting System

by

Yitian XING

A thesis
presented to the University of Waterloo
in fulfilment of the
thesis requirement for the degree of
Doctor of Philosophy
in
Mechanical and Mechatronics Engineering

Waterloo, Ontario, Canada, 2022

Examining Committee Membership

The following served on the Examining Committee for this thesis. The decision of the Examining Committee is by majority vote.

External Examiner:	Yongsheng Chen, Associate Professor Dept. of Earth and Space Science and Engineering York University
Supervisors:	Fue-Sang Lien, Professor Dept. of Mechanical and Mechatronics Engineering University of Waterloo
	William Melek, Professor Dept. of Mechanical and Mechatronics Engineering University of Waterloo
Internal Member:	John Wen, Professor Dept. of Mechanical and Mechatronics Engineering University of Waterloo
Internal Member:	Amir Khajepour, Professor Dept. of Mechanical and Mechatronics Engineering University of Waterloo
Internal-External Member:	Alexander Wong, Professor Dept. of Systems Design Engineering University of Waterloo

Author's Declaration

I hereby declare that I am the sole author of this thesis. This is a true copy of the thesis, including any required final revisions, as accepted by my examiners.

I understand that my thesis may be made electronically available to the public.

Abstract

Wind energy, as a renewable and green energy source with substantial value that is vital for sustainable human development, is gaining more and more attention around the world. The variability of wind implies that wind power is random, intermittent, and volatile. In order to overcome the unfavourable factors brought by wind power and enhance the reliable, stable, and secure operation of electrical grids that incorporate wind power systems, a multi-hour ahead wind power forecasting system consisting of an optimal combination of statistical, physical, and artificial intelligence (AI) models for real wind farm applications was proposed in this research.

Except for a direct persistence model that was able to produce wind power forecasts directly, an indirect persistence, an autoregressive integrated moving average (ARIMA), and a Weather Research and Forecasting (WRF) model were used to provide wind speed forecasts which, in turn, could be converted to wind power forecasts by using a power curve model. A technique for order of preference by similarity to ideal solution (TOPSIS) scheme was applied to construct a novel 5-in-1 (ensemble) WRF model for wind speed and wind power forecasting. An adaptive neuro-fuzzy inference system (ANFIS) model was employed to determine the power curve model, and another ANFIS model was utilised to build a wind speed correction model exclusively for correcting the wind speed forecasts provided by the 5-in-1 (ensemble) WRF model.

By using a set of 24-day historical wind speed and wind power measurements acquired from an operational wind turbine in a real wind farm located in North China, the multi-hour ahead wind power forecasting system was proposed comprising the following components over various forecast time horizons: the direct and indirect persistence models for 30-minute ahead forecasting, the ARIMA model for 1-hour ahead forecasting, and the WRF-TOPSIS model (with corrections obtained from the ANFIS-based wind speed correction model) for 1.5-hour to 24-hour (with a 30-minute temporal resolution) ahead forecasting. The primary contribution of this research is the novel WRF-TOPSIS model strategy used to select and combine the best-performing WRF models from a vast ensemble of possible models. The results demonstrated that the proposed multi-hour ahead wind power forecasting system has excellent predictive performance and is of practical relevance.

Acknowledgements

First and foremost, I would like to express my sincerest gratitude to my doctoral supervisors, Professor Fue-Sang Lien and Professor William Melek, for their invaluable guidance, unwavering support, and patience that cannot be underestimated throughout my PhD studies. I am deeply indebted to Professor Eugene Yee, who is my 'third supervisor', for all the helpful advice and constructive criticism. I also could not have undertaken this journey without the examining committee members, including Professor John Wen, Professor Amir Khajepour, Professor Alexander Wong, and Professor Yongsheng Chen, who generously provided insightful comments and suggestions.

This endeavour would not have been possible without the financial support from the Natural Sciences and Engineering Research Council of Canada (NSERC) Discovery Grants programme (grant numbers: 50503-10234 and 50503-10925). This work was made possible by the facilities of the Shared Hierarchical Academic Research Computing Network (SHARCNET: www.sharcnet.ca) and Compute/Calcul Canada.

I would like to give my special regards to Professor David Johnson and Professor Keith Hipel for the significant knowledge delivered in their courses. I am also grateful to Dr Deyong Wen, who took his precious time to teach me numerical weather prediction. Many thanks should also go to Dr Stefan Rehm, who improved my academic writing and speaking skills through English lectures. Last but not least, I would like to recognise the effort that I received from my parents, teachers, colleagues, classmates, and friends.

Dedication

This is dedicated to the one I love. It would be nice to see you in 2022!

Table of Contents

List of Figures

List of Tables

List of Abbreviations

AAE average absolute error. 19

ACF autocorrelation function. 44, 46, 108, 109, 112, 113, 117, 120, 160

ADALINE adaptive linear element. 20, 22

ADAM adaptive moment estimation. 26

AFWA Air Force Weather Agency. 48

AI artificial intelligence. iv, 8, 14, 18, 22, 23, 27, 29, 35, 241, 247–249, 251

AIC Akaike information criterion. 117, 120, 122, 134, 160

ANFIS adaptive neuro-fuzzy inference system. iv, 8–11, 18, 21–23, 25, 35, 36, 38, 57, 59, 66–69, 72–76, 94, 149, 155, 161, 214, 215, 218–220, 223, 226, 241, 249–251

ANN artificial neural network. 16–25, 27, 29, 30, 35, 36

AR autoregressive. 15, 16, 18, 30, 39–42, 44–47, 108, 113, 117, 121, 122, 134, 160

ARIMA autoregressive integrated moving average. iv, 8, 9, 11, 15–17, 19, 20, 23–25, 47, 103, 108, 117–120, 122, 123, 126, 129–131, 133–137, 142–144, 149, 154, 155, 159–163, 227, 234–236, 238–241, 243, 248, 250–252

ARMA autoregressive moving average. 15, 16, 39, 42, 46, 47

ARMINES Association for the Research and Development of Industrial Methods and Processes. 29

ARW Advanced Research Weather Research and Forecasting. 48, 49, 166

AWPPS ARMINES Wind Power Prediction System. 29

BMA Bayesian model averaging. 22

BP British Petroleum. 1

BPNN back-propagation neural network. 18, 19, 21–23

CENER National Renewable Energy Centre. 30

CEPRI China Electric Power Research Institute. 32

CEsA Research Centre for Wind Energy and Atmospheric Flows. 30

CFD computational fluid dynamics. 252

CFE Federal Electricity Commission. 19

CIEMAT Research Centre for Energy, Environment and Technology. 30

CNN convolutional neural network. 26

CPAR conditional parametric autoregressive. 16

DE differential evolution. 20

DGF double Gaussian function. 26

DTU Technical University of Denmark. 28, 31

DWD German Weather Service. 20, 30

ECCC Environment and Climate Change Canada. 181, 182

ECMWF European Centre for Medium-Range Weather Forecasts. 31

EE elliptic envelope. 26

EMD-FNN empirical mode decomposition based feed-forward neural network. 20, 21

EMS energy management system. 32

ENSMP Paris School of Mines. 29

EPSO enhanced particle swarm optimisation. 23

ESRL Earth System Research Laboratory. 48

f-ARIMA fractional-autoregressive integrated moving average. 17

FAA Federal Aviation Administration. 48

FFBP feed-forward back-propagation. 20

FIS fuzzy inference system. 11, 34, 35

FL fuzzy logic. 18, 21

FNN feed-forward neural network. 18–21

GA genetic algorithm. 26

GFDL Geophysical Fluid Dynamics Laboratory. 174

GFS Global Forecast System. 27, 57, 163, 169, 173, 241, 252

GRIB general regularly-distributed information in binary form. 164, 169

GWEC Global Wind Energy Council. 2

HEA hybrid evolutionary-adaptive. 25

HIRLAM High Resolution Limited Area Model. 27, 28, 30, 31

IA index of agreement. 62, 69, 72, 73, 76, 78, 84, 85, 87, 92–94, 100, 101, 103, 137, 142, 143, 149, 154, 155, 161, 162, 185, 187, 199, 210, 215, 218, 220, 223, 225, 226, 229, 235, 236, 238, 239, 243, 248–250

IF isolation forest. 26

IMD India Meteorological Department. 20

INEGI Institute of Mechanical Engineering and Industrial Management. 29

INESC Institute of Systems and Computer Engineering. 29

ISET Institute for Solar Energy Supply Technology. 30

ITSM improved time series method. 17

LS-SVM least-squares support vector machine. 21, 23, 24

MA moving average. 15, 39, 41, 42, 45–47, 108, 113, 115, 117, 120–122, 134, 160

MAE mean absolute error. 19–25, 62, 69, 72, 73, 78, 84, 85, 87, 92–94, 100, 101, 103, 137, 142, 143, 149, 154, 155, 161, 162, 185, 187, 199, 210, 215, 218, 220, 223, 225, 226, 229, 234–236, 238, 239, 243, 248, 250

MAPE mean absolute percentage error. 20–22, 24, 25, 62, 78, 84, 85, 137, 142, 143, 161, 185, 187, 199, 210, 215, 218, 225, 226

MAS multiple architecture system. 22, 23

MB mean bias. 62, 69, 72, 73, 78, 84, 85, 87, 92–94, 100, 101, 103, 137, 142, 143, 149, 154, 155, 161, 162, 185, 187, 199, 210, 215, 218, 220, 223, 225, 226, 229, 234, 236, 238, 239, 243, 248, 250

ME mean error. 23

MET Model Evaluation Tools. 49

MFNN multi-feedforward neural network. 26

MI mutual information. 25

MLE maximum likelihood estimate. 117, 120, 122, 134, 160

MLP multilayer perceptron. 21, 22, 26

MLR multiple linear regression. 22

MM5 Mesoscale Model 5. 30, 31

MOS Model Output Statistics. 31

MSAR Markov switching autoregressive. 16

MSE mean squared error. 19, 21, 23–25, 137

NCAR National Center for Atmospheric Research. 48

NCEP National Centers for Environmental Prediction. 31, 48

NCL NCAR Command Language. 49

NEA National Energy Administration. 62, 64, 228, 243, 248, 251

NetCDF network common data form. 166, 169, 173

NID normally independently distributed. 119, 122, 134, 161

NMM Non-Hydrostatic Mesoscale Model. 48

NNAM neural network assembling model. 30

NNWT neural network wavelet transform. 25

NOAA National Oceanic and Atmospheric Administration. 48

NRL Naval Research Laboratory. 48

NWP numerical weather prediction. 13, 23, 27–32, 48

OU University of Oklahoma. 48

PACF partial autocorrelation function. 43, 45, 46, 108, 114, 115, 117, 160

PCC Pearson correlation coefficient. 23

PE percentage error. 19

PSO particle swarm optimisation. 20, 25

RACF residual autocorrelation function. 126, 131, 160

RBF radial basis function. 20, 22, 23

RBFNN radial basis function neural network. 25, 26

REE Electrical Grid of Spain. 28

RIP4 Read/Interpolate/Plot 4. 49

RMSE root mean squared error. 16, 18, 20–22, 25, 62, 69, 72, 73, 78, 84, 85, 87, 92–94, 100, 101, 103, 137, 142, 143, 149, 154, 155, 161, 162, 185, 187, 199, 210, 215, 218, 220, 223, 225, 226, 229, 235, 236, 238, 239, 243, 248, 250

RNL Risø National Laboratory. 27, 31

RNN recurrent neural network. 18, 20

RRTMG Rapid Radiative Transfer Model for General Circulation Models. 174

RSAR regime-switching autoregressive. 16

SAM seasonal adjustment method. 25, 26

SARIMA seasonal autoregressive integrated moving average. 24, 29

SCADA supervisory control and data acquisition. 28, 29, 31

SDE standard deviation of the error. 25

SE standard error. 117, 120, 122, 134, 160

SMAPE symmetric mean absolute percentage error. 62, 78, 84, 85, 137, 142, 143, 161, 185, 187, 199, 210, 215, 218, 225, 226

SOWIE Simulation Model for the Operational Forecast of the Wind Energy Production in Europe. 27

SSE sum squared error. 25

SVM support vector machine. 18, 21, 22, 24

TOPSIS technique for order of preference by similarity to ideal solution. iv, 8–11, 51, 52, 163, 187, 199, 202, 204, 205, 225, 227, 228, 234–236, 238–241, 243, 248, 250–252

UC3M University Carlos III of Madrid. 28

UCAR University Corporation for Atmospheric Research. 57, 163

UCC University College Cork. 31

UO University of Oldenburg. 30

UPC Polytechnic University of Catalonia. 29

UTC Coordinated Universal Time. 57, 106, 168, 169, 175, 176

VAPOR Visualisation and Analysis Platform for Ocean, Atmosphere, and Solar Researchers. 49

VAR vector autoregression. 16

W2P wind-to-power. 30

WAsP Wind Atlas Analysis and Application Programme. 27, 32

WECS wind energy conversion system. 19, 23

WEPROG Weather and Wind Energy Prognosis. 31

WNF wavelet-neuro-fuzzy. 25

WPA wavelet transform, particle swarm optimisation, and adaptive-network-based fuzzy inference system. 25

WPFS Wind Power Forecast System. 32

WPMS Wind Power Management System. 30

WPP Weather Research and Forecasting Post Processor. 49

WPPT Wind Power Prediction Tool. 28, 29, 31

WPS Weather Research and Forecasting Pre-Processing System. 49, 164, 166, 167, 169, 170, 173, 179, 224, 225

WRF Weather Research and Forecasting. iv, 8–11, 25, 48, 49, 58, 163, 164, 166, 169, 170, 172, 173, 175–177, 179–186, 192–194, 197, 199, 200, 202–206, 208–210, 214, 215, 218–220, 223–228, 234–236, 238–241, 243, 248, 250–252

WRFDA Weather Research and Forecasting Data Assimilation. 49

WT wavelet transform. 25

WTT wavelet transform technique. 25, 26

List of Symbols

α_t	White noise	
$\bar{\omega}$	Normalised weight	
$\bar{y}$	Sample mean	
$\bar{Z}$	Mean of wind speed or wind power measurements	m/s or W
Δt	Time step	s
η	Efficiency	
γ	Autocovariance function	
$\hat{\gamma}$	Sample autocovariance	
$\hat{\rho}$	Sample autocorrelation function	
$\hat{y}_t$	Predicted value at the time t	
$\hat{Z}$	Wind speed or wind power forecast	m/s or W
λ	Characteristic root	
μ	Membership function	
∇	Differencing operator	
∇^k	kth order differencing	
ω	Weight	
Φ	Autoregressive coefficient polynomial	

ϕ	Autoregressive parameter	
ψ	Partial autocorrelation function	
ρ	Air density	$\mathrm{kg\,m^{-3}}$
ρ	Autocorrelation funtion	
Θ	Moving average coefficient polynomial	
θ	Moving average parameter	
ε_t	White noise	
φ	Autoregressive parameter	
A	Fuzzy set	
A	Swept area	$\mathrm{m^2}$
a_t	White noise term at the time t	s
B	Backshift operator	
B	Fuzzy set	
c	Constant	
C_p	Power coefficient	
Cap	Wind farm installed capacity	W
Cov	Autocovariance	
D^+	Distance between the alternative and positive ideal solution	
D^-	Distance between the alternative and negative ideal solution	
E	Expectation	
e_t	Prediction error at the time t	
f	Output	
k	Constant	

k	Time interval	s
L	Lag operator	
L^k	k-step lag operator	
M	Model	
max	Maximum	
min	Minimum	
n	Number	
O	Output	
P	Interpolation polynomial	
P	Wind power	W
p	Consequent parameter	
p	Constant	
p	Order of autoregressive	
P_n	Normalised wind power	W
Q	Qualification indicator	
q	Consequent parameter	
q	Constant	
q	Order of moving average	
r	Consequent parameter	
r	Constant	
S	Similarity	
t	Time	s
U	Wind speed	$\mathrm{m\,s^{-1}}$

U_n	Normalised wind speed	$\mathrm{m\,s^{-1}}$
v	Wind speed	$\mathrm{m\,s^{-1}}$
Var	Variance	
w	Weight	
X	Standardised evaluation matrix	
x	Input variable	
x	Interpolation node	
X_t	Wind speed or wind power forecast at the time t	m/s or W
Y	Positivised evaluation matrix	
y	Input variable	
y_t	Time series	
Z	Normalised evaluation matrix	
Z	Wind speed or wind power measurement	m/s or W
z	Output	
Z^+	Positive ideal solution	
Z^-	Negative ideal solution	
z_t	Historical wind speed measurement at the time t	$\mathrm{m\,s^{-1}}$
$y_t{}'$	Differenced time series	

Chapter 1

Introduction

1.1 Background

As the global population grows rapidly and the standard of living improves, energy demand is burgeoning. This trend has a significant influence on politics, economics, and culture all over the world. Professor Richard E. Smalley, from Rice University, the United States, who won the Nobel Prize in Chemistry in 1996, declared that energy is the first among the top 10 problems of humanity (energy, water, food, environment, poverty, terrorism and war, disease, education, democracy, and population) and plays the most vital role for people trying to solve the other nine problems [127]. Currently, the world's dominant energy is still conventional fossil fuels, namely coal, oil, and natural gas [136]. However, these sources of energy have two apparent drawbacks. One is resource depletion since these fossil fuels are non-renewable [55]. According to the Statistical Review of World Energy 2021 provided by British Petroleum (BP), the whole world proved coal reserves could support its production for around 139 years, while oil and natural gas would be used up in 53.5 and 48.8 years, respectively [11]. The other is environmental pollution, mainly reflected in global warming, acid rain, and ozone depletion [101]. In the face of these enormous threats, seeking a reliable and green energy supply that ensures sustainable human development is becoming more and more crucial.

Wind, a widely distributed and powerful source of energy, is inexhaustible. Besides, being different from conventional power generation, wind power is environmentally friendly without any air or water pollution. Compared with other clean energy supplies, wind power has exceptional advantages. For instance, unlike nuclear power, wind power has no disposal issues associated with toxic, hazardous, or radioactive waste, which means it

is safe; unlike hydroelectric power, wind power is flexible since it can be harnessed both onshore and offshore; unlike solar power, there are no day or night restrictions on wind power, so it is possible to realise a continuous power supply throughout the day. With recent technological innovations which have promoted the large-scale development and utilisation of available wind resources, wind power has become more and more economical. Specifically, the global weighted-average levelised cost of the electricity of onshore wind farms dramatically decreased from USD 0.311 per kWh in 1983 to USD 0.041 per kWh in 2020, which was cheaper than those of almost all power plants operating on fossil fuels, typically ranging from USD 0.04 to 0.14 per kWh. Moreover, it was also lower than those of electricity generation derived from other renewable energy sources, such as hydropower (USD 0.044 per kWh), solar photovoltaics (USD 0.057 per kWh), geothermal energy (USD 0.070 per kWh), and bioenergy (USD 0.076 per kWh) [59, 129].

Wind power, as the most mature and promising renewable energy technology with substantial commercial value, is gaining more and more attention worldwide [28, 119, 151]. In the last two decades, it has become a significant way of providing energy in some developed and developing countries. According to the Global Wind Report 2021 by the Global Wind Energy Council (GWEC), China, the United States, Brazil, the Netherlands, and Germany were the world's top five countries for the new installed wind capacity in 2020, occupying 80.6% of the global market share; while for the cumulative installed wind capacity, the world's top five markets were China, the United States, Germany, India, and Spain, making up 73% of the total wind power installations in the world [49].

Figures 1.1 and 1.2 show the global annual installed wind capacity 2001–2020 and cumulative installed wind capacity 2001–2020, respectively [49]. Specifically, Figure 1.1 indicates that the global annual installed wind capacity increased gradually between 2001 and 2015, although it did decrease in 2013. After that, it slightly went down for 3 years. However, 2019 saw a growth of 20% compared with 2018, and 2020 saw an increase of 53% compared with 2019. In 2020, a 93.0 GW wind capacity was installed globally, breaking the record in history. As a result, the global cumulative installed wind capacity went up year by year (see Figure 1.2). By the end of 2020, the global cumulative installed wind capacity reached 743 GW. As a whole, wind power is in a stage of rapid development at present.

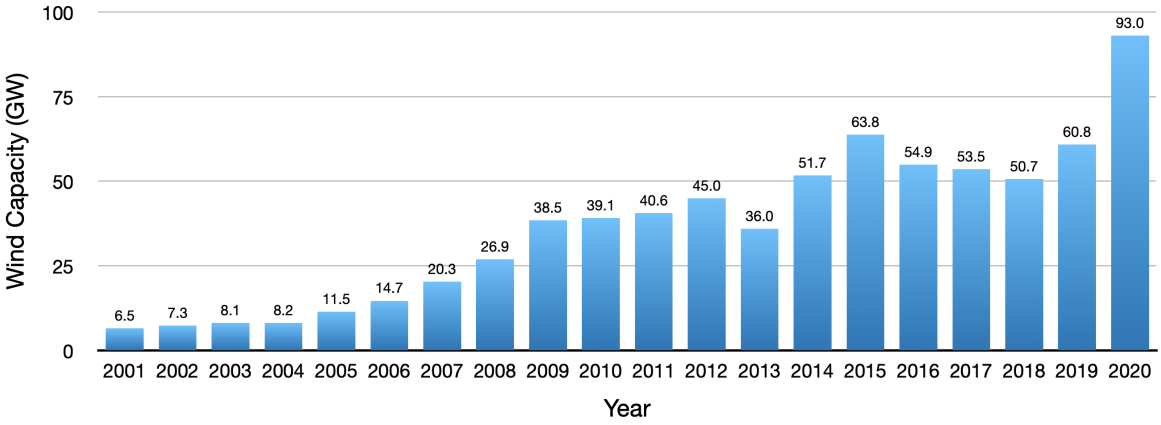

Figure 1.1. Global annual installed wind capacity 2001–2020.

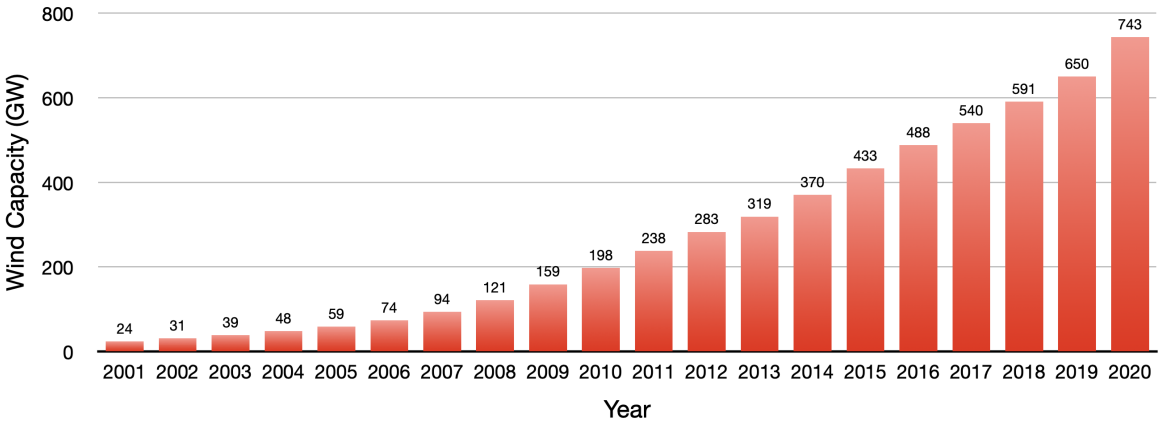

Figure 1.2. Global cumulative installed wind capacity 2001–2020.

China, where the average wind energy density is around 100 W/m^2, has abundant wind power resources. Liu, Tang, and Jiang [84] claimed that China's total wind energy reserves are about 3,226 GW, of which the available onshore wind energy for development and utilisation is 253 GW, and the exploitable offshore wind energy is 750 GW, adding up to 1,000 GW approximately. Figures 1.3 and 1.4 show China's annual installed wind capacity

2001–2020 and cumulative installed wind capacity 2001–2020, respectively [45, 46, 47, 48, 49]. The first 3 years saw the slow development of wind power. However, China's wind power industry has entered an accelerated development stage since 2004. By the end of 2003, the cumulative installed wind capacity was only 568 MW. Thereafter, the growth of the new installed wind capacity doubled for 6 consecutive years. 13,785 MW of new wind power installations were added in 2009, with year-over-year growth of 125.6%. During the following 11 years, the rise in the annual installed wind capacity remained at a high level with a tremendous fluctuation. The historical record of the annual installed wind capacity, reaching 48,940 MW, occurred in 2020. This number is impressive as it represented more than half of the world's market [49]. In 2020, China continued to lead the global wind power market in both onshore and offshore new installations, making up 56% and 50% of the world's share, respectively. As of the end of 2020, China's cumulative installed wind capacity was 278,324 MW, which was ranked first in the world and accounted for more than one third of the global share [49].

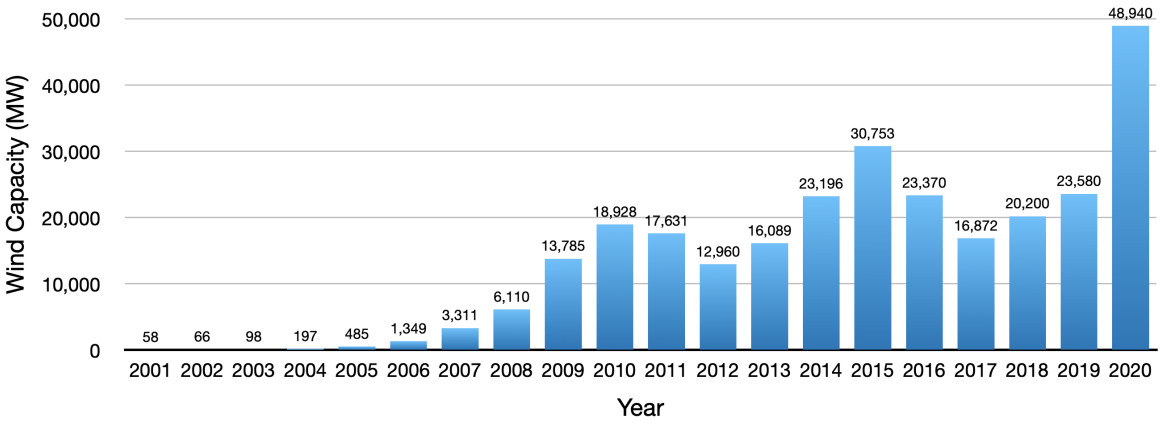

Figure 1.3. China's annual installed wind capacity 2001–2020.

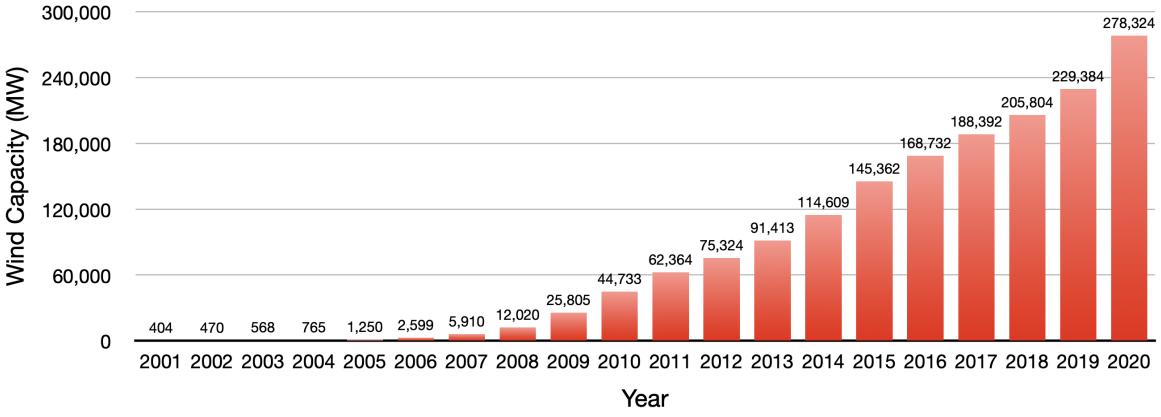

Figure 1.4. China's cumulative installed wind capacity 2001–2020.

In 2019, an additional 597 MW of new wind power capacity was installed in four provinces in Canada, representing the investment of more than one billion Canadian dollars in the field of wind energy. To be precise, two projects totalling 360 MW were constructed in Ontario, which is the leader of the Canadian wind power industry. Alberta took second place with one project of a 202 MW capacity. These two provinces took up 94.1% of the entire 2019 national market, followed by Saskatchewan and British Columbia with contributions of 20 MW and 15 MW, respectively. By the end of 2019, there were 301 wind farms with 6,771 wind turbines operating in Canada, and Canada's cumulative installed wind capacity reached 13,413 MW, which could meet the electricity demand of around 3.4 million Canadian homes [16]. Figure 1.5 shows Canada's annual installed wind capacity between 2001 and 2020. An upward trend with some fluctuations can be seen from 2001 to 2014, while the following 6 years saw a significant downward trend. Besides, Figure 1.6 shows Canada's cumulative installed wind capacity between 2001 and 2020, from which a steady increase from 198 MW to 13,577 MW can be found [45, 46, 47, 48, 49]. By the end of 2020, Canada was ranked the ninth wind power market in the world [49]. Evidently, fantastic development opportunities remain in Canada's wind power market. Moreover, wind energy has become the largest source of new power generation in Canada over the past 10 years and, indeed, continues to be a fast-growing contributor to Canada's hybrid electricity supply [15].

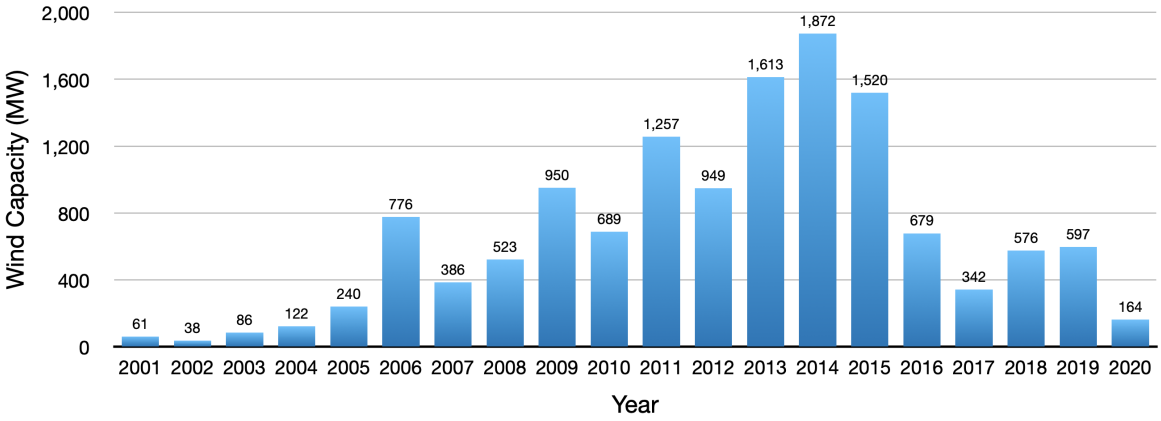

Figure 1.5. Canada's annual installed wind capacity 2001–2020.

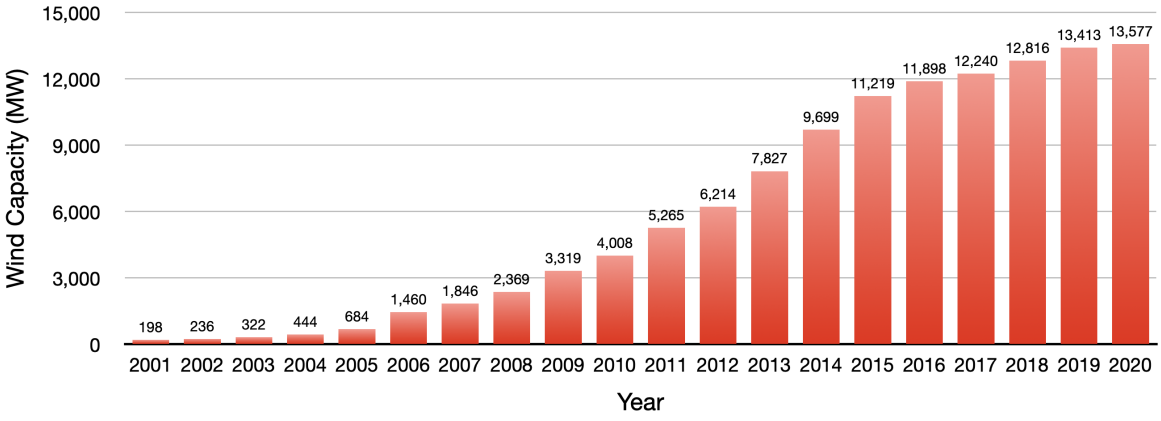

Figure 1.6. Canada's cumulative installed wind capacity 2001–2020.

With the continuous research and development of wind energy, the unit capacity of wind turbines is rising, and the construction scale of wind farms is expanding, resulting in wind power's higher and higher proportion in mixed electrical grids. Nevertheless, wind power is significantly affected by the characteristics of wind, which, by its very nature, is random, intermittent, and volatile [147]. It is true that when the capacity of a wind farm is small,

the above features will not make a severe impact on the power system. However, the higher the proportion of wind power in the electrical grid, the more noticeable influences on the power system will be in power quality, grid stability, and system security [3]. Sometimes, these effects may even compromise the whole power system. In consequence, wind power's larger and larger-scale grid connections bring new challenges to the reliable, stable, and secure operation of electrical grids that incorporate wind power systems.

1.2 Motivation

Developing a multi-hour ahead wind power forecasting system as the focus of this research was motivated by the following three potential outcomes:

(1) Greatly ensuring the stable, secure, and economical operation of electrical grids

Wind power forecasting allows power-dispatch divisions to know the future trend of wind power in advance and reduce the negative impacts on electrical grids resulting from random, intermittent, and volatile wind power by means of control. In addition, they can also adjust the schedules of mixed power generation supplies by increasing or decreasing reserve capacities in time to meet electricity demands and avoid financial losses as much as possible. Consequently, the stability, security, and efficiency of electrical grids improve, while the operating costs reduce [137].

(2) Effectively enhancing the reliability and market competitiveness of wind power

Wind farms have a risk of receiving financial penalties for unreliable power supplies. Compared with the other controllable methods of electricity generation, wind power's competitiveness is weak owing to its characteristics of randomness, intermittency, and volatility. Forecasting the power production of wind farms can effectively enhance the reliability of wind power and make wind power more competitive in the electricity market [148].

(3) Systematically scheduling the maintenance and repairs of wind turbines

Based on the results of wind power forecasting, technicians can be arranged to maintain and repair wind turbines when there is no wind or the wind speed is too low to start wind turbines, preventing the waste of wind resources and increasing the efficiency of wind turbines [109].

Hence, the research on multi-hour ahead wind power forecasting is imperative as it will predictably tackle the uncertainty associated with wind energy. Creating a wind power forecasting system and improving its forecast accuracy contribute to reducing the unfavourable influences caused by the randomness, intermittency, and volatility of wind energy. In the meantime, they are also in favour of improving the stability, security, economy, reliability, and efficiency of wind power systems.

1.3 Problem Statement

This research aimed to develop a comprehensive multi-hour ahead wind power forecasting system for real wind farm applications. Four categories of models, namely the wind data acquisition and pre-processing, wind speed forecasting, wind speed correction, and wind power forecasting models, were proposed as the main components of the whole system.

Historical wind speed and wind power measurements are acquired directly from wind farms, where these data are recorded at specific time intervals every day. Although these data are highly confidential, the operators of wind farms, as end-users, can enter historical wind speed and wind power measurements into the wind data acquisition and pre-processing model by themselves. The tricky part was wind speed forecasts provided by Weather Research and Forecasting (WRF) models. These data are predicted results that are not as accurate as wind speed measurements. Since all necessary resources, such as the WRF model, global geographical data, and historical meteorological data, are available online and free to download, wind speed forecasts can be obtained. However, WRF modelling requires a high level of meteorological knowledge and large amounts of computational resources. In addition, all wind data must be pre-processed before being input into the wind speed forecasting model, wind speed correction model, and wind power forecasting model.

The second problem tackled in this research was related to the generation of a multi-hour ahead wind speed forecasting model. After acquiring and pre-processing wind data, the next step was to process them. Three different methodologies based on a persistence, an autoregressive integrated moving average (ARIMA), and a WRF-technique for order of preference by similarity to ideal solution (TOPSIS) model were proposed to forecast wind speed multiple hours in advance.

The third problem was associated with correcting wind speed forecasts obtained from the WRF-TOPSIS model. An adaptive neuro-fuzzy inference system (ANFIS), belonging to artificial intelligence (AI), was suggested to amend wind speed forecasts according to the difference between historical wind speed measurements and wind speed forecasts.

The last problem was with a power curve model for converting the wind speed forecasts to wind power forecasts. An ANFIS model was recommended to delineate the mapping relationship between wind speed and wind power based on historically measured wind data. By making use of the outputs of the multi-hour ahead wind speed forecasting model as the inputs to the wind power forecasting model, wind power could be forecasted multiple hours in advance.

In summary, there were four major problems that needed to be solved in this research:

1) how to produce wind speed forecasts by using the WRF model;

2) how to employ the persistence, ARIMA, and WRF-TOPSIS models for multi-hour ahead wind speed forecasting;

3) how to correct the wind speed forecasts obtained from the WRF-TOPSIS model;

4) how to build the power curve model for converting the wind speed forecasts to wind power forecasts.

1.4 Proposed Contributions

The existing literature on wind power forecasting highlights two main issues of present models. One is that most researchers focused on very limited forecast time steps (one or a few); the other is that they applied meteorological forecasts provided by third parties instead of producing those data by themselves. In order to tackle these shortcomings, a comprehensive wind power forecasting system with multiple time horizons was proposed, and the application of WRF models to generate computational wind speed data was introduced.

In the process of developing the multi-hour ahead wind power forecasting system, the proposed contributions can be summarised as follows:

(1) Modelling of a multi-hour ahead wind speed forecasting model based on three different methodologies

A persistence, an ARIMA, and a WRF-TOPSIS model were used to forecast wind speed separately. According to their individual features, each wind speed forecasting model was recommended for one or more specific time horizons. Generally, shorter-term wind speed forecasting was only based on historically measured wind speeds. In

contrast, longer-term wind speed forecasting was based on historically measured wind speeds and computational wind speeds.

(2) Development of a multi-hour ahead wind power forecasting system by integrating wind speed forecasting models with a power curve model

An ANFIS model was employed to build a power curve model which aimed at mapping wind speed values into wind power values. Specifically, historically measured wind speed and wind power data were applied to form a training dataset. By inputting multi-hour ahead wind speed forecasts into a trained ANFIS model, the corresponding multi-hour ahead wind power forecasts could be generated as the outputs of the power curve model. That is to say, the wind speed forecasting models and the power curve model worked together to constitute the multi-hour ahead wind power forecasting system.

(3) A systematic method to select WRF models instead of an ad hoc method

In the process of WRF modelling, a couple of crucial physics options needed to be determined, and for each of them, there were lots of parameterisation schemes available. Previously for a case study in the laboratory, an ad hoc method mainly based on personal work experience was applied to establish a WRF model. However, a systematic method instead of it was proposed for the same case in this study. Specifically, after the preliminary screening according to the basic features of the parameterisation schemes, 10,800 parameterisation scheme combinations were chosen. Due to the combination restrictions, the number of the total practical parameterisation scheme combinations decreased to 1,334. Then, the predictive performance of the 1,334 candidate WRF models on the first day of the training dataset was examined, and the TOPSIS scheme selected the top 50 WRF models by using six evaluation metrics. Similarly, the predictive performance of the top 50 WRF models over the rest days of the training dataset was tested, and the TOPSIS scheme finally determined the top five WRF models for wind speed forecasting.

(4) A novel way of combining WRF models to enhance model reliability

The TOPSIS is a comprehensive evaluation method that can make full use of the information of original data, and its results can accurately reflect the gap among alternatives. In addition to ranking alternatives, it can also be utilised as an approach to assigning weights for them. Hence, combining the top five WRF models with the TOPSIS scheme was proposed according to their predictive performance on the training dataset. At last, the 5-in-1 (ensemble) WRF model was demonstrated to be more reliable than any single candidate WRF model.

(5) Development of an ANFIS model for the wind speed correction model

The errors in wind speed forecasts obtained from WRF models exist. An ANFIS model was proposed to detect the complicated relationship between wind speed forecasts and wind speed measurements according to the historical records and to correct wind speed forecasts before being input into the power curve model. The results demonstrated that this correction model is helpful for the improvement of wind power forecasting.

(6) Development of numerical methods to tune the ARIMA and ANFIS models

In terms of the ARIMA and ANFIS models, a couple of model parameters need to be decided. Different values of parameters lead to different results. Hence, the numerical analysis, comparing the model performance based on different parameter combinations, was applied to optimise the parameters of these models proposed in the research.

1.5 Structure of the Dissertation

This dissertation is organised as follows. In Chapter 1, the background, motivation, problem statement, proposed contributions, and structure of the dissertation are introduced. In Chapter 2, the classification of wind power forecasting, wind power forecasting models and software, fundamental theories of the Sugeno-type fuzzy inference system (FIS), ANFIS, and time series analysis, fundamental principle of the WRF model, and fundamental algorithm of the TOPSIS are reviewed. In Chapter 3, the analysis of factors affecting wind power, description of data sources, approaches of data pre-processing, spectral analysis of wind speed measurements, introduction of model evaluation metrics, interpretation of a 'forecast time horizon', and power curve modelling are presented. In Chapters 4 and 5, the statistics-based and physics-based modelling for multi-hour ahead wind speed and wind power forecasting are investigated based on a real case study, and the model predictive performance is assessed. In Chapter 6, the statistics-based and physics-based forecasting models are compared and analysed, and the multi-hour ahead wind power forecasting system is created and evaluated. In the last Chapter 7, the conclusions are drawn, and the future work is suggested.

Chapter 2

Literature Review

2.1 Classification of Wind Power Forecasting

According to the time horizon, wind power forecasting can be divided into four categories, namely very short-term, short-term, medium-term, and long-term forecasting [51]. However, there are no authoritative definitions for their ranges in the wind power industry. Different researchers have individual descriptions in their own studies. Besides, the actual applications of different forecast time horizons in electricity systems are consequential various. By referring to the relevant literature [22, 24, 51, 63, 122, 139, 156], the unit, range, and applications for each wind power forecast category are summarised in Table 2.1.

Table 2.1. Classification of wind power forecasting according to the time horizon.

Time horizon	Unit	Range	Applications
Very short-term	Minute	A few minutes to 30 minutes ahead	Wind turbine control, regulation actions, real-time grid operations, electricity market clearing, etc.
Short-term	Hour	1 hour to 72 hours ahead	Power dispatch schedules, load smart decisions, operational security in electricity markets, etc.
Medium-term	Day	3 days to 1 week ahead	Generator online/offline decisions, maintenance and repair schedules, reserve requirement decisions, unit commitment decisions, operation cost optimisation, operation management, etc.
Long-term	Year	1 year to several years ahead	Wind resource assessment, feasibility studies on wind farm design, etc.

According to the methodology, wind power forecasting can be divided into two categories, namely physical and statistical methods [139, 156].

2.1.1 Physical Methods

In physical methods, physical variables which influence wind power production, such as the landform of wind farms (roughness, obstacles, orography, etc.), surrounding weather conditions (wind speed, wind direction, temperature, pressure, humidity, etc.), and the layout of wind turbines, are usually incorporated into forecasting models [22, 63, 122]. These factors are considered in complicated mathematical models to calculate wind speeds in the future. After that, wind speed forecasts will be converted to wind power forecasts by using the power curves of wind turbines [51]. The essence of physical methods is to improve the resolution of meteorological data generated by numerical weather prediction (NWP) models as high as possible [156], for example, downscaling from tens of square kilometres to one square kilometre for the purpose of obtaining more accurate weather prediction. The advantages of physical methods are reflected in the fact that there is no need for a large number of historically measured data [63], as well as they are more suitable for complex terrain [74]. However, one of their drawbacks is the necessity of having

a wealth of meteorological knowledge and the understanding of physical characteristics to build forecasting models [74]. Additionally, physical methods require collecting physical information [66] and mostly need a tremendous amount of computational resources [73].

2.1.2 Statistical Methods

Statistical methods aim at establishing mapping relationships that can be either linear or non-linear between meteorological data (such as wind speed and wind direction) and wind power outputs [51]. For a statistical model, historically measured data are employed as a training dataset to determine the statistical relationship between inputs and outputs [63]. After being tuned by contrasting model forecasting results with wind power measurements, the statistical model parameters can be optimised for wind power forecasting [122]. In general, statistical methods contain time series analysis and AI [139]. One of the advantages of statistical methods is that their modelling processes are straightforward and affordable [63]. Besides, statistical methods can be easily adapted to different terrains of wind farms and various layouts of wind turbines [6], effectively ignoring some meteorological factors that have minor impacts on the power production of wind farms, such as temperature, pressure, and humidity [139]. Nevertheless, statistical methods have some inherent disadvantages. Although statistical models work well for short forecast time horizons, their forecast accuracy drops with the increase of the time scale [22]. Furthermore, it is difficult for statistical models to predict abrupt climate changes [154]. In addition, statistical methods require long-term data collection and large datasets for model training processes [139].

2.2 Overview of Wind Power Forecasting Models

2.2.1 Persistence Models

Persistence models, in which wind speed or wind power in the future is assumed to be equal to measured wind speed or wind power at the moment [156], are the most straightforward and economical approach in the field of wind power forecasting [22]. Another advantage of persistence models is that there are no additional variables, so there is no need to tune parameters [51]. Persistence models can be described by the following equations [22]:

$$v(t + \Delta t) = v(t) \ , \tag{2.1}$$

and

$$P(t + \Delta t) = P(t) \ , \tag{2.2}$$

where v is the wind speed, t is the time, Δt is the time step size, and P is the wind power.

However, the forecast errors of persistence models go up sharply with the expansion of the forecast time scale [145]. In the literature, this approach is usually applied as a benchmark to be compared with other advanced forecasting approaches in order to evaluate the improvements of those advanced models [128]. Typically, persistence models are designed for very short-term wind power forecasting and are widely used in the electrical industry [122].

2.2.2 Time Series Models

In addition to persistence models, statistical methods based on time series models are commonly applied for wind speed and wind power forecasting. Following three stages of model construction, namely identification, parameter estimation, and diagnostic checking, a mathematical model can finally be generated to describe studied data and then used to forecast wind speed or wind power [63].

Based on Box and Jenkins's research, classical time series models can be divided into four basic types, namely the autoregressive (AR), moving average (MA), autoregressive moving average (ARMA), and ARIMA models [86]. In general, time series models have the following form [51]:

$$X_t = c + \alpha_t + \sum_{i=1}^{p} \varphi_i X_{t-i} - \sum_{j=1}^{q} \theta_j \alpha_{t-j} \ , \tag{2.3}$$

where X_t is the wind speed (power) forecast at time t, c is a constant, α_t is the white noise at time t, p is the order of the AR component of the model, φ_i $(i = 1, 2, \ldots, p)$ are the AR model parameters, q is the order of the MA component of the model, and θ_j $(j = 1, 2, \ldots, q)$ are the MA model parameters. Equation (2.3) corresponds to the general form of the ARMA model. When either $p = 0$ or $q = 0$, the model reduces to an MA or an AR model, respectively [63]. Finally, the ARIMA model arises through the application of a differencing operation on the original data [86].

Huang and Chalabi [56] proposed a linear, time-varying AR model for wind speed forecasting based on a dataset acquired from a weather station in Herstmonceux, England.

The results indicated that the AR model was only applicable to forecast wind speed up to several hours in advance. Besides, the AR model was verified to be sufficient for the real-time control purpose.

Gallego et al. [36] suggested a conditional parametric autoregressive (CPAR) and a regime-switching autoregressive (RSAR) model which were constructed by replacing the fixed weights in linear AR models with functions depending on the wind speed and wind direction. This methodology was applied by these researchers to an offshore wind farm at Horns Rev in the North Sea near Denmark. The results showed that both the CPAR and RSAR models outperformed the base models (viz., the persistence, AR, and Markov switching autoregressive (MSAR) models) in terms of the 1-step ahead prediction of the wind speed and wind power for this very short time horizon forecasting application.

Kamal and Jafri [65] tested an ARMA model for a simulation of the hourly averaged wind speed values in Quetta, Pakistan, based on the data of 2-year wind speed measurements. In the process of the modelling, a couple of essential characteristics of wind speed data (viz., autocorrelation, non-Gaussian distribution, and diurnal non-stationarity) were considered. They proved that the wind speed forecasts with the 95% confidence interval provided by the ARMA model were acceptable up to 6 hours in advance.

Torres et al. [131] applied an ARMA and a persistence model to forecast the hourly average wind speed in Navarre, Spain, ranging from 1 to 10 hours in advance. The transformation and standardisation of the wind speed time series data were advised in the process of the ARMA modelling. Only in several 1-hour ahead forecasting cases, the errors of the persistence model were smaller than those of the ARMA model. For the other cases, the ARMA model consistently performed better than the persistence model. In addition, if the acceptable root mean squared error (RMSE) was limited to be not greater than 1.5 m/s, the proposed models in the study were only suitable for very short-term wind speed forecasting.

Erdem and Shi [29] presented four ARMA-based models (viz., a component, a traditional-linked ARMA, a vector autoregression (VAR), and a restricted VAR model) for providing the 1-hour ahead forecasts of wind speed and wind direction at two locations in North Dakota, the United States. Comparing these forecasts with the measurements acquired from the wind observation sites, these researchers claimed that the wind speed predictive performance of the traditional-linked ARMA, VAR, and restricted VAR models was comparable to one another, and each of these models was preferable to the component model. Nevertheless, the best models with regard to the wind direction forecasting were different, the component model for the first site and the VAR model for the second one.

An ARIMA and an artificial neural network (ANN) model were examined in Cadenas

and Rivera's [12] paper to forecast the monthly wind speed of the South Coast of Oaxaca, Mexico. After a comparative analysis, the superiority of the seasonal ARIMA model was revealed in the accuracy of wind speed forecasting. However, it was also concluded that the predictive performance of the ANN model might be enhanced by means of augmenting the number of training vectors.

Kavasseri and Seetharaman [67] investigated the application of fractional-autoregressive integrated moving average (f-ARIMA) models to forecast wind speed 24 and 48 hours in advance and applied the proposed methodology to four potential wind farms located in North Dakota, the United States. According to the power curve of the studied wind turbine, the wind speed forecasts were converted to the wind power forecasts. The conclusion was that the wind speed forecast errors of the f-ARIMA models were much lower than those of the persistence model, resulting in the improved forecasting of both the wind speed and wind power.

Liu et al. [81] reported an improved time series method (ITSM) based on an ARIMA model for forecasting the wind speed and wind power of a particular wind farm in China. A wavelet approach was employed to decompose the time series data into a couple of sub-series which were separately forecasted multi-step ahead and aggregately calculated. Finally, the forecasts of the original time series data were achieved. The results showed that the ITSM, which could be individually applied in wind speed or wind power forecasting, gave higher accuracy compared with a classical time series and a back-propagation network method.

According to the literature review of time series models listed above, it can be found that in most cases of wind speed and wind power forecasting, the forecasting models solely depend on the time series of wind speed or wind power measurements, and time is the only considered factor affecting results. The assumption is that the historical trend of wind data will influence the future wind data, and the continuity of change exists. The excellent effectiveness of time series models in short-term wind power forecasting has been validated [122]. Moreover, the structures of time series models are simple, and the required computational resources are comparatively low [51]. However, time series models need lots of historical data for modelling [86]. Since an essential assumption for time series modelling is that the data are stationary [92], it is tricky for time series models to deal with the condition of the data being non-stationary [157]. In addition, with the rise of the forecast time step, the corresponding forecast accuracy of time series models deteriorates mainly because these models rely on their own previous forecasts in the cases of multi-step ahead forecasting [63].

2.2.3 Artificial Intelligence Models

Thanks to the development of AI, a vast number of novel models based on AI are mushrooming in the field of wind speed and wind power forecasting in recent years [22]. The most widely used techniques involved in AI models are ANNs, support vector machines (SVMs), and fuzzy logic (FL) [86].

ANNs, composed of numerous simple processing units (neurons) interconnecting based on specific topological structures, imitate the human brain and its functions [85]. Two basic types of ANNs formed by different network architectures are feed-forward neural networks (FNNs) and recurrent neural networks (RNNs) [70]. Back-propagation is a pretty popular learning algorithm for training ANNs, and this type of ANNs is called back-propagation neural networks (BPNNs) [71]. Generally, an ANN model consists of one input layer, one or several hidden layers, and one output layer [2]. The weights of neurons' interconnections are learnt via a training process based on a training dataset [44]. After training, the ANN model is able to identify the intricate non-linear relationship between input and output variables [26]. Furthermore, ANNs have the abilities of self-learning, self-organising, and self-adapting [144].

SVMs, designed for classification and regression, are based on a statistical learning theory [41]. As a machine learning technique, SVMs can overcome some shortcomings of traditional ANNs, for example, overlearning and getting stuck at a local minimal point [133]. Basically, SVMs are more suitable for dealing with those non-linear problems with small sample sizes [153].

FL, in which the truth values of features are in the range of [0, 1] rather than either 0 or 1 in Boolean logic, is inspired by the fact that humans often make decisions according to uncertain and imprecise information [68]. Membership functions and linguistic fuzzy rules are implemented for FL modelling [103]. Additionally, FL can be combined with ANNs. An ANFIS, integrating FL with an ANN, is a good example [60, 134]. In this way, the ANFIS holds the advantages of the readability from FL and learning ability from the ANN [1].

Mohandes, Rehman, and Halawani [94] proposed an FNN model to forecast the mean monthly and daily wind speed in Jeddah, Saudi Arabia. Besides, an AR model was described as a benchmark. The results demonstrated that the FNN model was preferable to the AR model because of its lower RMSEs for the 1-step ahead monthly and daily forecasting cases. Moreover, the FNN model also showed its superiority in multi-step ahead forecasting compared with the AR model.

Sfetsos [121] introduced an FNN model for average hourly wind speed forecasting based

on time series analysis. In addition, a persistence and an ARIMA model were also presented for reference purposes. Two sets of 1-month wind speed data were employed: one was observed on the island of Crete, Greece, in March 1998; the other was measured in Oxfordshire, the United Kingdom, in June 1997. Because of producing the lowest errors for both of the cases studied, the FNN model was concluded to be better than the persistence and ARIMA models in terms of wind speed forecasting ability.

Mabel and Fernandez [87] presented an FNN model for the purpose of forecasting monthly wind power generated by the wind farms in Muppandal, India. To be precise, the FNN model was built with three input variables (viz., wind speed, relative humidity, and generation time) in the input layer and one output variable (wind power) in the output layer. After a couple of tests, the optimal numbers of the hidden layer and neurons in the hidden layer were determined to be one and four, respectively. The field data over 3 years between April 2002 and March 2005, provided by seven wind farms located in the studied area, were utilised in the research. A good agreement was discovered between the forecasted wind power values provided by the FNN model and the recorded data, with an overall percentage error (PE) of 4%.

Cadenas and Rivera [13] recommended an ANN model for the 1-hour ahead wind speed forecasting in Oaxaca, Mexico. A set of statistical tests on the 7-year hourly wind speed data, observed by the Federal Electricity Commission (CFE), verified that the wind speeds of each specific month in different years belonged to a same group. Hence, 12 specialised ANN models were established for every month of a year. Besides, four types of ANN models with different structures (viz., the different numbers of layers and neurons) were listed and compared with each other. It was surprising that the simplest ANN model with two layers and three neurons (two for the input layer and one for the output layer) overcame the other models with more complex configurations concerning the mean squared error (MSE) and mean absolute error (MAE). Moreover, this conclusion was confirmed by the cases of 12 months. These researchers claimed that the proposed wind speed forecasting model was sufficient for practical applications.

In order to forecast the power production of a wind energy conversion system (WECS) 10 minutes in advance, Chang [20] reported a BPNN model with three inputs in the input layer and one output in the output layer. A training dataset was created based on the 3-day historical power measurements of an operational WECS located on the Taichung coast, Taiwan, while the data of the following day was used as a test dataset. According to the results of a numerical approach, the optimal number of neurons in the hidden layer was determined to be 35. It was concluded that the proposed BPNN model was accurate and reliable for forecasting wind power with an average absolute error (AAE) of 0.2780%.

More and Deo [97] suggested an FNN and an RNN model for the wind speed forecasting of two coastal sites in India. As a conventional statistical time series analysis method, an ARIMA model was introduced to be a benchmark in their research. The actual wind speed observations between 1989 and 2000 in the coastal area of Colaba, provided by the India Meteorological Department (IMD), Mumbai, were employed to generate the forecasting models and validate model effectiveness. The results of the daily, weekly, and monthly wind speed forecasting confirmed that the proposed two neural network models outperformed the ARIMA model in terms of forecast accuracy.

Li and Shi [77] did a comprehensive investigation to compare the 1-hour ahead wind speed forecasting abilities of three typical neural network models, namely a feed-forward back-propagation (FFBP), a radial basis function (RBF), and an adaptive linear element (ADALINE) model. The collection of 1-year hourly average wind speed data acquired from two locations (Hann and Kulm) in North Dakota, the United States, was utilised in the research. It was concluded that the forecast accuracy of different neural network models varied. The choice of the neural network model type which contributed to the highest forecast accuracy depended on the data source. Nevertheless, the results indicated that even for the same dataset, there was no single neural network model that was able to consistently perform the best among all the presented models in terms of three metrics (viz., the MAE, RMSE, and mean absolute percentage error (MAPE)). In addition, for an individual neural network model, it was observed that the numbers of input variables and the learning rate affected the model forecast accuracy more or less.

In order to automatically specify the input variables and interior model parameters of an ANN and a nearest neighbour search model for 1-hour ahead wind power forecasting, Jursa and Rohrig [64] applied two evolutionary optimisation algorithms (viz., particle swarm optimisation (PSO) and differential evolution (DE)) to the forecasting models. The weather forecast data acquired from the German Weather Service (DWD), Germany, and the historically measured wind power data obtained from 10 wind farms located in north-western Germany, covering a period from the 1st of January 2004 to the 30th of June 2007, made up a database for the case study. The conclusion was that the precision of wind power forecasting could be enhanced through the proposed automatic specification approach.

Guo et al. [43] developed a modified empirical mode decomposition based feed-forward neural network (EMD-FNN) model for multi-step average monthly and daily wind speed forecasting. The EMD-FNN model was adjusted by removing a high-frequency component. The predictive performance of the modified EMD-FNN model was evaluated based on two datasets of wind speed measured in Zhangye, China. One was the monthly data from 2003 to 2006, and the other was the daily data between May 2006 and August 2006. Through a

comparative analysis, it was found that the modified EMD-FNN model was preferable to the FNN and unmodified EMD-FNN models. Specifically, the MSE, MAE, and MAPE for the modified EMD-FNN model were lower than those for the other two mentioned models in both of the case studies.

Mohandes et al. [95] examined an SVM model to forecast daily wind speed. The 12-year data of average daily wind speed observations in Madina, Saudi Arabia, were introduced to the case study. Another neural network method, a multilayer perceptron (MLP) model, was also generated as a reference model. According to the metric of the RMSE, it was concluded that the SVM model was more suitable than the MLP model for the wind speed forecasting. This judgement was supported by the systems with orders ranging from 1 to 11.

Zhou, Shi, and Li [158] stated a piece of detailed research on the application of a least-squares support vector machine (LS-SVM) model for 1-step ahead wind speed forecasting. In this study, these researchers introduced a linear, a Gaussian, and a polynomial kernel function to create three different LS-SVM models. The 1-year hourly wind speed data applied in this study were collected by a wind observation station in North Dakota, the United States. In order to avoid the seasonal influence, the entire dataset was divided into four seasonal datasets. It was found that the LS-SVM models were superior to the persistence model in terms of forecast accuracy for the spring, autumn, and winter datasets but not for the summer dataset.

Zhu et al. [159] advised a FL methodology for the forecasting of wind farm power output. The number of fuzzy rules used in this methodology was optimised based on a modified fuzzy c-means clustering algorithm, and a back-propagation algorithm was applied to tune the parameters of input and output membership functions. Wind speed, temperature, and wind power were taken into account as the three inputs of the FL model. In addition, a BPNN model was chosen as a benchmark. The measured wind speed and wind power data over a 25-day period with a temporal resolution of 10 minutes were acquired from an operational wind farm located in Inner Mongolia, China, and employed for model validation. After a comparative study, it was found that the FL model outperformed the BPNN model in terms of the 30-minute, 1-hour, and 2-hour ahead wind power forecasting since the RMSEs for the former kept lower than those for the latter in all the cases.

Potter and Negnevitsky [110] carried out a piece of research on applying an ANFIS model, which combined a FL and an ANN model, for very short-term (2.5-minute ahead) wind forecasting. Besides, the proposed model was utilised to forecast wind vectors instead of wind speed and wind power. The effectiveness of the ANFIS model was evaluated according to a 21-month wind speed and wind direction time series observed in Tasmania,

Australia. The results indicated that the ANFIS model performed much better than the persistence model, which was considered a benchmark. More specifically, the MAPE for the ANFIS model was lower than 4%, while the corresponding error for the persistence model was roughly 30%.

Nowadays, an increasing number of researchers are using AI models instead of conventional statistical models. The novel models listed above have verified the success of the AI technique in the field of wind speed and wind power forecasting. In general, AI models are preferable to time series models in terms of forecast accuracy. However, each AI model has individual pros and cons. An AI model which outperforms all other ones for all cases does not exist. That is because choosing a model for wind speed or wind power forecasting highly depends on many factors, including the data resource, forecast time horizon, wind farm location, and even season.

2.2.4 Hybrid Models

Hybrid models refer to the models in which two or more models based on various algorithms are combined together for forecasting [51]. The motivation behind hybrid models is to take advantage of the superiority of varied techniques and enhance overall predictive performance [145]. Although a combination of different models might not consistently outperform a single model [63], it is true that the combination method not only contributes to higher forecast accuracy in most situations [122] but also reduces the risk of forecast errors [53].

Li, Shi, and Zhou [78] presented a new two-step approach for hourly wind speed forecasting. To be precise, three ANN models, namely an ADALINE, a BPNN, and an RBF model, were introduced to forecast the wind speed individually, and a Bayesian model averaging (BMA) model was applied to combine the wind speed forecasts generated from the three single ANN models and then output the final wind speed forecasts. Two sets of 1-year mean hourly wind speed observations acquired from two locations in North Dakota, the United States, were used to prove the effectiveness of the proposed model. According to the evaluation metrics (viz., the MAE, RMSE, and MAPE), the adaptability, reliability, and accuracy of the proposed hybrid forecasting model were demonstrated to be robust, and the improvement of the hybrid model against each single ANN model was found.

Bouzgou and Benoudjit [9] introduced a multiple architecture system (MAS) including a multiple linear regression (MLR), an MLP, an RBF, and an SVM model for wind speed forecasting. Three methods (viz., an average, a weighted, and a non-linear method) were used to combine the wind speed forecasts produced by every individual model. A set of

10-year mean daily wind speed data measured by seven sites in Algeria from 1995 to 2004 was applied for the case study. Finally, the improvement of the proposed MAS over the individual forecasting models was observed.

Chang [21] declared a hybrid model based on an enhanced particle swarm optimisation (EPSO) algorithm to forecast wind power 10 minutes in advance. Particularly, a persistence, a BPNN, and an RBF model were employed to forecast wind power individually. Moreover, the EPSO algorithm was used to determine the best weights for every single model. Finally, the weighted outputs of the individual models were combined together to generate the final wind power forecasts. In order to validate the predictive performance of the hybrid model, a set of 1-year wind speed and wind power data recorded by a WECS located in Taichung, Taiwan, was applied in the research. By considering the seasonal influence, the data were split into four groups standing for the four seasons. The results proved the effectiveness of the proposed hybrid model because its forecast accuracy was consistently higher than that of the other models (viz., the persistence, BPNN, and RBF models) in the four seasonal case studies.

Liu, Wang, and Lu [83] stated a novel hybrid short-term wind power forecasting model. For this purpose, three AI models (viz., a BPNN, an RBF, and an LS-SVM model) were applied to provide the individual forecasts of the wind power 48 hours in advance. In order to choose appropriate inputs for these models, a Pearson correlation coefficient (PCC)-based approach was introduced to pre-process the raw data. Subsequently, the forecasts obtained from the three individual models were combined by using an ANFIS model to generate the final wind power forecasts. A case study with a 60-day dataset acquired from an operational wind farm in Sichuan, China, was used to evaluate the predictive performance of the proposed model. Besides, the actual meteorological observations (viz., wind speed, wind direction, and temperature) were employed instead of the forecasted meteorological data in this study because of the unavailability of NWP data. The comparative results showed that the proposed hybrid forecasting model was superable to each of the individual models in the cases of four seasons in terms of wind forecast accuracy.

Cadenas and Rivera [14] built a hybrid ARIMA-ANN model for wind speed forecasting. More specifically, the ARIMA model was employed to forecast the wind speed time series, and the ANN model was introduced to model the non-linear behaviour in the errors created by the ARIMA model. Three sets of hourly wind speed measurements obtained from three regions of Mexico, namely the Isla de Cedros in Baja California, the Cerro de la Virgen in Zacatecas, and Holbox in Quintana Roo, were applied to verify the forecasting ability of the proposed model. Three error metrics (viz., the mean error (ME), MSE, and MAE) were used to evaluate the model performance. A good agreement between the actual wind speed observations and wind speed forecasts provided by the proposed hybrid model was

found in the three case studies. Besides, the errors of the proposed model kept being lower than those of the single ARIMA and single ANN models in terms of wind speed forecasting.

Guo et al. [42] combined a seasonal autoregressive integrated moving average (SARIMA) and an LS-SVM model to forecast the average monthly wind speed in Hexi Corridor, China. Specifically, the SARIMA model was used to forecast the wind speed time series, and then the LS-SVM model was applied to describe the residuals of the SARIMA model. For the purpose of evaluation, two datasets of monthly average wind speed in Mazong Mountain and Jiuquan between January 2001 and December 2006 were employed in the case study. Moreover, an ARIMA, a SARIMA, an LS-SVM, an ARIMA-SVM, and a grey model were created based on the datasets for a comparative analysis. According to the three metrics (viz., the MSE, MAE, and MAPE), the hybrid model performed much better than the other models in both of the cases. These researchers declared that it was not only efficient but also easy to forecast the monthly wind speed in Hexi Corridor by utilising the proposed model.

Shi, Guo, and Zheng [123] suggested two hybrid models for wind speed and wind power forecasting, namely an ARIMA-ANN and an ARIMA-SVM model. The whole idea was that the ARIMA model was suitable for forecasting the linear component of a time series, while the ANN and SVM models were good at forecasting the non-linear component. In addition, the individual ARIMA, ANN, and SVM models were also introduced in this study for a comparative analysis. A set of 2-year hourly wind speed observations acquired from a wind observation station located in Colorado, the United States, and a set of 2-year hourly wind power measurements obtained from a wind turbine installed in North Dakota, the United States, were applied for the validation of the wind speed and wind power forecasting, respectively. The proposed wind forecasting models were tested for the different forecast time horizons (viz., 1-step, 3-step, 5-step, 7-step, and 9-step ahead). It was concluded that although it was promising to forecast wind speed and wind power by using the hybrid models, neither the ARIMA-ANN nor the ARIMA-SVM model outperformed the individual models for all the cases studied.

Liu, Tian, and Li [82] described two hybrid models, an ARIMA-ANN and an ARIMA-Kalman model, for wind speed forecasting. In detail, the ARIMA model was employed to optimise the structure of the ANN model in the ARIMA-ANN model and the initial parameters of the Kalman model in the ARIMA-Kalman model. Besides, a pure ARIMA model was considered a benchmark. Two sets of hourly wind speed data acquired from a wind farm in China were used to validate the effectiveness of the proposed models. The models were examined separately for the 1-step, 2-step, and 3-step ahead forecasting. The results proved that the proposed hybrid models were superable to the ARIMA model in both of the cases. Furthermore, it was discovered that the ARIMA-Kalman model

outperformed the ARIMA-ANN model in terms of the MAE, MSE, and MAPE.

Zhao et al. [155] recommended a novel hybrid model consisting of a WRF model, an ANN model, and a Kalman filter to forecast wind power 1 day in advance. Particularly, the WRF model was applied to generate meteorological forecasts including wind speed, wind direction, pressure, temperature, and humidity; the Kalman filter was utilised to post-process the raw wind speed forecasts obtained from the WRF model in order to increase the accuracy; and the enhanced wind speed forecasts together with the other forecasts provided by the WRF model were input to the ANN model to forecast wind power. A case study of the Lingyang wind farm in Nantong, China, was introduced in the research. Owing to the Kalman filter, the forecasting model's normalised RMSE reduced from 17.81% to 16.47%. In conclusion, the authors claimed that the proposed hybrid wind power forecasting model was beneficial to the growth of wind energy penetration in China.

For short-term wind power forecasting, Catalão, Pousinho, and Mendes [19] created a neural network wavelet transform (NNWT) model. Besides, a persistence, an ARIMA, and an ANN model were considered the reference models in the study. Four sets of wind power data acquired from a wind farm in Portugal were chosen for model construction and validation. Three error metrics, namely the MAPE, sum squared error (SSE), and standard deviation of the error (SDE), were used to evaluate the forecast accuracy. The numerical results showed that the proposed hybrid model was preferable to the reference models. In addition, it was pretty cost-effective in terms of computational consumption. Later on, these researchers presented a hybrid wavelet-neuro-fuzzy (WNF) model and tested it based on the same case study [17]. The results indicated that the WNF model outperformed the NNWT model. Still in the same year, they proposed a wavelet transform, particle swarm optimisation, and adaptive-network-based fuzzy inference system (WPA) model as another hybrid intelligent model [18]. The data applied in this research were precisely the same as those in the previous two studies. It was concluded that the WPA model had the highest forecast accuracy among all the seven reference models, including the NNWT and WNF models. Four years later, Osório, Matias, and Catalão [104] continued the identical case study in Portugal and announced a new model named the hybrid evolutionary-adaptive (HEA) model. In detail, the HEA model was composed of a mutual information (MI), a wavelet transform (WT), an evolutionary PSO, and an ANFIS model. A comparative analysis demonstrated that the HEA model was more accurate for short-term wind power forecasting than the other models, such as the NNWT, WNF, and WPA models investigated in the previous studies.

Zhang et al. [152] suggested a novel hybrid model for short-term wind speed forecasting. Since a wavelet transform technique (WTT), a seasonal adjustment method (SAM), and a radial basis function neural network (RBFNN) were included in the model, the model was

named WTT-SAM-RBFNN. To be precise, the WTT was used to pull out the primary features and get rid of the noise component from a raw time series; the SAM was applied to deal with the seasonal component; and the RBFNN was utilised to identify the trend component. Two sets of average hourly wind speed data recorded in Wuwei and Minqin, China, were employed to evaluate the proposed model. The experiments illustrated that the proposed hybrid model was preferable to the persistence, MLP, RBFNN, SAM-RBFNN, and WTT-RBFNN models as its errors were the lowest in both of the cases.

Hong and Riofloridо [54] established a hybrid deep learning neural network model to forecast wind power 24 hours in advance. More specifically, the novel model consisted of a convolutional neural network (CNN) and an RBFNN model. A double Gaussian function (DGF) was suggested as an activation function for the RBFNN model. Besides, the best parameters of the CNN and RBFNN models were selected according to an adaptive moment estimation (ADAM) approach. Through a convolution, a kernel, and a pooling operation, the features of wind power were captured by the CNN model. Moreover, the uncertain features were handled through the RBFNN-DGF model. The data of measured wind power acquired from the Changgong wind farm located in Changhua, Taiwan, between December 2014 and November 2015 were utilised to confirm the predictive performance of the proposed model. In addition, the entire data were split into four groups representing the four seasons. These researchers concluded that the proposed hybrid model was superable to the other models, namely the multi-feedforward neural network (MFNN)-genetic algorithm (GA), RBFNN-GA, RBFNN-DGF-GA, CNN-MFNN, and CNN-RBFNN models, in all the cases investigated in the study.

Lin, Liu, and Collu [79] integrated an isolation forest (IF) algorithm with deep learning neural networks and used this configuration for wind power forecasting. In the proposed hybrid model, the input variables were the wind speed, nacelle orientation, yaw error, blade pitch angle, and ambient temperature, while the output variable was the wind power. The 1-year data between July 2018 and June 2019 used in the case study were observed by an offshore wind turbine installed in Leven, the United Kingdom. Two anomaly detection techniques, namely the elliptic envelope (EE) and IF, were applied to filter the raw measurements separately, and the results of this filtering were compared with those obtained without anomaly detection. It was concluded that the deep learning neural networks were not able to identify the outliers, and an additional anomaly detection technique was necessary. Furthermore, IF performed better than EE in terms of wind forecast accuracy, especially when the statistics of the wind data did not conform (approximately or better) to a Gaussian distribution.

Recently, hybrid models are becoming more and more popular in the field of wind speed and wind power forecasting. Many researchers have proposed their own hybrid models and

demonstrated the effectiveness of those models. Several basic types of ideas for constructing hybrid models can be summarised as follows:

1) applying a couple of independent models for individual forecasting and employing an integration algorithm to combine the outputs of the independent models to generate the final forecasts;

2) linking a time series model with an AI model;

3) joining a physics-based model with an AI model;

4) connecting a time series decomposition technique with an AI model;

5) integrating deep learning neural networks with other techniques, such as an ANN or a filtering algorithm.

2.3 Overview of Wind Power Forecasting Software

A number of European developed countries, including Denmark, Spain, Germany, the United Kingdom, France, the Netherlands, Portugal, and Ireland, as well as the United States and China, have developed some pieces of wind power forecasting software which are or were being run in real wind farms, and the effectiveness has been verified in practice [33, 139].

Prediktor, developed by the Risø National Laboratory (RNL), Denmark, is a piece of short-term wind power forecasting software based on a physical method [132]. The basic idea is to tailor the NWP forecasts (viz., wind speed and wind direction) obtained from a High Resolution Limited Area Model (HIRLAM) for a target wind farm by applying the Wind Atlas Analysis and Application Programme (WAsP), which models the influences of local conditions including obstacles, surface roughness, and orography, together with a PARK model, which takes into account the wake and array effects among the wind turbines in a wind park. The power curves of wind turbines are employed to calculate the final wind power forecasts for the next 36 hours [72].

EuroWind GmbH, a German meteorological firm, launched a piece of commercial regional wind power forecasting software named the Simulation Model for the Operational Forecast of the Wind Energy Production in Europe (SOWIE) [75]. The SOWIE is a physics-based model that relies on the NWP data (viz., 3D wind and temperature forecasts) of a HIRLAM and the Global Forecast System (GFS) and the information database

of all the wind turbines in Europe. Moreover, its forecast time horizon is expanded to 120 hours in advance [96].

Besides the physical method, the statistical method is another primary methodology widely utilised in wind power forecasting software. For example, a British company, Garrad Hassan, created GH Forecaster based on an adaptive multi-parameter statistical regression technique [106]. The location-specific meteorological forecasts (viz., wind speed, wind direction, air temperature, and air pressure) transformed from the global NWP forecasts provided by the Met Office, the United Kingdom, are input to a power model to be converted to wind farm power generation [40].

In response to the increasing wind power in Spain, Sipreólico was developed by the cooperation between University Carlos III of Madrid (UC3M) and the Electrical Grid of Spain (REE), Spain [120]. The forecasting software is based on adaptive non-parametric statistical models with the inputs of the NWP forecasts provided by the Spanish HIRLAM and hourly real-time power records obtained from a supervisory control and data acquisition (SCADA) system together with various power curve models [66]. For different data availability, there are nine statistical models. To be precise, one of them does not use NWP forecasts; another three only take forecasted wind speed into account; another three consider wind direction besides wind speed; the rest two are the hybrids of the others with the extra non-parametric prediction of a diurnal cycle. Final forecasts are produced relying on the combination of these alternative models according to the recent forecast errors of every single model with a memory (a forgetting factor) of 24 hours [38]. Additionally, the forecast time horizon of Sipreólico is 36 hours in advance with a temporal resolution of 1 hour [96].

The Technical University of Denmark (DTU) developed the Wind Power Prediction Tool (WPPT), which is able to forecast the wind power generation of an individual wind farm, a group of wind farms, and an area of wind farms with a time horizon up to 2 days [88]. In order to forecast the wind power of an area, a two-branch method is introduced. Specifically, in the first branch, the online records and NWP forecasts of the representative wind farms are used to generate the wind power forecasts of the representative wind farms in each sub-area; then, the wind power forecasts of the representative wind farms are combined and upscaled to calculate the production of each sub-area; and then the wind power production of the area is achieved through integrating the production of each sub-area. In the second branch, the offline wind power records of the sub-areas and the NWP forecasts of the area are utilised to compute the wind power production of the sub-areas; once again, the area's production is achieved through integrating the production of the sub-areas. Finally, the total production is the weighted mean of the wind power forecasts provided by these two branches.

A conditional parametric approach which builds the relationship between meteorological variables (viz., wind speed and wind direction) and the output of wind power is employed in the WPPT consisting of four models. To be precise, a wind farm model converts NWP forecasts and online observations to the wind power of a wind farm by using wind direction dependent power curves; an upscaling model calculates the wind power production of a sub-area by integrating the forecasts of the representative wind farms based on an upscaling function; an area model converts NWP forecasts and offline records to the wind power production of an area based on a similar method in the wind farm model; and a total model integrates the forecasts obtained from the two branches by using a weighted mean method [88]. In response to the changes either in surroundings or in NWP models, an adaptive parameters estimation method is employed based on a recursive least squares and exponential forgetting algorithm. In addition, the WPPT offers the assessment of wind power forecasting uncertainty [96].

Moreover, AI is applied to a couple of statistics-based software models. For instance, a Spanish firm, AleaSoft, developed AleaWind with the assistance from the Polytechnic University of Catalonia (UPC). An exclusive model called AleaModel is applied in AleaWind for wind power forecasting. Particularly, an ANN and a SARIMA model are combined for the software architecture. The parameters of AleaWind are assessed online. Besides, the wind speed and wind direction forecasts obtained from NWP models and wind power measurements acquired from wind farms are applied as the inputs of AleaWind, which is able to forecast the wind power production of an individual wind farm, a region, and a whole nation with a time horizon of 1 to 2 days [96].

The Association for the Research and Development of Industrial Methods and Processes (ARMINES) and the Paris School of Mines (ENSMP), France, codeveloped the ARMINES Wind Power Prediction System (AWPPS) by integrating five types of models [39]. To be precise, the short-term models based on a statistical time series method are generated to forecast wind power 10 hours in advance. The long-term models based on fuzzy neural networks with the inputs of real-time SCADA data and NWP forecasts provide 3-day ahead wind power forecasts. A hybrid model based on an intelligent weighting method combines the forecasts of the short-term and long-term models to optimise the overall predictive performance. The upscaling prediction models based on a cascaded and a clustering method with reference wind farms are created by applying adaptive fuzzy neural networks and used for regional and national forecasting. An uncertainty estimation model based on the methods of adapted resampling and prediction risk indices assesses the confidence intervals of short-term and long-term forecasting [96].

At the request of a group of Portuguese wind farm owners, the Institute of Systems and Computer Engineering (INESC), the Institute of Mechanical Engineering and Industrial

Management (INEGI), and the Research Centre for Wind Energy and Atmospheric Flows (CEsA), Portugal, worked together to develop a piece of 3-day ahead wind power forecasting software which is named EPREV [96]. There are three types of statistical models, namely a wind-to-power (W2P) model, an AR model, and a neural network assembling model (NNAM), applied in EPREV. To be precise, the W2P model converts NWP forecasts to wind power forecasts; the AR model is specific for very short-term forecasting; and the NNAM is for the fusion of the W2P and AR models. In addition, an error prediction model is designed to assess the uncertainty of wind power forecasting [116].

The Institute for Solar Energy Supply Technology (ISET), Germany, developed the Wind Power Management System (WPMS) based on a statistical method. In the WPMS, the Lokalmodell of the DWD is regarded as an input model fed into an ANN model. For the purpose of improving the Lokalmodell, the Klimamodell Mainz (a numerical mesoscale atmospheric model) is applied to transform wind forecasts specifically for the site of wind farms [30]. The WPMS performs the following two operations: real-time monitoring the current wind power output of control areas and partial regions; and forecasting the wind power of individual wind farms, control areas, and partial regions up to 3 days in advance. Moreover, regional wind power forecasts are calculated by aggregating and upscaling the forecasts of every single wind farm through a conversion model [117].

In order to further improve the accuracy of wind power forecasting, the hybrid method with the combination of the physical and statistical methods is employed in the software. LocalPred and RegioPred, provided by the National Renewable Energy Centre (CENER) and the Research Centre for Energy, Environment and Technology (CIEMAT), Spain, is a set of wind power forecasting software based on a hybrid method [89]. RegioPred is a model for regional forecasting according to the results obtained from the single wind farm forecasting model LocalPred. Specifically, regional forecasts are worked out by adding up the forecasts of every individual wind farm or reference wind farms selected by cluster analysis. Besides, LocalPred, containing an adaptive NWP inputs optimisation model based on principal component analysis, time series modelling, mesoscale modelling with Mesoscale Model 5 (MM5), and power curve modelling, is specifically designed for the wind power forecasting of those wind farms in complex terrain. In addition, 72-hour ahead meteorological variables forecasting is done by MM5 with a spatial resolution of one square kilometre [90].

Following the principle of Prediktor, the University of Oldenburg (UO), Germany, presented a pretty similar software model called Previento [32]. They formerly implemented the Deutschlandmodell [8] and now the Lokalmodell [32] of the DWD instead of a HIRLAM for NWP. Besides, stricter physical downscaling and innovative linear upscaling are introduced in Previento [139]. The forecast time horizon is up to 48 hours [32]. Along with wind

power forecasts, the uncertainty of forecasted results is also provided by Previento [76].

Aeolis Forecasting Services, the Netherlands, launched a piece of software called Scirocco, which is based on a hybrid method [96]. The various NWP models including the HIRLAM, MM5, the European Centre for Medium-Range Weather Forecasts (ECMWF) model, and the National Centers for Environmental Prediction (NCEP) model are applied to generate meteorological forecasts, which are used as the inputs of Scirocco. Besides, there are three schemes for adjustment purposes in Scirocco. Specifically, a Model Output Statistics (MOS) scheme is designed to adjust the systematic errors of NWP models as a post-processing procedure. Another scheme is utilised to transform global NWP forecasts to site-specific ones with local orography and roughness conditions. The other MOS scheme is employed to deal with the features of wind turbines and wind farms. Finally, forecasted wind speed is converted to wind power via power curves provided by manufacturers. Moreover, regional wind power production can be forecasted by using an upscaling model according to the representative wind farms. The forecast time horizon relies on NWP outputs. It is worth noting that Scirocco has the ability of self-learning that it is able to adapt to a target wind farm by adjusting all the parameters in the schemes according to the forecast errors during its operation in the first couple of months.

University College Cork (UCC), Ireland, developed the Weather and Wind Energy Prognosis (WEPROG), which comprises a weather prediction model operating every 6 hours and a power prediction model using historical and real-time SCADA data [96]. A multi-scheme ensemble prediction approach is applied to the weather prediction model, while a training procedure building the relationship between meteorological forecasts and historical wind power measurements is implemented in the power prediction model. The WEPROG can be used to forecast the wind power generation of either a wind farm or a region.

Prediktor and the WPPT were integrated and extended to be a new piece of software called Zephyr, under the collaboration between the RNL and the DTU, Denmark [37]. The motivation of this hybrid method is to join the advantages of the two models together [124]. In Zephyr, a wind power forecasting model is allocated to a wind farm based on data availability. For example, when the information of a wind farm is limited to the type, number, and location of wind turbines, a simplified physics-based Prediktor model is employed with the only inputs of NWP forecasts. Nevertheless, if all the data of a wind farm are available, in that case, a statistics-based WPPT model will be added to forecast wind power together [96].

Apart from the European countries, the United States also has its wind power forecasting software named eWind, developed by a U.S. company AWS Truewind [4]. The

ForeWind numerical weather model, as a mesoscale model using the boundary conditions obtained from a regional weather model, is run in the commercial software eWind. Unlike Prediktor applying once-and-for-all parameterisation for local influences with the WAsP, more physical processes can be captured and regional NWP forecasts can be better refined to a specific location through this approach. Besides, an adaptive statistical method is utilised to deal with systematic errors. The forecast time horizon of eWind is 2 days [38].

In addition, it is worth noting that as a developing country, China successfully developed the Wind Power Forecast System (WPFS) with the support from the China Electric Power Research Institute (CEPRI). The WPFS, taking NWP forecasts and wind farm historical measurements into account, is a hybrid model based on a physical and a statistical method. Specifically, there are five modules integrated into the WPFS, namely a NWP, a prediction system database, a prediction programme, a user interface, and an energy management system (EMS) interface module [139]. However, Canada still does not have its own wind power forecasting software at the moment. Therefore, it is meaningful for Canada to develop a piece of forecasting software with independent intellectual property rights.

Table 2.2 gives a list of wind power forecasting software with the corresponding developers, methods, and countries and regions of application [33, 96, 139].

Table 2.2. Wind power forecasting software.

Software	Developer(s)	Method	Countries & regions of application
Prediktor	Risø Nationallaboratoriet, Denmark	Physical	Denmark, Spain, Ireland, Northern Ireland, France, Germany, the United States, Scotland, and Japan
SOWIE	EuroWind GmbH, Germany	Physical	Germany, Austria, and Switzerland
AleaWind	AleaSoft & Universidad Politécnica de Cataluña, Spain	Statistical	Spain
AWPPS	Association pour la Recherche et le Développement des Méthodes et Processus Industriels & École Nationale Supérieure des Mines de Paris, France	Statistical	Ireland, Crete, Madeira, and the Azores

Software	Developer(s)	Method	Countries & regions of application
EPREV	Instituto de Engenharia de Sistemas e Computadores, Instituto de Engenharia Mecânica e Gestão Industrial, and Centro de Estudos de Energia Eólica e Escoamentos Atmosféricos, Portugal	Statistical	Portugal
GH Forecaster	Garrad Hassan, the United Kingdom	Statistical	Great Britain, Greece, and the United States
Sipreólico	Universidad Carlos III de Madrid & Red Eléctrica de España, Spain	Statistical	Spain
WPMS	Institut für Solare Energieversorgungstechnik, Germany	Statistical	Germany, Austria, and Italy
WPPT	Danmarks Tekniske Universitet, Denmark	Statistical	Denmark, Australia, Canada, Ireland, Northern Ireland, the Netherlands, Sweden, and Greece
eWind	AWS Truewind, the United States	Hybrid	the United States
LocalPred & RegioPred	Centro Nacional de Energías Renovables & Centro de Investigaciones Energéticas, Medioambientales y Tecnológicas, Spain	Hybrid	Spain & Ireland
Previento	Carl von Ossietzky Universität Oldenburg, Germany	Hybrid	Germany & Northern Ireland
Scirocco	Aeolis Forecasting Services, the Netherlands	Hybrid	The Netherlands, Germany, and Spain
WEPROG	Coláiste na hOllscoile Corcaigh, Ireland	Hybrid	Denmark, Germany, Ireland, and Australia
WPFS	China Electric Power Research Institute, China	Hybrid	China

Software	Developer(s)	Method	Countries & regions of application
Zephyr	Risø Nationallaboratoriet & Danmarks Tekniske Universitet, Denmark	Hybrid	Denmark & Australia

2.4 Fundamental Theory of the Sugeno-Type Fuzzy Inference System

The Sugeno-type FIS, also known as the Takagi-Sugeno-Kang system, was first proposed in 1985 [130]. Its output membership functions are limited to either constant or linear. If the output membership functions are constant, it is called a zero-order system; if the output membership functions are linear, it is called a first-order system.

A typical form of the fuzzy rules in the zero-order Sugeno-type FIS is

$$if\ x\ is\ A\ and\ y\ is\ B,\ then\ z = k\ , \tag{2.4}$$

where x and y are the input variables, A and B are the fuzzy sets, z is the output, and k is a constant. The output membership functions of all the rules in the zero-order Sugeno-type FIS are a singleton set [143].

The first-order Sugeno-type FIS, which is more popular in practical applications, has the following form of fuzzy rules:

$$if\ x\ is\ A\ and\ y\ is\ B,\ then\ z = px + qy + r\ , \tag{2.5}$$

where x and y are the input variables, A and B are the fuzzy sets, z is the output, and p, q, and r are constants. The first-order Sugeno-type FIS, in which each rule defines the location of a moving singleton set, can be regarded as the extension of the zero-order Sugeno-type FIS [143].

In each fuzzy rule, the relationship between input variables and the output is linear. After computation, a smooth non-linear input-output curve can be produced via interpolation [143]. The Sugeno-type FIS, widely used in the field of system modelling and control, is a simple and effective way of applying a linear approach to a non-linear system [102].

In addition, a higher-order Sugeno-type FIS is theoretically feasible. Nevertheless, the growth in the order makes the system extremely complex, but it does not bring significant advantages in terms of more precise modelling or control. Thus, the application of the higher-order Sugeno-type FIS is relatively rare in practice.

In general, the advantages of the Sugeno-type FIS can be summarised as follows [102]:

1) it ensures the continuity of the output curve;

2) it has high computational efficiency;

3) it is pretty suitable for mathematical analysis;

4) it can be well combined with existing linear system theories;

5) it can be applied together with optimisation and adaptive algorithms.

2.5 Fundamental Theory of the Adaptive Neuro-Fuzzy Inference System

The FIS goes through a series of mapping processes in inference, namely mapping the characteristics of input variables to input membership functions, mapping input membership functions to fuzzy rules, mapping fuzzy rules to the characteristics of the output, mapping the characteristics of the output to output membership functions, and mapping output membership functions to a single value or decision [61]. In a typical FIS, either given (expert experience) or arbitrarily selected (intuitive experience) membership functions are employed. Essentially, the fuzzy rules of the established FIS, explaining system characteristics, are acquired in advance based on the knowledge and experience of experts or professionals [68]. Structurally, the FIS is usually represented by if-then conditional sentences (rules), which are very suitable for presenting human qualitative or fuzzy knowledge and experience. However, a lack of corresponding knowledge or experience will lead to unsatisfactory results.

In the past few decades, the development of the FIS and ANN has made considerable progress in intelligent control. Although both FIS and ANN belong to the field of AI, their fundamental theories are entirely different. An obvious shortcoming of the FIS is that it does not have a self-learning function, so its application is greatly restricted. On the other hand, the ANN cannot express the fuzzy language. The ANFIS, combining the FIS and

ANN, not only can express human knowledge but also has the self-learning ability. It is an effective tool for the modelling and control of complex systems [60].

A typical architecture of an ANFIS is shown in Figure 2.1. Each node in the same layer has a similar function, and the functions in each layer of the ANFIS are described as follows [99]:

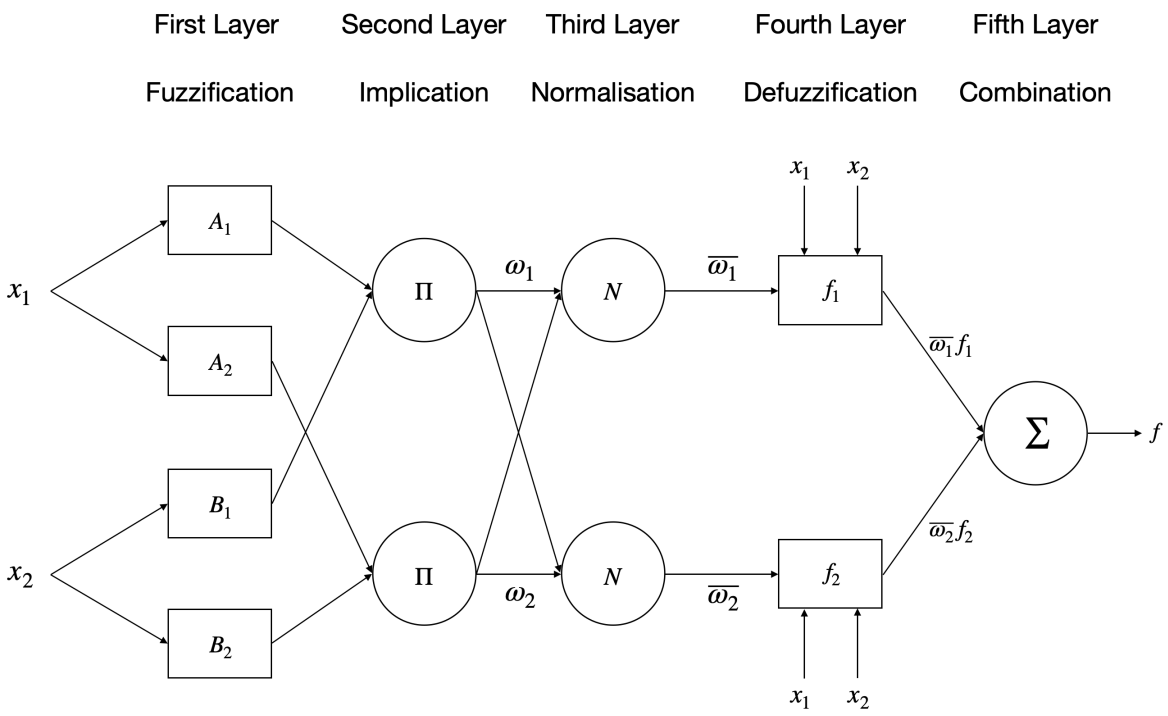

Figure 2.1. Typical architecture of an ANFIS.

(1) First layer

Each node in this layer is an adaptive node and represented by a node function given by

$$O_{1,\,i} = \mu_{A_i}(x_1), \quad i = 1,\ 2\ , \tag{2.6}$$

and

$$O_{1,\ i} = \mu_{B_{i-2}}(x_2), \quad i = 3,\ 4\ , \tag{2.7}$$

where $O_{1,\ i}$ is the output of the i-th node in the first layer, μ_{A_i} and $\mu_{B_{i-2}}$ are the membership functions, A_i and B_{i-2} are the fuzzy sets, and x_1 and x_2 are the inputs to the nodes.

(2) Second layer

Each node in this layer is a fixed node represented by Π. The inputs are multiplied by each other, and the resulting product is the output, so

$$O_{2,\ i} = \omega_i = \mu_{A_i}(x_1)\mu_{B_i}(x_2), \quad i = 1,\ 2\ , \tag{2.8}$$

where $O_{2,\ i}$ is the output of the i-th node in the second layer, ω_i is the weight of the i-th node, μ_{A_i} and μ_{B_i} are the membership functions, A_i and B_{i-2} are the fuzzy sets, and x_1 and x_2 are the inputs to the nodes.

(3) Third layer

Each node in this layer is a fixed node represented by N. The ratio of the weight of the i-th rule to the sum of the weights of the rules is calculated as the output of the node, so

$$O_{3,\ i} = \overline{\omega_i} = \frac{\omega_i}{\omega_1 + \omega_2}, \quad i = 1,\ 2\ , \tag{2.9}$$

where $O_{3,\ i}$ is the output of the i-th node in the third layer, $\overline{\omega_i}$ is the normalised weight of the i-th node, and ω_i is the weight of the i-th node.

(4) Fourth layer

Each node in this layer is an adaptive node and represented by a node function given by

$$O_{4,\ i} = \overline{\omega_i} f_i = \overline{\omega_i}(p_i x_1 + q_i x_2 + r_i), \quad i = 1,\ 2\ , \tag{2.10}$$

where $O_{4,\ i}$ is the output of the i-th node in the fourth layer, $\overline{\omega_i}$ is the normalised weight of the i-th node, f_i is the output of the i-th rule, p_i, q_i, and r_i are the consequent parameters, and x_1 and x_2 are the inputs to the nodes.

(5) Fifth layer

The single node in this layer is a fixed node that calculates the final output of all the input signals:

$$O_{5,\ i} = f = \sum_i \overline{\omega_i} f_i = \frac{\sum_i \omega_i f_i}{\sum_i \omega_i}, \quad i = 1,\ 2\ , \tag{2.11}$$

where $O_{5,\ i}$ is the output of the i-th node in the fifth layer, f is the sum of the outputs of the rules, $\overline{\omega_i}$ is the normalised weight of the i-th node, f_i is the output of the i-th rule, and ω_i is the weight of the i-th node.

The ANFIS can reflect the features of the studied data correctly since its fuzzy rules and membership functions are learnt according to the given information [118]. In general, the ANFIS is mainly applied to the following situations [34]:

1) a large number of input-output data pairs are available for modelling;

2) the analytical model of the system is not available in advance based on existing input and output variables.

2.6 Fundamental Theory of Time Series Analysis

2.6.1 Stationary Time Series

In statistics, stationarity means that the statistical properties of a time series do not change over time. If a random time series y_t, for any time t, meets all of the following conditions:

1) expectation, $E(y_t) = \mu < \infty$, is a constant independent of time t;

2) variance, $Var(y_t) = E(y_t - \mu)^2 = \sigma^2$, is a constant independent of time t;

3) autocovariance, $Cov(y_t,\ y_{t-k}) = E[(y_t - \mu)(y_{t-k} - \mu)] = \gamma_k$, is a constant only related to the time interval k and independent of time t,

then y_t is called a stationary time series, and γ_k is called an autocovariance function [52].

2.6.2 Autocorrelation Function of a Stationary Time Series

The definition of the autocorrelation function of the time series y_t is shown as follows [10]:

$$\rho_k = \frac{\gamma_k}{\gamma_0} \ . \tag{2.12}$$

In fact, it is impossible to calculate the theoretical expectation, autocovariance, and autocorrelation function according to the definition. Instead, the corresponding estimated values, namely the sample mean, sample autocovariance, and sample autocorrelation function, are calculated based on sample data. If n observations of a random time series are given, then the formulae are shown as follows [10]:

(1) Sample mean:

$$\overline{y} = \frac{1}{n}\sum_{t=1}^{n} y_t \ . \tag{2.13}$$

(2) Sample autocovariance:

$$\hat{\gamma}(k) = \frac{1}{n}\sum_{t=1}^{n-k}(y_t - \overline{y})(y_{t-k} - \overline{y}) \ . \tag{2.14}$$

(3) Sample autocorrelation function:

$$\hat{\rho}(k) = \frac{\hat{\gamma}(k)}{\hat{\gamma}(0)} \ . \tag{2.15}$$

2.6.3 Autoregressive and Moving Average Model

The previous information of the variable and disturbance terms is applied to find the changing rules in a single-variable time series model. The ARMA model, which is the most popular model used to fit a single-variable stationary time series, can be divided into three types, namely the AR, MA, and ARMA models [50].

(1) AR model

A model with the following structure is called a p-order AR model, which can be simply written as AR (p):

$$\begin{cases} y_t = \phi_1 y_{t-1} + \phi_2 y_{t-2} + \cdots + \phi_p y_{t-p} + \varepsilon_t \\ \phi_p \neq 0 \\ E(\varepsilon_t) = 0,\ Var(\varepsilon_t) = \sigma_\varepsilon^2,\ E(\varepsilon_t \varepsilon_s) = 0,\ s \neq t \\ E(y_s \varepsilon_t) = 0,\ \forall s < t \end{cases} . \tag{2.16}$$

The AR (p) model has the following conditions:

1) $\phi_p \neq 0$, ensuring that the highest order of the model is p;
2) $E(\varepsilon_t) = 0,\ Var(\varepsilon_t) = \sigma_\varepsilon^2,\ E(\varepsilon_t \varepsilon_s) = 0,\ s \neq t$, asking that the random disturbance series ε_t is a zero-mean white noise series;
3) $E(y_s \varepsilon_t) = 0,\ \forall s < t$, indicating that the current random disturbance term is independent of the past values of the series.

Introduce the lag operator L, and let L^k be the k-step lag operator:

$$L^k y_t = y_{t-k} \ , \tag{2.17}$$

then the AR (p) model can be simplified as follows:

$$\Phi(L) y_t = \varepsilon_t \ , \tag{2.18}$$

where $\Phi(L) = 1 - \phi_1 L - \phi_2 L^2 - \cdots - \phi_p L^p$, which is called a p-order AR coefficient polynomial.

Moreover, $\Phi(L) = 0$ is called the characteristic equation of the AR (p) model. The p roots λ_i $(i = 1,\ 2,\ \ldots,\ p)$ of the characteristic equation are called the characteristic roots of the AR (p) model. If all of the p characteristic roots are outside of the unit circle:

$$|\lambda_i| > 1, \quad i = 1,\ 2,\ \ldots,\ p \ , \tag{2.19}$$

then the AR (p) model is called a stationary AR model, and the series y_t fitting this model is called a stationary AR series. Equation (2.19) is called the stationary

condition of the AR model. Since $\Phi(L) = 0$ is a polynomial related to the lag operator L, the stationarity of the AR model depends on the parameters $\phi_1,\ \phi_2,\ \ldots,\ \phi_p$.

(2) MA model

A model with the following structure is called a q-order MA model, which can be simply written as MA (q):

$$\begin{cases} y_t = \varepsilon_t - \theta_1\varepsilon_{t-1} - \theta_2\varepsilon_{t-2} - \cdots - \theta_q\varepsilon_{t-q} \\ \theta_q \neq 0 \\ E(\varepsilon_t) = 0,\ Var(\varepsilon_t) = \sigma_\varepsilon^2,\ E(\varepsilon_t\varepsilon_s) = 0,\ s \neq t \end{cases} . \tag{2.20}$$

The MA (q) model has the following conditions:

1) $\theta_q \neq 0$, ensuring that the highest order of the model is q;
2) $E(\varepsilon_t) = 0,\ Var(\varepsilon_t) = \sigma_\varepsilon^2,\ E(\varepsilon_t\varepsilon_s) = 0,\ s \neq t$, requiring that the random disturbance series ε_t is a zero-mean white noise series.

Apply the lag operator L, and then the MA (q) model can be simplified as follows:

$$y_t = \Theta(L)\varepsilon_t\ , \tag{2.21}$$

where $\Theta(L) = 1 - \theta_1 L - \theta_2 L^2 - \cdots - \theta_q L^q$, which is called a q-order MA coefficient polynomial.

Moreover, $\Theta(L) = 0$ is called the characteristic equation of the MA (q) model. The q roots λ_k $(k = 1,\ 2,\ \ldots,\ q)$ of the characteristic equation are called the characteristic roots of the MA (q) model. If all of the q characteristic roots are outside of the unit circle:

$$|\lambda_k| > 1, \quad k = 1,\ 2,\ \ldots,\ q\ , \tag{2.22}$$

then the MA (q) model is called an invertible MA model, and the series y_t fitting this model is called an invertible MA series. Equation (2.22) is called the invertible condition of the MA model. Since $\Theta(L) = 0$ is a polynomial related to the lag operator L, the invertibility of the MA model depends on the parameters $\theta_1,\ \theta_2,\ \ldots,\ \theta_q$.

(3) ARMA model

A model with the following structure is called an ARMA model, which can be simply written as ARMA (p, q):

$$\begin{cases} y_t = \phi_1 y_{t-1} + \phi_2 y_{t-2} + \cdots + \phi_p y_{t-p} + \varepsilon_t - \theta_1 \varepsilon_{t-1} - \theta_2 \varepsilon_{t-2} - \cdots - \theta_q \varepsilon_{t-q} \\ \phi_p \neq 0,\ \theta_q \neq 0 \\ E(\varepsilon_t) = 0,\ Var(\varepsilon_t) = \sigma_\varepsilon^2,\ E(\varepsilon_t \varepsilon_s) = 0,\ s \neq t \\ E(y_s \varepsilon_t) = 0,\ \forall s < t \end{cases} . \tag{2.23}$$

The ARMA (p, q) model has all the conditions mentioned above in the AR (p) and MA (q) models.

Apply the lag operator L, and then the ARMA (p, q) model can be simplified as follows:

$$\Phi(L) y_t = \Theta(L) \varepsilon_t \ , \tag{2.24}$$

where $\Phi(L) = 1 - \phi_1 L - \phi_2 L^2 - \cdots - \phi_p L^p$, which is called a p-order AR coefficient polynomial, and $\Theta(L) = 1 - \theta_1 L - \theta_2 L^2 - \cdots - \theta_q L^q$, which is called a q-order MA coefficient polynomial.

Obviously, when $q = 0$, the ARMA (p, q) model is equivalent to the AR (p) model; when $p = 0$, the ARMA (p, q) model is equivalent to the MA (q) model. It can be seen that the AR (p) and MA (q) models are the special cases of the ARMA (p, q) model. Therefore, if the roots of $\Phi(L) = 0$ have all modulus greater than 1, ARMA (p, q) is a stationary ARMA model; if the roots of $\Theta(L) = 0$ have all modulus greater than 1, ARMA (p, q) is an invertible ARMA model; and if the roots of $\Phi(L) = 0$ and $\Theta(L) = 0$ have all modulus greater than 1, ARMA (p, q) is a stationary and invertible ARMA model.

2.6.4 Model Identification

By investigating the properties of the sample autocorrelation function and sample partial autocorrelation function of a stationary time series, an appropriate model can be selected to be fitted to the time series of observations [35].

(1) Partial autocorrelation function

Set y_t to be a stationary time series. When the values of y_{t-1}, y_{t-2}, ..., y_{t-k} are given to predict y_t, the predicted value is the linear combination of y_{t-j}:

$$\hat{y}_t = \sum_{j=1}^{k} g_{kj} y_{t-j} \ . \tag{2.25}$$

The prediction error is

$$e_t = y_t - \hat{y}_t = y_t - \sum_{j=1}^{k} g_{kj} y_{t-j} \ . \tag{2.26}$$

Minimise the square of the prediction error. Set the selected parameters ψ_{kj} ($j = 1,\ 2,\ \ldots,\ k$), which let

$$E(e_t^2) = E[(y_t - \sum_{j=1}^{k} g_{kj} y_{t-j})^2] = min \ , \tag{2.27}$$

then $\hat{y}_t = \sum_{j=1}^{k} \psi_{kj} y_{t-j}$ is called a linear minimum variance estimation. Besides, ψ_{kj} ($j = 1,\ 2,\ \ldots,\ k$) is called the partial autocorrelation function (PACF) of the stationary time series y_t.

Expanding and simplifying Equation (2.27), the following equation can be obtained:

$$\sum_{i=1}^{k} \psi_{ki} \rho_{j-i} = \rho_j, \quad j = 1,\ 2,\ \ldots,\ k \ . \tag{2.28}$$

Its matrix form is

$$\begin{bmatrix} 1 & \rho_1 & \cdots & \rho_{k-1} \\ \rho_1 & 1 & \cdots & \rho_{k-2} \\ \vdots & \vdots & \ddots & \vdots \\ \rho_{k-1} & \rho_{k-2} & \cdots & 1 \end{bmatrix} \begin{bmatrix} \psi_{k1} \\ \psi_{k2} \\ \vdots \\ \psi_{kk} \end{bmatrix} = \begin{bmatrix} \rho_1 \\ \rho_2 \\ \vdots \\ \rho_k \end{bmatrix} \ . \tag{2.29}$$

According to Equation (2.29), the recursive equation of the PACF ψ_{kk} is shown as follows:

$$\psi_{kk} = \begin{cases} \rho_1, & k = 1 \\ \dfrac{\rho_k - \sum_{j=1}^{k-1} \psi_{k-1,\ j}\rho_{k-j}}{1 - \sum_{j=1}^{k-1} \psi_{k-1,\ j}\rho_j}, & k = 2,\ 3,\ \ldots \end{cases}, \tag{2.30}$$

in which

$$\psi_{kj} = \psi_{k-1,\ j} - \psi_{kk}\psi_{k-1,\ k-j}, \quad j = 1,\ 2,\ \ldots,\ k\ . \tag{2.31}$$

(2) Identification of the AR model

Multiply both sides of the stationary time series model $y_t = \phi_1 y_{t-1} + \phi_2 y_{t-2} + \cdots + \phi_p y_{t-p} + \varepsilon_t$ by y_{t-k} ($\forall k \geq 1$), and then calculate the expectation:

$$E(y_t y_{t-k}) = \phi_1 E(y_{t-1}y_{t-k}) + \phi_2 E(y_{t-2}y_{t-k}) + \cdots + \phi_p E(y_{t-p}y_{t-k}) + E(\varepsilon_t y_{t-k}), \quad \forall k \geq 1\ . \tag{2.32}$$

According to the third condition of the AR (p) model:

$$E(\varepsilon_t y_{t-k}) = 0, \quad \forall k \geq 1\ , \tag{2.33}$$

the following recursive equation of the autocovariance function can be obtained:

$$\gamma_k = \phi_1\gamma_{k-1} + \phi_2\gamma_{k-2} + \cdots + \phi_p\gamma_{k-p}\ . \tag{2.34}$$

Since $\rho_k = \frac{\gamma_k}{\gamma_0}$, divide both sides of Equation (2.34) by the variance function γ_0, and then the recursive equation of the autocorrelation function (ACF) can be obtained:

$$\rho_k = \phi_1\rho_{k-1} + \phi_2\rho_{k-2} + \cdots + \phi_p\rho_{k-p}\ . \tag{2.35}$$

The ACF of the stationary AR (p) model has two significant properties: one is tailing off, which means ρ_k always has a non-zero value and will not invariably be equal to zero when k is greater than a certain constant; the other is that ρ_k decays by the negative exponent.

For the AR (p) model

$$\begin{cases} \rho_1 = \phi_1 + \phi_2\rho_1 + \cdots + \phi_p\rho_{p-1} \\ \rho_2 = \phi_1\rho_1 + \phi_2 + \cdots + \phi_p\rho_{p-2} \\ \qquad\qquad \vdots \\ \rho_p = \phi_1\rho_{p-1} + \phi_2\rho_{p-2} + \cdots + \phi_p \end{cases}, \tag{2.36}$$

its matrix form is

$$\begin{bmatrix} \rho_1 \\ \rho_2 \\ \vdots \\ \rho_p \end{bmatrix} = \begin{bmatrix} 1 & \rho_1 & \cdots & \rho_{p-1} \\ \rho_1 & 1 & \cdots & \rho_{p-2} \\ \vdots & \vdots & \ddots & \vdots \\ \rho_{p-1} & \rho_{p-2} & \cdots & 1 \end{bmatrix} \begin{bmatrix} \phi_1 \\ \phi_2 \\ \vdots \\ \phi_p \end{bmatrix}. \tag{2.37}$$

It can be proved that the PACF ψ_{kk} of the stationary AR (p) model cuts off after the lag p, which means $\psi_{kk} = 0,\ \forall k > p$. Conversely, if the PACF ψ_{kk} of a time series cuts off after the lag p, then the time series fits the AR (p) model. The mathematical expression is shown as follows:

$$\psi_{kj} = \begin{cases} \phi_j, & j = 1,\ 2,\ \ldots,\ p \\ 0, & j = p+1,\ p+2,\ \ldots,\ k \end{cases}. \tag{2.38}$$

(3) Identification of the MA model

For the invertible MA (q) model $y_t = \varepsilon_t - \theta_1\varepsilon_{t-1} - \theta_2\varepsilon_{t-2} - \cdots - \theta_q\varepsilon_{t-q}$, the autocovariance function is

$$\gamma_k = E(y_t y_{t-k}) = E[(\varepsilon_t - \theta_1\varepsilon_{t-1} - \cdots - \theta_q\varepsilon_{t-q})(\varepsilon_{t-k} - \theta_1\varepsilon_{t-k-1} - \cdots - \theta_q\varepsilon_{t-k-q})]\ . \tag{2.39}$$

According to the second condition of the MA (q) model:

$$E(\varepsilon_t\varepsilon_s) = 0, \quad s \neq t\ , \tag{2.40}$$

the following recursive equation of the autocovariance function can be obtained:

$$\gamma_k = \begin{cases} (1+\theta_1^2+\cdots+\theta_q^2)\sigma_\varepsilon^2, & k=0 \\ (-\theta_k+\sum_{i=1}^{q-k}\theta_i\theta_{k+1})\sigma_\varepsilon^2, & 1\le k\le q \\ 0, & k>q \end{cases}. \tag{2.41}$$

Since $\rho_k = \frac{\gamma_k}{\gamma_0}$, divide both sides of Equation (2.41) by the variance function γ_0, and then the recursive equation of the ACF can be obtained:

$$\rho_k = \begin{cases} 1, & k=0 \\ \dfrac{-\theta_k+\sum_{i=1}^{q-k}\theta_i\theta_{k+1}}{1+\theta_1^2+\cdots+\theta_q^2}, & 1\le k\le q \\ 0, & k>q \end{cases}. \tag{2.42}$$

It can be proved that the ACF ρ_k of the invertible MA (q) model cuts off after the lag q, which means $\rho_k = 0,\ \forall k > q$. Conversely, if the ACF ρ_k of a time series cuts off after the lag q, then the time series fits the MA (q) model.

The PACF of the invertible MA (q) model has two significant properties: one is tailing off, which means ψ_{kk} always has a non-zero value and will not invariably be equal to zero when k is greater than a certain constant; the other is that ψ_{kk} decays by the negative exponent.

(4) Identification of the ARMA model

The criteria for the identification of the ARMA model are summarised as follows:

1) if the ACF of a stationary time series y_t tails off, and its PACF cuts off, then the series y_t is an AR series;
2) if the ACF of a stationary time series y_t cuts off, and its PACF tails off, then the series y_t is an MA series;
3) if both the ACF and PACF of a stationary time series y_t tail off, then the series y_t is an ARMA series.

2.6.5 Stationary Model of a Non-Stationary Time Series

The AR, MA, and ARMA models mentioned above are all used to describe stationary time series. However, in practice, many time series are non-stationary. In order to smooth a time

series, a first-order or second-order differencing operation is usually applied to transform the original time series into a stationary time series. If a non-stationary time series can be transformed into a stationary time series by differencing, then the series is called a homogeneous non-stationary time series, and the number of differencing times is called a homogeneous order [10].

Set ∇ to be a differencing operator, then the first-order differencing is

$$\nabla y_t = y_t - y_{t-1} \ , \tag{2.43}$$

and the second-order differencing is

$$\nabla^2 y_t = \nabla(y_t - y_{t-1}) = y_t - 2y_{t-1} + y_{t-2} \ . \tag{2.44}$$

It can be deduced that

$$\nabla^k = (1 - L)^k \ . \tag{2.45}$$

If y_t is a d-th order homogeneous non-stationary time series, then the new time series transformed by the d-th order differencing

$$y_t{}' = (1 - L)^d y_t \tag{2.46}$$

is a stationary time series.

If the new time series $y_t{}'$ fits the ARMA (p, q) model $\Phi(L)y_t{}' = \Theta(L)\varepsilon_t$, then the original time series y_t fits

$$\Phi(L)(1 - L)^d y_t = \Theta(L)\varepsilon_t \ , \tag{2.47}$$

where $\Phi(L) = 1 - \phi_1 L - \phi_2 L^2 - \cdots - \phi_p L^p$, which is the AR coefficient polynomial of the stationary and invertible ARMA (p, q) model; $\Theta(L) = 1 - \theta_1 L - \theta_2 L^2 - \cdots - \theta_q L^q$, which is the MA coefficient polynomial of the stationary and invertible ARMA (p, q) model; and ε_t is a zero-mean white noise series.

The model is called an ARIMA model, and the original non-stationary time series y_t fits the ARIMA (p, d, q) model.

2.7 Fundamental Principle of the Weather Research and Forecasting Model

2.7.1 Introduction

The WRF model, jointly developed by a large number of scientific research institutions including the National Center for Atmospheric Research (NCAR), the National Oceanic and Atmospheric Administration (NOAA), represented by the NCEP and the Earth System Research Laboratory (ESRL), the Air Force Weather Agency (AFWA), the Naval Research Laboratory (NRL), the University of Oklahoma (OU), and the Federal Aviation Administration (FAA), is a next-generation mesoscale NWP system with high resolution [126]. This system is designed not only for operational numerical weather forecasting applications, for example, daily weather and severe storm, air-quality, wildland fire, and wind and solar forecasts, but also for atmospheric numerical simulation research, including data assimilation research, atmospheric physics/parameterisation research, regional climate and seasonal time-scale research, land surface-atmosphere interaction simulations, air-sea coupling simulations, and idealised simulations at multiple scales [112].

To be precise, the WRF model is a fully compressible and non-hydrostatic model (with a hydrostatic option) written in the Fortran 90 language [108]. The Arakawa C-grid (a staggered grid) is applied in the horizontal direction, while a terrain-following hydrostatic pressure coordinate is employed in the vertical direction [105]. Besides, a second-order and a third-order Runge-Kutta algorithm are used for time integration schemes [135]. In addition, the WRF model features two dynamical cores (the Advanced Research Weather Research and Forecasting (ARW) and Non-Hydrostatic Mesoscale Model (NMM) cores), one data assimilation system, and one scalable software architecture that supports parallel computing and system extensibility [69]. In terms of the model framework, programme optimisation, and numerical calculations, the state-of-the-art technology is utilised for the WRF model in which the robust data assimilation technology, powerful nesting capability, and advanced physical processes are combined together to allow researchers to simulate real atmospheric data or ideal atmospheric conditions [113].

The WRF model has a number of advantages, such as scalability, portability, high efficiency, and easy maintenance. Moreover, it can also be coupled to those prediction models from different industries [138]. At present, the WRF model, as a free and shared resource holding over 30,000 registered users from more than 150 countries, has become a mainstream weather prediction model that is suitable for the scale range of tens of metres to thousands of kilometres [125].

2.7.2 WRF Model Structure

A WRF modelling system flow chart is shown in Figure 2.2, from which it can be seen that the system consists of three main components, namely a Weather Research and Forecasting Pre-Processing System (WPS), a WRF model, and a post-processing and visualisation system [27]. Specifically, the WPS is used for real-world simulations. The functions of the WPS include defining the simulation domains, interpolating static geographical data (such as topography, the land-use type, and the soil type) into the simulated domains, and interpolating the gridded meteorological data obtained from other models into the simulated domains. The WRF model is made up of two parts. One is called a Weather Research and Forecasting Data Assimilation (WRFDA) system, which is not mandatory. Nevertheless, the WRFDA system can be utilised to add observation data to the interpolation analysis created by the WPS. When the WRF model is running in cyclic mode, the WRFDA system can also be used to update the initialisation conditions of the WRF model. The other is an ARW solver, which is the critical component of the WRF modelling system. The ARW solver is composed of several initialisation programmes and is used for the simulations and numerical integrations of ideal and real data. The post-processing and visualisation system supports multiple graphics and verification tools, such as the Visualisation and Analysis Platform for Ocean, Atmosphere, and Solar Researchers (VAPOR), the NCAR Command Language (NCL), ARWpost, Read/Interpolate/Plot 4 (RIP4), the Weather Research and Forecasting Post Processor (WPP), and Model Evaluation Tools (MET).

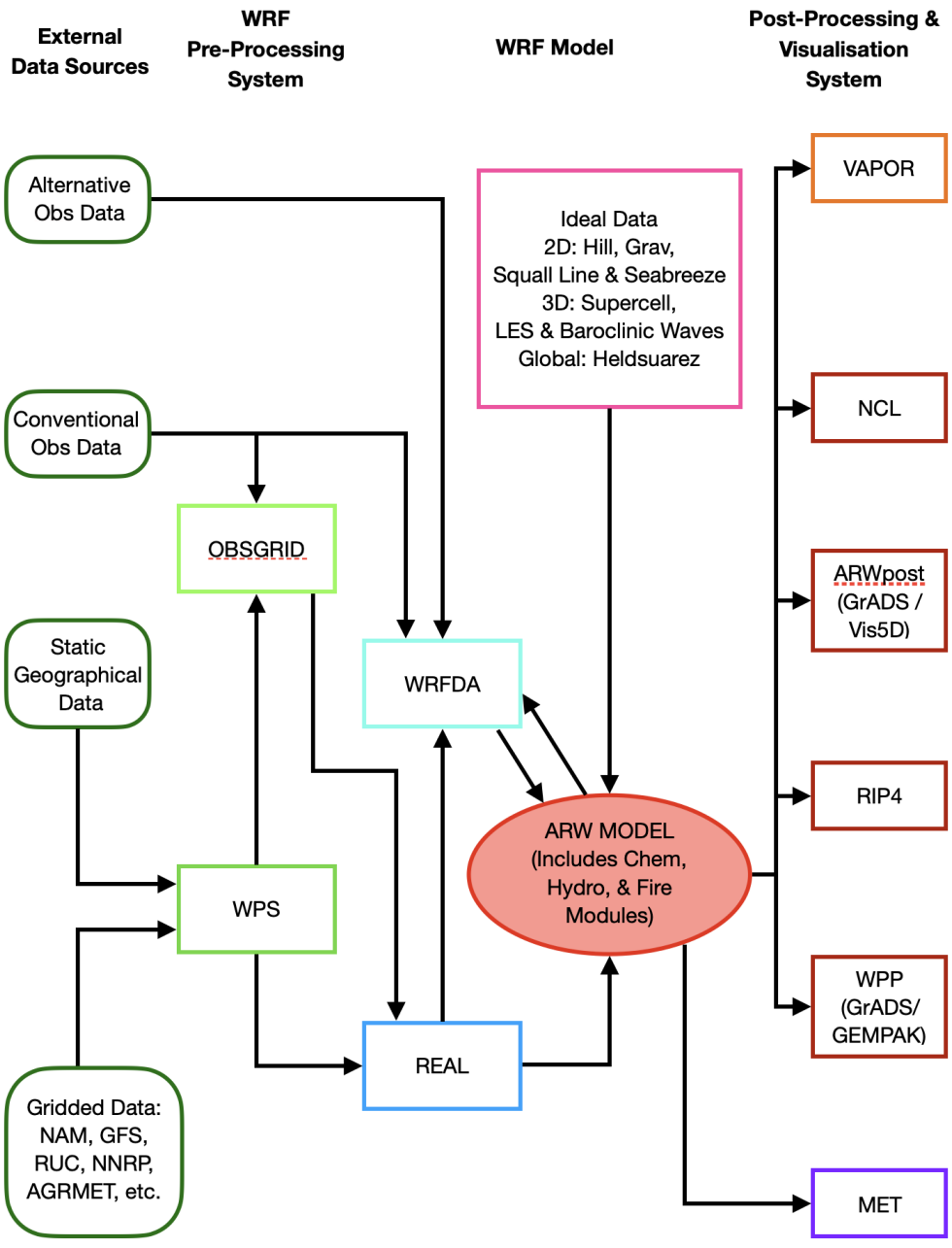

Figure 2.2. WRF modelling system flow chart.

2.8 Fundamental Algorithm of the Technique for Order of Preference by Similarity to Ideal Solution

2.8.1 Introduction

The TOPSIS, designed for solving multi-criteria decision making problems, was first proposed by Hwang and Yoon in 1981 [58] and further developed by Yoon in 1987 [149] and Hwang, Lai, and Liu in 1993 [57]. It is a comprehensive evaluation method that can make full use of the information of the original data, and its results can accurately reflect the gap among alternatives [150]. The positive and negative ideal solutions are the two fundamental concepts of the TOPSIS method [140]. To be precise, the attribute values of the positive and negative ideal solutions are the best and worst ones for all the evaluation criteria, respectively [141]. The basic principle of the TOPSIS is to compare each alternative with both the positive and negative ideal solutions. The one which is the closest to the positive ideal solution and farthest from the negative ideal solution is the best option among all the alternatives [31]. In terms of the advantages of the TOPSIS, it is simple in structure and computationally efficient [111]. Moreover, there are no strict requirements concerning the criterion type, criterion amount, sample size, and data distribution [23]. In addition to ranking alternatives, the TOPSIS can also serve as an approach to assigning weights for various alternatives.

2.8.2 TOPSIS Scheme

The TOPSIS scheme is implemented by carrying out the following key steps [5, 93, 146]:

(1) Step 1

Create a standardised evaluation matrix X consisting of m alternatives and n criteria:

$$X = \begin{bmatrix} x_{11} & x_{12} & \cdots & x_{1n} \\ x_{21} & x_{22} & \cdots & x_{2n} \\ \vdots & \vdots & \ddots & \vdots \\ x_{m1} & x_{m2} & \cdots & x_{mn} \end{bmatrix}. \tag{2.48}$$

(2) Step 2

Positivise the original matrix X:

$$Y = P(X) = \begin{bmatrix} y_{11} & y_{12} & \cdots & y_{1n} \\ y_{21} & y_{22} & \cdots & y_{2n} \\ \vdots & \vdots & \ddots & \vdots \\ y_{m1} & y_{m2} & \cdots & y_{mn} \end{bmatrix} . \tag{2.49}$$

As shown in Table 2.3, there are four common types of criteria used in the TOPSIS scheme. Specifically, the first type is called the benefit criterion, the characteristic of which is the bigger, the better. The second one is called the cost criterion, which is contrary to the benefit criterion, with the characteristic of the smaller, the better. Besides, there is a type called the intermediate criterion, and its characteristic is the closer to a specific value, the better. The last one is named the interval criterion, instead of a value, its characteristic is the closer to a particular interval, the better. Positivisation refers to the conversion of all non-benefit criteria into benefit ones.

Table 2.3. Four common types of criteria and their characteristics.

Type	Characteristic
Benefit criterion	The bigger, the better.
Cost criterion	The smaller, the better.
Intermediate criterion	The closer to a specific value, the better.
Interval criterion	The closer to a specific interval, the better.

For each non-benefit criterion, there is a formula that can be applied to convert it to a benefit criterion. The details are shown as follows:

1) cost criterion $\longrightarrow$ benefit criterion:

$$y_i = max\{x_i\} - x_i \ . \tag{2.50}$$

2) intermediate criterion $\longrightarrow$ benefit criterion:

$$y_i = 1 - \frac{|x_i - x_0|}{M} \ , \tag{2.51}$$

in which

$$M = max\{|x_i - x_0|\} \ . \tag{2.52}$$

3) interval criterion $\longrightarrow$ benefit criterion:

$$y_i = \begin{cases} 1 - \dfrac{a - x_i}{M}, & x_i < a \\ 1, & a \le x_i \le b \\ 1 - \dfrac{x_i - b}{M}, & k > b \end{cases} , \tag{2.53}$$

in which

$$M = max\{a - min\{x_i\}, max\{x_i\} - b\} . \tag{2.54}$$

(3) Step 3

Normalise the positivised matrix Y to eliminate the influence of different criterion dimensions:

$$Z = N(Y) = \begin{bmatrix} z_{11} & z_{12} & \cdots & z_{1n} \\ z_{21} & z_{22} & \cdots & z_{2n} \\ \vdots & \vdots & \ddots & \vdots \\ z_{m1} & z_{m2} & \cdots & z_{mn} \end{bmatrix} , \tag{2.55}$$

in which

$$z_{ij} = \frac{y_{ij}}{\sqrt{\sum_{i=1}^{m} {y_{ij}}^2}} . \tag{2.56}$$

(4) Step 4

Define the positive ideal solution Z^+ and negative ideal solution Z^-:

$$\begin{aligned} Z^+ &= (Z_1^+, Z_2^+, \ldots, Z_n^+) \\ &= (max\{z_{11}, z_{21}, \ldots, z_{m1}\}, max\{z_{12}, z_{22}, \ldots, z_{m2}\}, \ldots, max\{z_{1n}, z_{2n}, \ldots, z_{mn}\}) \end{aligned} , \tag{2.57}$$

and

$$\begin{aligned} Z^- &= (Z_1^-, Z_2^-, \ldots, Z_n^-) \\ &= (min\{z_{11}, z_{21}, \ldots, z_{m1}\}, min\{z_{12}, z_{22}, \ldots, z_{m2}\}, \ldots, min\{z_{1n}, z_{2n}, \ldots, z_{mn}\}) \end{aligned} . \tag{2.58}$$

The nature of Equations (2.57) and (2.58) is to pick out the maximum and minimum values of each criterion, respectively.

(5) Step 5

Calculate the distances between each alternative and the positive and negative ideal solutions:

$$D_i^+ = \sqrt{\sum_{j=1}^{n} (Z_j^+ - Z_{ij})^2} \ , \tag{2.59}$$

and

$$D_i^- = \sqrt{\sum_{j=1}^{n} (Z_j^- - Z_{ij})^2} \ . \tag{2.60}$$

(6) Step 6

Calculate the similarity scores of all the alternatives to the positive ideal solution:

$$S_i = \frac{D_i^-}{D_i^+ + D_i^-} \ . \tag{2.61}$$

The range of S_i is between 0 and 1. Specifically, if the distance between the alternative and negative ideal solution D_i^- is 0, which means the alternative is just the negative ideal solution, its similarity score S_i will be 0. If the distance between the alternative and positive ideal solution D_i^+ is 0, which means the alternative is just the positive ideal solution, its similarity score S_i will be 1.

(7) Step 7

Rank all the alternatives according to their similarity scores S_i.

Chapter 3

Preliminary Work

3.1 Analysis of Factors Affecting Wind Power

The electricity of wind farms is produced by wind turbines which first convert the kinetic energy of wind into the mechanical energy of blades and then into electrical energy via electromagnetic induction. The output power of a wind turbine can be described by the following formula [98]:

$$P = \frac{1}{2} C_p \eta \rho A U^3 \ , \tag{3.1}$$

where P is the wind power (W), C_p is the power coefficient, η is the efficiency, ρ is the air density (kg/m^3), A is the swept area (m^2), and U is the wind speed (m/s).

(1) Wind speed

According to Formula (3.1), it can be seen that the wind power (P) is proportional to the cube of the wind speed (U). That is to say, eight times the wind power can be obtained by doubling the wind speed. A typical wind turbine power curve is shown in Figure 3.1 [7], from which it can be found that a slight change in the wind speed leads to a great influence on the wind power when the wind speed is in the range between the cut-in and rated speeds. Specifically, the cut-in speed is the minimum required wind speed to start the wind turbine. Usually, its value is from 3 to 4 m/s. Besides, the rated output speed, typically between 12 and 17 m/s, is the wind speed at which the output power reaches the rated power of the wind turbine. Moreover, the cut-out speed

is the maximum wind speed for wind turbine safe operation, and its common value is 25 m/s [114]. While the wind speed is between the rated output and cut-out speeds, the wind turbine can keep running at the maximum output power level. Nevertheless, when the wind speed is either lower than the cut-in speed or higher than the cut-out speed, the wind turbine will not work, so that the output power is 0. Hence, the wind speed is the most important variable that affects the wind power.

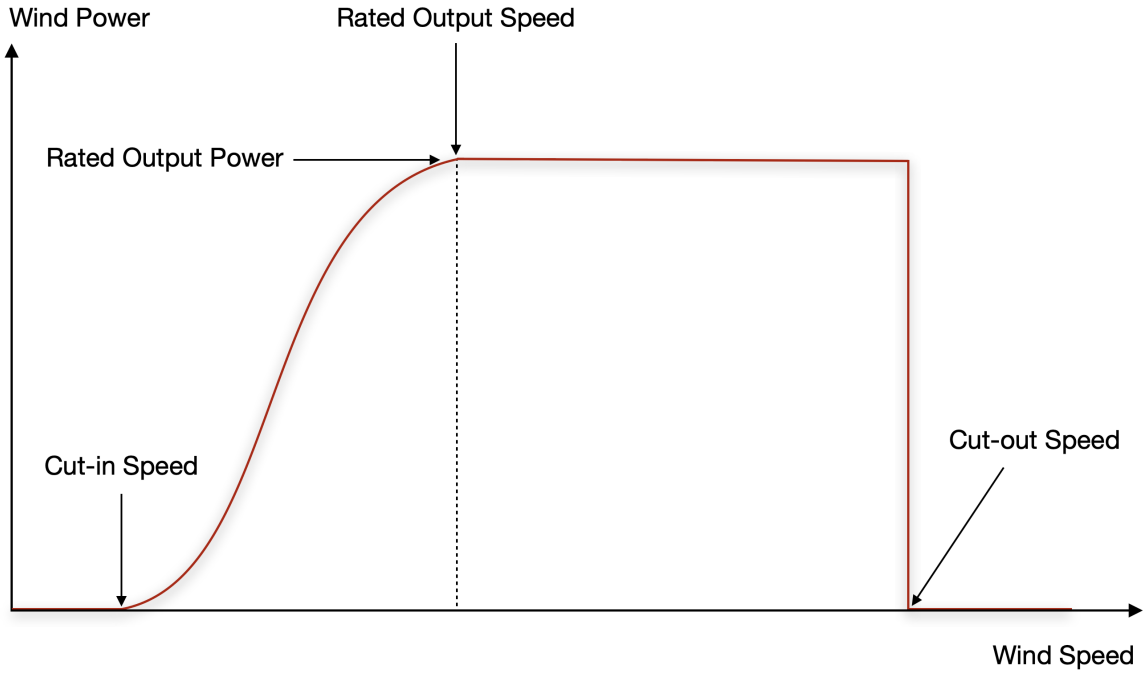

Figure 3.1. Typical wind turbine power curve.

(2) Wind direction

When the wind turbine is facing directly into the wind, the output wind power will be very close to the designed value. However, when there is a certain angle between the horizontal axis of the wind turbine and wind direction, the wind energy cannot be fully captured by the wind turbine, resulting in the lower output power. Although a yaw drive, installed in the horizontal wind turbine, is capable of intelligently orienting the wind turbine to face the wind by sensors when the wind direction changes, the response action costs time. Therefore, the wind direction variable affects the wind power as well.

(3) Air density

Formula (3.1) illustrates that the air density (ρ) is another variable that affects the wind power. With the rise of the air density, the output power of the wind turbine goes up. In addition, the air density varies with the changes in the atmospheric pressure, temperature, and humidity, which are also regarded as the factors that have influences on the wind power.

(4) Power coefficient, efficiency, and swept area

As shown in Formula (3.1), the power coefficient (C_p), efficiency (η), and swept area (A) all affect the output power. However, these properties are fixed for any given wind turbine. In other words, they are factors affecting the wind power but not variables.

3.2 Description of Data Sources

Three sets of time series data were used for developing the multi-hour ahead wind power forecasting system in this study. More specifically, two of these datasets were acquired from a real wind farm located in North China. These datasets consisted of the historical wind speed measurements obtained at the wind turbine hub height and wind power measurements for a single operational wind turbine for the time period from 00:00:00 Coordinated Universal Time (UTC) on the 11th of August 2015 to 23:30:00 UTC on the 3rd of September 2015. The sampling time of the data was 30 minutes. In total, each of the two sets of data had 1,152 samples acquired over a period of 24 days. The remaining dataset consisted of the meteorological forecasts obtained from the GFS with a temporal resolution of 6 hours for the same period of time. In order to build the forecasting models and assess their predictive performance, these three sets of data were divided into two groups. In particular, the data from the first 20 days were used as a training dataset, and the remaining data from the last 4 days were used as a test dataset. Additionally, for the ANFIS-based power curve model and wind speed correction model, the last-day data of the first 20-day data were set as a checking dataset for validation (preventing overfitting of the training dataset), which means the length of the training dataset reduced to 19 days.

Besides, there was a set of geographic coordinate data for each of the 66 wind turbines in the wind farm. The centre point of all the wind turbines could be determined: the location centroid was 41.06° N and 114.81° E. This was regarded herein as the location of the target wind turbine at which wind speed and wind power forecasts would be made. In addition, a set of static geographical data provided by the University Corporation for

Atmospheric Research (UCAR), the United States, was available for WRF (physics-based) modelling.

3.3 Approaches of Data Pre-Processing

(1) Use interpolation for missing data

In the actual operation of wind farms, incomplete wind data are very common. This problem may result from system failures or may be caused by human errors. Therefore, for a set of raw data, the first step is to apply an approach to complete it. The Lagrange polynomial is a proper interpolation method for solving the problem of missing data. The mathematical description is shown as follows [25].

A set of $n+1$ different data points, $a = x_0 < x_1 < \cdots < x_n = b$, in the range of $[a,\ b]$ is given, and the values of the function $y = f(x)$ are set to be $y_0,\ y_1,\ \ldots,\ y_n$. If there is a polynomial

$$P_n(x) = a_0 + a_1 x + a_2 x^2 + \cdots + a_n x^n \tag{3.2}$$

let

$$P_n(x_i) = y_i, \quad i = 0,\ 1,\ 2,\ \ldots,\ n\ , \tag{3.3}$$

then $P_n(x)$ is called the interpolation polynomial of $y = f(x)$, $x_0,\ x_1,\ \ldots,\ x_n$ are the interpolation nodes, $[a,\ b]$ is the interpolation interval, and Equation (3.3) is the interpolation condition.

(2) Clear negative data

In the original wind data, some values of historically measured wind speed and wind power were negative, which was abnormal. In order to generate the forecasting models properly, all the negative data had to be cleared. A simple way was to regard all of them to be 0:

$$U_i = 0, \quad if\ U_i < 0\ , \tag{3.4}$$

and

$$P_i = 0, \quad if \ P_i < 0 \ , \tag{3.5}$$

where U_i is the i-th wind speed, and P_i is the i-th wind power.

(3) Normalise data

For the purpose of the fast convergence of an ANFIS model, both input and output data should be normalised in the range between 0 and 1 before training and testing procedures. In this study, the input was the wind speed, and the output was the wind power. A popular min-max normalisation technique was employed [107]:

$$x_{n,\ i} = \frac{(x_i - x_{min})(y_{max} - y_{min})}{x_{max} - x_{min}} + y_{min} \ , \tag{3.6}$$

where $x_{n,\ i}$ is the i-th normalised wind speed (power), x_i is the i-th wind speed (power), x_{min} is the minimum wind speed (power), y_{max} is the normalised maximum wind speed (power), y_{min} is the normalised minimum wind speed (power), and x_{max} is the maximum wind speed (power).

In this study, the minimum wind speed and wind power were both 0; the maximum wind speed and wind power were 25 m/s and 1,500 kW, respectively; the normalised minimum wind speed and wind power were both 0; and the normalised maximum wind speed and wind power were both 1. Thus, Equation (3.6) can be simplified as follows:

$$U_{n,\ i} = \frac{U_i}{25} \ , \tag{3.7}$$

and

$$P_{n,\ i} = \frac{P_i}{1500} \ , \tag{3.8}$$

where $U_{n,\ i}$ is the i-th normalised wind speed, U_i is the i-th wind speed, $P_{n,\ i}$ is the i-th normalised wind power, and P_i is the i-th wind power.

3.4 Spectral Analysis of Wind Speed Measurements

In nature, wind varies owing to large-scale slowly evolving weather patterns and small-scale influences such as topography and local stability. Therefore, the wind at a fixed location

may appear multi-time-scale variability. It is best to perform a spectral analysis of wind speed measurements and use the results to guide statistical models. The spectral analysis decomposes a set of time series observed data into underlying sine and cosine functions of different frequencies for the purpose of identifying those frequencies that appear particularly strong or significant. If a large correlation between the sine and cosine functions of different frequencies and observations is pinpointed, it can be concluded that a strong periodicity of the respective frequency in the data exists [142]. As mentioned in Section 3.2, the wind speed measurements used in this research were a set of 24-day time series data. The spectrum of the time series was calculated, and the smoothed periodogram is shown in Figure 3.2, from which it can be seen that no evident periodicity was detected for this limited-length data. In addition, there was no diurnal variability of the wind identified in this case.

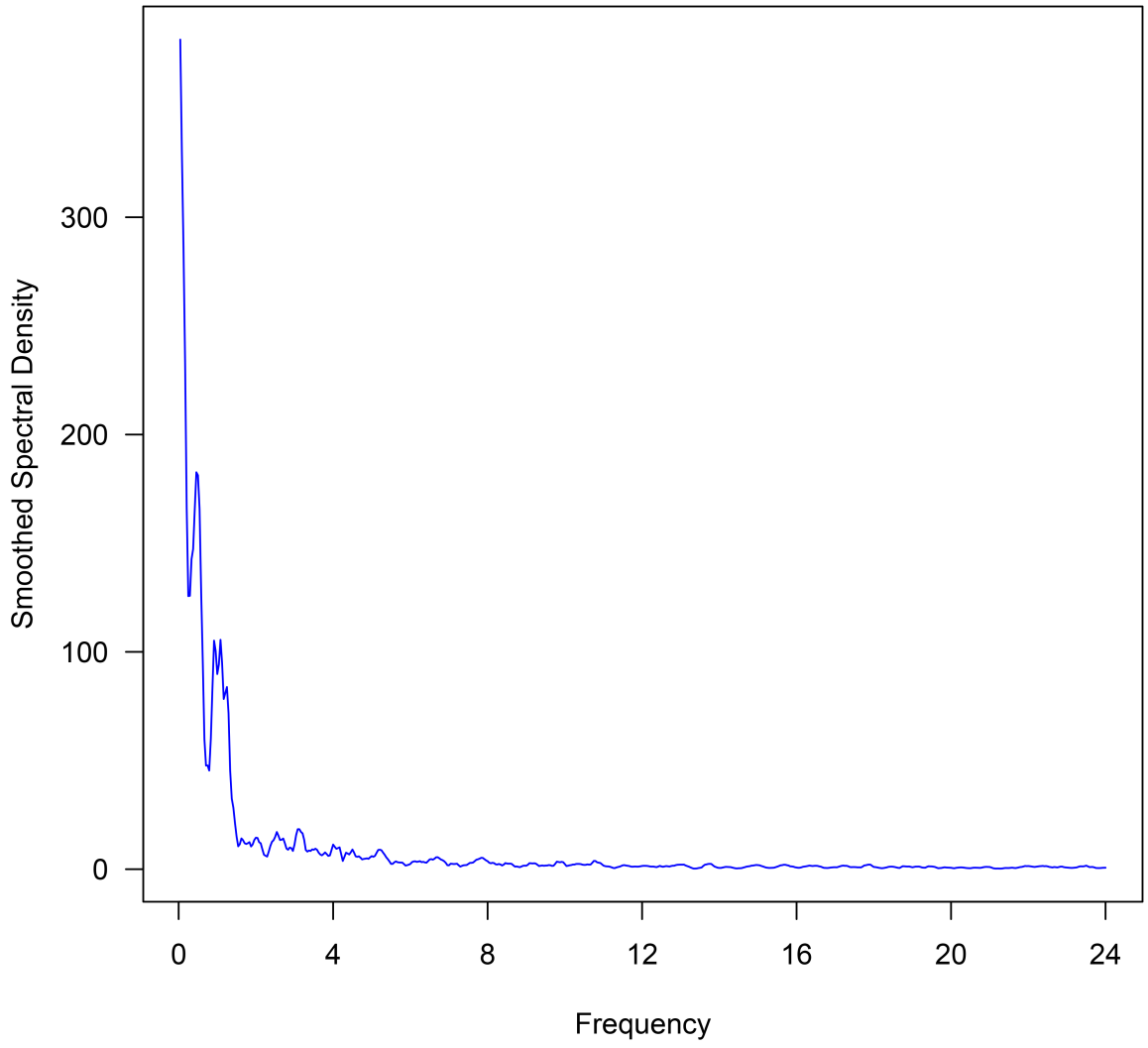

Figure 3.2. Smoothed periodogram of the spectral analysis of the 24-day wind speed measurements.

3.5 Introduction of Model Evaluation Metrics

In order to evaluate the predictive performance of the forecasting models, six of the most widely used statistical metrics, namely the mean bias (MB), MAE, RMSE, index of agreement (IA), MAPE, and symmetric mean absolute percentage error (SMAPE), were selected in this study [80, 115, 156]. Furthermore, an official document released by the National Energy Administration (NEA), China, recommends two additional wind power forecast metrics for validation, namely the accuracy rate and qualification rate [100]. In the following, the definitions of these eight evaluation metrics are given in detail.

(1) Mean bias (for wind speed and wind power) is defined as

$$\mathrm{MB} = \frac{\sum_{i=1}^{n}(\hat{Z}_i - Z_i)}{n} , \tag{3.9}$$

where n is the total number of assessment time points per day, $\hat{Z}_i$ is the i-th wind speed (power) forecast, and Z_i is the i-th wind speed (power) measurement.

(2) Mean absolute error (for wind speed and wind power) is defined as

$$\mathrm{MAE} = \frac{\sum_{i=1}^{n}|\hat{Z}_i - Z_i|}{n} , \tag{3.10}$$

where n is the total number of assessment time points per day, $\hat{Z}_i$ is the i-th wind speed (power) forecast, and Z_i is the i-th wind speed (power) measurement.

(3) Root mean squared error (for wind speed and wind power) is defined as

$$\mathrm{RMSE} = \sqrt{\frac{\sum_{i=1}^{n}(\hat{Z}_i - Z_i)^2}{n}} , \tag{3.11}$$

where n is the total number of assessment time points per day, $\hat{Z}_i$ is the i-th wind speed (power) forecast, and Z_i is the i-th wind speed (power) measurement.

(4) Index of agreement (for wind speed and wind power) is defined as

$$\mathrm{IA} = 1 - \frac{\sum_{i=1}^{n}(\hat{Z}_i - Z_i)^2}{\sum_{i=1}^{n}(|\hat{Z}_i - \bar{Z}| + |Z_i - \bar{Z}|)^2} , \tag{3.12}$$

where n is the total number of assessment time points per day, $\hat{Z}_i$ is the i-th wind speed (power) forecast, Z_i is the i-th wind speed (power) measurement, and $\bar{Z}$ is the mean of the wind speed (power) measurements.

(5) Mean absolute percentage error (for wind speed only) is defined as

$$\text{MAPE} = \frac{\sum_{i=1}^{n} \left| \frac{\hat{Z}_i - Z_i}{Z_i} \right|}{n} \times 100\% \ , \tag{3.13}$$

where n is the total number of assessment time points per day, $\hat{Z}_i$ is the i-th wind speed forecast, and Z_i is the i-th wind speed measurement.

(6) Symmetric mean absolute percentage error (for wind speed only) is defined as

$$\text{SMAPE} = \frac{\sum_{i=1}^{n} \frac{|\hat{Z}_i - Z_i|}{(|\hat{Z}_i| + |Z_i|)/2}}{n} \times 100\% \ , \tag{3.14}$$

where n is the total number of assessment time points per day, $\hat{Z}_i$ is the i-th wind speed forecast, and Z_i is the i-th wind speed measurement.

(7) Accuracy rate (for wind power only) is defined as

$$\text{accuracy rate} = \left(1 - \sqrt{\frac{\sum_{i=1}^{n} \left(\frac{\hat{Z}_i - Z_i}{Cap} \right)^2}{n}} \right) \times 100\% \ , \tag{3.15}$$

where n is the total number of assessment time points per day, $\hat{Z}_i$ is the i-th wind power forecast, Z_i is the i-th wind power measurement, and Cap is the wind farm installed capacity. The monthly or yearly average accuracy rate for wind power forecasting is the arithmetic mean of the daily accuracy rates for that month or year.

(8) Qualification rate (for wind power only) is defined as

$$\text{qualification rate} = \frac{\sum_{i=1}^{n} Q_i}{n} \times 100\% \ , \tag{3.16}$$

with

$$\left(1-\frac{|\hat{Z}_i-Z_i|}{Cap}\right)\times 100\% \geq 75\%, \quad Q_i=1\ ; \tag{3.17}$$

and

$$\left(1-\frac{|\hat{Z}_i-Z_i|}{Cap}\right)\times 100\% < 75\%, \quad Q_i=0\ . \tag{3.18}$$

Herein, n is the total number of assessment time points per day, Q_i indicates whether the i-th wind power forecast is qualified, $\hat{Z}_i$ is the i-th wind power forecast, Z_i is the i-th wind power measurement, and Cap is the wind farm installed capacity. The monthly or yearly average qualification rate for wind power forecasting is the arithmetic mean of the daily qualification rates for that month or year.

3.6 Interpretation of a 'Forecast Time Horizon'

In order to strengthen and standardise the operational management of wind farms, implement the requirement of the guaranteed full purchase of wind power, ensure the safe and reliable operation of power systems, and promote the healthy and orderly development of wind power, the NEA [100] officially clarified the industry requirements for grid-connected operational wind farms in China. Specifically, all the operators of the wind farms in China have to report their wind power forecasts (with a temporal resolution of 15 minutes) for 24 hours of the next day to the power-dispatch agency. Due to the limitations of the temporal resolution of the currently available wind data, the time interval used in this study was 30 minutes. However, the idea was precisely the same. For example, assume that it is 00:00 currently. For 24-hour ahead wind power forecasting, not only is the wind power forecast at 24:00 required, but also the wind power forecasts from 00:30 to 23:30 with a time interval of 30 minutes are necessary. In other words, 48 wind power forecasts should be reported for the 24-hour ahead wind power forecasting of the next day. It is straightforward to understand that for a forecast time horizon of 24 hours, only reporting the last wind power forecast, which is really 24 hours later from now, is meaningless. The trend of wind power and how it will perform during these 24 hours are significant, and this is why wind power forecasts every 30 minutes in 24-hour ahead wind power forecasting are necessary.

For the purpose of forecasting the wind power for the next 24 hours as accurately as possible, all the wind data up to the forecast time point should be fully utilised. This point

is worth emphasising since among the 48 wind power forecasts for the next 24 hours, only the last wind power forecast is really reported 24 hours in advance, and the others are not. For instance, the first wind power forecast is reported 30 minutes from now. Basically, it is a 30-minute ahead wind power forecast, but it still belongs to the 24-hour ahead wind power forecasting results. The same applies to the other 46 wind power forecasts. There is no doubt that when generating the first wind power forecast for the next 24 hours, the real 24-hour ahead wind power forecasting can be applied. However, by doing so, there is no access to any wind data from the past 24 hours. Instead, the wind data from 24 hours ago are employed. This method can be used for the first 47 wind power forecasts, and, as a result, all the wind power forecasts are truly determined 24 hours in advance. Nevertheless, this way of forecasting will cause the forecast accuracy rate to decrease appreciably. Obviously, it does not make any sense to do the 24-hour ahead wind power forecasting like this.

In conclusion, in actual applications, the 24-hour ahead wind power forecasting does not mean forecasting a single point 24 hours later from now or forecasting every point 24 hours in advance. All the available data at the moment should be used to forecast wind power for the next 24 hours. In this way, the first wind power forecast is forecasted 30 minutes in advance, the second one is 1 hour in advance, the third one is 1.5 hours in advance, ..., the 47th one is 23.5 hours in advance, and only the last one is a true 24-hour ahead forecast. However, this forecasting scheme is still referred to as 24-hour ahead wind power forecasting. This concept can be extended to other forecast time horizons. For instance, the 4-hour ahead wind power forecasting requires the wind power forecasts for the next 4 hours with a time interval of 30 minutes, leading to reporting eight wind power forecasts.

3.7 Power Curve Modelling

3.7.1 Introduction

A power curve indicates the relationship between wind speed and wind power. Once wind speed forecasts are obtained, the corresponding wind power forecasts can be calculated according to the power curve via mapping the wind speed to wind power.

Every wind turbine comes with a power curve provided by the manufacturer. However, in this study, the specific model of the studied wind turbine was unknown, which means the manufacturer's power curve was unavailable. Even though the power curve was given,

it only represented the designed relationship between wind speed and wind power. As discussed in Section 3.1, the output power of a wind turbine is influenced by changeable surroundings. In practice, the relationship between wind speed and wind power is hard to strictly follow the manufacturer's power curve. Hence, the method of the power curve modelling based on historical wind speed and wind power measurements was suggested. It was believed that the power curve model created in this way was able to reflect the actual performance of the wind turbine.

3.7.2 Power Curve Modelling Based on an ANFIS Model

An ANFIS was proposed to model the power curve in this study. The wind speed was set as the input of the ANFIS model, while the wind power was the output. The historical wind speed and wind power data measured from the 11th of August 2015 to the 3rd of September 2015 with a time interval of 30 minutes were employed for the power curve modelling. In total, each set of data had 1,152 measurements for 24 days. Both sets of data were divided into three groups in the time series. In particular, the data from the first 19 days were used as a training dataset for model training, the data from the 20th day were used as a checking dataset for model validation, and the remaining data from the last 4 days were used as a test dataset for evaluating the mapping performance of the model.

A scatter plot revealing the relationship between the historical wind speed and wind power measurements from the training dataset is shown in Figure 3.3. The objective of the power curve modelling was to create a single curve based on the scatter points by minimising the errors.

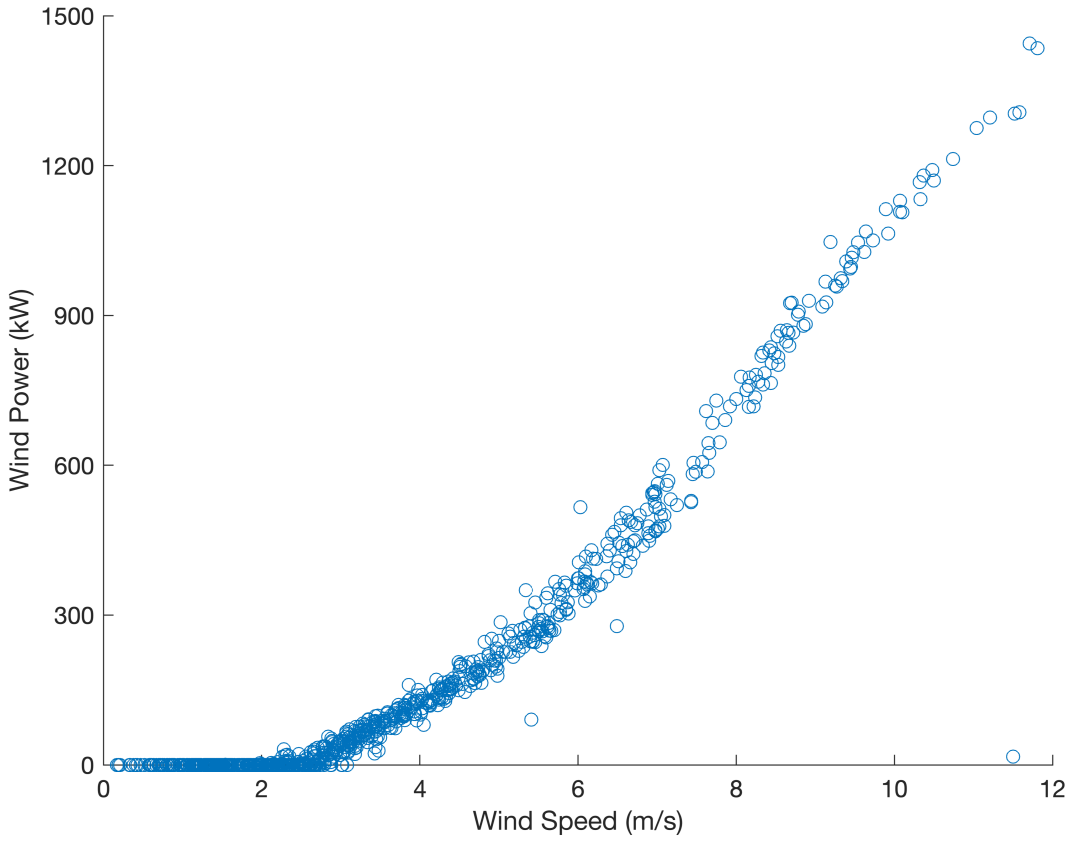

Figure 3.3. Relationship between the historical wind speed and wind power measurements from the 20-day training dataset.

In the ANFIS modelling, some model parameters need to be set by users. One of the vital model parameters is the membership function type associated with the input. According to the shape of the power curve shown in Figure 3.1, a generalised bell-shaped membership function was selected in this case. Another crucial model parameter is the number of membership functions. More membership functions contribute to an ANFIS model with a more complex structure but not necessarily better performance. In this case, it was found that the ANFIS model failed in the power curve modelling as long as the number of membership functions was greater than 3. For example, Figure 3.4 shows a power curve provided by an ANFIS model with four membership functions. Roughly speaking, there was a drop in the wind power when the wind speed rose from 10 to 11 m/s. Obviously,

this trend went against the truth. The same thing happened in the experiments with the increasing number of membership functions. Since at least two membership functions are required for ANFIS learning, the appropriate number of membership functions for the power curve modelling was either 2 or 3. Moreover, when the wind speed was between 0 and 3 m/s, some corresponding wind power values were negative, which was not valid. This negative wind power issue could be solved simply by setting all negative values to 0. In addition, all the wind power values had to be adjusted to 0 when the wind speed was lower than 2 m/s since the wind turbine will stop working once the wind speed does not reach the cut-in speed value.

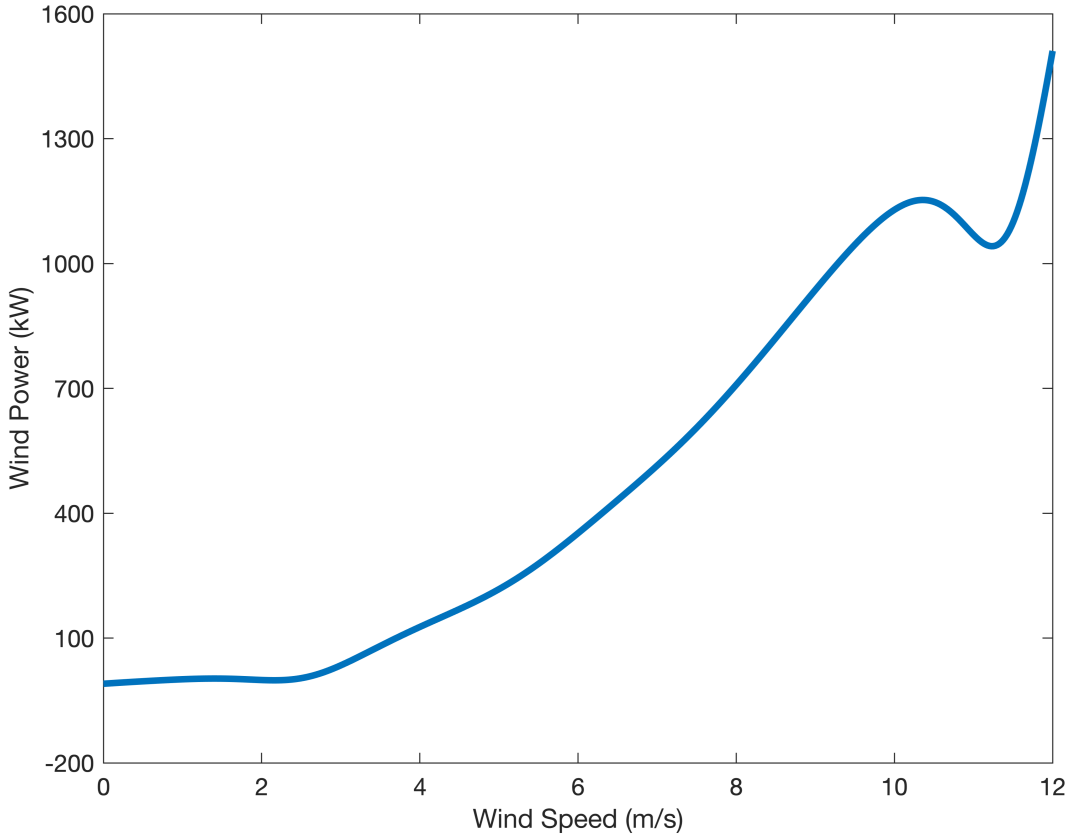

Figure 3.4. Power curve provided by an ANFIS model with four membership functions.

Another model parameter that needs to be highlighted is the training epoch number.

The combinations of the different numbers of membership functions and training epochs were applied to train the ANFIS model. The other parameters inside the ANFIS model were determined through self-learning during the training process. Next, the wind speed measurements from the test dataset were input to the trained ANFIS model, and then the corresponding wind power computations were obtained as the model output. According to the model evaluation metrics explained in Section 3.5, the MBs, MAEs, RMSEs, IAs, accuracy rates, and qualification rates were calculated based on the differences between the wind power computations provided by the ANFIS model and the wind power measurements from the test dataset. For the simplicity purpose, the 4-day average value (viz., the arithmetic mean over a period of 4 days represented by the test dataset) of each metric was used to compare the mapping performance of the ANFIS models with different numbers of membership functions and training epochs. The corresponding results are shown in Tables 3.1 to 3.6.

Table 3.1. Four-day average MBs for the ANFIS models with different numbers of membership functions and training epochs evaluated by using the 4-day test dataset.

4-day average MB (kW)		Number of membership functions	
		2	3
Number of training epochs	10	0.9	0.6
	100	1.2	0.2
	200	1.2	0.0
	500	1.2	-0.1
	1,000	1.1	-0.1
	2,000	1.1	-0.1
	5,000	1.1	-0.1
	10,000	1.1	-0.1

Table 3.2. Four-day average MAEs for the ANFIS models with different numbers of membership functions and training epochs evaluated by using the 4-day test dataset.

4-day average MAE (kW)		Number of membership functions	
		2	3
Number of training epochs	10	12.9	10.2
	100	10.8	10.2
	200	10.7	10.2
	500	10.6	10.2
	1,000	10.6	10.2
	2,000	10.6	10.2
	5,000	10.6	10.2
	10,000	10.6	10.2

Table 3.3. Four-day average RMSEs for the ANFIS models with different numbers of membership functions and training epochs evaluated by using the 4-day test dataset.

4-day average RMSE (kW)		Number of membership functions	
		2	3
Number of training epochs	10	21.6	17.0
	100	18.0	17.2
	200	17.8	17.2
	500	17.6	17.3
	1,000	17.5	17.3
	2,000	17.5	17.3
	5,000	17.5	17.3
	10,000	17.5	17.3

Table 3.4. Four-day average IAs for the ANFIS models with different numbers of membership functions and training epochs evaluated by using the 4-day test dataset.

4-day average IA		Number of membership functions	
		2	3
Number of training epochs	10	1.00	1.00
	100	1.00	1.00
	200	1.00	1.00
	500	1.00	1.00
	1,000	1.00	1.00
	2,000	1.00	1.00
	5,000	1.00	1.00
	10,000	1.00	1.00

Table 3.5. Four-day average accuracy rates for the ANFIS models with different numbers of membership functions and training epochs evaluated by using the 4-day test dataset.

4-day average accuracy rate		Number of membership functions	
		2	3
Number of training epochs	10	98.56%	98.87%
	100	98.80%	98.86%
	200	98.81%	98.85%
	500	98.83%	98.85%
	1,000	98.84%	98.85%
	2,000	98.84%	98.85%
	5,000	98.84%	98.85%
	10,000	98.83%	98.85%

Table 3.6. Four-day average qualification rates for the ANFIS models with different numbers of membership functions and training epochs evaluated by using the 4-day test dataset.

4-day average qualification rate		Number of membership functions	
		2	3
Number of training epochs	10	100.00%	100.00%
	100	100.00%	100.00%
	200	100.00%	100.00%
	500	100.00%	100.00%
	1,000	100.00%	100.00%
	2,000	100.00%	100.00%
	5,000	100.00%	100.00%
	10,000	100.00%	100.00%

From Tables 3.1 to 3.6, it can be found that most of the ANFIS models were incredibly close to each other in terms of the evaluation metrics. To be precise, the 4-day average qualification rate was 100.00% for every ANFIS model. Besides, the 4-day average IAs were all 1.00, except that one for the ANFIS model with two membership functions and 10 training epochs, which was 0.99 (almost reaching 1.00). In general, the ANFIS model with three membership functions performed better than that with two membership functions since the former always had a lower 4-day average MB absolute value, MAE, and RMSE and a higher 4-day average accuracy rate compared with the latter under the condition of the same number of training epochs. In addition, it can be seen that for the ANFIS model with three membership functions, the increasing number of training epochs did not improve the 4-day average MAE, IA, and qualification rate at all and even had the adverse effects on the 4-day average RMSE and accuracy rate. Although the 4-day average MB absolute value for the ANFIS model with three membership functions and 10 training epochs was higher than those for the other ANFIS models with the same number of membership functions but more training epochs, all of the 4-day average MB absolute values were lower than 1.0 kW. Under the consideration of computational costs, the combination of three membership functions and 10 training epochs was selected for the power curve modelling. In conclusion, three key model parameters, namely the type of membership functions, number of membership functions, and number of training epochs, were finally determined

to be generalised bell-shaped, 3, and 10, respectively.

3.7.3 Model Evaluation

A comparison between the wind power predictions provided by the selected ANFIS model and the historical wind power measurements from the test dataset is shown in Figure 3.5. Intuitively, the conformance between the wind power computations and measurements was excellent. Numerically, the 4-day average MB, MAE, and RMSE were 0.6 kW, 10.2 kW, and 17.0 kW, respectively. These values for the three evaluation metrics were relatively small in comparison with the rated power of the wind turbine (1,500 kW). Furthermore, the 4-day average IA, accuracy rate, and qualification rate were 1.00, 98.87%, and 100.00%, respectively. In other words, if the wind speed forecasts were equal to the wind speed measurements for these 4 days, the 4-day average IA and qualification rate for the wind power forecasting would both correspond to their maximum values (perfect scores). Moreover, the 4-day average accuracy rate would reach 98.87%. In view of this, the selected ANFIS model provided an excellent model for the power curve of the wind turbine for this case. Finally, it is noted that the 1.13% wind power prediction error, as characterised by the accuracy rate, mainly resulted from the systematic errors, model errors, and neglect of other variables that affected the wind power.

In this research, the historical wind speed measurements were treated as the 'truth'. Nevertheless, wind speed measurements are not perfect. For example, wind speeds measured by an anemometer typically have errors on the order of 1 m/s. In wind power forecasting, the relationship between wind speed and wind power measurements matters rather than the accuracy of the wind speed measurements. Although there were measurement errors, the selected ANFIS model indicated that if the wind speed forecasts were equal to the wind speed measurements, the prediction error for the 4-day test dataset would be only 1.13%. Furthermore, this was the main reason for generating a power curve model by using the real wind speed and wind power measurements instead of employing the power curve provided by the manufacturer. The ANFIS-based power curve model is able to correct partial errors caused by measurement.

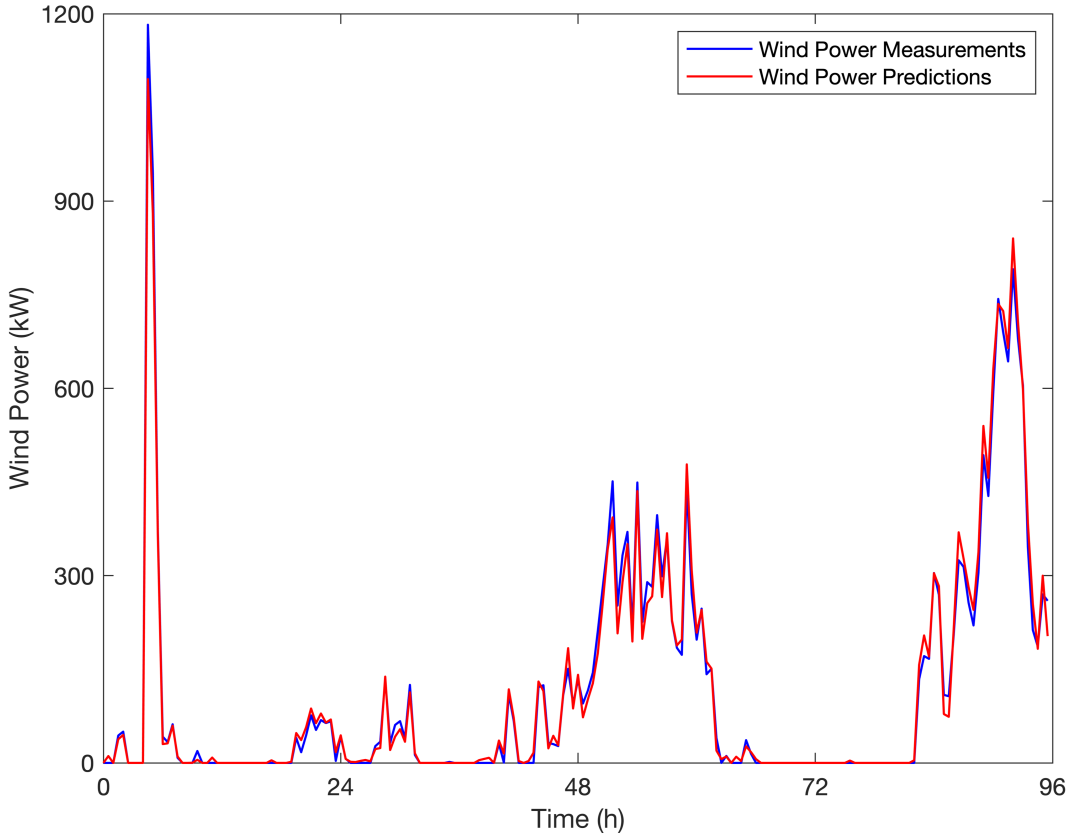

Figure 3.5. Evaluation of the power curve model by using the historical wind speed and wind power measurements from the 4-day test dataset.

3.7.4 Power Curve

The final power curve created by using the selected ANFIS model is shown in Figure 3.6, from which it can be seen that this power curve which successfully described the relationship between the wind speed and wind power when the wind speed ranged between 0 and 12 m/s looks very similar to the left part of the typical one given in Figure 3.1. The main drawback of this power curve was that the wind power tended to have a maximum value lower than 1,200 kW at the end of the curve. Nevertheless, the rated power of the studied wind turbine was 1,500 kW. Obviously, this ANFIS model did not capture the features of the power curve when the wind speed was between the rated and cut-out speed values or

higher than the cut-out speed value, which means the mapping performance of this ANFIS model would definitely deteriorate when the wind speed was greater than 12 m/s. All these problems were due to the limitation of the given training dataset. From Figure 3.3, it can be seen that the maximum wind speed in the training dataset was less than 12 m/s, and only a few points fell in the wind speed values ranging from 11 to 12 m/s. Therefore, it was impossible for the ANFIS model to learn the right part of the typical power curve because of the lack of facts in this case. It is strongly recommended to collect a considerable number of historically measured wind data for complete power curve modelling. Fortunately, the power curve in Figure 3.6 was sufficient for the case study in this research simply because the maximum wind speed measurement in the test dataset was lower than 12 m/s, and the maximum wind power measurement was less than 1,200 kW.

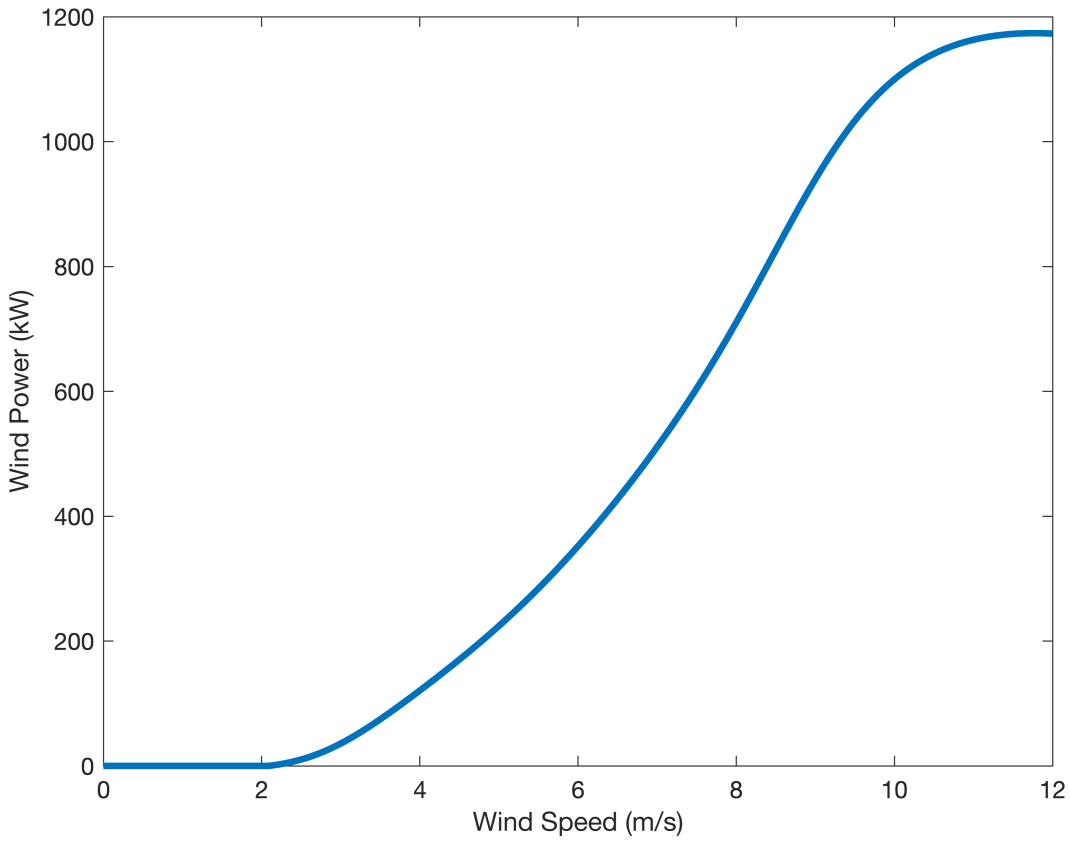

Figure 3.6. Final power curve created by using the selected ANFIS model.

3.7.5 Summary

The role of a power curve is to map wind speed forecasts to wind power forecasts. In this case, an ANFIS was proposed to model the power curve by using a set of historically measured wind speed and wind power data over a period of 24 days. Specifically, the first 19-day wind data were employed as a training dataset, the wind data from the 20th day were a checking dataset, and the remaining 4-day data were a test dataset. Besides, the wind speed was set as the model input, while the wind power was the output. Through a comparative analysis, three key ANFIS model parameters, namely the type of membership functions, number of membership functions, and number of training epochs, were determined to be generalised bell-shaped, 3, and 10, respectively. The mapping performance of the trained ANFIS model was assessed according to the test dataset. The effectiveness of the selected ANFIS model was verified as the model IA, accuracy rate, and qualification rate were 1.00, 98.87%, and 100.00%, respectively. The 1.13% wind power prediction error, as characterised by the accuracy rate, mainly resulted from the systematic errors, model errors, and neglect of other variables that affected the wind power. Finally, the power curve created by using the selected ANFIS model was obtained. Because of the limitation of the training dataset, this power curve could only handle the cases when the wind speed was lower than 12 m/s. However, the established power curve was sufficient in this study simply because there were no wind speed values higher than 12 m/s and no wind power values higher than 1,200 kW in the test dataset.

Chapter 4

Statistics-Based Modelling

4.1 Persistence Modelling

4.1.1 Introduction

Nowadays, the persistence model is widely used in the electrical industry, especially for very short-term wind speed and wind power forecasting. In fact, it is the most straightforward and economical approach: the basic idea here is to view a past wind speed or wind power measurement as the future wind speed or wind power forecast (for example, the persistence model considers that the wind speed or wind power at time $t + 1$ is simply equal to the wind speed or wind power at time t). More specifically, the persistence model asserts the following relationships:

$$v_i = v_{i-\Delta t} \ , \tag{4.1}$$

and

$$P_i = P_{i-\Delta t} \ , \tag{4.2}$$

where v_i is the wind speed at time i, Δt is the time step size, and P_i is the wind power at time i.

From Equations (4.1) and (4.2), it can be seen that the structure of the persistence model is quite simple. Specifically, there are no variables except the time step size, and no model parameters need to be tuned.

4.1.2 Wind Speed Forecasting Based on a Persistence Model

In total, there was a set of 24-day historical wind speed measurements. However, in order to compare the predictive performance of the persistence model with that of the advanced models in the following sections, only the last 5 days of wind speed measurements were utilised for the wind speed forecasting in this case. In addition, the persistence model was evaluated over the last 4 days of available wind speed measurements. The first day of the last 5 days was included because the wind speed measurements for that day were applied to provide the wind speed forecasts for the second day.

For a comprehensive assessment of the persistence model in the wind speed forecasting, the different forecast time step sizes ranging from 1 to 48 steps were tested in the experiment. According to Equation (4.1), the wind speed forecasts based on the different time step sizes for the last 4 days were acquired. Since the temporal resolution of the wind speed measurements was 30 minutes, 1-step, 2-step, 3-step, 4-step, 6-step, 8-step, 12-step, 16-step, 24-step, and 48-step ahead corresponded to 30 minutes, 1 hour, 1.5 hours, 2 hours, 3 hours, 4 hours, 6 hours, 8 hours, 12 hours, and 24 hours in advance, respectively. According to Equations (3.9) to (3.14), the MBs, MAEs, RMSEs, IAs, MAPEs, and SMAPEs for the wind speed forecasting by using the persistence model and their 4-day average values were calculated. The corresponding results are shown in Tables 4.1 to 4.6.

Table 4.1. MBs for the wind speed forecasting by using the persistence model applied to the 4-day test dataset.

MB (m/s)		Forecast day				Average
		1	2	3	4	
Forecast time horizon	30 minutes	-0.01	-0.02	0.04	-0.07	-0.01
	1 hour	-0.04	-0.05	0.10	-0.15	-0.03
	1.5 hours	-0.07	-0.06	0.15	-0.21	-0.05
	2 hours	-0.07	-0.04	0.19	-0.30	-0.05
	3 hours	-0.13	-0.02	0.29	-0.56	-0.11
	4 hours	-0.22	-0.05	0.43	-0.88	-0.18
	6 hours	-0.30	-0.06	0.49	-1.41	-0.32
	8 hours	-0.33	-0.18	0.54	-1.72	-0.42
	12 hours	-0.26	-0.32	0.29	-1.98	-0.57
	24 hours	-0.19	0.02	-1.17	-0.34	-0.42

Table 4.2. MAEs for the wind speed forecasting by using the persistence model applied to the 4-day test dataset.

MAE (m/s)		Forecast day				Average
		1	2	3	4	
Forecast time horizon	30 minutes	0.70	0.56	0.61	0.59	0.61
	1 hour	1.10	0.67	0.71	0.83	0.83
	1.5 hours	1.30	0.80	0.90	0.97	0.99
	2 hours	1.41	0.89	0.99	1.11	1.10
	3 hours	1.49	0.92	1.11	1.37	1.22
	4 hours	1.56	1.16	1.33	1.58	1.41
	6 hours	1.75	1.10	1.80	1.80	1.62
	8 hours	1.79	1.09	2.14	2.09	1.78
	12 hours	1.70	1.43	2.86	2.87	2.22
	24 hours	1.59	1.07	2.29	3.69	2.16

Table 4.3. RMSEs for the wind speed forecasting by using the persistence model applied to the 4-day test dataset.

RMSE (m/s)		Forecast day				Average
		1	2	3	4	
Forecast time horizon	30 minutes	1.41	0.71	0.78	0.75	0.91
	1 hour	2.08	0.89	0.90	1.11	1.24
	1.5 hours	2.36	1.05	1.09	1.29	1.45
	2 hours	2.39	1.08	1.23	1.46	1.54
	3 hours	2.35	1.12	1.46	1.79	1.68
	4 hours	2.43	1.37	1.64	1.99	1.86
	6 hours	2.56	1.33	2.07	2.29	2.07
	8 hours	2.74	1.28	2.60	2.67	2.32
	12 hours	2.69	1.67	3.14	3.58	2.77
	24 hours	2.34	1.57	2.68	4.10	2.67

Table 4.4. IAs for the wind speed forecasting by using the persistence model applied to the 4-day test dataset.

IA		Forecast day				Average
		1	2	3	4	
Forecast time horizon	30 minutes	0.86	0.95	0.98	0.99	0.94
	1 hour	0.70	0.92	0.97	0.97	0.89
	1.5 hours	0.61	0.89	0.96	0.96	0.86
	2 hours	0.60	0.89	0.95	0.94	0.85
	3 hours	0.61	0.88	0.92	0.92	0.83
	4 hours	0.59	0.82	0.90	0.90	0.80
	6 hours	0.54	0.83	0.85	0.87	0.77
	8 hours	0.48	0.84	0.76	0.82	0.72
	12 hours	0.50	0.73	0.65	0.67	0.64
	24 hours	0.62	0.76	0.75	0.56	0.67

Table 4.5. MAPEs for the wind speed forecasting by using the persistence model applied to the 4-day test dataset.

MAPE		Forecast day				Average
		1	2	3	4	
Forecast time horizon	30 minutes	25.48%	27.64%	18.32%	20.00%	22.86%
	1 hour	38.92%	34.83%	25.32%	26.74%	31.46%
	1.5 hours	47.26%	41.26%	35.73%	29.21%	38.37%
	2 hours	51.72%	43.10%	44.15%	31.84%	42.70%
	3 hours	61.54%	55.66%	58.83%	37.69%	53.43%
	4 hours	64.06%	68.58%	68.36%	43.77%	61.19%
	6 hours	72.08%	71.71%	89.43%	45.14%	69.59%
	8 hours	85.95%	58.45%	127.90%	49.28%	80.40%
	12 hours	69.72%	80.03%	164.96%	78.80%	98.38%
	24 hours	62.99%	51.97%	94.90%	148.03%	89.47%

Table 4.6. SMAPEs for the wind speed forecasting by using the persistence model applied to the 4-day test dataset.

SMAPE		Forecast day				Average
		1	2	3	4	
Forecast time horizon	30 minutes	24.71%	24.53%	17.75%	19.72%	21.68%
	1 hour	35.78%	28.85%	23.32%	25.95%	28.47%
	1.5 hours	41.41%	33.47%	30.62%	28.84%	33.58%
	2 hours	45.98%	37.57%	34.26%	32.56%	37.59%
	3 hours	50.03%	40.01%	38.59%	41.48%	42.53%
	4 hours	55.10%	48.87%	42.52%	49.95%	49.11%
	6 hours	63.42%	47.56%	54.43%	57.63%	55.76%
	8 hours	63.93%	48.63%	59.66%	64.21%	59.11%
	12 hours	58.81%	62.39%	78.48%	86.79%	71.62%
	24 hours	55.87%	41.96%	73.91%	97.77%	67.38%

From Tables 4.1 to 4.6, it can be seen that the persistence model performed well for the 30-minute ahead wind speed forecasting. Specifically, its 4-day average MB absolute value was only 0.01 m/s, which was almost equal to 0; its 4-day average MAE and RMSE were 0.61 m/s and 0.91 m/s, respectively, which were both less than 1 m/s; its 4-day average IA was 0.94, which was the only one above the level of 0.90; and its 4-day average MAPE and SMAPE were 22.86% and 21.68%, respectively, which were just slightly higher than 20.00%. Nevertheless, it is not surprising that with the rise in the forecast time horizon from 30 minutes to 12 hours, the 4-day average MB absolute value, MAE, RMSE, MAPE, and SMAPE for the wind speed forecasting by using the persistence model went up gradually. In the end, the values of these evaluation metrics for the 12-hour ahead wind speed forecasting, reaching 0.57 m/s, 2.22 m/s, 2.77 m/s, 98.38%, and 71.62%, respectively, were much higher than those for the 30-minute ahead wind speed forecasting. Additionally, the corresponding 4-day average IA decreased gradually with the increasing forecast time horizon. The 4-day average IA for the 12-hour ahead wind speed forecasting, as low as 0.64, was much worse than that for the 30-minute ahead wind speed forecasting. One interesting discovery is that the predictive performance of the 24-hour ahead wind speed forecasting was a little better than that of the 12-hour ahead wind speed forecasting according to

every single metric in this case. However, this can only be explained as an accidental phenomenon since it does not make any sense.

Another point that needs to be highlighted is that although the MBs for the 30-minute ahead wind speed forecasting were close to each other for the 4 single days, the differences among them became much larger as the forecast time horizon increased from 30 minutes to 24 hours. The same applied to the MAEs, RMSEs, IAs, MAPEs, and SMAPEs. For instance, the MB, MAE, RMSE, IA, MAPE, and SMAPE for the second day changed from -0.02 to 0.02 m/s, 0.56 to 1.07 m/s, 0.71 to 1.57 m/s, 0.95 to 0.76, 27.64% to 51.97%, and 24.53% to 41.96%, respectively, while these metrics for the fourth day changed from -0.07 to -0.34 m/s, 0.59 to 3.69 m/s, 0.75 to 4.10 m/s, 0.99 to 0.56, 20.00% to 148.03%, and 19.72% to 97.77%, respectively. These findings indicated that with the expansion of the forecast time horizon, the wind speed predictive performance of the persistence model became unstable, and the model reliability went down.

In the actual operation of wind farms, 30 minutes, 4 hours, and 24 hours are the most common wind power forecast time horizons as required. A comparison of the 30-minute, 4-hour, and 24-hour ahead wind speed forecasts provided by the persistence model and the historical wind speed measurements from the test dataset is shown in Figure 4.1. It is easy to see that the 30-minute ahead wind speed forecasts were incredibly close to the historical wind speed measurements. The 4-hour ahead wind speed predictive performance seemed still acceptable, although the errors at some time points were not small. In contrast, the difference between the 24-hour ahead wind speed forecasts and historical wind speed measurements was quite large. Especially in the last 2 days, there were clear opposite trends between the forecasts and measurements most of the time.

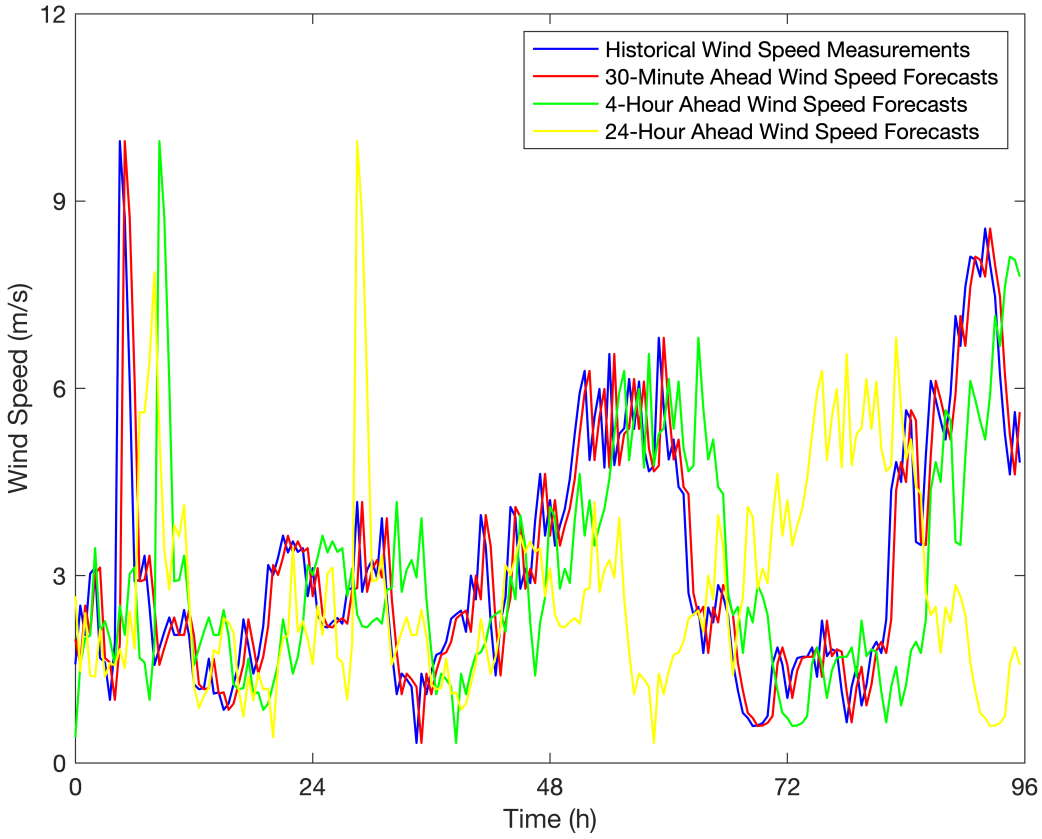

Figure 4.1. Comparison of the 30-minute, 4-hour, and 24-hour ahead wind speed forecasts provided by the persistence model and the historical wind speed measurements from the 4-day test dataset.

4.1.3 Wind Power Forecasting Based on a Persistence Model

Same as the wind speed forecasting based on a persistence model in Section 4.1.2, the predictive performance of the wind power forecasting based on a persistence model was assessed over the last 4 days of wind data. There are two ways of forecasting wind power based on the persistence model: direct forecasting and indirect forecasting.

(1) Direct forecasting

In this method, historical wind power measurements are the only necessary data and are simply regarded as future wind power forecasts. The 5-day historical wind power measurements in the identical time period as the historical wind speed measurements in Section 4.1.2 were used in this case. For a comprehensive assessment of the direct persistence model in the wind power forecasting, the different forecast time step sizes ranging from 1 to 48 steps were tested in the experiment. According to Equation (4.2), the direct wind power forecasts based on the different time step sizes for the last 4 days were acquired. The correspondence between the time step size and time horizon was the same as that explained in Section 4.1.2. According to Equations (3.9) to (3.12) and (3.15) to (3.18), the MBs, MAEs, RMSEs, IAs, accuracy rates, and qualification rates for the wind power forecasting by using the direct persistence model and their 4-day average values were calculated. The corresponding results are shown in Tables 4.7 to 4.12.

Table 4.7. MBs for the wind power forecasting by using the direct persistence model applied to the 4-day test dataset.

MB (kW)		Forecast day				Average
		1	2	3	4	
Forecast time horizon	30 minutes	-0.1	-1.9	2.0	-5.4	-1.4
	1 hour	-1.5	-3.6	5.1	-11.0	-2.8
	1.5 hours	-2.8	-4.6	7.4	-14.9	-3.7
	2 hours	-3.5	-3.7	7.9	-19.4	-4.7
	3 hours	-6.2	-2.3	9.2	-39.1	-9.6
	4 hours	-7.4	-6.2	14.3	-69.8	-17.3
	6 hours	-8.3	-5.3	14.3	-125.4	-31.2
	8 hours	-8.3	-9.7	17.6	-154.5	-38.7
	12 hours	-8.3	-9.7	1.2	-177.4	-48.5
	24 hours	-16.5	35.6	-123.1	-50.7	-38.7

Table 4.8. MAEs for the wind power forecasting by using the direct persistence model applied to the 4-day test dataset.

MAE (kW)		Forecast day				Average
		1	2	3	4	
Forecast time horizon	30 minutes	58.2	26.6	59.0	50.7	48.6
	1 hour	98.5	33.5	63.0	81.5	69.1
	1.5 hours	114.9	38.0	74.6	93.5	80.3
	2 hours	117.7	41.7	80.3	110.1	87.5
	3 hours	119.3	37.6	89.6	135.5	95.5
	4 hours	119.6	48.2	112.4	149.3	107.4
	6 hours	124.4	39.0	155.4	146.9	116.4
	8 hours	122.4	37.5	192.2	164.2	129.1
	12 hours	123.6	46.2	247.2	212.4	157.3
	24 hours	109.9	70.0	158.4	307.3	161.4

Table 4.9. RMSEs for the wind power forecasting by using the direct persistence model applied to the 4-day test dataset.

RMSE (kW)		Forecast day				Average
		1	2	3	4	
Forecast time horizon	30 minutes	199.4	46.0	90.9	82.7	104.7
	1 hour	285.0	54.1	92.0	128.2	139.8
	1.5 hours	312.4	57.9	105.6	156.9	158.2
	2 hours	312.8	59.6	116.8	181.7	167.7
	3 hours	312.5	53.1	131.7	217.4	178.7
	4 hours	318.1	65.5	154.4	228.7	191.7
	6 hours	319.8	56.0	191.5	224.1	197.9
	8 hours	319.7	57.6	227.3	253.9	214.6
	12 hours	319.7	64.1	271.3	313.7	242.2
	24 hours	264.0	209.1	202.7	360.7	259.1

Table 4.10. IAs for the wind power forecasting by using the direct persistence model applied to the 4-day test dataset.

IA		Forecast day				Average
		1	2	3	4	
Forecast time horizon	30 minutes	0.74	0.68	0.90	0.97	0.82
	1 hour	0.33	0.49	0.89	0.92	0.66
	1.5 hours	0.10	0.40	0.85	0.88	0.56
	2 hours	0.10	0.37	0.82	0.84	0.53
	3 hours	0.10	0.56	0.77	0.75	0.54
	4 hours	0.09	0.21	0.66	0.68	0.41
	6 hours	0.09	0.45	0.47	0.66	0.42
	8 hours	0.09	0.38	0.26	0.57	0.33
	12 hours	0.09	0.23	0.02	0.40	0.18
	24 hours	0.12	0.24	0.41	0.06	0.21

Table 4.11. Accuracy rates for the wind power forecasting by using the direct persistence model applied to the 4-day test dataset.

Accuracy rate		Forecast day				Average
		1	2	3	4	
Forecast time horizon	30 minutes	86.71%	96.94%	93.94%	94.49%	93.02%
	1 hour	81.00%	96.40%	93.87%	91.45%	90.68%
	1.5 hours	79.17%	96.14%	92.96%	89.54%	89.45%
	2 hours	79.15%	96.03%	92.21%	87.89%	88.82%
	3 hours	79.17%	96.46%	91.22%	85.51%	88.09%
	4 hours	78.80%	95.63%	89.71%	84.75%	87.22%
	6 hours	78.68%	96.27%	87.23%	85.06%	86.81%
	8 hours	78.69%	96.16%	84.85%	83.08%	85.69%
	12 hours	78.69%	95.72%	81.91%	79.09%	83.85%
	24 hours	82.40%	86.06%	86.49%	75.95%	82.73%

Table 4.12. Qualification rates for the wind power forecasting by using the direct persistence model applied to the 4-day test dataset.

Qualification rate		Forecast day				Average
		1	2	3	4	
Forecast time horizon	30 minutes	95.83%	100.00%	100.00%	100.00%	98.96%
	1 hour	91.67%	100.00%	100.00%	97.92%	97.40%
	1.5 hours	91.67%	100.00%	100.00%	93.75%	96.35%
	2 hours	91.67%	100.00%	100.00%	93.75%	96.35%
	3 hours	91.67%	100.00%	97.92%	85.42%	93.75%
	4 hours	91.67%	100.00%	97.92%	79.17%	92.19%
	6 hours	91.67%	100.00%	95.83%	91.67%	94.79%
	8 hours	91.67%	100.00%	89.58%	81.25%	90.62%
	12 hours	91.67%	100.00%	87.50%	81.25%	90.10%
	24 hours	91.67%	95.83%	91.67%	75.00%	88.54%

From Tables 4.7 to 4.12, it can be found that the predictive performance of the direct persistence model for the 30-minute ahead wind power forecasting was good. To be precise, its 4-day average MB absolute value, MAE, RMSE, IA, accuracy rate, and qualification rate were 1.4 kW, 48.6 kW, 104.7 kW, 0.82, 93.02%, and 98.96%, respectively. However, it is not surprising that as the forecast time horizon expanded from 30 minutes to 24 hours, the 4-day average MB absolute value, MAE, and RMSE for the wind power forecasting by using the direct persistence model increased gradually, while the corresponding 4-day average IA, accuracy rate, and qualification rate decreased. At last, the values of these evaluation metrics for the 24-hour ahead direct wind power forecasting, reaching 38.7 kW, 161.4 kW, 259.1 kW, 0.21, 82.73%, and 88.54%, respectively, were much worse than those for the 30-minute ahead direct wind power forecasting. Nevertheless, a few exceptions existed in this case. Specifically, the 4-day average MB absolute value for the 24-hour ahead direct wind power forecasting was a little smaller than that for the 12-hour ahead direct wind power forecasting; the 4-day average IAs for the 3-hour, 6-hour, and 24-hour ahead direct wind power forecasting were a little higher than those for the 2-hour, 4-hour, and 12-hour ahead direct wind power forecasting, respectively; and the 4-day average qualification rate for

the 6-hour ahead direct wind power forecasting was a little higher than those for the 4-hour and 3-hour ahead direct wind power forecasting. All of them can be regarded as accidental phenomena since they do not make any sense.

Another point that needs to be highlighted is that although the MBs for the 30-minute ahead direct wind power forecasting were close to each other for the 4 single days, the differences among them became much larger as the forecast time horizon increased from 30 minutes to 24 hours. The same applied to the MAEs, RMSEs, IAs, accuracy rates, and qualification rates. For instance, the MB, MAE, RMSE, IA, accuracy rate, and qualification rate for the second day changed from -1.9 to 35.6 kW, 26.6 to 70.0 kW, 46.0 to 209.1 kW, 0.68 to 0.24, 96.94% to 86.06%, and 100.00% to 95.83%, respectively, while these metrics for the fourth day changed from -5.4 to -50.7 kW, 50.7 to 307.3 kW, 82.7 to 360.7 kW, 0.97 to 0.06, 94.49% to 75.95%, and 100.00% to 75.00%, respectively. These findings indicated that with the expansion of the forecast time horizon, the wind power predictive performance of the direct persistence model became unstable, and the model reliability went down.

In the actual operation of wind farms, 30 minutes, 4 hours, and 24 hours are the most common wind power forecast time horizons as required. A comparison of the 30-minute, 4-hour, and 24-hour ahead wind power forecasts provided by the direct persistence model and the historical wind power measurements from the test dataset is shown in Figure 4.2. It is easy to see that the 30-minute ahead direct wind power forecasts were incredibly close to the historical wind power measurements. The 4-hour ahead direct wind power predictive performance seemed still acceptable, although the errors at some time points were not small. In contrast, the difference between the 24-hour ahead direct wind power forecasts and historical wind power measurements was quite large. Especially in the last 2 days, there were clearly different trends between the forecasts and measurements most of the time.

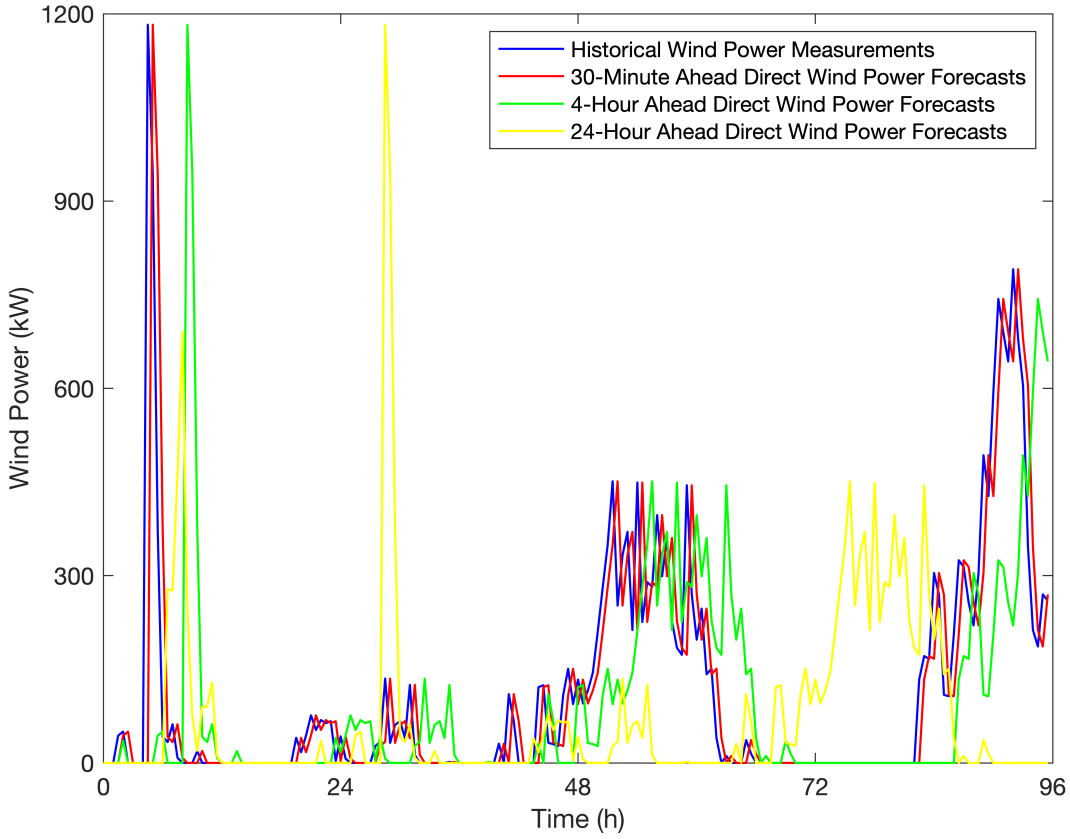

Figure 4.2. Comparison of the 30-minute, 4-hour, and 24-hour ahead wind power forecasts provided by the direct persistence model and the historical wind power measurements from the 4-day test dataset.

(2) Indirect forecasting

In this method, historical wind speed measurements are considered future wind speed forecasts that can be converted to wind power forecasts by using a power curve model. As discussed in Section 4.1.2, the wind speed forecasts provided by the persistence model for the multiple forecast time horizons were obtained. In this case, all the wind speed forecasts for the last 4 days were input to the ANFIS-based power curve model created in Section 3.7, and then the corresponding indirect wind power forecasts could be acquired as the output of the power curve model. According to Equations (3.9) to (3.12) and (3.15) to (3.18), the MBs, MAEs, RMSEs, IAs, accuracy rates, and

qualification rates for the wind power forecasting by using the indirect persistence model and their 4-day average values were calculated. The corresponding results are shown in Tables 4.13 to 4.18.

Table 4.13. MBs for the wind power forecasting by using the indirect persistence model applied to the 4-day test dataset.

MB (kW)		Forecast day				Average
		1	2	3	4	
Forecast time horizon	30 minutes	-2.1	-0.4	-4.6	5.1	-0.5
	1 hour	-3.5	-2.8	-0.8	-1.1	-2.0
	1.5 hours	-4.8	-3.7	1.5	-4.9	-3.0
	2 hours	-5.0	-2.7	2.1	-10.3	-4.0
	3 hours	-8.1	-0.9	3.5	-30.7	-9.1
	4 hours	-10.1	-4.1	8.6	-62.9	-17.1
	6 hours	-11.1	-3.5	8.9	-120.2	-31.5
	8 hours	-11.2	-8.4	12.8	-151.9	-39.7
	12 hours	-11.0	-8.8	-3.5	-175.5	-49.7
	24 hours	-14.5	33.9	-122.1	-57.2	-40.0

Table 4.14. MAEs for the wind power forecasting by using the indirect persistence model applied to the 4-day test dataset.

MAE (kW)		Forecast day				Average
		1	2	3	4	
Forecast time horizon	30 minutes	54.7	28.3	64.2	56.2	50.8
	1 hour	94.7	33.1	67.0	78.9	68.4
	1.5 hours	110.3	38.7	76.7	93.7	79.8
	2 hours	114.4	41.6	83.1	111.1	87.6
	3 hours	116.2	36.8	92.2	135.0	95.1
	4 hours	115.9	46.6	113.3	147.3	105.7
	6 hours	120.7	38.1	155.2	147.7	115.4
	8 hours	119.1	35.7	186.3	165.6	126.7
	12 hours	120.9	48.4	239.9	211.5	155.2
	24 hours	110.0	66.2	161.3	300.6	159.5

Table 4.15. RMSEs for the wind power forecasting by using the indirect persistence model applied to the 4-day test dataset.

RMSE (kW)		Forecast day				Average
		1	2	3	4	
Forecast time horizon	30 minutes	193.6	45.9	93.8	85.4	104.7
	1 hour	275.5	52.8	98.1	129.0	138.9
	1.5 hours	301.8	57.6	112.2	158.8	157.6
	2 hours	302.4	59.4	121.2	183.7	166.7
	3 hours	302.4	51.6	137.5	218.3	177.5
	4 hours	306.6	63.9	160.1	227.2	189.5
	6 hours	308.9	54.3	191.2	225.1	194.9
	8 hours	308.9	55.3	224.6	253.1	210.5
	12 hours	309.1	65.2	262.9	313.5	237.7
	24 hours	262.7	193.6	204.9	354.6	254.0

Table 4.16. IAs for the wind power forecasting by using the indirect persistence model applied to the 4-day test dataset.

IA		Forecast day				Average
		1	2	3	4	
Forecast time horizon	30 minutes	0.74	0.68	0.88	0.97	0.82
	1 hour	0.33	0.49	0.87	0.93	0.65
	1.5 hours	0.11	0.38	0.83	0.89	0.55
	2 hours	0.10	0.36	0.80	0.84	0.53
	3 hours	0.10	0.58	0.74	0.76	0.54
	4 hours	0.10	0.22	0.62	0.70	0.41
	6 hours	0.10	0.47	0.45	0.67	0.42
	8 hours	0.10	0.42	0.25	0.58	0.34
	12 hours	0.10	0.20	0.03	0.40	0.18
	24 hours	0.12	0.26	0.40	0.07	0.21

Table 4.17. Accuracy rates for the wind power forecasting by using the indirect persistence model applied to the 4-day test dataset.

Accuracy rate		Forecast day				Average
		1	2	3	4	
Forecast time horizon	30 minutes	87.09%	96.94%	93.74%	94.31%	93.02%
	1 hour	81.63%	96.48%	93.46%	91.40%	90.74%
	1.5 hours	79.88%	96.16%	92.52%	89.42%	89.49%
	2 hours	79.84%	96.04%	91.92%	87.76%	88.89%
	3 hours	79.84%	96.56%	90.83%	85.45%	88.17%
	4 hours	79.56%	95.74%	89.33%	84.85%	87.37%
	6 hours	79.41%	96.38%	87.26%	84.99%	87.01%
	8 hours	79.40%	96.32%	85.03%	83.12%	85.97%
	12 hours	79.39%	95.65%	82.47%	79.10%	84.15%
	24 hours	82.48%	87.09%	86.34%	76.36%	83.07%

Table 4.18. Qualification rates for the wind power forecasting by using the indirect persistence model applied to the 4-day test dataset.

Qualification rate		Forecast day				Average
		1	2	3	4	
Forecast time horizon	30 minutes	95.83%	100.00%	100.00%	100.00%	98.96%
	1 hour	91.67%	100.00%	100.00%	97.92%	97.40%
	1.5 hours	91.67%	100.00%	100.00%	93.75%	96.35%
	2 hours	91.67%	100.00%	100.00%	93.75%	96.35%
	3 hours	91.67%	100.00%	95.83%	85.42%	93.23%
	4 hours	91.67%	100.00%	97.92%	85.42%	93.75%
	6 hours	91.67%	100.00%	95.83%	91.67%	94.79%
	8 hours	91.67%	100.00%	91.67%	81.25%	91.15%
	12 hours	91.67%	100.00%	89.58%	81.25%	90.62%
	24 hours	91.67%	95.83%	91.67%	77.08%	89.06%

From Tables 4.13 to 4.18, it can be found that the predictive performance of the indirect persistence model for the 30-minute ahead wind power forecasting was good. To be precise, its 4-day average MB absolute value, MAE, RMSE, IA, accuracy rate, and qualification rate were 0.5 kW, 50.8 kW, 104.7 kW, 0.82, 93.02%, and 98.96%, respectively. However, it is not surprising that as the forecast time horizon expanded from 30 minutes to 24 hours, the 4-day average MB absolute value, MAE, and RMSE for the wind power forecasting by using the indirect persistence model increased gradually, while the corresponding 4-day average IA, accuracy rate, and qualification rate decreased. At last, the values of these evaluation metrics for the 24-hour ahead indirect wind power forecasting, reaching 40.0 kW, 159.5 kW, 254.0 kW, 0.21, 83.07%, and 89.06%, respectively, were much worse than those for the 30-minute ahead indirect wind power forecasting. Nevertheless, a few exceptions existed in this case. Specifically, the 4-day average MB absolute value for the 24-hour ahead indirect wind power forecasting was a little smaller than that for the 12-hour ahead indirect wind power forecasting; the 4-day average IAs for the 3-hour, 6-hour, and 24-hour ahead indirect wind power forecasting were a little higher than those for the 2-hour, 4-hour, and 12-hour ahead indirect wind power forecasting, respectively; and the 4-day average qualification rate

for the 6-hour ahead indirect wind power forecasting was a little higher than that for the 4-hour ahead indirect wind power forecasting, which was a little higher than that for the 3-hour ahead indirect wind power forecasting. All of them can be regarded as accidental phenomena since they do not make any sense.

Another point that needs to be highlighted is that although the MBs for the 30-minute ahead indirect wind power forecasting were close to each other for the 4 single days, the differences among them became much larger as the forecast time horizon increased from 30 minutes to 24 hours. The same applied to the MAEs, RMSEs, IAs, accuracy rates, and qualification rates. For instance, the MB, MAE, RMSE, IA, accuracy rate, and qualification rate for the second day changed from -0.4 to 33.9 kW, 28.3 to 66.2 kW, 45.9 to 193.6 kW, 0.68 to 0.26, 96.94% to 87.09%, and 100.00% to 95.83%, respectively, while these metrics for the fourth day changed from 5.1 to -57.2 kW, 56.2 to 300.6 kW, 85.4 to 354.6 kW, 0.97 to 0.07, 94.31% to 76.36%, and 100.00% to 77.08%, respectively. These findings indicated that with the expansion of the forecast time horizon, the wind power predictive performance of the indirect persistence model became unstable, and the model reliability went down.

In the actual operation of wind farms, 30 minutes, 4 hours, and 24 hours are the most common wind power forecast time horizons as required. A comparison of the 30-minute, 4-hour, and 24-hour ahead wind power forecasts provided by the indirect persistence model and the historical wind power measurements from the test dataset is shown in Figure 4.3. It is easy to see that the 30-minute ahead indirect wind power forecasts were incredibly close to the historical wind power measurements. The 4-hour ahead indirect wind power predictive performance seemed still acceptable, although the errors at some time points were not small. In contrast, the difference between the 24-hour ahead indirect wind power forecasts and historical wind power measurements was quite large. Especially in the last 2 days, there were clearly different trends between the forecasts and measurements most of the time.

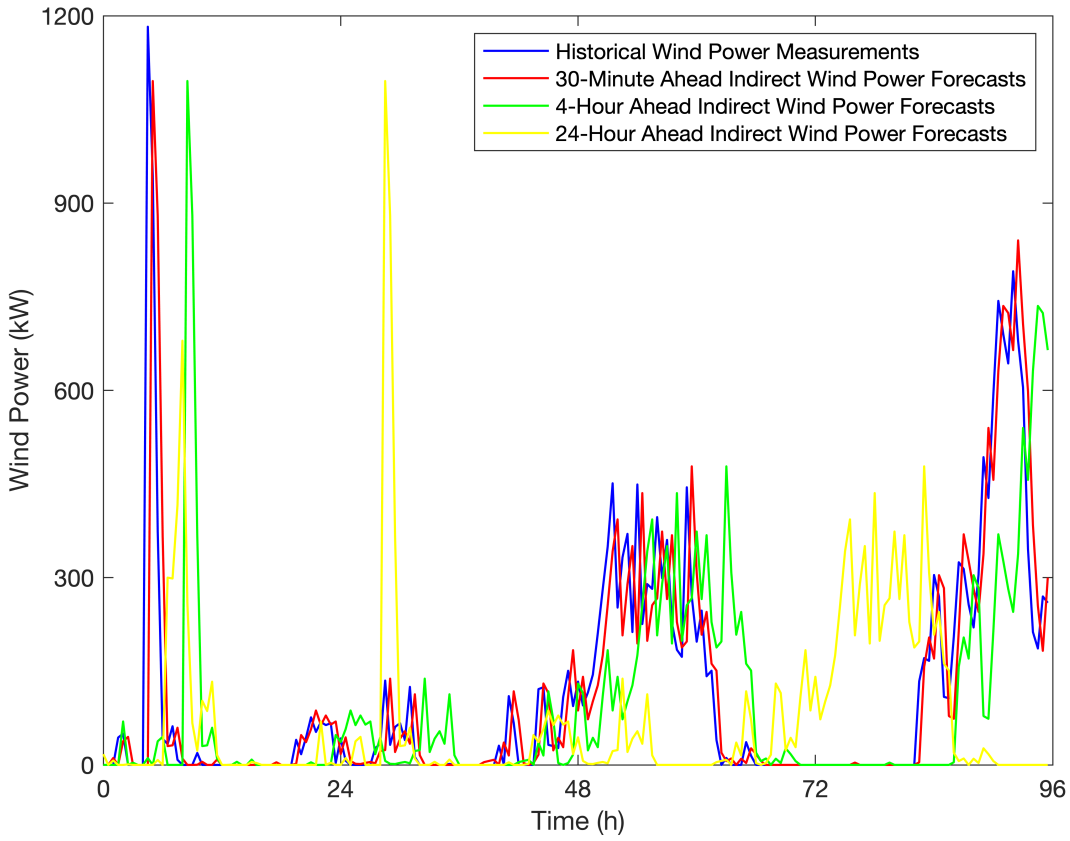

Figure 4.3. Comparison of the 30-minute, 4-hour, and 24-hour ahead wind power forecasts provided by the indirect persistence model and the historical wind power measurements from the 4-day test dataset.

4.1.4 Summary

The persistence modelling, a widely used statistical approach for wind speed and wind power forecasting in the electrical industry at the moment, is presented in Section 4.1. Basically, there are two ways of forecasting wind power based on a persistence model. One is called direct forecasting. In this method, historical wind power measurements are the only necessary data and are simply regarded as future wind power forecasts. The other is indirect forecasting, in which historical wind speed measurements are considered future wind speed forecasts that can be converted to wind power forecasts by utilising a power

curve model. In this case study, both the direct and indirect wind power forecasting were tested for 10 different forecast time horizons ranging from 30 minutes to 24 hours. The results revealed that the direct and indirect persistence models performed quite well for the 30-minute ahead wind power forecasting. However, with the rise in the forecast time horizon, the MB, MAE, RMSE, IA, accuracy rate, and qualification rate for the wind power forecasting by using the direct and indirect persistence models deteriorated.

4.2 ARIMA Time Series Modelling

4.2.1 Introduction

The ARIMA time series modelling, as a classical statistical method, was proposed for wind speed and wind power forecasting in this study. Its general idea was to use an ARIMA model to forecast wind speed first and then convert wind speed forecasts to wind power forecasts by using a power curve model. In order to create the ARIMA model and evaluate its predictive performance, the original 24-day historical wind speed measurements were divided into two groups. In particular, the data from the first 20 days were used as a training dataset, and the remaining data from the last 4 days were used as a test dataset. According to the training dataset, the most appropriate ARIMA model could be finally determined and employed to forecast the wind speeds for the last 4 days. The details of the ARIMA model configuration and predictive performance evaluation are described in the following subsections within this section.

4.2.2 Exploratory Data Analysis

In order to figure out the significant properties of given data, an exploratory data analysis is usually the first step for time series modelling. One of the most basic and practical exploratory graphical approaches is to plot the data in the time series. The graph of the 24-day historical wind speed measurements against time is given in Figure 4.4. Not only the obvious but also the less clear statistical features of the studied data can be gleaned from the visual interpretation of the plot. The details of the analysis are represented as follows.

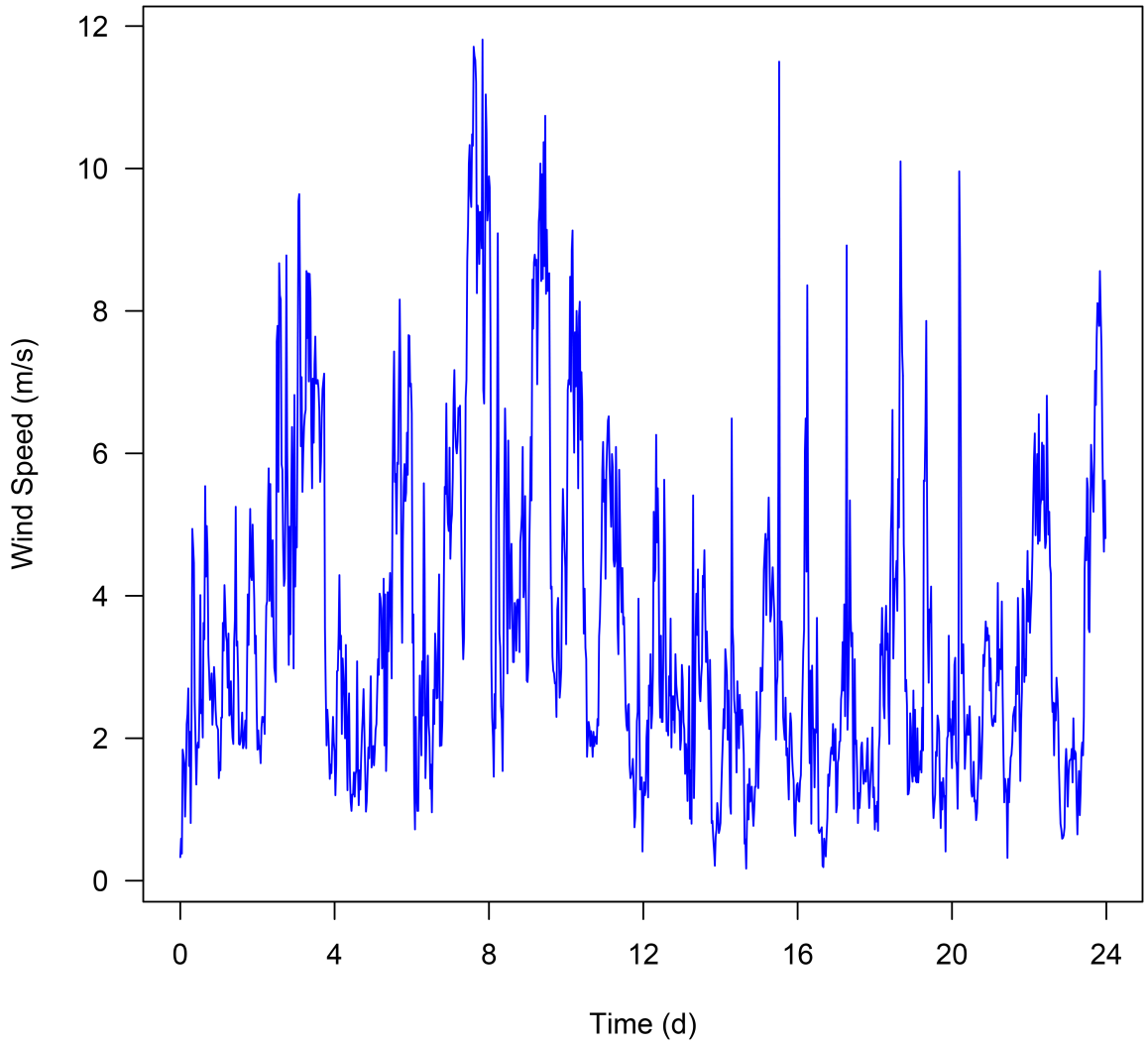

Figure 4.4. Time series of the 24-day historical wind speed measurements.

(1) Autocorrelation

From Figure 4.4, it was discovered that at some specific sections of the time series, the wind speed measurements were consistently above the overall mean level, whereas at

the other locations, the wind speed measurements below the mean level were grouped together. These patterns of persistence signified that the historical wind speed measurements were probably autocorrelated.

(2) Seasonality

Wind speed is affected by climate and meteorological conditions, which vary greatly in the four seasons. Since the time period of the historical wind speed measurements applied in this study was only 24 days, it did not make sense to argue that the season had a significant influence on the data. Besides, Figure 4.4 demonstrates that there were no obvious cycles in the data. Hence, the historical wind speed measurements were supposed to be not seasonal or periodic.

(3) Non-stationarity

From Figure 4.4, it was found that the historical wind speed measurements fluctuated and followed the overall mean level in general. This plot was not similar to those ones of typical non-stationarity. Therefore, this time series of the historical wind speed measurements seemed to be stationary. However, when data were only marginally non-stationary, it might not be sure whether a differencing operation was needed to account for homogeneous non-stationarity.

(4) Trends

The existence of trends in data is one of the non-stationarity forms. As shown in Figure 4.4, there were no uptrends or downtrends in the historical wind speed measurements against time. Neither deterministic nor stochastic trend was present here. This finding followed the previous statement that the studied data in this case might be stationary.

(5) Need for a transformation

At this stage, it was hard to determine whether a transformation was required for the studied data just from the plot. Nevertheless, at the diagnostic checking stage of the model construction, this issue would be detected by examining the properties of the residuals.

(6) Extreme values

The existence of the extreme wind speed values was easily detected in Figure 4.4. By comparing the plots of the time series of the 24-day historical wind speed measurements (see Figure 4.4) and the corresponding time series of the 24-day historical wind power measurements (see Figure 4.5), it was concluded that all the extreme wind speed values

were correct because they contributed to the corresponding extreme wind power values at their specific time points, except the extreme wind speed value on the 16th day. By looking up the original wind dataset, the wind speed value was 11.5 m/s at 12:30 UTC on the 26th of August 2015, while the corresponding wind power value was 16.8 kW. Apparently, these two values did not match each other, which means it was very likely that either the wind speed value or the wind power value was incorrectly recorded. However, among the total 1,152 values, only one wrong extreme value would not significantly affect the model construction.

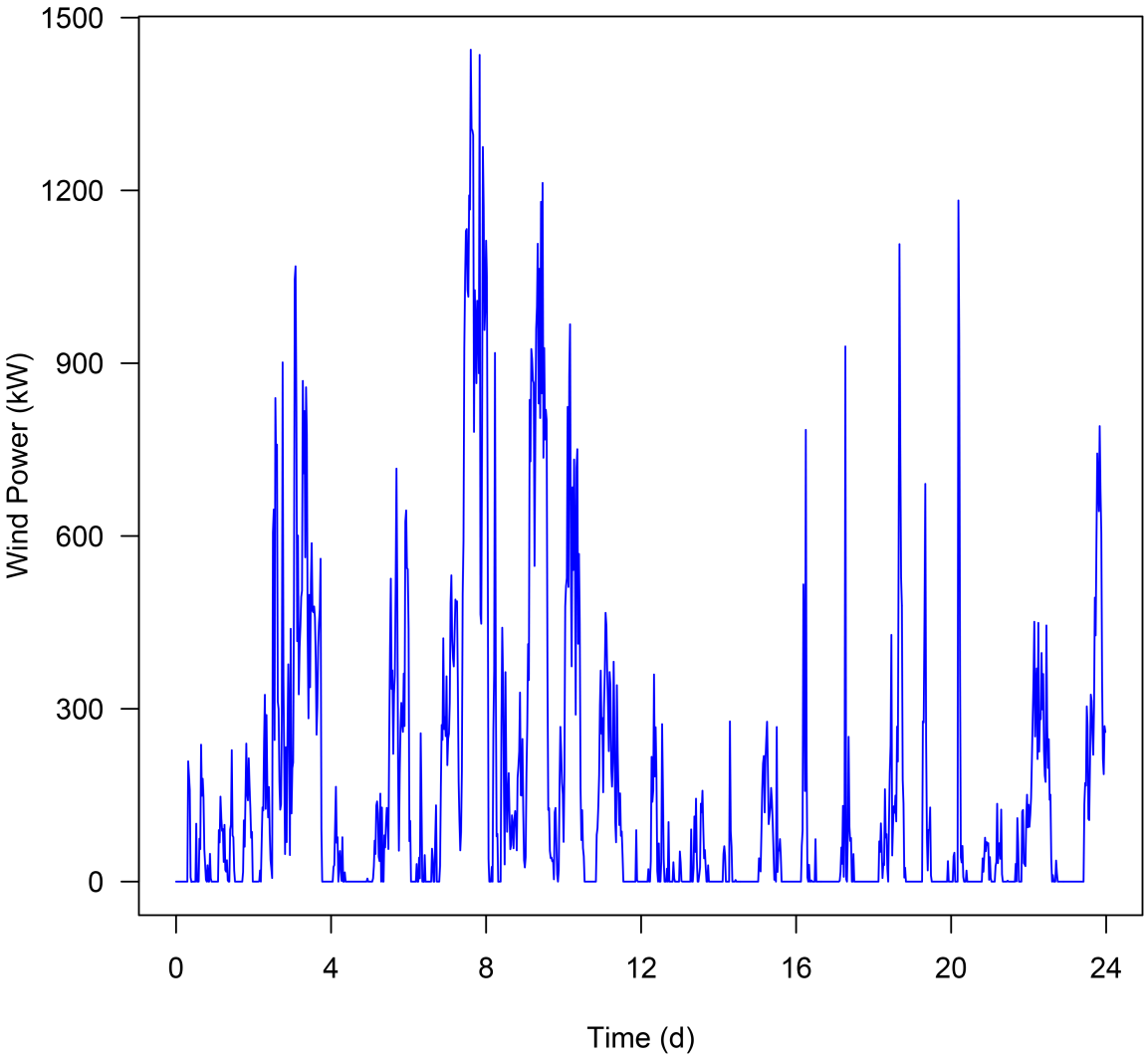

Figure 4.5. Time series of the 24-day historical wind power measurements.

(7) Long term cycles

Actually, this set of 24-day historical wind speed measurements was too short to detect any long-term cycles graphically.

(8) Known or unknown interventions

There were no known interventions to the historical wind speed measurements in the studied wind farm. Nevertheless, the operator of the wind farm sometimes does intervene in the running of the wind turbines. For instance, a wind turbine may be stopped by human operations for maintenance or repair purposes even if the wind speed is good for the wind turbine running. By comparing Figures 4.4 and 4.5, it was concluded that the studied wind turbine was running normally during the period of 24 days. Moreover, the plot of the historical wind speed measurements (see Figure 4.4) also indicates that there were no apparent changes in the mean level of the historical wind speed measurements due to unknown interventions.

(9) Proposed type of time series models

According to the results of the exploratory data analysis on the historical wind speed measurements discussed above, the non-seasonal ARIMA model was entertained as the most appropriate type of time series models to be fitted to the time series of the historical wind speed measurements.

4.2.3 Confirmatory Data Analysis

After proposing the non-seasonal ARIMA model as the most suitable time series model to describe the historical wind speed measurements from the training dataset against time, the next step of the time series modelling was the confirmatory data analysis. Following the three stages of model construction, namely identification, parameter estimation, and diagnostic checking, the most appropriate ARIMA model could finally be created to describe the studied data in the time series.

4.2.3.1 Identification

In order to create the most appropriate ARIMA (p, d, q) model, there are three numbers of orders, namely the number of AR terms (the p value), number of differencing operations (the d value), and number of MA terms (the q value), need to be identified. At the stage of identification, the graphs of the sample ACF and sample PACF are usually examined to determine the values of these parameters.

(1) Sample autocorrelation function

The sample ACF of the time series of the historical wind speed measurements from the training dataset was calculated and is plotted against lag 30 in Figure 4.6. As shown in Figure 4.6, the sample ACF of the non-seasonal historical wind speed measurements attenuated relatively slow, revealing that it might be advisable to difference the data once.

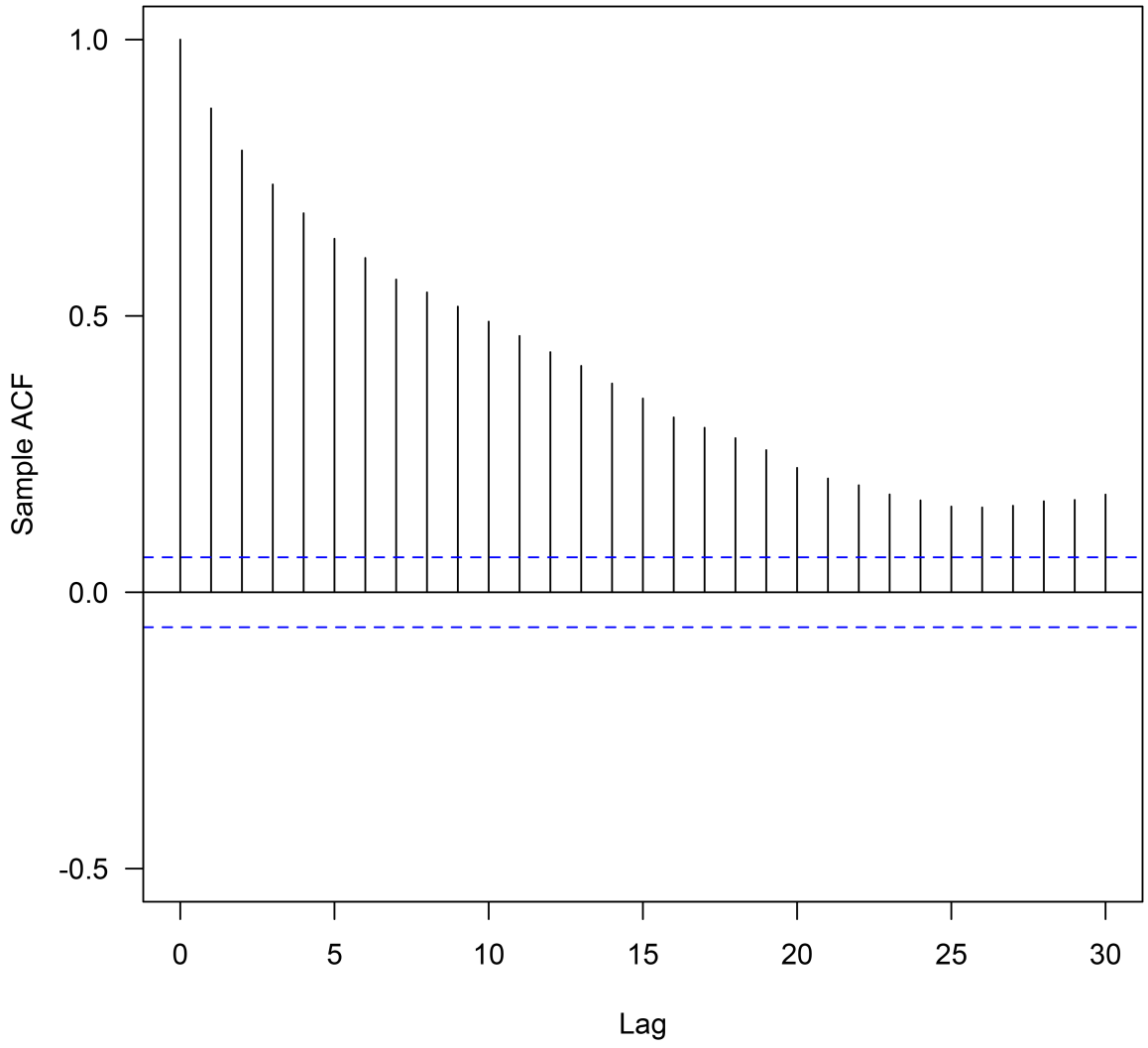

Figure 4.6. Sample ACF of the time series of the historical wind speed measurements from the 20-day training dataset.

The historical wind speed measurements from the training dataset against time were differenced according to Equation (2.43), and the results are shown in Figure 4.7,

from which it can be visually found that the mean level of the differenced historical wind speed measurements decreased to about 0. More specifically, the mean value was calculated to be 0.001720542 m/s, which was approximately equal to 0 m/s. Furthermore, compared with the original time series of the historical wind speed measurements (see Figure 4.4), the time series of the differenced historical wind speed measurements looked much more stationary.

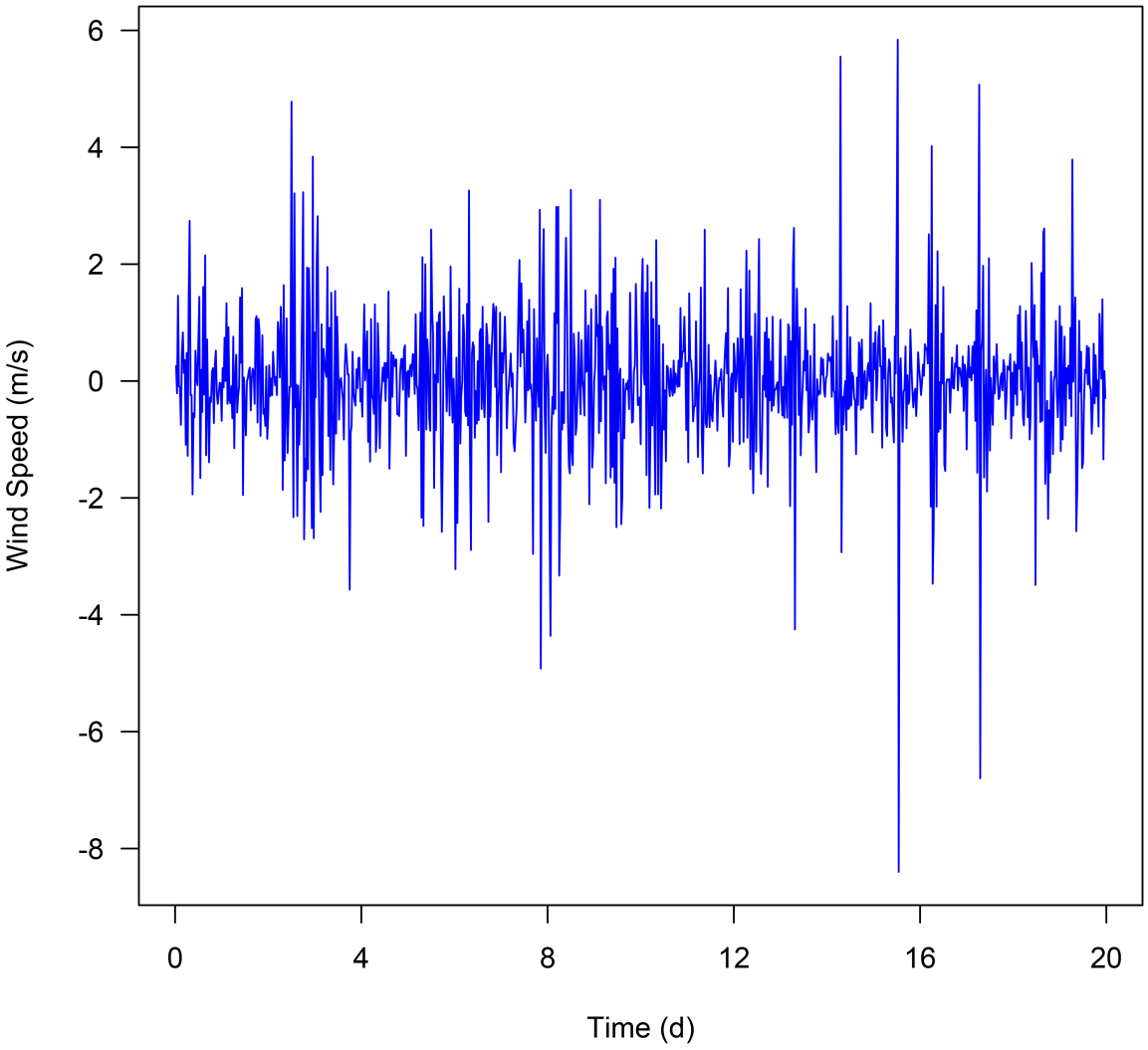

Figure 4.7. Time series of the differenced historical wind speed measurements from the 20-day training dataset.

The sample ACF of the time series of the differenced historical wind speed measurements from the training dataset was calculated and is plotted against lag 30 in Fig-

ure 4.8, from which it can be seen that after differencing the original historical wind speed measurements once, the homogeneous non-stationarity was removed, and the sample ACF died off quite quickly. In addition, the sample ACF damped out but did not appear to truncate, indicating the need for AR terms to model the time series of the differenced historical wind speed measurements. Nevertheless, one might also argue that the sample ACF cut off and was not significantly different from 0 after lag 1. Therefore, a pure MA model might be proposed as well.

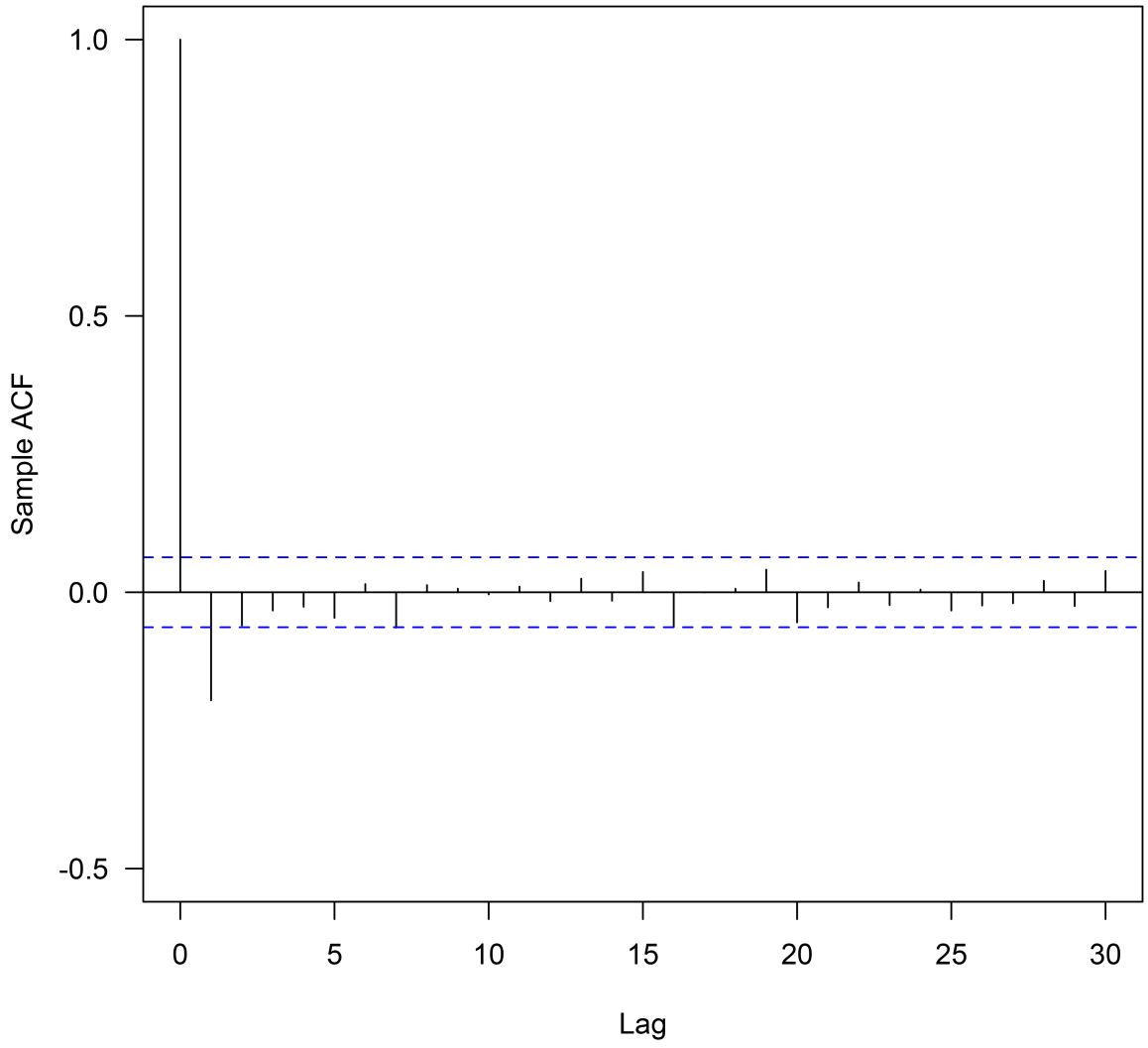

Figure 4.8. Sample ACF of the time series of the differenced historical wind speed measurements from the 20-day training dataset.

(2) Sample partial autocorrelation function

The sample PACF of the time series of the differenced historical wind speed mea-

surements from the training dataset was calculated and is plotted against lag 30 in Figure 4.9. Particularly, the sample PACF attenuated but did not appear to cut off, which suggested the need for MA terms to model the time series of the differenced historical wind speed measurements.

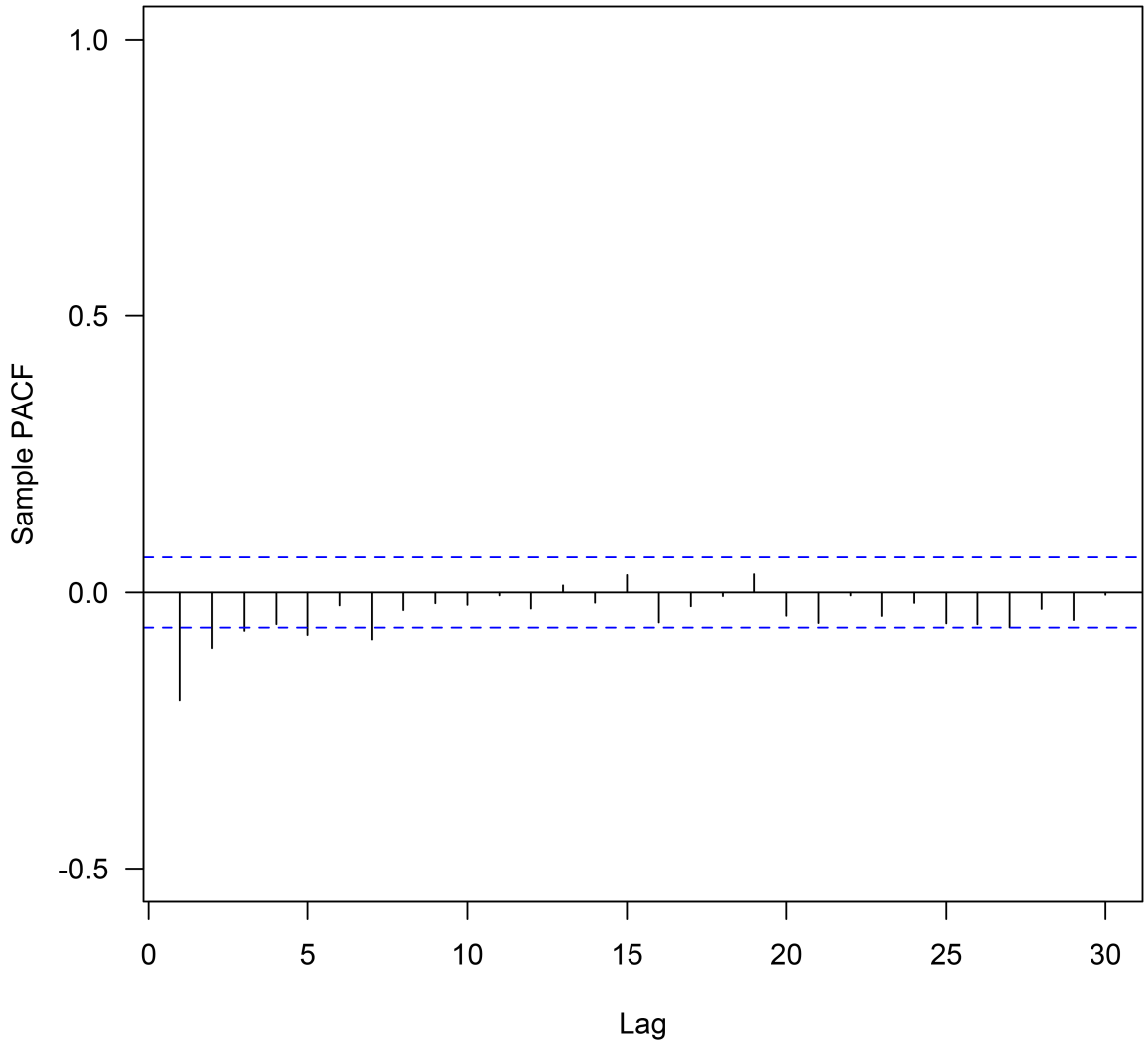

Figure 4.9. Sample PACF of the time series of the differenced historical wind speed measurements from the 20-day training dataset.

(3) Proposed ARIMA models

As discussed above, the original historical wind speed measurements from the train-

ing dataset were required to be differenced once to remove the homogeneous non-stationarity since the sample ACF of the time series of the original historical wind speed measurements died off relatively slow. Thus, the d value was determined to be 1. Besides, the sample ACF of the time series of the differenced historical wind speed measurements was not significantly different from 0 after lag 1. Hence, the q value was proposed to be 1. Additionally, the sample PACF of the time series of the differenced historical wind speed measurements was not significantly different from 0 after lag 7. Since the sample PACFs at lags 4 and 6 were within the confidence interval, the p value was proposed to be 1, 2, 3, 5, or 7. Moreover, a pure MA model was also proposed in the above sample ACF section. In conclusion, the orders of the proposed ARIMA models were summarised as follows: $(0, 1, 1)$, $(1, 1, 1)$, $(2, 1, 1)$, $(3, 1, 1)$, $(5, 1, 1)$, and $(7, 1, 1)$.

4.2.3.2 Parameter Estimation

By examining the figures of the sample ACF and PACF of the time series of the differenced historical wind speed measurements from the training dataset (see Figures 4.8 and 4.9), the orders required for the ARIMA model were ascertained. In total, there were six tentative models identified to describe the differenced historical wind speed measurements in the time series. At this stage, an approach of maximum likelihood is usually used to calculate the maximum likelihood estimates (MLEs) and standard errors (SEs) for the parameters of the AR and MA terms in the ARIMA models. Besides, the Akaike information criterion (AIC) method is advised to select the most appropriate model from the tentative ones.

The MLEs, SEs, and AICs of the tentative ARIMA models fitted to the time series of the differenced historical wind speed measurements from the training dataset were calculated and are shown in Table 4.19. Among the six tentative ARIMA models, the ARIMA $(3, 1, 1)$ model had the minimum AIC value (2,949.48). However, for the ϕ_3 in the ARIMA $(3, 1, 1)$ model, its absolute value of the MLE was less than 1.96 times that of the SE. Thus, it could be claimed that the estimate for the ϕ_3 was not significantly different from 0, and the ϕ_3 should be left out of the model. Consequently, the ARIMA $(2, 1, 1)$ model might be the best choice. To be precise, for the parameters of the AR and MA terms in the ARIMA $(2, 1, 1)$ model, the absolute values of the MLEs were all greater than 1.96 times those of the corresponding SEs. Therefore, it could be declared that even at the level of 1% significance, these estimates for the parameters were significantly different from 0, and the parameters should be included in the model. In addition, the AIC value of the ARIMA $(2, 1, 1)$ model was just a little bit higher than that of the ARIMA $(3, 1, 1)$ model and was the second smallest among those of the six tentative ARIMA models. As a result, the

ARIMA $(2, 1, 1)$ model was selected as the best model to be fitted to the time series of the differenced historical wind speed measurements from the training dataset.

Table 4.19. MLEs, SEs, and AICs of the tentative ARIMA models fitted to the time series of the differenced historical wind speed measurements from the 20-day training dataset.

ARIMA (p, d, q)	Parameter	MLE	SE	AIC
$(0, 1, 1)$	θ_1	-0.2442	0.0352	2,979.85
	σ_a^2	1.304	/	
$(1, 1, 1)$	ϕ_1	0.6151	0.1083	2,962.4
	θ_1	-0.8249	0.0835	
	σ_a^2	1.277	/	
$(2, 1, 1)$	ϕ_1	0.7351	0.0334	2,949.77
	ϕ_2	0.1272	0.0330	
	θ_1	-0.9856	0.0090	
	σ_a^2	1.257	/	
$(3, 1, 1)$	ϕ_1	0.7313	0.0332	2,949.48
	ϕ_2	0.0929	0.0399	
	ϕ_3	0.0496	0.0328	
	θ_1	-0.9880	0.0080	
	σ_a^2	1.254	/	
$(5, 1, 1)$	ϕ_1	0.7314	0.0330	2,952.69
	ϕ_2	0.0906	0.0400	
	ϕ_3	0.0315	0.0401	
	ϕ_4	0.0128	0.0401	
	ϕ_5	0.0162	0.0327	
	θ_1	-0.9896	0.0075	
	σ_a^2	1.253	/	

ARIMA (p, d, q)	Parameter	MLE	SE	AIC
$(7, 1, 1)$	ϕ_1	0.3238	0.3542	2,969.86
	ϕ_2	-0.0082	0.0903	
	ϕ_3	-0.0263	0.0587	
	ϕ_4	-0.0326	0.0487	
	ϕ_5	-0.0492	0.0454	
	ϕ_6	0.0041	0.0481	
	ϕ_7	-0.0668	0.0448	
	θ_1	-0.5633	0.3556	
	σ_a^2	1.271	/	

As mentioned in Section 4.2.3.1, the mean value of the differenced historical wind speed measurements from the training dataset was approximately equal to 0 m/s. According to the estimates for the parameters given in Table 4.19, the selected ARIMA $(2, 1, 1)$ model can be written as

$$(1 - B)(1 - 0.7351B - 0.1272B^2)z_t = (1 + 0.9856B)a_t \ , \tag{4.3}$$

where B is the backshift operator, z_t is the differenced historical wind speed measurement at time t, and a_t is the white noise term at time t that is normally independently distributed (NID) with a mean of 0 and a variance of 1.257 (i.e., NID $(0, 1.257)$).

4.2.3.3 Diagnostic Checking

For the purpose of ensuring that the proposed ARIMA $(2, 1, 1)$ model was adequate to describe the time series of the differenced historical wind speed measurements from the training dataset, a couple of statistical tests had to be performed at the stage of diagnostic checking. More specifically, overfitting, consisting of one or more additional parameters in the model, was employed to test the adequacy of the proposed model at first. Then, a whiteness, a normality, and a constant variance test were applied to check if the estimated innovations or residuals of the calibrated ARIMA model were satisfied with the assumptions of independence, normality, and homoscedasticity, respectively. The details of these tests are explained as follows.

(1) Overfitting

Overfitting means fitting a more complex ARIMA model than the proposed one to check whether adding one or more parameters contributes to enhancing the fit. By referring to Figure 4.8, the sample ACF of the time series of the differenced historical wind speed measurements from the training dataset died off and was not significantly different from 0 after lag 1. Nevertheless, the sample ACF value at lag 2 was just on the lower limit of the confidence interval, which implied that the second order of the MA term might be helpful for the model construction. Hence, a test model generated by overfitting the proposed ARIMA $(2, 1, 1)$ model was the ARIMA $(2, 1, 2)$ model. For the purpose of a comprehensive study, the ARIMA $(0, 1, 2)$, ARIMA $(1, 1, 2)$, ARIMA $(3, 1, 2)$, ARIMA $(5, 1, 2)$, and ARIMA $(7, 1, 2)$ models were involved in the test as well. The MLEs, SEs, and AICs of the overfitted ARIMA models fitted to the time series of the differenced historical wind speed measurements from the training dataset were calculated and are shown in Table 4.20.

Table 4.20. MLEs, SEs, and AICs of the overfitted ARIMA models fitted to the time series of the differenced historical wind speed measurements from the 20-day training dataset.

ARIMA (p, d, q)	Parameter	MLE	SE	AIC
$(0, 1, 2)$	θ_1	-0.2370	0.0322	2,973.32
	θ_2	-0.1015	0.0346	
	σ_a^2	1.292	/	
$(1, 1, 2)$	ϕ_1	0.8929	0.0231	2,948.05
	θ_1	-1.1556	0.0426	
	θ_2	0.1660	0.0399	
	σ_a^2	1.254	/	
$(2, 1, 2)$	ϕ_1	1.1836	0.2421	2,948.34
	ϕ_2	-0.2476	0.2087	
	θ_1	-1.4405	0.2327	
	θ_2	0.4461	0.2293	
	σ_a^2	1.252	/	

ARIMA (p, d, q)	Parameter	MLE	SE	AIC
$(3, 1, 2)$	ϕ_1	0.6772	0.8175	2,951.96
	ϕ_2	0.1276	0.6273	
	ϕ_3	0.0717	0.0866	
	θ_1	-0.9355	0.8160	
	θ_2	-0.0526	0.8031	
	σ_a^2	1.254	/	
$(5, 1, 2)$	ϕ_1	0.0054	0.2647	2,954.49
	ϕ_2	0.6218	0.1948	
	ϕ_3	0.1000	0.0446	
	ϕ_4	0.0585	0.0331	
	ϕ_5	0.0026	0.0351	
	θ_1	-0.2626	0.2628	
	θ_2	-0.7178	0.2602	
	σ_a^2	1.252	/	
$(7, 1, 2)$	ϕ_1	0.1982	0.3431	2,956.22
	ϕ_2	0.4809	0.2525	
	ϕ_3	0.0788	0.0478	
	ϕ_4	0.0265	0.0379	
	ϕ_5	-0.0052	0.0365	
	ϕ_6	0.0527	0.0344	
	ϕ_7	-0.0049	0.0387	
	θ_1	-0.4556	0.3419	
	θ_2	-0.5298	0.3391	
	σ_a^2	1.249	/	

From Table 4.20, it can be found that for the parameters of the AR and MA terms in

the ARIMA $(3,1,2)$ and ARIMA $(7,1,2)$ models, the absolute values of the MLEs were all less than 1.96 times those of the corresponding SEs. Therefore, these two models would not be chosen in this case. Besides, for the ϕ_4 and ϕ_5 in the ARIMA $(5,1,2)$ model, their absolute values of the MLEs were both less than 1.96 times those of the SEs, indicating that these two parameters should not be considered for the ARIMA model. It had been proved that the ARIMA $(3,1,2)$ model was not suitable, and neither was the ARIMA $(5,1,2)$ model. Similarly, for the ϕ_2 and θ_2 in the ARIMA $(2,1,2)$ model, their absolute values of the MLEs were both less than 1.96 times those of the SEs. Hence, these two estimates for the parameters were not significantly different from 0, and the parameters should be left out of the model. It had been proved that the ARIMA $(1,1,1)$ model was inferior to the ARIMA $(2,1,1)$ model, and so was the ARIMA $(2,1,2)$ model. In addition, the ARIMA $(0,1,2)$ model would not be selected since its AIC value was the highest among all of those of the overfitted ARIMA models.

The most impressive find was the ARIMA $(1,1,2)$ model. To be precise, it had the smallest AIC value among the total 12 proposed ARIMA models mentioned above. Moreover, for the parameters in this model, the absolute values of the MLEs were all greater than 1.96 times those of the corresponding SEs. Thus, it could be announced that even at the level of 1% significance, these estimates for the parameters were significantly different from 0, and the parameters should be included in the model.

As mentioned in Section 4.2.3.1, the mean value of the differenced historical wind speed measurements from the training dataset was approximately equal to 0 m/s. According to the estimates for the parameters given in Table 4.20, the selected ARIMA $(1,1,2)$ model can be written as

$$(1-B)(1-0.8929B)z_t = (1+1.1556B-0.1660B^2)a_t \ , \tag{4.4}$$

where B is the backshift operator, z_t is the differenced historical wind speed measurement at time t, and a_t is the white noise term at time t that is NID with a mean of 0 and a variance of 1.254 (i.e., NID $(0, 1.254)$).

In strict, the ARIMA $(1,1,2)$ model could not be simply regarded as an overfitted model based on the previously selected ARIMA $(2,1,1)$ model. The reason was that although the second order of the MA term was added to the ARIMA $(2,1,1)$ model, the second order of the AR term was removed. In conclusion, it was hard to figure out which one was better to be fitted to the time series of the differenced historical wind speed measurements from the training dataset between the ARIMA $(2,1,1)$ and ARIMA $(1,1,2)$ models at this stage.

(2) Whiteness test

The residuals of the ARIMA $(2, 1, 1)$ and ARIMA $(1, 1, 2)$ models fitted to the time series of the differenced historical wind speed measurements from the training dataset were calculated and are plotted against time in Figures 4.10 and 4.11, respectively.

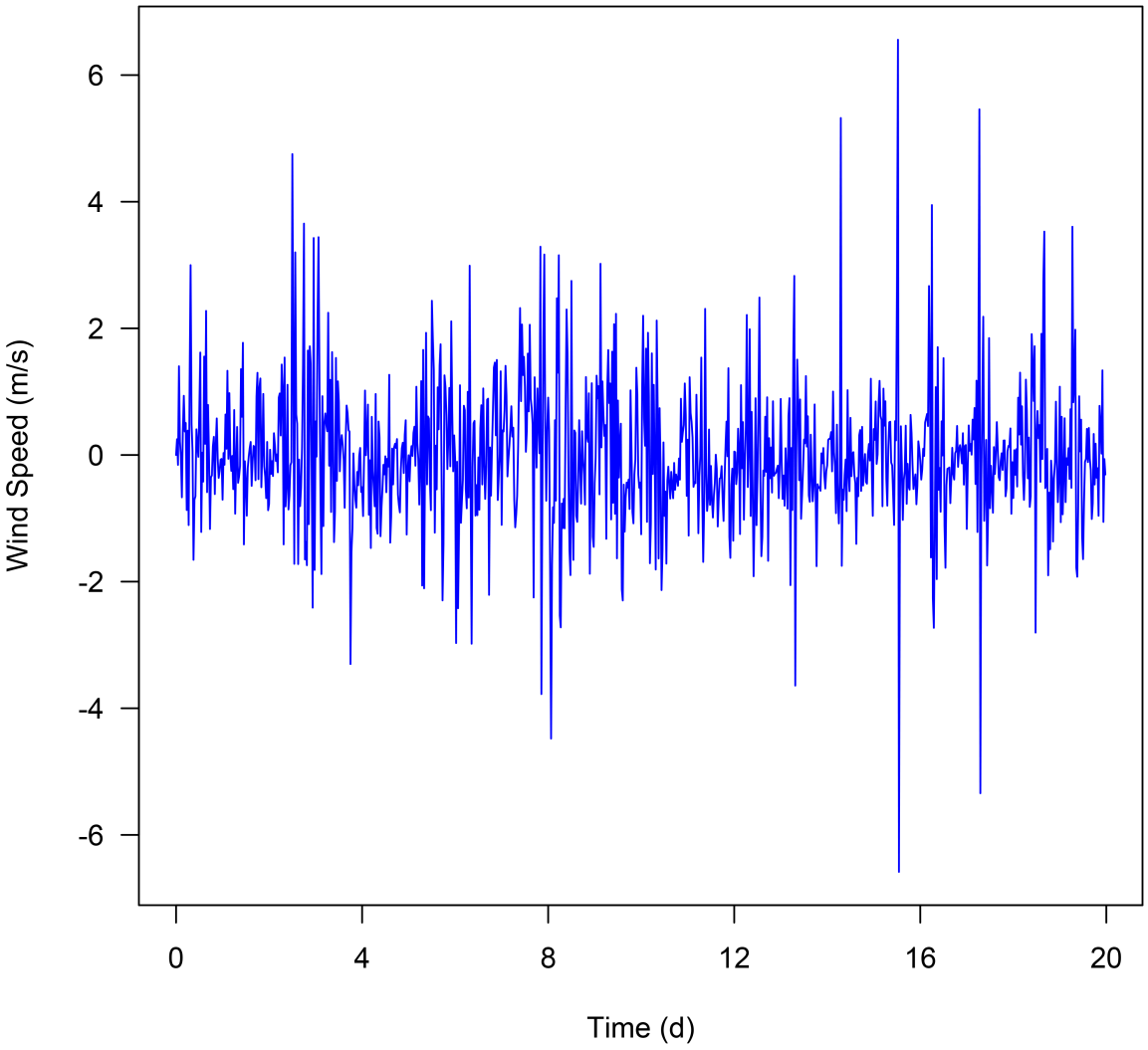

Figure 4.10. Time series of the residuals of the ARIMA $(2, 1, 1)$ model fitted to the time series of the differenced historical wind speed measurements from the 20-day training dataset.

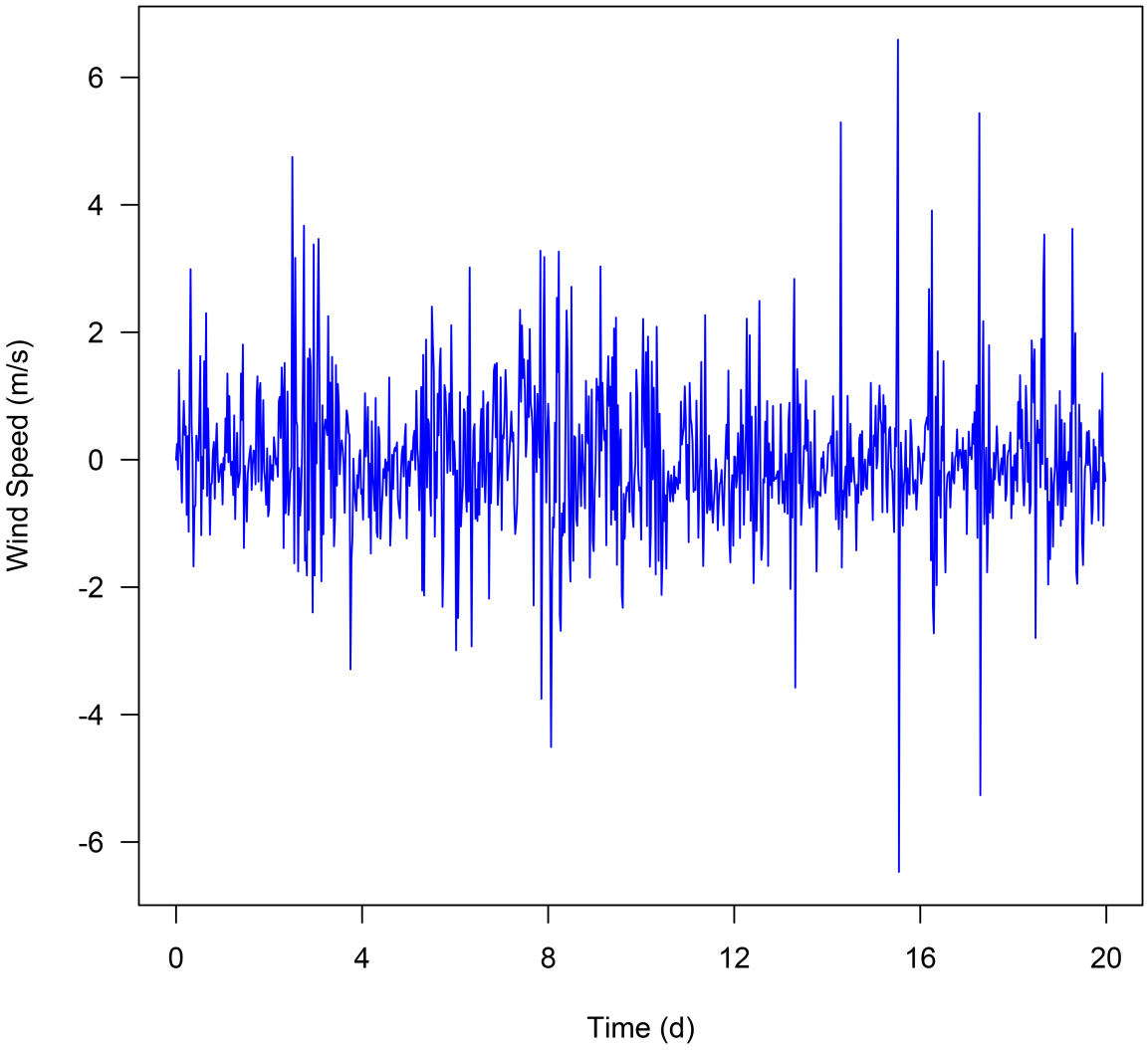

Figure 4.11. Time series of the residuals of the ARIMA $(1, 1, 2)$ model fitted to the time series of the differenced historical wind speed measurements from the 20-day training dataset.

Among the three assumptions for innovations, independence is the principal one. The most informative method to check whether the estimated residuals are uncorrelated or

white is to examine the graph of the residual autocorrelation function (RACF). The sample RACFs of the ARIMA $(2, 1, 1)$ and ARIMA $(1, 1, 2)$ models fitted to the time series of the differenced historical wind speed measurements from the training dataset were calculated and are plotted against lag 30 in Figures 4.12 and 4.13, respectively. From Figures 4.12 and 4.13, it can be found that the values of the sample RACFs of the ARIMA $(2, 1, 1)$ and ARIMA $(1, 1, 2)$ models were all within the 95% confidence interval after lag 0, which means all the residuals were uncorrelated and indicates that the innovations of the selected ARIMA $(2, 1, 1)$ and ARIMA $(1, 1, 2)$ models for the differenced historical wind speed measurements from the training dataset satisfied the whiteness assumption.

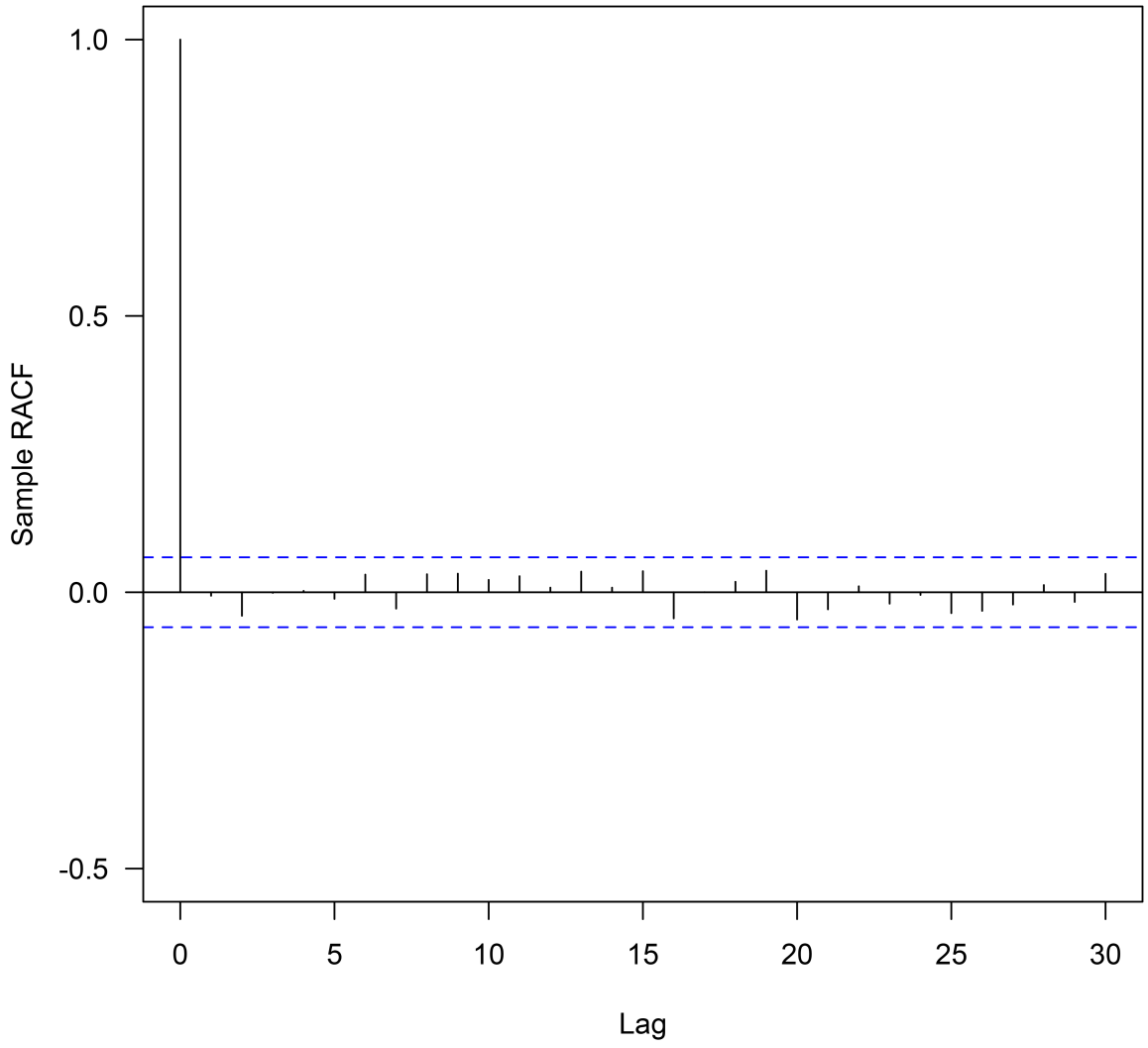

Figure 4.12. Sample RACF of the ARIMA $(2, 1, 1)$ model fitted to the time series of the differenced historical wind speed measurements from the 20-day training dataset.

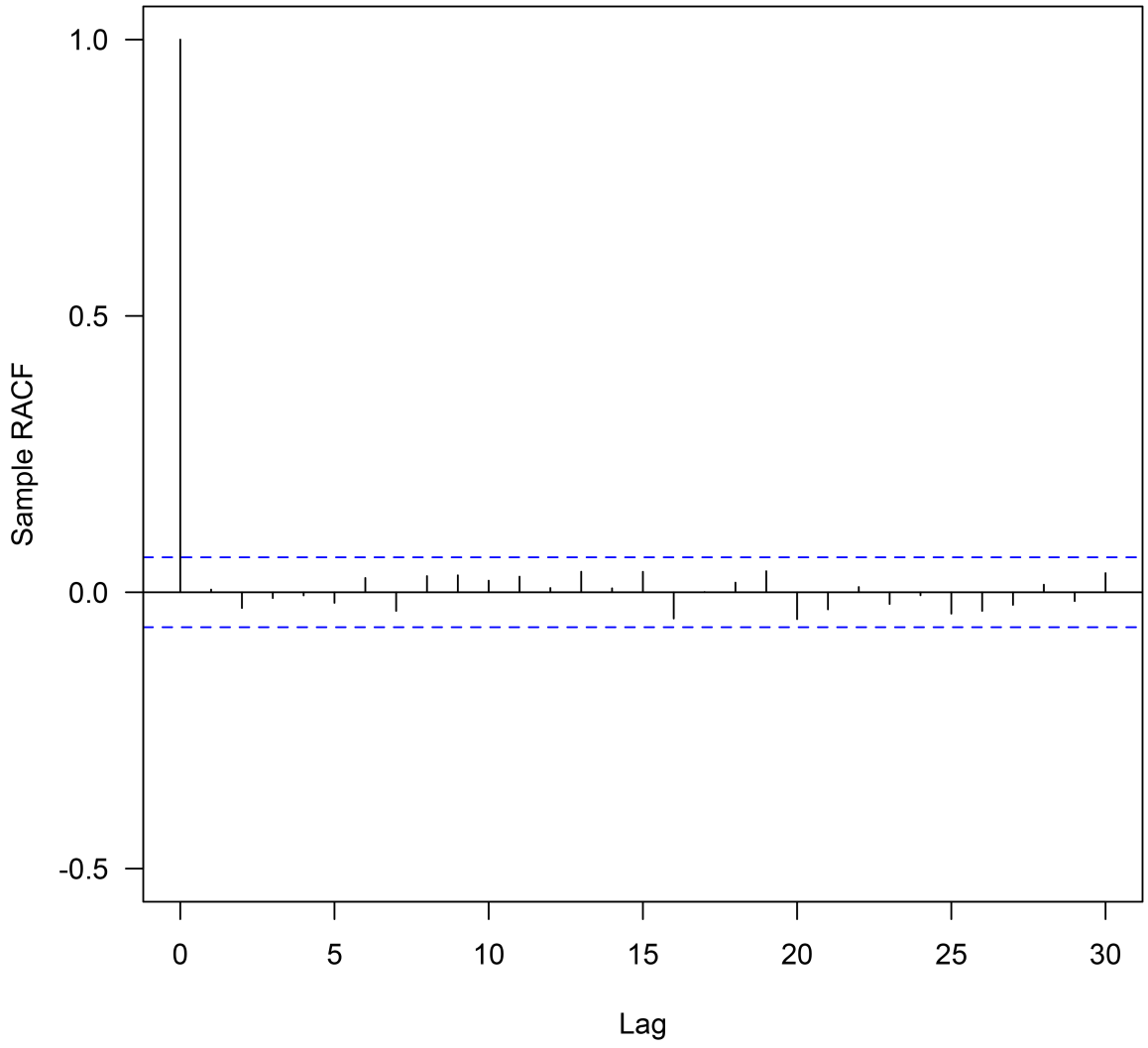

Figure 4.13. Sample RACF of the ARIMA $(1, 1, 2)$ model fitted to the time series of the differenced historical wind speed measurements from the 20-day training dataset.

(3) Normality test

Innovations, represented by a_t, are assumed to be identically and independently dis-

tributed for ARIMA models. In particular, in the maximum likelihood estimation method, innovations are developed to be Gaussian or normally distributed. The normality tests for the residuals of the ARIMA $(2, 1, 1)$ and ARIMA $(1, 1, 2)$ models fitted to the time series of the differenced historical wind speed measurements from the training dataset were performed, and the results are shown in Table 4.21. Additionally, the Lilliefors (Kolmogorov-Smirnov) normality test was applied here.

Table 4.21. Results of the normality tests for the residuals of the ARIMA $(2, 1, 1)$ and ARIMA $(1, 1, 2)$ models fitted to the time series of the differenced historical wind speed measurements from the 20-day training dataset.

Proposed model	D value	p value
ARIMA $(2, 1, 1)$	0.069885	5.781E-12
ARIMA $(1, 1, 2)$	0.069918	5.622E-12

From Table 4.21, it can be seen that the p values of the residuals of the fitted ARIMA $(2, 1, 1)$ and ARIMA $(1, 1, 2)$ models (5.781E-12 and 5.622E-12, respectively) were extremely small. Hence, the null hypothesis was rejected, implying that the innovations did not follow a normal distribution. In view of this situation, a Box-Cox transformation method was proposed to transform the differenced historical wind speed measurements from the training dataset. Then, the ARIMA $(2, 1, 1)$ and ARIMA $(1, 1, 2)$ models needed to be refitted to the differenced-and-transformed historical wind speed measurements from the training dataset in order to calculate the new parameters for the proposed models. Finally, the residuals could be corrected.

For the Box-Cox transformation, the critical point was to determine an appropriate parameter λ. The automatic selection for the Box-Cox transformation parameter by R (a programming language) was around 0.33. For the comparative analysis purpose, the additional values of λ in the range of 0.05 to 0.60 with an interval of 0.05 were examined in the time series of the differenced historical wind speed measurements from the training dataset, and the results are shown in Table 4.22.

Table 4.22. Results of the normality tests for the residuals of the ARIMA $(2, 1, 1)$ and ARIMA $(1, 1, 2)$ models refitted the time series of the differenced-and-transformed historical wind speed measurements from the 20-day training dataset.

λ	Refitted ARIMA $(2, 1, 1)$		Refitted ARIMA $(1, 1, 2)$	
	D value	p value	D value	p value
0.05	0.053483	8.28E-07	0.054198	5.317E-07
0.10	0.047562	2.511E-05	0.047724	2.302E-05
0.15	0.044724	0.0001093	0.042509	0.00032
0.20	0.043041	0.0002488	0.039694	0.001141
0.25	0.041953	0.0004148	0.038127	0.002212
0.30	0.038636	0.001791	0.037041	0.003435
0.33	0.036299	0.004599	0.035792	0.005589
0.35	0.03635	0.004508	0.035586	0.006044
0.40	0.034676	0.008485	0.034238	0.009951
0.45	0.033991	0.01087	0.035043	0.007409
0.50	0.03683	0.003735	0.036585	0.004113
0.55	0.039697	0.00114	0.039744	0.001117
0.60	0.04239	0.0003384	0.044344	0.000132

From Table 4.22, it can be seen that all the p values were greater than those in Table 4.21, while all the D values were smaller than those in Table 4.21. These results of the normality tests suggested that the Box-Cox transformation acted on the studied data indeed. The residuals of the ARIMA $(2, 1, 1)$ and ARIMA $(1, 1, 2)$ models refitted the time series of the differenced-and-transformed historical wind speed measurements from the training dataset were much closer to a normal distribution. In general, to pass a normality test, the p value should be greater than 0.05, so that the null hypothesis can be accepted, which means the distribution of data is normal. Unfortunately, there were no p values greater than 0.05 in this case. Nevertheless, the maximum p value (0.01087) occurred when the parameter of the Box-Cox transformation was 0.45, and the refitted model was the ARIMA $(2, 1, 1)$ model. At least, this p value was greater

than 0.01. In other words, the null hypothesis of the residuals satisfying a normal distribution could not be rejected with 99% confidence. Besides, the corresponding D value was the smallest one among all the D values. Therefore, the Box-Cox transformation with the parameter of 0.45 was determined to transform the differenced historical wind speed measurements from the training dataset, and the ARIMA $(2, 1, 1)$ model was selected.

In addition, the sample RACF of the ARIMA $(2, 1, 1)$ model refitted to the time series of the differenced-and-transformed historical wind speed measurements from the training dataset was calculated and is plotted against lag 30 in Figure 4.14, from which it can be found that the values of the sample RACF of the refitted ARIMA $(2, 1, 1)$ model were all within the 95% confidence interval after lag 0, which means all the residuals were uncorrelated and indicates that the innovations of the ARIMA $(2, 1, 1)$ model refitted to the differenced-and-transformed historical wind speed measurements from the training dataset satisfied the whiteness assumption.

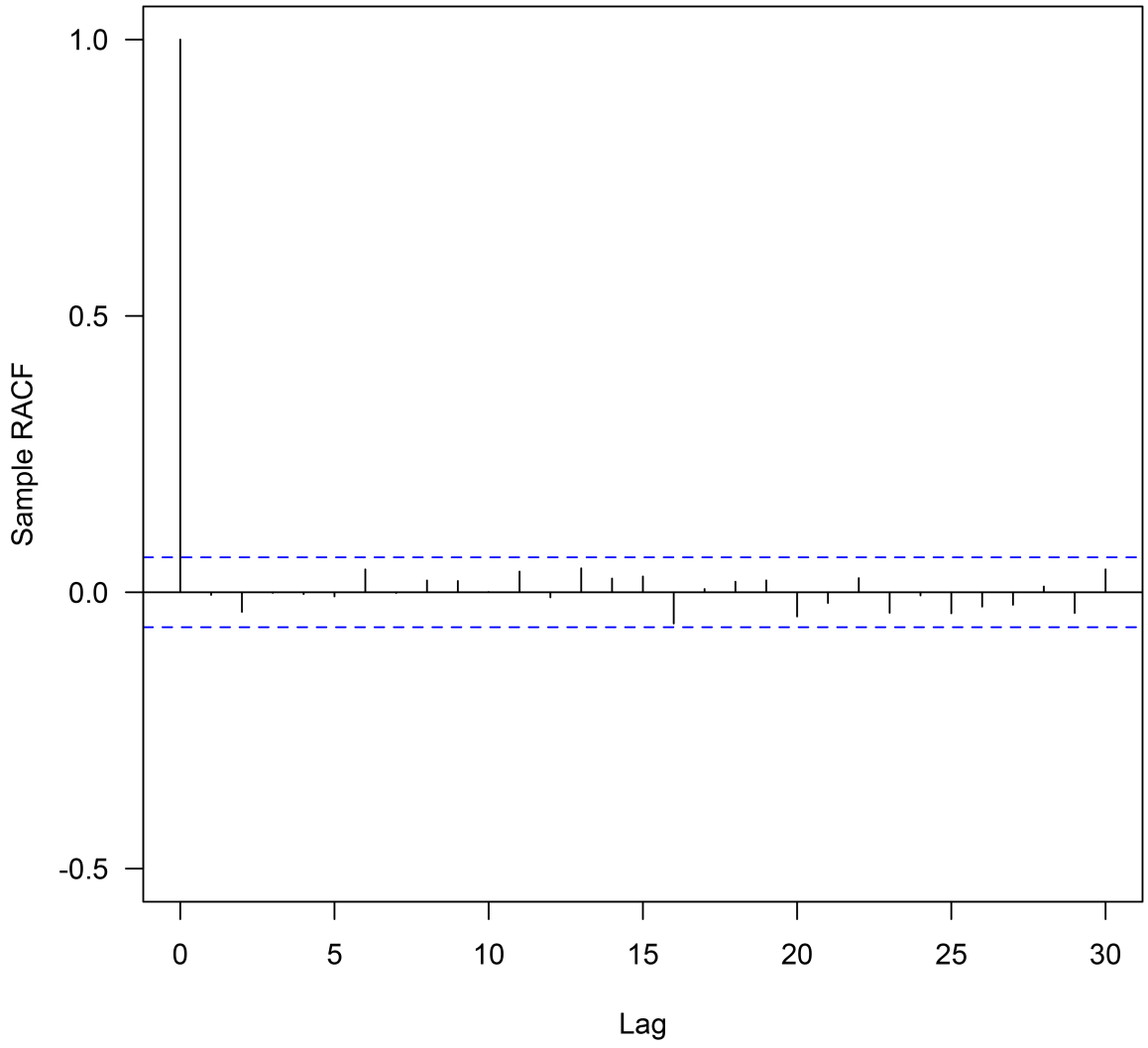

Figure 4.14. Sample RACF of the ARIMA $(2, 1, 1)$ model refitted to the time series of the differenced-and-transformed historical wind speed measurements from the 20-day training dataset.

(4) Constant variance test

A constant variance, called homoscedasticity in statistics, is assumed to exist in the residuals of a fitted ARIMA model. Levene's test was used for testing the homogeneity of the variance of the innovations in this study. The constant variance tests for the residuals of the ARIMA $(2, 1, 1)$ models fitted to the differenced and refitted to the differenced-and-transformed historical wind speed measurements from the training dataset were performed, and the results are shown in Table 4.23.

Table 4.23. Results of the constant variance tests for the residuals of the ARIMA $(2, 1, 1)$ models fitted to the differenced and refitted to the differenced-and-transformed historical wind speed measurements from the 20-day training dataset.

Type of data	$P_r\ (> F)$
Differenced historical wind speed measurements from the training dataset	0.1806
Differenced-and-transformed historical wind speed measurements from the training dataset	0.9238

As can be seen in Table 4.23, the P_r value of the ARIMA $(2, 1, 1)$ model fitted to the differenced historical wind speed measurements from the training dataset was 0.1806, which was greater than 0.05, indicating that the null hypothesis could not be rejected. In other words, the innovations passed the constant variance test. By contrast, the P_r value of the ARIMA $(2, 1, 1)$ model fitted to the differenced-and-transformed historical wind speed measurements from the training dataset, 0.9238, was much larger than that of the ARIMA $(2, 1, 1)$ model fitted to the differenced historical wind speed measurements from the training dataset and quite close to 1. This result showed the contribution of the Box-Cox transformation once again. By applying the Box-Cox transformation, the innovations could be announced to be homoscedastic with much more confidence.

4.2.3.4 Most Appropriate Model

Following the identification (see Section 4.2.3.1), parameter estimation (see Section 4.2.3.2), and diagnostic checking (see Section 4.2.3.3) stages, the most appropriate model, ARIMA $(2, 1, 1)$, to describe the differenced-and-transformed historical wind speed measurements from the training dataset was constructed. In the process of refitting the ARIMA $(2, 1, 1)$ model to the time series of the differenced historical wind speed measurements from the

training dataset transformed by applying the Box-Cox transformation with the parameter of 0.45, the MLEs, SEs, and AIC of the ARIMA $(2, 1, 1)$ model were calculated and are shown in Table 4.24.

Table 4.24. MLEs, SEs, and AIC of the ARIMA $(2, 1, 1)$ model refitted to the differenced-and-transformed historical wind speed measurements from the 20-day training dataset.

ARIMA (p, d, q)	Parameter	MLE	SE	AIC
$(2, 1, 1)$	ϕ_1	0.7395	0.0333	1,535.4
	ϕ_2	0.1220	0.0329	
	θ_1	-0.9858	0.0085	
	σ_a^2	0.2876	/	

From Table 4.24, it can be found that for the parameters of the AR and MA terms in the ARIMA $(2, 1, 1)$ model fitted to the differenced-and-transformed historical wind speed measurements from the training dataset, the absolute values of the MLEs were all greater than 1.96 times those of the corresponding SEs. Therefore, it could be declared that even at the level of 1% significance, these estimates for the parameters were significantly different from 0, and the parameters should be included in the model. By comparing Table 4.24 with Tables 4.19 and 4.20, it can be seen that the variance of the white noise of the ARIMA $(2, 1, 1)$ model fitted to the Box-Cox transformed time series, 0.2876, was much smaller than those of the ARIMA models fitted to the untransformed time series. Furthermore, the AIC value of the ARIMA $(2, 1, 1)$ model fitted to the Box-Cox transformed time series, 1,535.4, dropped dramatically. All of these findings revealed the benefits provided by the Box-Cox transformation.

As mentioned in Section 4.2.3.1, the mean value of the differenced historical wind speed measurements from the training dataset was approximately equal to 0 m/s. According to the estimates for the parameters given in Table 4.24, the most appropriate model, ARIMA $(2, 1, 1)$ fitted to the Box-Cox transformed time series, can be written as

$$(1 - B)(1 - 0.7395B - 0.1220B^2)z_t^{(0.45)} = (1 + 0.9858B)a_t \ , \tag{4.5}$$

where B is the backshift operator, z_t is the differenced historical wind speed measurement at time t, and a_t is the white noise term at time t that is NID with a mean of 0 and a variance of 0.2876 (i.e., NID $(0, 0.2876)$).

4.2.4 Wind Speed Forecasting Based on an ARIMA Model

Following the exploratory data analysis (see Section 4.2.2) and confirmatory data analysis (see Section 4.2.3), the most appropriate model, ARIMA $(2, 1, 1)$, fitted to the time series of the differenced-and-transformed historical wind speed measurements from the training dataset was generated. A comparison between the wind speed fits provided by the ARIMA $(2, 1, 1)$ model and the historical wind speed measurements from the training dataset is shown in Figure 4.15.

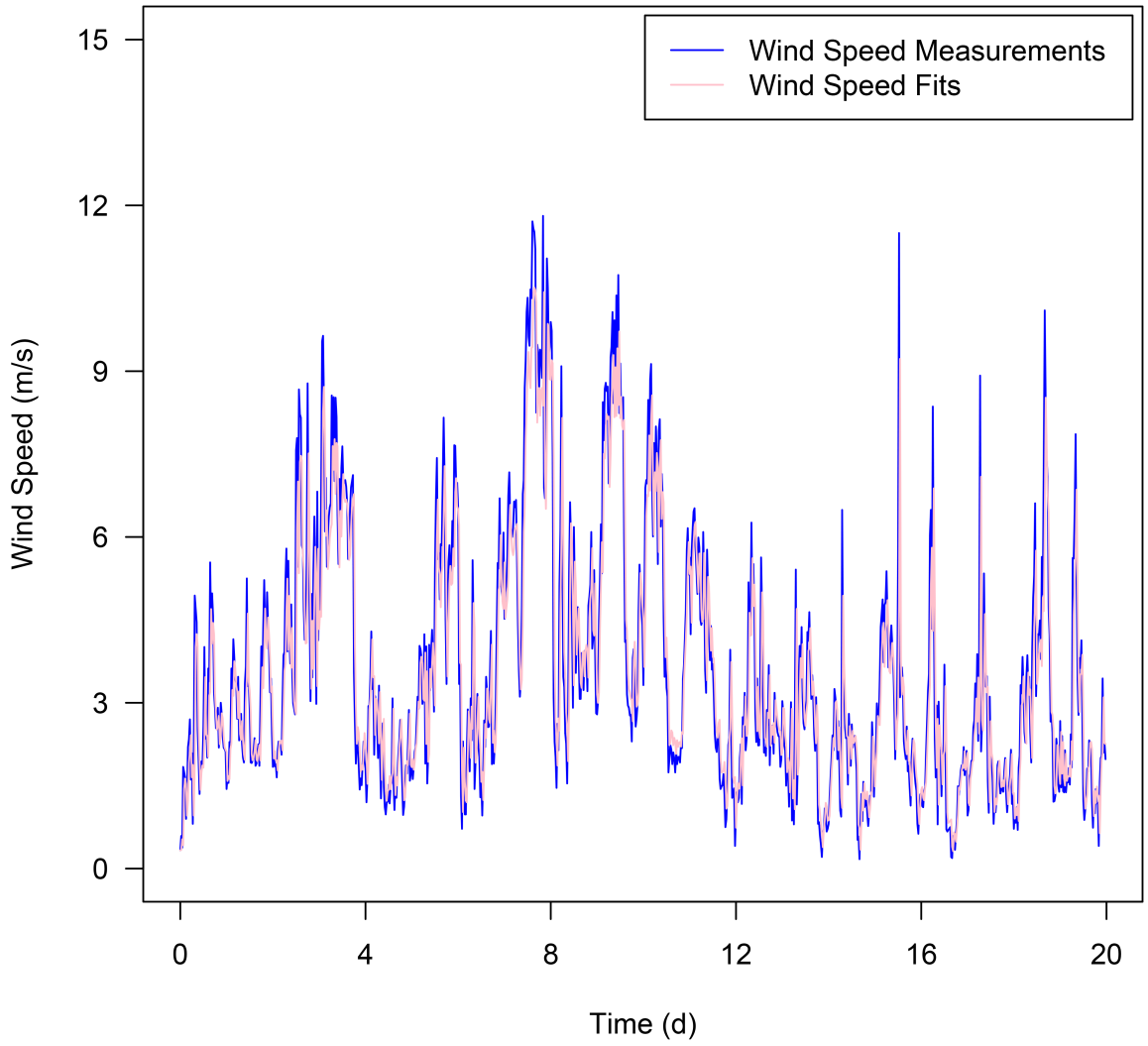

Figure 4.15. Comparison between the wind speed fits provided by the ARIMA $(2, 1, 1)$ model and the historical wind speed measurements from the 20-day training dataset.

From Figure 4.15, it can be visually found that the wind speed fits obtained from the ARIMA $(2, 1, 1)$ model provided an excellent conformance with the historical wind speed

measurements from the training dataset in the period of 20 days. The characteristics of the wind speed measurements were captured and described by the ARIMA $(2, 1, 1)$ model successfully. Next, the ARIMA $(2, 1, 1)$ model was applied to the wind speed forecasting for the purpose of providing the best estimates of what would happen at the specified time points in the future. In addition, the method of minimum MSE forecasts was used here.

For a comprehensive assessment of the ARIMA $(2, 1, 1)$ model in the wind speed forecasting, the different forecast time step sizes ranging from 1 to 48 steps were tested in the experiment. According to Equation (4.5), the wind speed forecasts based on the different time step sizes for the test dataset were acquired. The correspondence between the time step size and time horizon was the same as that explained in Section 4.1.2. According to Equations (3.9) to (3.14), the MBs, MAEs, RMSEs, IAs, MAPEs, and SMAPEs for the wind speed forecasting by using the ARIMA $(2, 1, 1)$ model and their 4-day average values were calculated. The corresponding results are shown in Tables 4.25 to 4.30.

Table 4.25. MBs for the wind speed forecasting by using the ARIMA $(2, 1, 1)$ model applied to the 4-day test dataset.

MB (m/s)		Forecast day				Average
		1	2	3	4	
Forecast time horizon	30 minutes	-0.08	-0.07	-0.12	-0.29	-0.14
	1 hour	-0.04	-0.13	-0.23	-0.41	-0.20
	1.5 hours	-0.22	-0.09	-0.31	-0.54	-0.29
	2 hours	-0.11	-0.14	-0.25	-0.72	-0.31
	3 hours	-0.11	-0.10	-0.29	-0.62	-0.28
	4 hours	-0.47	-0.21	-0.31	-0.82	-0.45
	6 hours	0.11	-0.09	-0.21	-1.07	-0.32
	8 hours	-0.45	-0.11	-0.63	-1.49	-0.67
	12 hours	-0.30	-0.37	-0.32	-1.36	-0.59
	24 hours	-0.31	-0.12	-1.06	-1.63	-0.78

Table 4.26. MAEs for the wind speed forecasting by using the ARIMA $(2, 1, 1)$ model applied to the 4-day test dataset.

MAE (m/s)		Forecast day				Average
		1	2	3	4	
Forecast time horizon	30 minutes	0.67	0.52	0.62	0.63	0.61
	1 hour	0.75	0.60	0.69	0.82	0.72
	1.5 hours	0.99	0.65	0.80	0.87	0.83
	2 hours	1.12	0.67	0.94	1.08	0.95
	3 hours	1.10	0.64	1.00	1.07	0.95
	4 hours	1.10	0.78	1.04	1.31	1.06
	6 hours	1.41	0.81	1.65	1.41	1.32
	8 hours	1.17	0.85	1.50	1.94	1.37
	12 hours	1.02	0.86	2.10	1.96	1.49
	24 hours	1.04	0.75	1.75	2.22	1.44

Table 4.27. RMSEs for the wind speed forecasting by using the ARIMA $(2, 1, 1)$ model applied to the 4-day test dataset.

RMSE (m/s)		Forecast day				Average
		1	2	3	4	
Forecast time horizon	30 minutes	1.37	0.67	0.78	0.83	0.91
	1 hour	1.47	0.78	0.89	1.07	1.05
	1.5 hours	1.84	0.88	1.01	1.23	1.24
	2 hours	1.99	0.86	1.18	1.43	1.36
	3 hours	1.90	0.80	1.27	1.50	1.37
	4 hours	1.94	0.97	1.33	1.76	1.50
	6 hours	1.99	1.00	1.86	1.85	1.67
	8 hours	1.83	1.05	1.76	2.45	1.77
	12 hours	1.74	1.05	2.33	2.56	1.92
	24 hours	1.75	0.94	2.10	2.83	1.91

Table 4.28. IAs for the wind speed forecasting by using the ARIMA $(2, 1, 1)$ model applied to the 4-day test dataset.

IA		Forecast day				Average
		1	2	3	4	
Forecast time horizon	30 minutes	0.87	0.96	0.98	0.98	0.95
	1 hour	0.85	0.94	0.97	0.97	0.93
	1.5 hours	0.76	0.93	0.96	0.96	0.90
	2 hours	0.72	0.93	0.95	0.95	0.89
	3 hours	0.75	0.94	0.94	0.94	0.89
	4 hours	0.74	0.91	0.94	0.92	0.88
	6 hours	0.72	0.90	0.88	0.91	0.85
	8 hours	0.77	0.90	0.89	0.85	0.85
	12 hours	0.79	0.89	0.81	0.83	0.83
	24 hours	0.79	0.91	0.85	0.80	0.84

Table 4.29. MAPEs for the wind speed forecasting by using the ARIMA $(2, 1, 1)$ model applied to the 4-day test dataset.

MAPE		Forecast day				Average
		1	2	3	4	
Forecast time horizon	30 minutes	25.32%	26.82%	20.75%	20.37%	23.31%
	1 hour	30.33%	32.35%	24.97%	23.39%	27.76%
	1.5 hours	34.67%	33.19%	30.80%	23.45%	30.53%
	2 hours	42.81%	36.07%	38.42%	29.00%	36.57%
	3 hours	41.42%	33.97%	44.48%	27.51%	36.85%
	4 hours	42.84%	47.45%	39.87%	39.29%	42.36%
	6 hours	58.66%	49.93%	79.46%	33.96%	55.50%
	8 hours	48.20%	50.09%	67.75%	50.59%	54.16%
	12 hours	41.88%	47.08%	102.59%	50.77%	60.58%
	24 hours	42.84%	44.39%	67.99%	55.48%	52.67%

Table 4.30. SMAPEs for the wind speed forecasting by using the ARIMA $(2, 1, 1)$ model applied to the 4-day test dataset.

SMAPE		Forecast day				Average
		1	2	3	4	
Forecast time horizon	30 minutes	24.21%	22.55%	19.63%	19.50%	21.47%
	1 hour	28.08%	26.36%	22.37%	22.89%	24.92%
	1.5 hours	33.45%	26.16%	26.81%	23.55%	27.49%
	2 hours	39.11%	28.33%	31.37%	31.37%	32.22%
	3 hours	36.61%	26.76%	31.58%	28.12%	30.76%
	4 hours	41.62%	33.36%	33.01%	37.42%	36.35%
	6 hours	48.78%	34.53%	52.25%	36.34%	42.97%
	8 hours	44.43%	35.30%	48.56%	54.24%	45.63%
	12 hours	37.60%	37.01%	64.40%	51.93%	47.73%
	24 hours	38.43%	31.73%	55.25%	59.72%	46.28%

From Tables 4.25 to 4.30, it can be seen that the ARIMA $(2, 1, 1)$ model performed well for the 30-minute ahead wind speed forecasting. Specifically, its 4-day average MB absolute value was only 0.14 m/s, which was close to 0; its 4-day average MAE and RMSE were 0.61 m/s and 0.91 m/s, respectively, which were both less than 1 m/s; its 4-day average IA was 0.95, which was the only one reaching the level of 0.95; and its 4-day average MAPE and SMAPE were 23.31% and 21.47%, respectively, which were just slightly higher than 20.00%. Nevertheless, it is not surprising that with the rise in the forecast time horizon from 30 minutes to 12 hours, the 4-day average MB absolute value, MAE, RMSE, MAPE, and SMAPE for the wind speed forecasting by using the ARIMA $(2, 1, 1)$ model went up gradually, although there were a few exceptions. To be precise, the 4-day average MB absolute values for the 3-hour, 6-hour, and 12-hour ahead wind speed forecasting were a little smaller than those for the 2-hour, 4-hour, and 8-hour ahead wind speed forecasting, respectively; the 4-day average MAPE for the 8-hour ahead wind speed forecasting was a little smaller than that for the 6-hour ahead wind speed forecasting; and the 4-day average SMAPE for the 3-hour ahead wind speed forecasting was a little smaller than that for the 2-hour ahead wind speed forecasting. In the end, the values of these evaluation metrics for the 12-hour ahead wind speed forecasting, reaching 0.59 m/s, 1.49 m/s, 1.92 m/s, 60.58%,

and 47.73%, respectively, were much higher than those for the 30-minute ahead wind speed forecasting. Additionally, the corresponding 4-day average IA decreased gradually with the increasing forecast time horizon. The 4-day average IA for the 12-hour ahead wind speed forecasting, as low as 0.83, was relatively worse than that for the 30-minute ahead wind speed forecasting. This is because for the 1-step ahead wind speed forecasting, all of the wind speed forecasts were calculated according to the historical wind speed measurements. However, for the multi-step ahead wind speed forecasting, half or most of the wind speed forecasts depended on the wind speed estimates previously calculated. Thus, the wind speed forecast error gradually accumulated with the expansion of the forecast time step size, resulting in a larger and larger error. One interesting discovery is that the predictive performance of the 24-hour ahead wind speed forecasting was a little better than that of the 12-hour ahead wind speed forecasting according to every single metric except the MB in this case. However, this can only be explained as an accidental phenomenon since it does not make any sense.

Another point that needs to be highlighted is that although the MBs for the 30-minute ahead wind speed forecasting were close to each other for the 4 single days, the differences among them became much larger as the forecast time horizon increased from 30 minutes to 24 hours. The same applied to the MAEs, RMSEs, IAs, MAPEs, and SMAPEs. For instance, the MB, MAE, RMSE, IA, MAPE, and SMAPE for the second day changed from -0.07 to -0.12 m/s, 0.52 to 0.75 m/s, 0.67 to 0.94 m/s, 0.96 to 0.91, 26.82% to 44.39%, and 22.55% to 31.73%, respectively, while these metrics for the fourth day changed from -0.29 to -1.63 m/s, 0.63 to 2.22 m/s, 0.83 to 2.83 m/s, 0.98 to 0.80, 20.37% to 55.48%, and 19.50% to 59.72%, respectively. These findings indicated that with the expansion of the forecast time horizon, the wind speed predictive performance of the ARIMA $(2, 1, 1)$ model became unstable, and the model reliability went down.

In the actual operation of wind farms, 30 minutes, 4 hours, and 24 hours are the most common wind power forecast time horizons as required. The individual comparisons between the 30-minute, 4-hour, and 24-hour ahead wind speed forecasts (together with the 90% confidence interval) provided by the ARIMA $(2, 1, 1)$ model and the historical wind speed measurements from the test dataset are shown in Figures 4.16, 4.17, and 4.18, respectively. It is easy to see that the 30-minute ahead wind speed forecasts were incredibly close to the historical wind speed measurements, and the corresponding 90% confidence interval covered almost all the wind speed measurements. One 30-minute ahead forecast provided by the ARIMA $(2, 1, 1)$ model was predicted one step in advance based on the previous two points. Hence, it was expected to be close to the past measurement, resulting in a lag display. The 4-hour ahead wind speed predictive performance seemed still acceptable, although the errors at some time points were not small, and the corresponding 90%

confidence interval covered almost all the wind speed measurements as well. In contrast, the difference between the 24-hour ahead wind speed forecasts and historical wind speed measurements was quite large. In fact, the 24-hour ahead wind speed forecasts did not capture the characteristics of the wind speed measurements at all. Nevertheless, the corresponding 90% confidence interval still covered most of the wind speed measurements. It should be noted that the ARIMA $(2, 1, 1)$ model was fitted to the time series of Box-Cox transformed historical wind speed measurements. The Box-Cox transformed wind speed forecasts were in the middle of the confidence intervals. However, in order to produce the real wind speed forecasts shown in Figures 4.16 to 4.18, an inverse Box-Cox transformation was performed. After that, the wind speed forecasts were not in the middle of the confidence intervals anymore. In addition, a comparison of the 30-minute, 4-hour, and 24-hour ahead wind speed forecasts provided by the ARIMA $(2, 1, 1)$ model and the historical wind speed measurements from the test dataset is shown in Figure 4.19.

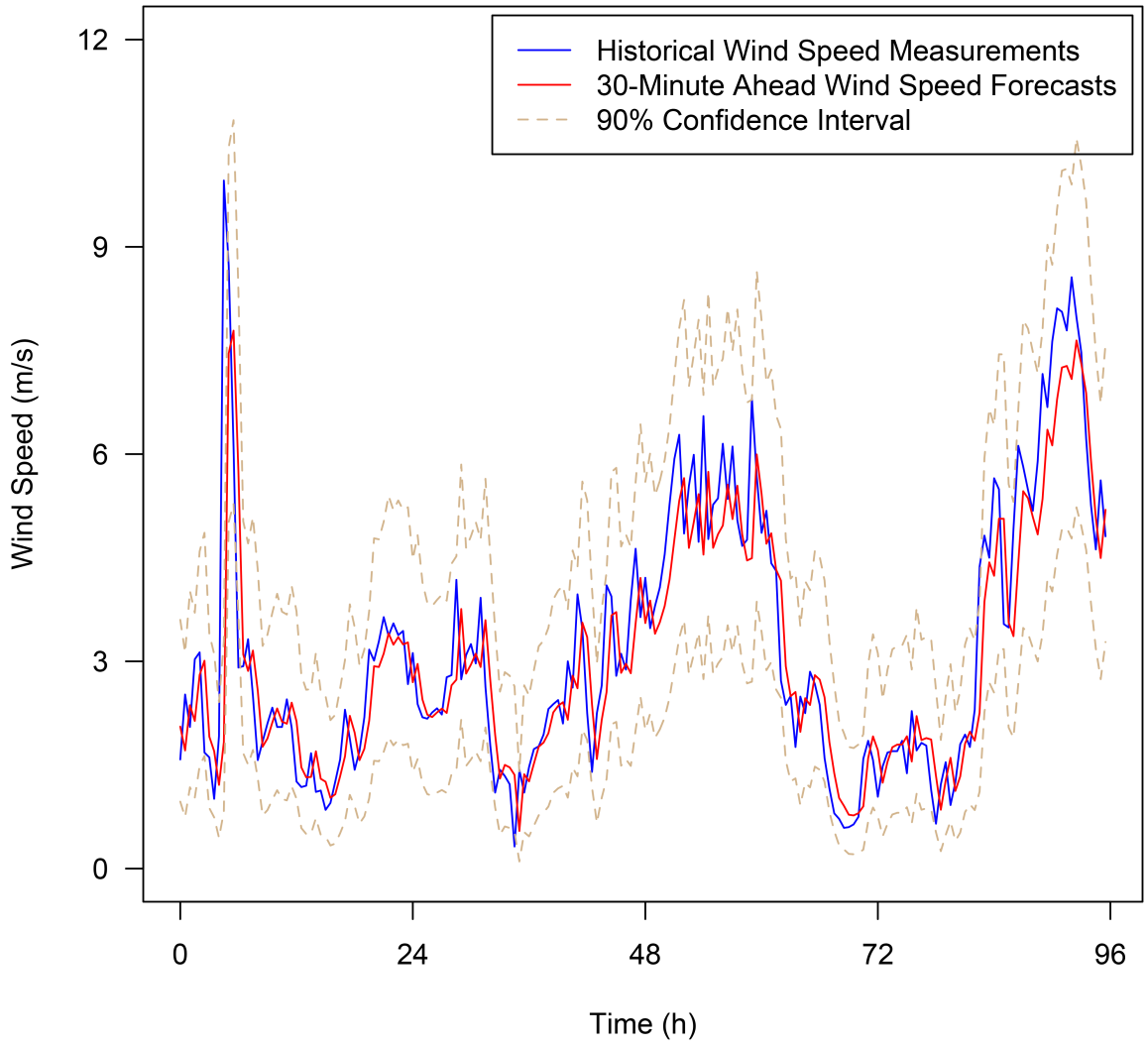

Figure 4.16. Comparison between the 30-minute ahead wind speed forecasts (together with the 90% confidence interval) provided by the ARIMA $(2, 1, 1)$ model and the historical wind speed measurements from the 4-day test dataset.

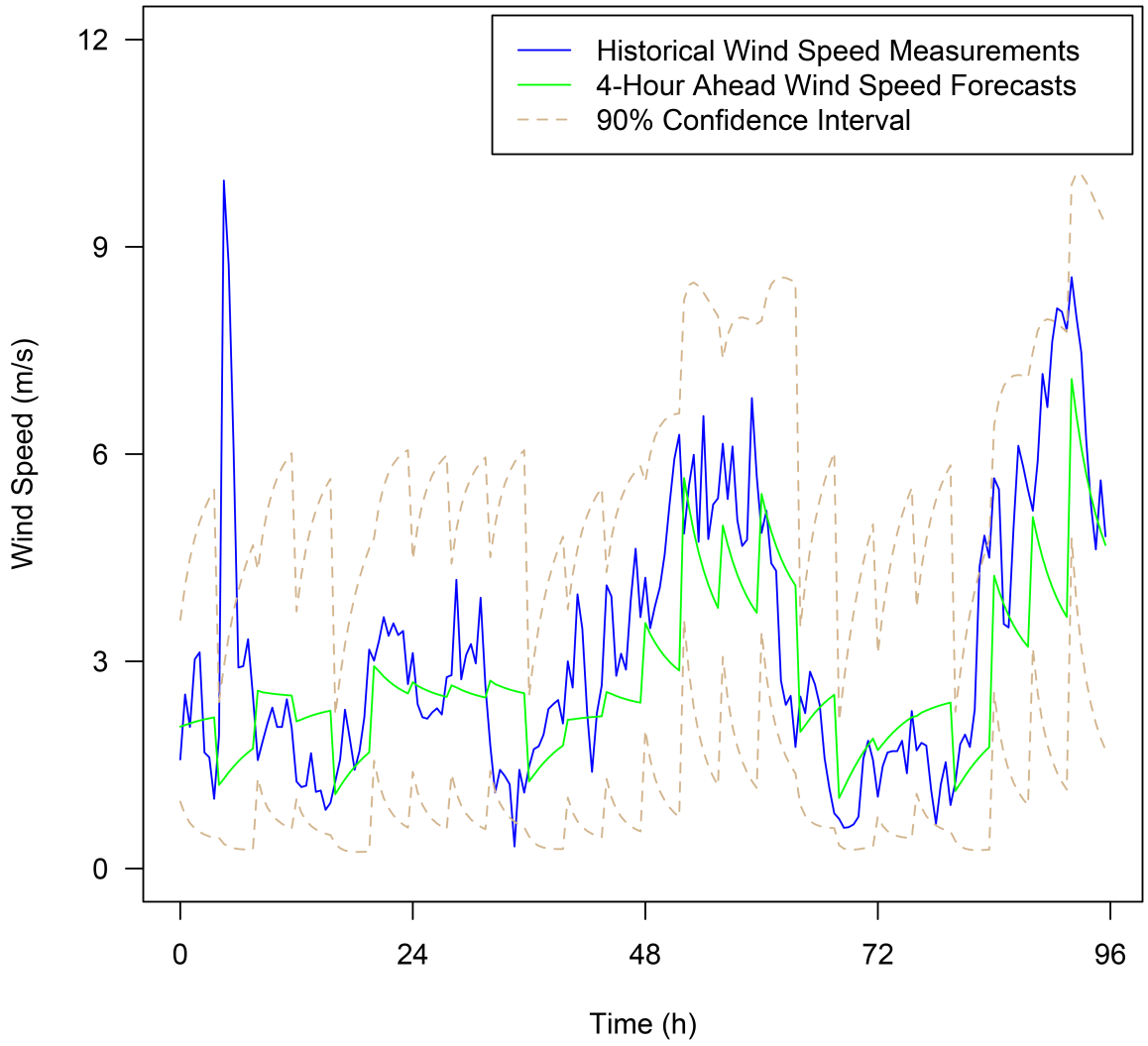

Figure 4.17. Comparison between the 4-hour ahead wind speed forecasts (together with the 90% confidence interval) provided by the ARIMA $(2, 1, 1)$ model and the historical wind speed measurements from the 4-day test dataset.

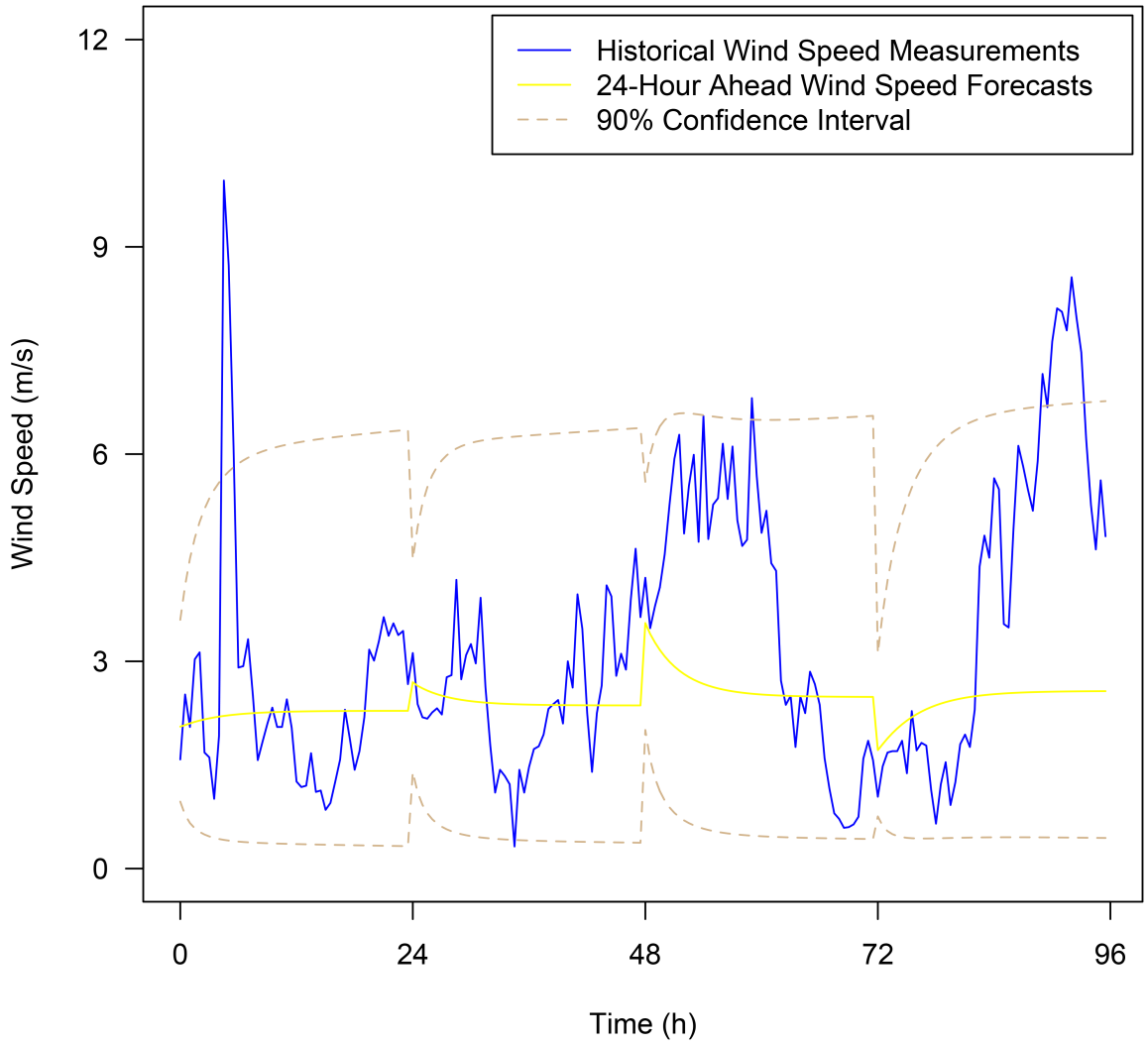

Figure 4.18. Comparison between the 24-hour ahead wind speed forecasts (together with the 90% confidence interval) provided by the ARIMA $(2, 1, 1)$ model and the historical wind speed measurements from the 4-day test dataset.

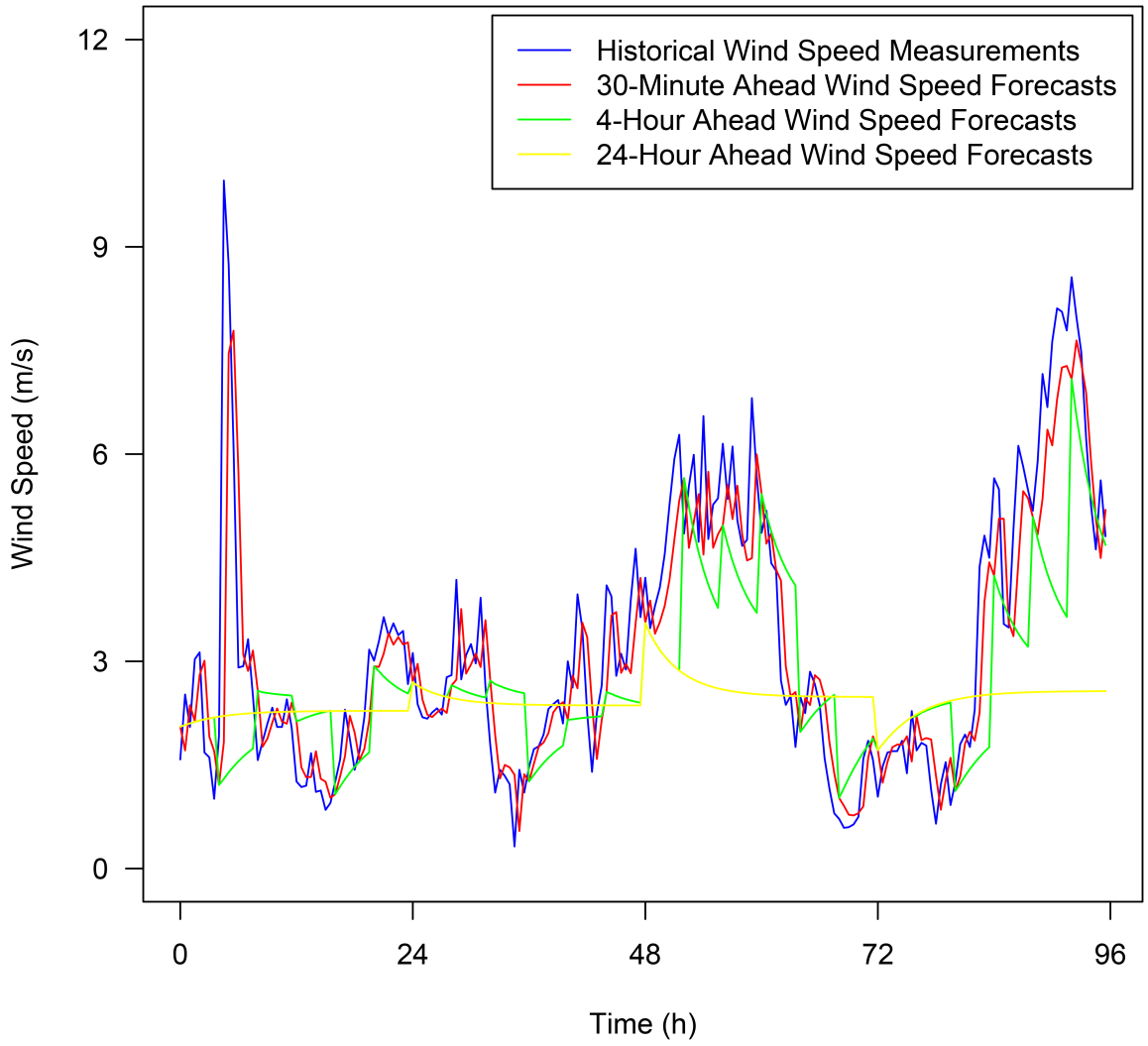

Figure 4.19. Comparison of the 30-minute, 4-hour, and 24-hour ahead wind speed forecasts provided by the ARIMA $(2, 1, 1)$ model and the historical wind speed measurements from the 4-day test dataset.

4.2.5 Wind Power Forecasting Based on an ARIMA Model

As discussed in Section 4.2.4, the wind speed forecasts provided by the ARIMA $(2, 1, 1)$ model for the multiple forecast time horizons were obtained. In this case, all the 4-day wind speed forecasts for the test dataset were input to the ANFIS-based power curve model created in Section 3.7, and then the corresponding wind power forecasts could be acquired as the output of the power curve model. According to Equations (3.9) to (3.12) and (3.15) to (3.18), the MBs, MAEs, RMSEs, IAs, accuracy rates, and qualification rates for the wind power forecasting by using the ARIMA $(2, 1, 1)$ model and their 4-day average values were calculated. The corresponding results are shown in Tables 4.31 to 4.36.

Table 4.31. MBs for the wind power forecasting by using the ARIMA $(2, 1, 1)$ model applied to the 4-day test dataset.

MB (kW)		Forecast day				Average
		1	2	3	4	
Forecast time horizon	30 minutes	-20.9	-6.9	-30.6	-37.7	-24.0
	1 hour	-21.9	-10.2	-44.5	-56.8	-33.3
	1.5 hours	-41.7	-10.7	-55.9	-74.8	-45.7
	2 hours	-37.6	-17.2	-50.2	-93.2	-49.5
	3 hours	-36.6	-11.9	-62.8	-87.7	-49.7
	4 hours	-60.8	-22.3	-59.7	-111.5	-63.6
	6 hours	-29.6	-15.8	-73.5	-139.8	-64.7
	8 hours	-62.4	-22.5	-103.9	-169.6	-89.6
	12 hours	-63.2	-26.2	-80.3	-178.5	-87.1
	24 hours	-63.5	-23.3	-135.8	-196.0	-104.6

Table 4.32. MAEs for the wind power forecasting by using the ARIMA $(2, 1, 1)$ model applied to the 4-day test dataset.

MAE (kW)		Forecast day				Average
		1	2	3	4	
Forecast time horizon	30 minutes	52.8	25.4	60.6	57.1	49.0
	1 hour	53.2	27.5	66.8	81.2	57.2
	1.5 hours	75.5	34.7	75.7	89.5	68.9
	2 hours	78.5	30.5	83.1	104.1	74.0
	3 hours	83.5	31.3	90.3	108.2	78.3
	4 hours	66.1	30.5	93.4	118.3	77.1
	6 hours	96.0	32.1	133.5	140.6	100.5
	8 hours	69.3	34.0	118.7	172.2	98.6
	12 hours	66.7	31.3	166.7	182.4	111.8
	24 hours	67.1	31.6	142.4	199.8	110.2

Table 4.33. RMSEs for the wind power forecasting by using the ARIMA $(2, 1, 1)$ model applied to the 4-day test dataset.

RMSE (kW)		Forecast day				Average
		1	2	3	4	
Forecast time horizon	30 minutes	187.8	41.4	92.4	96.0	104.4
	1 hour	186.5	44.3	101.6	127.7	115.0
	1.5 hours	232.5	51.7	113.4	150.5	137.0
	2 hours	233.6	48.1	122.1	167.3	142.8
	3 hours	235.4	46.5	130.4	189.8	150.5
	4 hours	226.2	49.8	138.1	203.4	154.4
	6 hours	237.1	48.7	172.8	219.7	169.6
	8 hours	226.2	52.6	169.7	267.7	179.0
	12 hours	225.9	52.8	203.2	291.5	193.4
	24 hours	226.0	51.0	199.4	305.9	195.6

Table 4.34. IAs for the wind power forecasting by using the ARIMA $(2, 1, 1)$ model applied to the 4-day test dataset.

IA		Forecast day				Average
		1	2	3	4	
Forecast time horizon	30 minutes	0.65	0.67	0.86	0.95	0.78
	1 hour	0.64	0.57	0.82	0.90	0.73
	1.5 hours	0.18	0.37	0.76	0.86	0.54
	2 hours	0.17	0.40	0.73	0.81	0.53
	3 hours	0.17	0.46	0.69	0.75	0.52
	4 hours	0.19	0.40	0.67	0.72	0.50
	6 hours	0.14	0.36	0.45	0.65	0.40
	8 hours	0.19	0.34	0.56	0.52	0.40
	12 hours	0.19	0.40	0.28	0.47	0.34
	24 hours	0.19	0.39	0.48	0.45	0.38

Table 4.35. Accuracy rates for the wind power forecasting by using the ARIMA $(2, 1, 1)$ model applied to the 4-day test dataset.

Accuracy rate		Forecast day				Average
		1	2	3	4	
Forecast time horizon	30 minutes	87.48%	97.24%	93.84%	93.60%	93.04%
	1 hour	87.57%	97.04%	93.23%	91.49%	92.33%
	1.5 hours	84.50%	96.55%	92.44%	89.97%	90.86%
	2 hours	84.43%	96.79%	91.86%	88.85%	90.48%
	3 hours	84.31%	96.90%	91.31%	87.34%	89.96%
	4 hours	84.92%	96.68%	90.80%	86.44%	89.71%
	6 hours	84.19%	96.75%	88.48%	85.35%	88.69%
	8 hours	84.92%	96.49%	88.69%	82.15%	88.06%
	12 hours	84.94%	96.48%	86.46%	80.57%	87.11%
	24 hours	84.93%	96.60%	86.70%	79.61%	86.96%

Table 4.36. Qualification rates for the wind power forecasting by using the ARIMA $(2, 1, 1)$ model applied to the 4-day test dataset.

Qualification rate		Forecast day				Average
		1	2	3	4	
Forecast time horizon	30 minutes	97.92%	100.00%	100.00%	100.00%	99.48%
	1 hour	97.92%	100.00%	100.00%	97.92%	98.96%
	1.5 hours	95.83%	100.00%	100.00%	95.83%	97.92%
	2 hours	95.83%	100.00%	97.92%	93.75%	96.88%
	3 hours	95.83%	100.00%	100.00%	89.58%	96.35%
	4 hours	95.83%	100.00%	97.92%	91.67%	96.35%
	6 hours	95.83%	100.00%	95.83%	83.33%	93.75%
	8 hours	95.83%	100.00%	95.83%	85.42%	94.27%
	12 hours	95.83%	100.00%	91.67%	81.25%	92.19%
	24 hours	95.83%	100.00%	91.67%	81.25%	92.19%

From Tables 4.31 to 4.36, it can be found that the predictive performance of the ARIMA $(2, 1, 1)$ model for the 30-minute ahead wind power forecasting was good. To be precise, its 4-day average MB absolute value, MAE, RMSE, IA, accuracy rate, and qualification rate were 24.0 kW, 49.0 kW, 104.4 kW, 0.78, 93.04%, and 99.48%, respectively. However, it is not surprising that as the forecast time horizon expanded from 30 minutes to 24 hours, the 4-day average MB absolute value, MAE, and RMSE for the wind power forecasting by using the ARIMA $(2, 1, 1)$ model increased gradually, while the corresponding 4-day average IA, accuracy rate, and qualification rate decreased. At last, the values of these evaluation metrics for the 24-hour ahead wind power forecasting, reaching 104.6 kW, 110.2 kW, 195.6 kW, 0.38, 86.96%, and 92.19%, respectively, were much worse than those for the 30-minute ahead wind power forecasting. Nevertheless, a few exceptions existed in this case. Specifically, the 4-day average MB absolute value for the 12-hour ahead wind power forecasting was a little smaller than that for the 8-hour ahead wind power forecasting; the 4-day average MAEs for the 4-hour, 8-hour, and 24-hour ahead wind power forecasting were a little smaller than those for the 3-hour, 6-hour, and 12-hour ahead wind power forecasting, respectively; the 4-day average IA for the 24-hour ahead wind power forecasting was a little higher than that for the 12-hour ahead wind power forecasting; and the 4-day

average qualification rate for the 8-hour ahead wind power forecasting was a little higher than that for the 6-hour ahead wind power forecasting. All of them can be regarded as accidental phenomena since they do not make any sense.

Another point that needs to be highlighted is that although the MBs for the 30-minute ahead wind power forecasting were close to each other for the 4 single days, the differences among them became much larger as the forecast time horizon increased from 30 minutes to 24 hours. The same applied to the MAEs, RMSEs, IAs, accuracy rates, and qualification rates. For instance, the MB, MAE, RMSE, IA, accuracy rate, and qualification rate for the second day changed from -6.9 to -23.3 kW, 25.4 to 31.6 kW, 41.4 to 51.0 kW, 0.67 to 0.39, 97.24% to 96.60%, and 100.00% to 100.00%, respectively, while these metrics for the fourth day changed from -37.7 to -196.0 kW, 57.1 to 199.8 kW, 96.0 to 305.9 kW, 0.95 to 0.45, 93.60% to 79.61%, and 100.00% to 81.25%, respectively. These findings indicated that with the expansion of the forecast time horizon, the wind power predictive performance of the ARIMA $(2, 1, 1)$ model became unstable, and the model reliability went down.

In the actual operation of wind farms, 30 minutes, 4 hours, and 24 hours are the most common wind power forecast time horizons as required. In the same way as mapping the wind speed forecasts to wind power forecasts by using the ANFIS-based power curve model created in Section 3.7, the 90% confidence intervals for the different forecast time horizons could also be generated. The individual comparisons between the 30-minute, 4-hour, and 24-hour ahead wind power forecasts (together with the 90% confidence interval) provided by the ARIMA $(2, 1, 1)$ model and the historical wind power measurements from the test dataset are shown in Figures 4.20, 4.21, and 4.22, respectively. It is easy to see that the 30-minute ahead wind power forecasts were incredibly close to the historical wind power measurements, and the corresponding 90% confidence interval covered almost all the wind power measurements. The 4-hour ahead wind power predictive performance seemed still acceptable, although the errors at some time points were not small, and the corresponding 90% confidence interval covered almost all the wind power measurements as well. In contrast, the difference between the 24-hour ahead wind power forecasts and historical wind power measurements was quite large. In fact, the 24-hour ahead wind power forecasts did not capture the characteristics of the wind power measurements at all. Nevertheless, the corresponding 90% confidence interval still covered most of the wind power measurements. In addition, a comparison of the 30-minute, 4-hour, and 24-hour ahead wind power forecasts provided by the ARIMA $(2, 1, 1)$ model and the historical wind power measurements from the test dataset is shown in Figure 4.23.

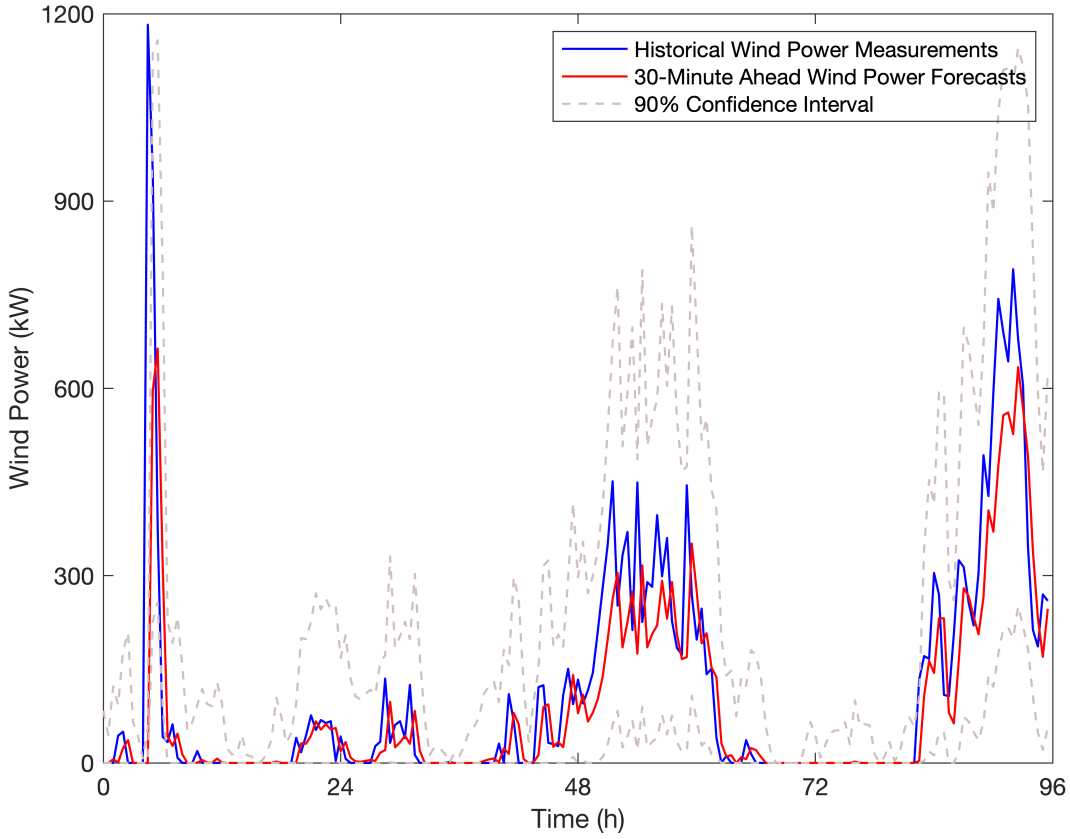

Figure 4.20. Comparison between the 30-minute ahead wind power forecasts (together with the 90% confidence interval) provided by the ARIMA $(2, 1, 1)$ model and the historical wind power measurements from the 4-day test dataset.

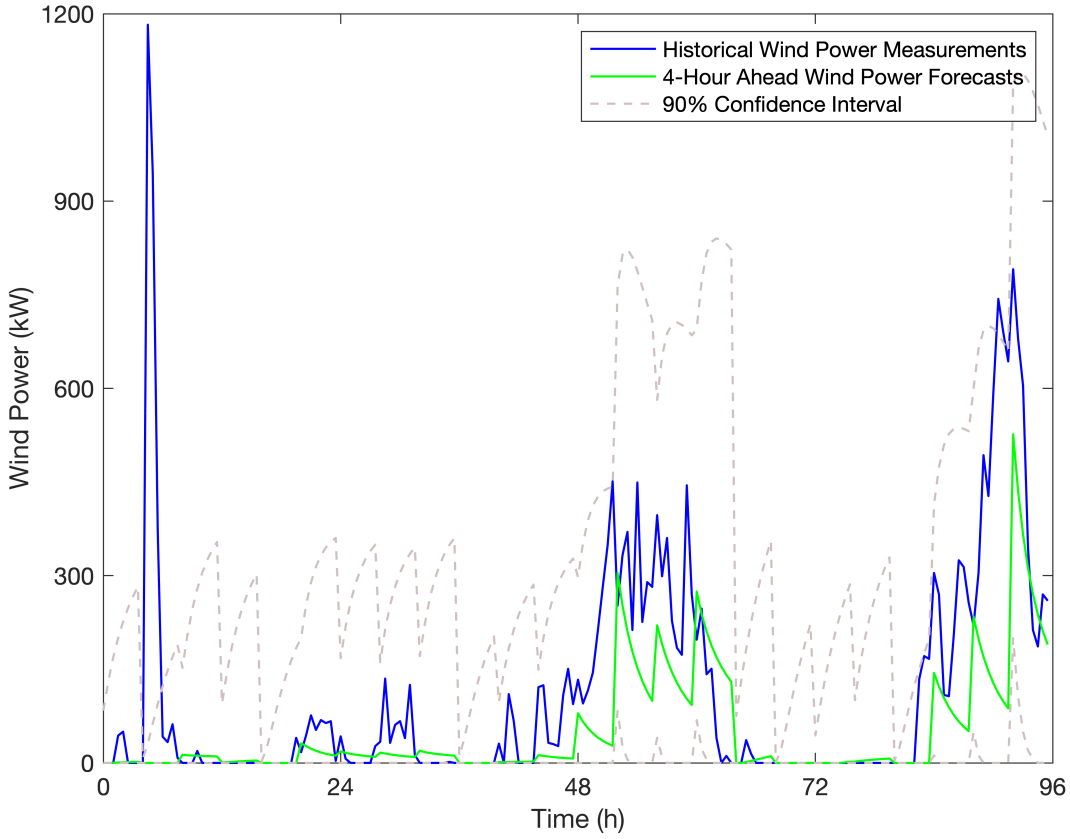

Figure 4.21. Comparison between the 4-hour ahead wind power forecasts (together with the 90% confidence interval) provided by the ARIMA $(2, 1, 1)$ model and the historical wind power measurements from the 4-day test dataset.

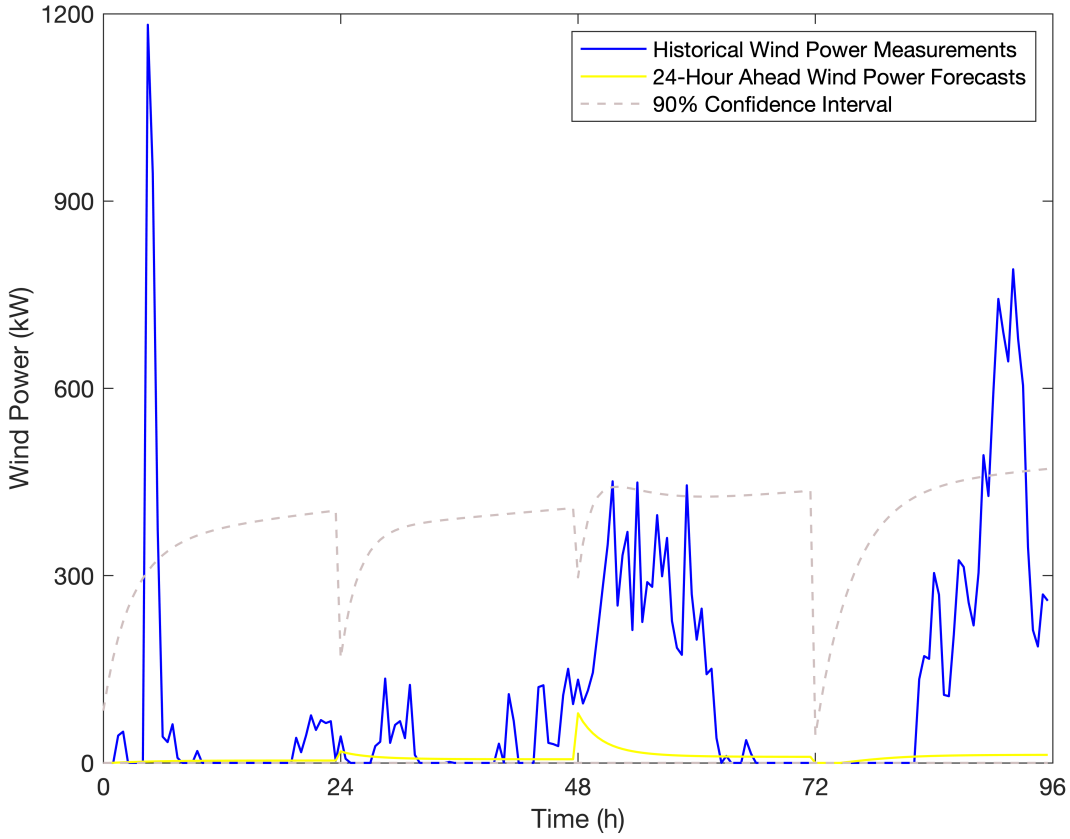

Figure 4.22. Comparison between the 24-hour ahead wind power forecasts (together with the 90% confidence interval) provided by the ARIMA $(2, 1, 1)$ model and the historical wind power measurements from the 4-day test dataset.

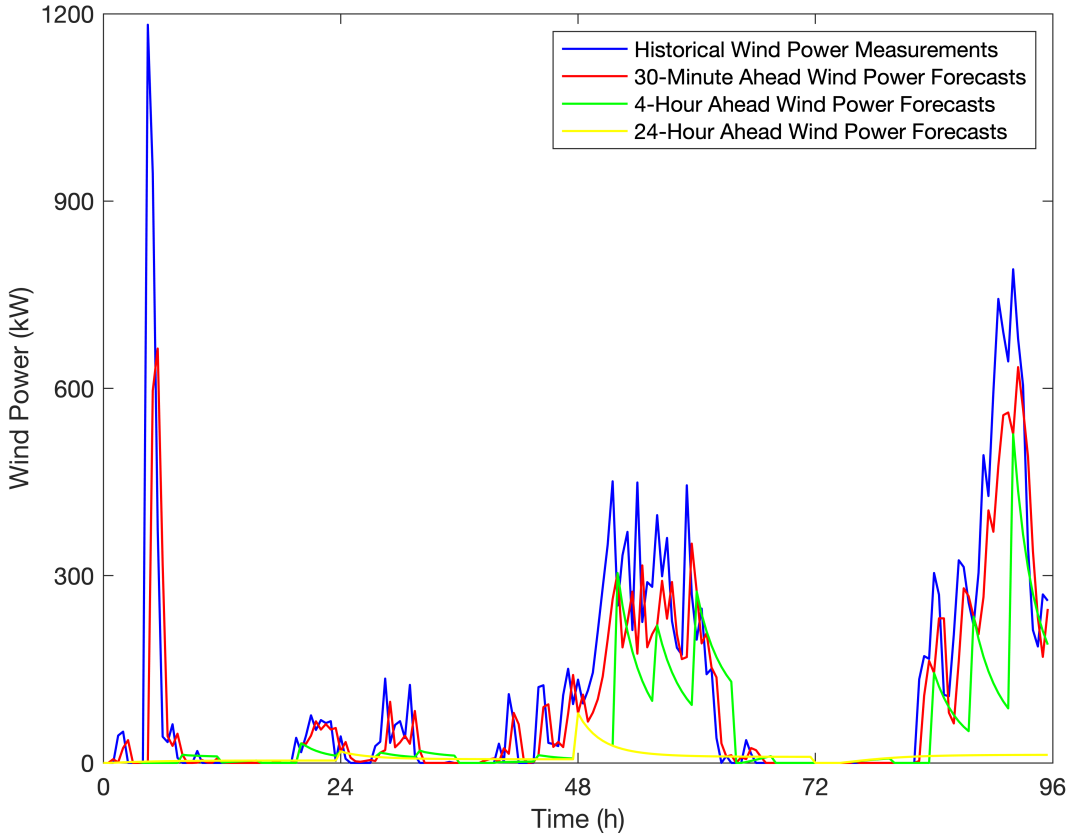

Figure 4.23. Comparison of the 30-minute, 4-hour, and 24-hour ahead wind power forecasts provided by the ARIMA $(2, 1, 1)$ model and the historical wind power measurements from the 4-day test dataset.

4.2.6 Summary

The ARIMA time series modelling, as a classical statistical method for wind speed and wind power forecasting, is presented in Section 4.2. First of all, an exploratory data analysis was applied to the 24 days of historical wind speed measurements. Through the visual interpretations of the characteristics of the historical wind speed measurements, such as autocorrelation, non-seasonality, no trends, no long term cycles, and no known or unknown interventions, a non-seasonal ARIMA model was entertained as the most

appropriate type of time series models to be fitted to the time series of the historical wind speed measurements.

Then, a confirmatory data analysis was employed. To be precise, in the first stage of identification, the plot of the sample ACF of the time series of the historical wind speed measurements from the training dataset implied that a differencing operation was necessary for the original data. According to the plots of the sample ACF and sample PACF of the time series of the differenced historical wind speed measurements from the training dataset, the orders of the ARIMA models were proposed to be $(0, 1, 1)$, $(1, 1, 1)$, $(2, 1, 1)$, $(3, 1, 1)$, $(5, 1, 1)$, and $(7, 1, 1)$. In the second stage of parameter estimation, an approach of maximum likelihood was used to calculate the MLEs and SEs for the parameters of the AR and MA terms in the ARIMA models, together with the AIC method, the ARIMA $(2, 1, 1)$ model was selected from the six tentative models as the most appropriate one.

In the third stage of diagnostic checking, overfitting was tested at first, and the ARIMA $(1, 1, 2)$ model was found as the second most promising model since the AIC value of the ARIMA $(1, 1, 2)$ model was even lower than that of the ARIMA $(2, 1, 1)$ model, and the estimates for the parameters of the AR and MA terms in the ARIMA $(1, 1, 2)$ model were all significantly different from 0. After that, a whiteness test was applied to the residuals of the ARIMA $(2, 1, 1)$ and ARIMA $(1, 1, 2)$ models. Their plots of the sample RACF indicated that the residuals of these two models were uncorrelated. Therefore, both of the models satisfied the whiteness assumption. However, these two models failed a normality test. In view of this situation, applying a Box-Cox transformation to the differenced historical wind speed measurements from the training dataset was suggested. Then, the ARIMA $(2, 1, 1)$ and ARIMA $(1, 1, 2)$ models were refitted to the differenced-and-transformed historical wind speed measurements from the training dataset. The results of the normality test for the residuals of the refitted ARIMA models verified the contributions of the Box-Cox transformation. The maximum p value of 0.01087, considerably larger than the previous ones (5.781E-12 and 5.622E-12), occurred when the parameter of the Box-Cox transformation was 0.45, and the ARIMA $(2, 1, 1)$ model was employed. Unfortunately, this p value was still less than the desired value of 0.05. Nevertheless, it was at least greater than 0.01. In other words, the null hypothesis of the residuals satisfying a normal distribution could not be rejected with 99% confidence. In addition. the corresponding D value was the smallest one among all the D values. Hence, the Box-Cox transformation with the parameter of 0.45 was proposed to transform the differenced historical wind speed measurements from the training dataset, and the ARIMA $(2, 1, 1)$ model was selected. Moreover, the refitted ARIMA $(2, 1, 1)$ model passed the whiteness test as well.

And then, a constant variance test was applied to the residuals of the ARIMA $(2, 1, 1)$ models fitted to the differenced and differenced-and-transformed historical wind speed

measurements from the training dataset. The results showed that both of the models passed the constant variance test. Owing to the Box-Cox transformation, the innovations of the refitted ARIMA $(2, 1, 1)$ model could be announced to be homoscedastic with much more confidence. The most appropriate model for the wind speed forecasting was determined to be the ARIMA $(2, 1, 1)$ model and can be written as

$$(1 - B)(1 - 0.7395B - 0.1220B^2)z_t^{(0.45)} = (1 + 0.9858B)a_t \ , \tag{4.6}$$

where B is the backshift operator, z_t is the differenced historical wind speed measurement at time t, and a_t is the white noise term at time t that is NID with a mean of 0 and a variance of 0.2876 (i.e., NID $(0, 0.2876)$).

Next, the selected ARIMA $(2, 1, 1)$ model was utilised to forecast the wind speeds for the test dataset. The wind speed forecasting was tested for 10 different forecast time horizons ranging from 30 minutes to 24 hours, and the predictive performance was assessed by using the six evaluation metrics described in Section 3.5. It was concluded that the ARIMA $(2, 1, 1)$ model performed well for the 30-minute ahead wind speed forecasting, with the 4-day average MB absolute value of 0.14 m/s, MAE of 0.61 m/s, RMSE of 0.91 m/s, IA of 0.95, MAPE of 23.31%, and SMAPE of 21.47%. Besides, the corresponding 90% confidence interval covered almost all the wind speed measurements. Nevertheless, with the rise in the forecast time horizon, the 4-day average MB absolute value, MAE, RMSE, MAPE, and SMAPE for the wind speed forecasting by using the ARIMA $(2, 1, 1)$ model went up gradually, while the corresponding 4-day average IA decreased. This is because for the 1-step ahead wind speed forecasting, all of the wind speed forecasts were calculated according to the historical wind speed measurements. However, for the multi-step ahead wind speed forecasting, half or most of the wind speed forecasts depended on the wind speed estimates previously calculated. Thus, the wind speed forecast error gradually accumulated with the expansion of the forecast time step size, resulting in a larger and larger error. Although there were some exceptions in this case, they can only be explained as accidental phenomena since they do not make any sense. Additionally, the differences among the MBs for the 4 single days of the test dataset became much larger as the forecast time horizon increased from 30 minutes to 24 hours. The same applied to the other five evaluation metrics. These findings indicated that with the expansion of the forecast time horizon, the wind speed predictive performance of the ARIMA $(2, 1, 1)$ model became unstable, and the model reliability dropped.

Finally, the wind speed forecasts provided by the ARIMA $(2, 1, 1)$ model were converted to the wind power forecasts by using the ANFIS-based power curve model created in Section 3.7. Like the wind speed forecasting, the wind power forecasting was tested for 10

different forecast time horizons ranging from 30 minutes to 24 hours, and the predictive performance was assessed by using the six evaluation metrics described in Section 3.5. It was concluded that the ARIMA $(2, 1, 1)$ model performed well for the 30-minute ahead wind power forecasting, with the 4-day average MB absolute value of 24.0 kW, MAE of 49.0 kW, RMSE of 104.4 kW, IA of 0.78, accuracy rate of 93.04%, and qualification rate of 99.48%. Similarly to the wind speed forecasting, the corresponding 90% confidence interval covered almost all the wind power measurements. However, with the rise in the forecast time horizon, the 4-day average MB absolute value, MAE, and RMSE for the wind power forecasting by using the ARIMA $(2, 1, 1)$ model increased gradually, while the corresponding 4-day average IA, accuracy rate, and qualification rate went down. Although there were some exceptions in this case, they can only be explained as accidental phenomena since they do not make any sense. In addition, the differences among the MBs for the 4 single days of the test dataset became much larger as the forecast time horizon increased from 30 minutes to 24 hours. The same applied to the other five evaluation metrics. These findings indicated that with the expansion of the forecast time horizon, the wind power predictive performance of the ARIMA $(2, 1, 1)$ model became unstable, and the model reliability dropped.

Chapter 5

Physics-Based Modelling

5.1 Introduction

In Chapter 4, the statistics-based modelling (viz., the persistence modelling and ARIMA time series modelling) for wind speed and wind power forecasting is explained in detail. Besides, another primary methodology, widely used in the field of wind speed and wind power forecasting as well, is called physics-based modelling. By applying real geographical and meteorological data, the physics-based forecasting method is supposed to be more suitable for longer forecast time horizons. The general idea of the physics-based modelling for wind power forecasting in this study was to produce wind speed forecasts by using a WRF model first and then convert the wind speed forecasts to wind power forecasts by using a power curve model.

In order to determine the most reliable WRF model and evaluate its predictive performance, the same historical wind data used for the statistics-based modelling were employed for the physics-based modelling in this case. Specifically, the original 24 days of historical wind speed and wind power measurements were divided into two groups: the first 20 days of wind data were used as a training dataset, and the remaining 4 days of wind data were used as a test dataset. In addition, the real geographical data provided by the UCAR and the meteorological data provided by the GFS were both open resources that could be downloaded from the websites. Moreover, in the process of physics-based modelling, the different combinations of model parameters contributed to the different WRF models and different wind speed forecasts as well. Therefore, a TOPSIS scheme was proposed to select and combine the WRF models to generate the best wind speed forecasts. The details of

the WRF model configuration and predictive performance evaluation are described in the following sections within this chapter.

5.2 Setting up and Running a WPS Programme

In a WPS programme, there are three independent subprogrammes, namely *geogrid*, *ungrib*, and *metgrid*, that cooperate together to prepare the inputs to a *real* programme for real-data simulations in the WRF model. Every single subprogramme has its own role of preparation. Particularly, the *geogrid* programme is used to define the model domains and interpolate static geographical data to the model grids; the *ungrib* programme is able to read gridded meteorological fields from the files in the format of the general regularly-distributed information in binary form (GRIB) and write these data in an intermediate format; and the *metgrid* programme interpolates the extracted gridded meteorological fields to the defined model grids horizontally. In addition, a vertical interpolation of the extracted gridded meteorological fields to the WRF eta levels is implemented in the *real* programme. A WPS flow chart is shown in Figure 5.1.

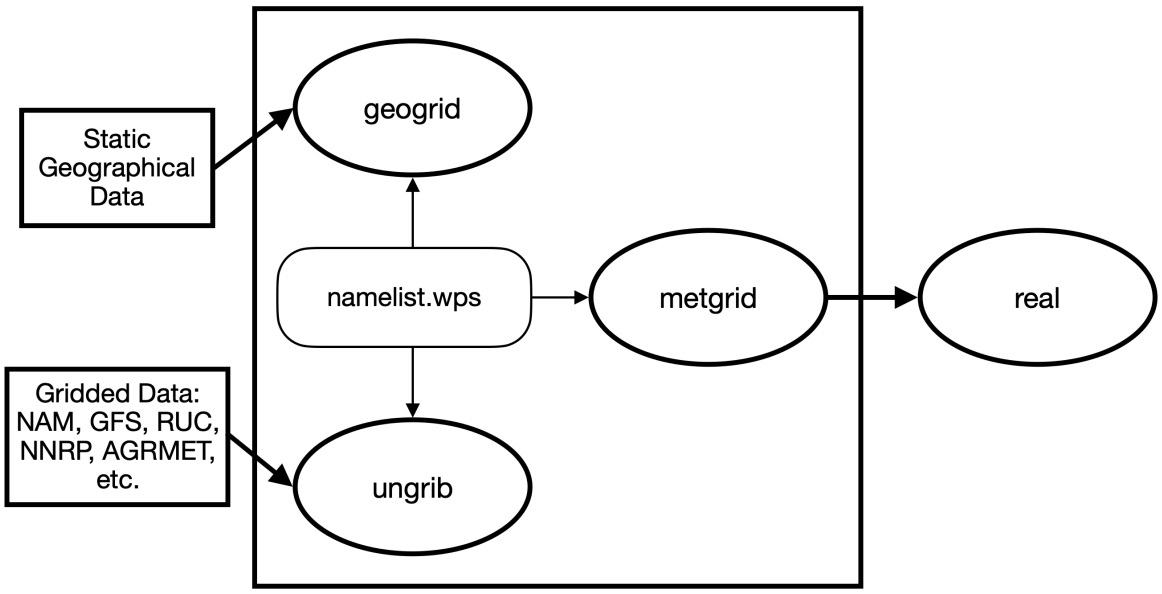

Figure 5.1. WPS flow chart.

As shown in Figure 5.1, the variables of the *geogrid*, *ungrib*, and *metgrid* programmes are controlled in a file called *namelist.wps*, which consists of a shared namelist record for all the programmes and three individual namelist records for each programme. The content of the edited *namelist.wps* file for this study is shown below:

```
&share
wrf_core = 'ARW',
max_dom = 4,
start_date = '2015-08-10_00:00:00', '2015-08-10_00:00:00', '2015-08-10_00:00:00', '2015-08-10_00:00:00',
end_date = '2015-09-04_00:00:00', '2015-09-04_00:00:00', '2015-09-04_00:00:00', '2015-09-04_00:00:00',
interval_seconds = 21600,
active_grid = .true., .true., .true., .true.,
io_form_geogrid = 2,
opt_output_from_geogrid_path = './output/',
/
&geogrid
parent_id = 1, 1, 2, 3,
parent_grid_ratio = 1, 3, 3, 3,
i_parent_start = 1, 116, 71, 71,
j_parent_start = 1, 78, 48, 48,
e_we = 301, 211, 211, 211,
e_sn = 202, 142, 142, 142,
geog_data_res = 'default', 'default', '30s', '30s',
dx = 27000,
dy = 27000,
map_proj = 'lambert',
ref_lat = 41.06,
ref_lon = 114.81,
truelat1 = 30.0,
truelat2 = 60.0,
stand_lon = 114.81,
geog_data_path = '/home/greendou/scratch/WPS_GEOG/',
opt_geogrid_tbl_path = './geogrid/',
/
&ungrib
out_format = 'WPS',
```

prefix = ‘./output/FILE’,
/
&metgrid
fg_name = ‘./output/FILE’,
opt_metgrid_tbl_path = ‘./metgrid/’,
io_form_metgrid = 2,
opt_output_from_metgrid_path = ‘./output/’,
/

5.2.1 Setting up and Running a *geogrid* Programme

Before running the *geogrid* programme, some variables in the *share* and *geogrid* sections in the *namelist.wps* file needed to be edited. First of all, in the *share* section, since the WPS prepared the input data for the ARW simulations in this study, the *wrf_core* variable, specifying the WRF dynamical core, was set to be ‘ARW’. The *max_dom* variable, specifying the total number of domains/nests (including the parent domain) in the simulation, was set to be 4 as it was designed to have four domains. The meaning of the nests can be explained as they contribute to a higher resolution with lower computational costs. From the content of the *namelist.wps* file shown above, it can be found that for some variables, there were four columns that represented the individual values for the four domains. The *active_grid* variable was set to be a list of four .true.’s as each grid of the four domains would be processed by the *geogrid* and *metgrid* programmes. The *io_form_geogrid* variable was left at the default value of 2 as the domain files generated by the *geogrid* programme would be written in the format of the network common data form (NetCDF), which was expected by the *metgrid* programme. The *opt_output_from_geogrid_path* variable gave the path to the location where the domain files from the *geogrid* programme would be written to and read from. These mentioned variables in the *share* section were all relevant to the *geogrid* programme. However, the other variables, namely *start_date*, *end_date*, and *interval_seconds*, would be ignored by the *geogrid* programme, which only produced time-independent data.

In the *geogrid* section, the *parent_id* variable, specifying the domain number of each nest’s parent, was set to be 1, 1, 2, 3, which means that domain 1 was the parent domain, and domains 2, 3, and 4 were inside domains 1, 2, and 3, respectively. The *parent_grid_ratio* variable, specifying the ratio of each nest’s parent grid distance to the corresponding nest’s grid distance, was set to be 1, 3, 3, 3, which means that the grid lengths of domains 1, 2, and 3 were three times those of domains 2, 3, and 4, respectively. The *i_parent_start* and *j_parent_start* variables, specifying the x and y coordinates of the lower-left corner of

each nest in the corresponding parent domain, were set to be 1, 116, 71, 71 and 1, 78, 48, 48, respectively, indicating that the coordinates of the lower-left corners of domain 2 in domain 1, domain 3 in domain 2, and domain 4 in domain 3 were (116, 78), (71, 48), and (71, 48), respectively. The basis of these settings was keeping the nest boundaries away from the corresponding coarse domain boundaries and roughly putting the nests at the centre of their parent domains. The *e_we* and *e_sn* variables, specifying each domain's full west-east and south-north dimensions, were set to be 301, 211, 211, 211 and 202, 142, 142, 142, respectively, indicating that domain 1 had 301 grid points in the west-east dimension and 202 grid points in the south-north dimension, and domains 2, 3, and 4 all had 211 grid points in the west-east dimension and 142 grid points in the south-north dimension. The *geog_data_res* variable, specifying the resolution of the source data to be employed when the static terrestrial data being interpolated to the nest's grid, was set to be 'default', 'default', '30s', '30s'. The *dx* and *dy* variables, specifying the grid distances (in metres) in the x and y directions, respectively, were both set to be 27000 as recommended by the model developers that these two variables preferably have the same value for a Lambert conformal projection, which means that the grid distance of domain 1 was 27×27 km^2. Based on the values specified for the *parent_id* and *parent_grid_ratio* variables, the grid distances of domains 2, 3, and 4 were 9×9 km^2, 3×3 km^2, and 1×1 km^2, respectively. The *map_proj* variable specifies the projection of the simulation domain. There are four optional projection types, namely Lambert conformal ('lambert'), polar stereographic ('polar'), Mercator ('mercator'), and regular latitude-longitude ('lat-lon'). 'lambert' was selected in this study because the studied wind turbine was located in a mid-latitude area for which the Lambert conformal projection was the most suitable one. The *ref_lat* and *ref_lon* variables specify the latitude and longitude of the centre point of the coarse domain, respectively. In order to place the studied wind turbine at the centre point, the *ref_lat* and *ref_lon* variables were set to be 41.06 and 114.81, respectively, by referring to the estimated location of the wind turbine (41.06° N, 114.81° E) in Section 3.2. The *truelat1* and *truelat2* variables were set to be 30.0 and 60.0, respectively, indicating that the surface of the Lambert conformal projection intersected the surface of the earth at the latitudes of 30.0° N and 60.0° N. The *stand_lon* variable, specifying the longitude parallel with the y-axis in the Lambert conformal projection, was set to be the same value (114.81) as the *ref_lon* variable, which means that the coarsest domain would be centred. The *geog_data_path* and *opt_geogrid_tbl_path* variables gave the paths to the directories where the static geographical data and *GEOGRID.TBL* file were stored, respectively.

Once the simulation coarse and nested domains were correctly defined in the *namelist.wps* file, the WPS domain configuration used for the numerical weather forecasts over the wind farm was finished. A picture of the domain configuration is displayed in Figure 5.2, in

which the four nested domains (centred on the location of the wind farm) are labelled as d01 (coarsest corresponding to the entire domain), d02, d03, and d04 (finest). By running the *geogrid* programme, the domain files were produced.

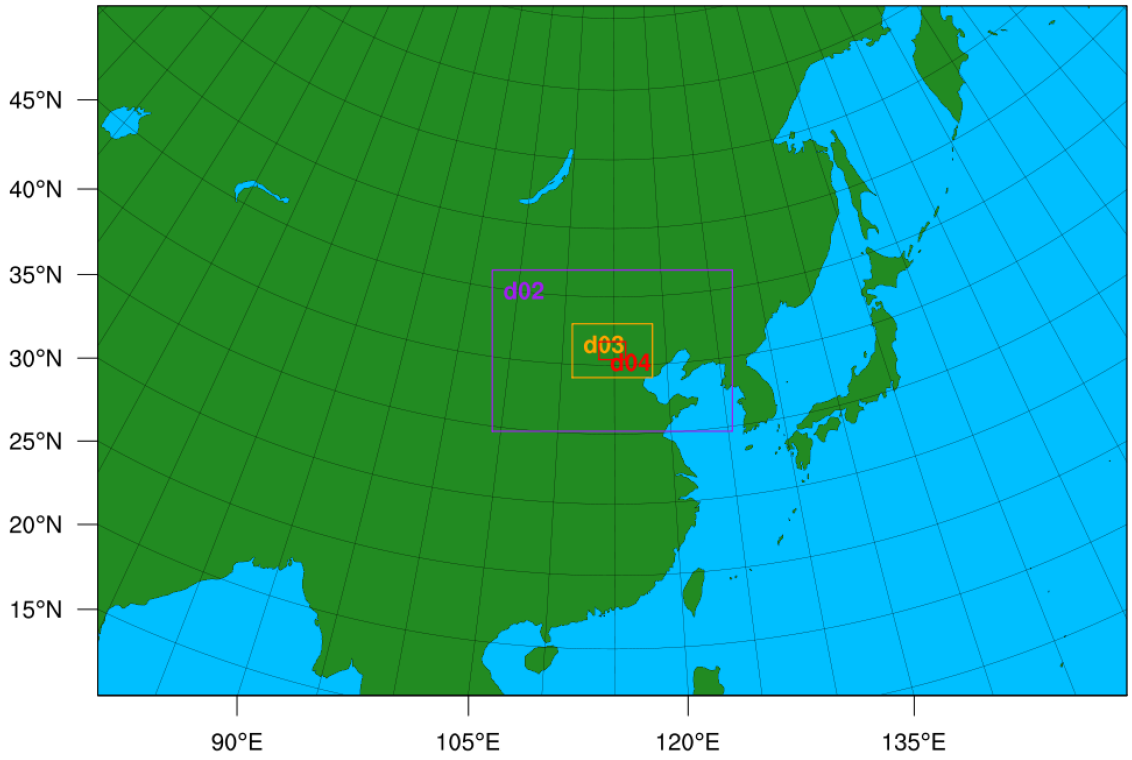

Figure 5.2. WPS domain configuration used for the numerical weather forecasts over the wind farm.

5.2.2 Setting up and Running an *ungrib* Programme

Before running the *ungrib* programme, some variables in the *share* and *ungrib* sections in the *namelist.wps* file needed to be edited. First of all, in the *share* section, the *start_date* and *end_date* variables, specifying the starting and ending UTC dates and times of the simulation for each domain, were set to be '2015-08-10_00:00:00', '2015-08-10_00:00:00', '2015-08-10_00:00:00', '2015-08-10_00:00:00' and '2015-09-04_00:00:00', '2015-09-04_00:00:00', '2015-09-04_00:00:00', '2015-09-04_00:00:00', respectively, indicating that

the simulation for each domain would start from 00:00:00 UTC on the 10th of August 2015 and end at 00:00:00 UTC on the 4th of September 2015. The *interval_seconds* variable, specifying the time interval (in seconds) between the meteorological input files, was set to be 21600 since the input files were available with a temporal resolution of 6 hours. In the *ungrib* section, the *out_format* variable, specifying the format of the intermediate files written by the *ungrib* programme, was set to be 'WPS' as the *ungrib* programme was executed in the WPS programme. The *prefix* variable identified the path and prefix of the intermediate files.

After suitably editing the variables related to the *ungrib* programme in the *namelist.wps* file, the variable table (*Vtable*) of the codes to identify the variables and levels in the GRIB files was supplied. Moreover, the GRIB files obtained from the GFS had to be linked to the filenames that were expected by the *ungrib* programme. By running the *ungrib* programme, the meteorological fields from the GRIB files were extracted, and the files of meteorological data were produced in the intermediate format.

5.2.3 Setting up and Running a *metgrid* Programme

Some variables in the *share* and *metgrid* sections are relevant to the running of the *metgrid* programme. However, at this stage, there was no need to modify any variable in the *share* section because all of the variables were set appropriately for the runnings of the *geogrid* and *ungrib* programmes in Sections 5.2.1 and 5.2.2, respectively. In the *metgrid* section, the *fg_name* variable identified the path and prefix of the intermediate meteorological data files. The *opt_metgrid_tbl_path* variable gave the path to the directory where the *METGRID.TBL* file was stored. The *io_form_metgrid* variable was left at the default value of 2 as the outputs generated by the *metgrid* programme would be written in the format of the NetCDF, which was expected by the *real* programme. The *opt_output_from_metgrid_path* variable gave the path to the location where the output files from the *metgrid* programme would be written to.

After suitably editing the variables related to the *metgrid* programme in the *namelist.wps* file, the *METGRID.TBL* file appropriate for the WRF core had to be linked in the *metgrid* directory. By running the *metgrid* programme, the meteorological fields extracted by the *ungrib* programme were horizontally interpolated to the model domains defined by the *geogrid* programme.

5.3 Setting up and Running a WRF Programme

After successfully running the WPS programme, which is required for the real-data simulations, the next step is to set up a WRF programme. Similar to the WPS programme, there is a *namelist.input* file in which the parameters of the WRF programme can be edited. An example of a *namelist.input* file for this study is shown below:

&time_control
run_days = 0,
run_hours = 0,
run_minutes = 0,
run_seconds = 0,
start_year = 2015, 2015, 2015, 2015,
start_month = 08, 08, 08, 08,
start_day = 10, 10, 10, 10,
start_hour = 18, 18, 18, 18,
start_minute = 00, 00, 00, 00,
start_second = 00, 00, 00, 00,
end_year = 2015, 2015, 2015, 2015,
end_month = 08, 08, 08, 08,
end_day = 12, 12, 12, 12,
end_hour = 00, 00, 00, 00,
end_minute = 00, 00, 00, 00,
end_second = 00, 00, 00, 00,
interval_seconds = 108000,
input_from_file = .true., .true., .true., .true.,
history_interval = 30, 30, 30, 30,
frames_per_outfile = 9000, 9000, 9000, 9000,
restart = .false.,
restart_interval = 4320,
io_form_history = 2,
io_form_restart = 2,
io_form_input = 2,
io_form_boundary = 2,
/
&domains
time_step = 162,
time_step_fract_num = 0,

time_step_fract_den = 1,
max_dom = 4,
e_we = 301, 211, 211, 211,
e_sn = 202, 142, 142, 142,
e_vert = 50, 50, 50, 50,
p_top_requested = 5000,
num_metgrid_levels = 27,
num_metgrid_soil_levels = 4,
dx = 27000, 9000, 3000, 1000,
dy = 27000, 9000, 3000, 1000,
grid_id = 1, 2, 3, 4,
parent_id = 1, 1, 2, 3,
i_parent_start = 1, 116, 71, 71,
j_parent_start = 1, 78, 48, 48,
parent_grid_ratio = 1, 3, 3, 3,
parent_time_step_ratio = 1, 3, 3, 3,
feedback = 1,
smooth_option = 0,
/
&physics
mp_physics = 5, 5, 5, 5,
cu_physics = 2, 2, 0, 0,
bl_pbl_physics = 6, 6, 6, 6,
sf_sfclay_physics = 5, 5, 5, 5,
sf_surface_physics = 3, 3, 3, 3,
num_soil_layers = 9,
ra_lw_physics = 4, 4, 4, 4,
ra_sw_physics = 4, 4, 4, 4,
radt = 27, 27, 27, 27,
co2tf = 1,
bldt = 0, 0, 0, 0,
cudt = 0, 0, 0, 0,
icloud = 1,
num_land_cat = 21,
sf_urban_physics = 0, 0, 0, 0,
/
&dynamics
w_damping = 1,

```
diff_opt = 2, 2, 2, 2,
km_opt = 4, 4, 4, 4,
diff_6th_opt = 2, 2, 2, 2,
diff_6th_factor = 0.12, 0.12, 0.12, 0.12,
base_temp = 290,
damp_opt = 3,
zdamp = 5000, 5000, 5000, 5000,
dampcoef = 0.2, 0.2, 0.2, 0.2,
khdif = 0, 0, 0, 0,
kvdif = 0, 0, 0, 0,
non_hydrostatic = .true., .true., .true., .true.,
moist_adv_opt = 1, 1, 1, 1,
scalar_adv_opt = 1, 1, 1, 1,
gwd_opt = 0,
/
&bdy_control
spec_bdy_width = 5,
spec_zone = 1,
relax_zone = 4,
specified = .true.,
nested = .false., .true., .true., .true.,
/
```

Unlike the *namelist.wps* file (see Section 5.2), in which the values of all the variables were fixed after being edited, some parameters in the *namelist.input* file had a number of optional values, implying that there were different candidate WRF models for the wind speed and wind power forecasting in this study. In order to facilitate the description of the parameter settings, the parameters in the *namelist.input* file are split into two parts: one is the fixed parameters, and the other is the variable parameters.

5.3.1 Settings of Fixed Parameters

In the *time_control* section, the *run_days*, *run_hours*, *run_minutes*, and *run_seconds* parameters, specifying the simulation run time in days, hours, minutes, and seconds, respectively, were all simply set to be 0, which means that the time to run the model simulation would entirely depend on the starting and ending times. The *interval_seconds* parameter, specifying the periodic frequency of incoming real data in seconds, was set to be 108000, which

means that there were no updated real data within 30 hours. Although the resolution of the GFS data was 6 hours, the WRF model aimed to forecast wind speeds one day in advance in this research. Therefore, the model lateral boundaries were not able to be updated every 6 hours. The *input_from_file* parameter was set to be .true. for the four domains, indicating that the nested run would have input files for each domain. The *history_interval* parameter was set to be 30 for each domain as the frequency of recording data to the history file was 30 minutes. The *frames_per_outfile* parameter, specifying the number of time periods that would be written to each history file, was set to be 9000 for each domain, and it was big enough to generate one output file containing all output times. The *restart* parameter was set to be .false. as a restart run would never be done, because of which the *restart_interval* parameter, specifying the time interval (in minutes) of restart output files, would be ignored. The *io_form_history*, *io_form_restart*, *io_form_input*, and *io_form_boundary* parameters, specifying the formats for the history output, restart output, input, and boundary files, respectively, were all left at the default value of 2 (the NetCDF) as recommended by the model developers.

In the *domains* section, the *time_step* parameter, specifying the time step (in seconds) for integration, was set to be 162 as the model developers recommend applying a value of $6 \times dx$ in km for a typical case. The *time_step_fract_num* and *time_step_fract_den* parameters, specifying the numerator and denominator for the fractional time step, were set to be 0 and 1, respectively, indicating that the time step was an integer. The *max_dom* parameter, specifying the number of domains for running, was set to be 4, which means that all the domains were going to be run. The *e_we* and *e_sn* parameters, specifying each domain's full west-east and south-north dimensions, were set to be 301, 211, 211, 211 and 202, 142, 142, 142, respectively, indicating that domain 1 had 301 grid points in the west-east dimension and 202 grid points in the south-north dimension, and domains 2, 3, and 4 all had 211 grid points in the west-east dimension and 142 grid points in the south-north dimension. The *e_vert* parameter, specifying the number of vertical levels onto which the *real* programme would interpolate the incoming data, was set to be 50 for each domain as a level range of 40 to 60 is recommended by the model developers. The *p_top_requested* parameter, specifying the pressure top (in Pa) to use in the model, was left at the default value of 5000 as recommended by the model developers. The *num_metgrid_levels* parameter was set to be 27 as there were 27 incoming vertical levels in the input data. The *num_metgrid_soil_levels* parameter was set to be 4 as there were four soil levels in the WPS outputs. The *dx* and *dy* parameters, specifying the grid distances (in metres) in the x and y directions, respectively, were both set to be 27000, 9000, 3000, 1000, which means that the grid distances of domains 1, 2, 3, and 4 were 27×27 km^2, 9×9 km^2, 3×3 km^2, and 1×1 km^2, respectively. The *grid_id* parameter, specifying the domain numbers, was set to

be 1, 2, 3, 4 as there were four domains. The *parent_id* parameter, specifying the domain number of each nest's parent, was set to be 1, 1, 2, 3, which means that domains 1, 2, 3, and 4 had domains 1, 1, 2, and 3 as parents, respectively. The *i_parent_start* and *j_parent_start* parameters, specifying the x and y coordinates of the lower-left corner of each nest in the corresponding parent domain, were set to be 1, 116, 71, 71 and 1, 78, 48, 48, respectively, indicating that the coordinates of the lower-left corners of domain 1 in domain 1, domain 2 in domain 1, domain 3 in domain 2, and domain 4 in domain 3 were (1, 1), (116, 78), (71, 48), and (71, 48), respectively. The *parent_grid_ratio* parameter, specifying the ratio of each nest's parent grid distance to the corresponding nest's grid distance, was set to be 1, 3, 3, 3, which means that the grid lengths of domains 1, 2, and 3 were three times those of domains 2, 3, and 4, respectively. The *parent_time_step_ratio* parameter, specifying the parent-to-nest time step ratio, was set to be 1, 3, 3, 3 as recommended by the model developers. The *feedback* parameter was set to be 1 as the feedback from the nests to their corresponding parent domains would be used and the run would be a two-way nested run. The *smooth_option* parameter was set to be 0, which means that the smoothing option for each parent domain in the area of the nest was turned off as recommended by the model developers.

In the *physics* section, the *ra_lw_physics* and *ra_sw_physics* parameters, specifying the longwave and shortwave radiation options, respectively, were both set to be 4 (the Rapid Radiative Transfer Model for General Circulation Models (RRTMG) scheme) for each domain as recommended by the model developers. The *radt* parameter, specifying the minutes between radiation physics calls, was set to be 27 for each domain as the model developers recommend applying 1 minute per km of *dx*. Since the *co2tf* parameter is the flag of the CO_2 transmission function for the Geophysical Fluid Dynamics Laboratory (GFDL) radiation only, it would be ignored in this case. The *bldt* and *cudt* parameters, specifying the minutes between boundary layer physics calls and cumulus physics calls, respectively, were both set to be 0 for each domain as every time step is recommended by the model developers. The *icloud* parameter was left at the default value of 1, indicating that the cloud effect on the optical depth in radiation would be applied. The *num_land_cat* parameter was set to be 21 as there were 21 land categories in the input data. The *sf_urban_physics* parameter was set to be 0 for each domain, indicating that the urban canopy model would not be activated.

In the *dynamics* section, the *w_damping* parameter was set to be 1, which means that the vertical velocity damping flag was turned on as this is required for the model stability of the operational run. The *diff_opt* parameter, as a turbulence and mixing option, was set to be 2 for each domain, which means evaluating mixing terms in physical space. The *km_opt* parameter, as an eddy coefficient option, was set to be 4 (the horizontal Smagorinsky

first-order closure) for each domain as it is recommended by the model developers for real-data cases. The *diff_6th_opt* parameter was set to be 2 for each domain, indicating that the sixth-order numerical diffusion without up-gradient diffusion would be applied. The *diff_6th_factor* parameter, specifying the sixth-order numerical diffusion non-dimensional rate, was left at the default value of 0.12 for each domain. The *base_temp* parameter, specifying the base state sea-level temperature (in K), was left at the default value of 290 as a typical value ranges from 270 to 300 K. The *damp_opt* parameter, as the upper-level damping flag, was set to be 3 (with the Rayleigh damping) as it is suitable for real-data cases. The *zdamp* parameter, specifying the damping depth (in metres) from the model top, was left at the default value of 5000 for each domain. The *dampcoef* parameter, specifying the damping coefficient, was left at the default value of 0.2 for each domain. The *khdif* and *kvdif* parameters, specifying the horizontal and vertical diffusion constants (in m^2/s), were both left at the default value of 0 for each domain. The *non_hydrostatic* parameter was set to be .true. for each domain, indicating that the model was run in non-hydrostatic mode. The *moist_adv_opt* and *scalar_adv_opt* parameters were both left at the default value of 1 for each domain, indicating that the positive-definite advection would be applied for moisture and scalars. The *gwd_opt* parameter was set to be 0, indicating that the gravity wave drag option was turned off.

In the *bdy_control* section, the *spec_bdy_width* parameter was set to be 5, indicating that there were five rows for specified boundary value nudging. The *spec_zone* and *relax_zone* parameters, specifying the numbers of points in the specified and relaxation zones, were set to be 1 and 4, respectively. The *specified* parameter was set to be .true., indicating that the specified boundary condition was turned on. The *nested* parameter was set to be .false., .true., .true., .true. as the nested boundary conditions had to be applied to the nests.

5.3.2 Settings of Variable Parameters

In the *time_control* section, the *start_year*, *start_month*, *start_day*, *start_hour*, *start_minute*, *start_second*, *end_year*, *end_month*, *end_day*, *end_hour*, *end_minute*, and *end_second* parameters, specifying the starting and ending times for the model domains in the year, month, day, hour, minute, and second, respectively, are the variable parameters. In this study, the forecast time horizon was 24 hours. Besides, the spin-up time required for the WRF model to stabilise and build up the dynamic structure of the atmospheric motions was taken to be 6 hours. As a consequence, the total simulation time for each case was 30 hours. The WRF model took a cold start at 18:00 one day before every forecast day. For instance, for the case of the first forecast day, the WRF model started from 18:00 UTC on the 10th of

August 2015 and ended at 00:00 UTC on the 12th of August 2015. The parameter settings of the starting and ending times for the first day are presented in the *namelist.input* file in Section 5.3. In the meantime, the introduction of the spin-up time ensures that final wind power forecasts can be reported before the next day a couple of hours in advance. The earliest reporting time depends on the computational time of the WRF model. Since the time length of the original wind data was 24 days, there were 24 pairs of starting and ending time parameters in total.

In the *physics* section, the *mp_physics*, *cu_physics*, *bl_pbl_physics*, *sf_sfclay_physics*, and *sf_surface_physics* parameters, as the critical physics options that need to be determined in the WRF modelling, were selected as the variable parameters in this study. To be precise, the *mp_physics*, *cu_physics*, *bl_pbl_physics*, *sf_sfclay_physics*, and *sf_surface_physics* parameters represent the microphysics, cumulus, planetary boundary-layer, surface-layer, and land-surface parameterisations, respectively. The direct interactions between the various WRF physics options are displayed in Figure 5.3. In addition, there is another variable parameter called *num_soil_layers*, which represents the number of soil layers in the land-surface model. For each land-surface model, the number of soil layers is fixed. Since the *num_soil_layers* parameter depends on the *sf_surface_physics* parameter, the *num_soil_layers* parameter will not be considered in the following discussion.

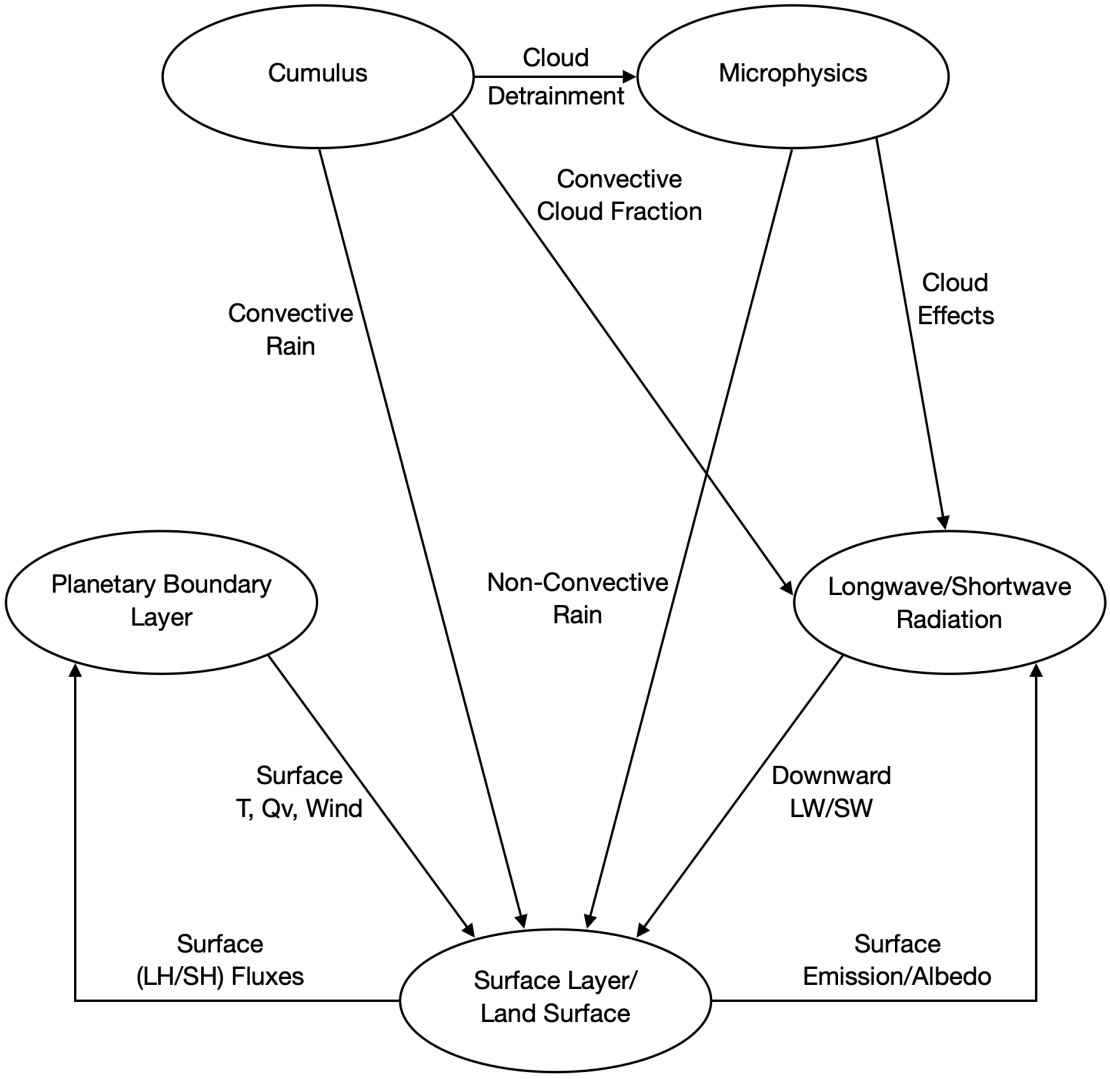

Figure 5.3. Direct interactions between the various WRF physics options.

For each physics option, there are many parameterisation schemes available. Some of them are simple and used for coarse domains or ideal cases, while the others are complex and suitable for high-resolution real-world simulations. The various parameterisation schemes (used in this research) for the five physics options in the WRF model are summarised in Table 5.1.

Table 5.1. The various parameterisation schemes for the five physics options in the WRF model.

No.	mp_physics	cu_physics	bl_pbl_physics	sf_sfclay_physics	sf_surface_physics
1	Purdue Lin	Kain-Fritsch	Yonsei University	Revised MM5	Rapid Update Cycle
2	Ferrier Eta	Betts-Miller-Janjic	Mellor-Yamada-Janjic	Eta Similarity	Noah-Multi-Physics
3	WRF Single-Moment 6-Class	Grell-Freitas	Quasi-Normal Scale Elimination	Quasi-Normal Scale Elimination	Community Land Model Version 4
4	Thompson et al.	Grell 3D	Mellor-Yamada Nakanishi and Niino Level 3	Mellor-Yamada Nakanishi and Niino	
5	Milbrandt-Yau Double-Moment 7-Class	Zhang-McFarlane	BouLac	Total Energy - Mass Flux	
6	Stony Brook University (Y. Lin)	Kain-Fritsch-Cumulus Potential	University of Washington		
7	WRF Double-Moment 6-Class	Multi-Scale Kain-Fritsch	Total Energy - Mass Flux		
8	NSSL Single-Moment 6-Class	New Tiedtke	Shin-Hong		
9	NSSL-LFO Single-Moment 6-Class		Grenier-Bretherton-McCaa		

No.	mp_physics	cu_physics	bl_pbl_physics	sf_sfclay_physics	sf_surface_physics
10	Thompson Aerosol-Aware				

From Table 5.1, it can be seen that the numbers of selected physical parameterisation schemes for the microphysics, cumulus, planetary boundary-layer, surface-layer, and land-surface physics options were 10, eight, nine, five, and three, respectively. Mathematically, there were 10,800 physical parameterisation scheme combinations. However, a number of restrictions on the various scheme combinations exist. For example, the planetary boundary-layer scheme is fixed to one or two specific surface-layer schemes: when the *bl_pbl_physics* parameters are set to be 1, 2, 4, 6, 8, 9, 10, 11, and 12, the *sf_sfclay_physics* parameters have to be 1, 2, 4, 5, 1 or 2, 1 or 2, 10, 1, and 1, respectively. Any other combination between the planetary boundary-layer and surface-layer schemes does not work. Besides, the multi-scale Kain-Fritsch scheme only matches the Yonsei University scheme, and the Zhang-McFarlane scheme requires the Mellor-Yamada-Janjic or University of Washington scheme, which are the fixed combinations between the cumulus and planetary boundary-layer schemes. The community land model scheme is not compatible with the Mellor-Yamada-Janjic or quasi-normal scale elimination scheme, which are the conflicts between the land-surface and planetary boundary-layer schemes. Additionally, some WRF models with certain scheme combinations cannot generate full results. Consequently, the number of total practical scheme combinations was 1,334, which was relatively small compared with that of possible scheme combinations (10,800).

5.3.3 Running a *real* and a *wrf* Programme

After suitably editing the parameters in the *namelist.input* file, a *real* programme can be run. The *real* programme is an initialisation programme required by real simulations. Specifically, it plays the role of taking the 2D outputs created by the WPS programme and performing the vertical interpolation for 3D meteorological fields and sub-surface soil data. After that, the boundary and initial condition files for each domain are produced and will be fed into a *wrf* programme. Running the *wrf* programme is the last step of running the WRF model. Finally, the output files containing all the meteorological forecasts were generated.

5.4 Estimating Wind Speed Forecasts at the Wind Turbine Hub Height

WRF output files contain a large number of different meteorological forecasts, and wind speed forecasts were the only meteorological data needed in this research. As explained in Section 5.3, in the vertical direction, the WRF model domain was discretised by utilising 50 levels extending from the ground surface to a height corresponding to an atmospheric pressure of 5,000 Pa. The corresponding heights of the first 12 levels are shown in Table 5.2.

Table 5.2. Heights of the first 12 vertical levels in the WRF models.

Model level	Height (m)
1	0
2	52.6
3	119.75
4	205.06
5	312.82
6	447.9
7	615.71
8	821.93
9	1072.74
10	1373.08
11	1725.85
12	2132.68

The hub height of the studied wind turbine was 65 m. By referring to Table 5.2, it can be found that the hub height was between the second and third vertical levels. Since the wind speed forecasts for each vertical level were available, an interpolation method could be applied to estimate the wind speed forecasts at the 65-m height. Moreover, as most weather stations observe wind speeds at the height of 10 m, WRF models automatically estimate 10-m height wind speed forecasts and provide these data for users. Hence, a more

convenient solution was proposed herein—converting wind speed forecasts at the 10-m height to those at the 65-m height by the wind profile power law shown as below [62]:

$$U_{hub} = U_r(\frac{h_{hub}}{h_r})^{\alpha} \ , \tag{5.1}$$

where U_{hub} is the wind speed (m/s) at the hub height, U_r is the given wind speed (m/s) at a reference height, h_{hub} is the hub height (m), h_r is the reference height (m), and α is the wind shear. When wind speed measurements at different heights are unavailable, the wind shear exponent α is taken as 1/7 (or 0.143) as an approximation.

The estimation process of the wind speed forecasts at the wind turbine hub height is described as follows:

(1) Read a WRF output file;

(2) Extract the x-wind components at the 10-m height at all times;

(3) Extract the y-wind components at the 10-m height at all times;

(4) Find the nearest grid index to the wind turbine location;

(5) Extract the x-wind components at the 10-m height for the wind turbine location;

(6) Extract the y-wind components at the 10-m height for the wind turbine location;

(7) Calculate the wind speed forecasts at the 10-m height based on the zonal and meridional wind components by the Pythagorean theorem;

(8) Estimate the wind speed forecasts at the hub height by the wind profile power law.

5.5 Selecting and Combining WRF Models Based on a TOPSIS Scheme

Dr Deyong Wen is now an atmospheric scientist and a data analyst working at Environment and Climate Change Canada (ECCC). When he did research in our laboratory as a postdoctoral fellow a few years ago, he produced a set of wind speed forecasts by using the WRF model for the same wind turbine case. The previous WRF model was created mainly based on Dr Wen's working experience. In particular, a couple of physical parameterisation

scheme combinations were examined based on a very short test dataset, and then a specific scheme combination was chosen according to the model predictive performance. Although those data (wind speed forecasts) have not been published, the methodology of building the WRF model is very similar to that one applied in Dr Wen's paper 'Short-term wind speed and power forecasting using an ensemble of mixture density neural networks' [91], which was published in the journal of Renewable Energy in 2016. His current status as an expert at ECCC and his published papers show that he has sufficient professional meteorological knowledge to build reliable WRF models and calculate wind speed forecasts. Therefore, the wind speed forecasts he generated for the specific wind turbine, as the early results of our laboratory, are believed to be able to represent a general level in the industry and be regarded as a benchmark in this research. In order to distinguish them from the previous wind speed forecasts, the wind speed forecasts obtained in this case were called new wind speed forecasts. The choices of the physical parameterisation scheme combinations for the various physics options provide different WRF models that generate different wind speed forecasts. Nevertheless, there are no rules for selecting the parameterisation scheme for each physics option. All physical parameterisation schemes were developed by different research groups, and each of these schemes has its own characteristic features. The assumption in this study was that for the studied wind farm with its distinctive geographical factors and climatic conditions, one or several specific physical parameterisation scheme combinations might consistently outperform other scheme combinations. In addition, it was speculated that among the five selected physics options, the planetary boundary-layer, surface-layer, and land-surface parameterisations were even more sensitive than the microphysics and cumulus parameterisations.

Instead of the ad hoc method previously applied, a systematic approach was proposed to select the WRF models. In total, there were wind speeds over a 24-day period that needed to be forecasted. However, 1,334 possible physical parameterisation scheme combinations implied that there were 1,334 individual WRF model forecasts that needed to be considered. Because of the substantial computational time and cost that this would require, it was extremely burdensome to run 1,334 individual WRF models to provide wind speed forecasts for each day of the 24-day period. A practical solution proposed in the study was to run the entire set of 1,334 WRF models for the first day and select the top 50 from them according to their predictive performance. A comparison of the new wind speed forecasts provided by the 1,334 different WRF models, Dr Wen's wind speed forecasts, and the historical wind speed measurements for the first day of the dataset is exhibited in Figure 5.4. A careful perusal of this figure shows that the predictive performance of the 1,334 WRF models (with specific choices for the parameterisations of the various physical processes) varied greatly. Besides, the general trend of the new wind speed forecasts was roughly the same

as that of Dr Wen's wind speed forecasts. Nevertheless, it is a little bit tricky to tell how well the new wind speed forecasts perform compared with Dr Wen's wind speed forecasts according to Figure 5.4. It should be noted that the wind speed measurements fell out of the coverage of the wind speed forecasts provided by the 1,334 WRF models most of the time. However, this one-day period was too short to indicate statistical significance. Furthermore, atmospheric motion is a complicated process, and the predictive performance of WRF models varies every day. At this stage, the goal was to find relatively accurate WRF models which had the potential to be further improved by using a wind speed correction model.

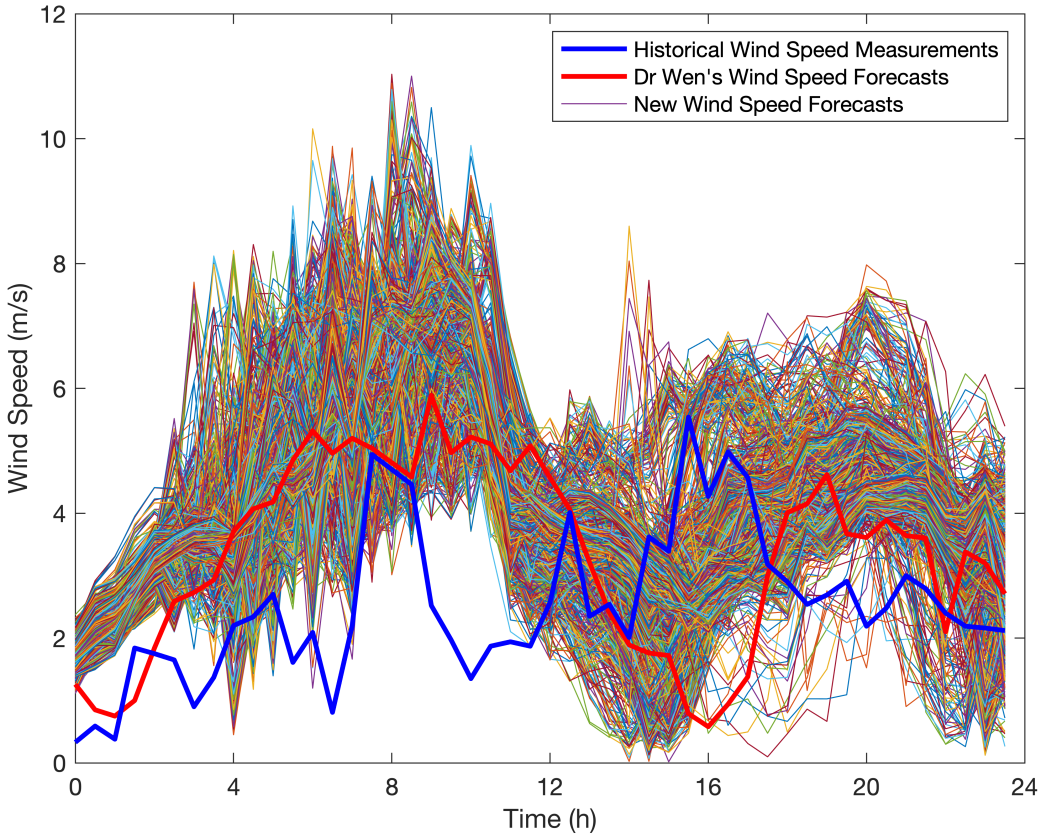

Figure 5.4. Comparison of the new wind speed forecasts provided by the 1,334 different WRF models, Dr Wen's wind speed forecasts, and the historical wind speed measurements for the first day of the dataset (the 11th of August 2015).

A short version of the dataset of the historical wind speed measurements (indicated by WSM), Dr Wen's wind speed forecasts (indicated by WSF 0), and the new wind speed forecasts provided by the 1,334 different WRF models (indicated by WSFs 1 to 1,334) for the first day of the dataset is shown in Table 5.3.

Table 5.3. Short version of the dataset of the historical wind speed measurements (indicated by WSM), Dr Wen's wind speed forecasts (indicated by WSF 0), and the new wind speed forecasts provided by the 1,334 different WRF models (indicated by WSFs 1 to 1,334) for the first day of the dataset (the 11th of August 2015).

Month	Day	Hour	Minute	WSM (m/s)	WSF 0 (m/s)	WSF 1 (m/s)	WSF 2 (m/s)	⋯	WSF 1,333 (m/s)	WSF 1,334 (m/s)
8	11	0	0	0.33	1.26	1.80	1.92	⋯	1.68	1.62
8	11	0	30	0.59	0.85	2.18	2.40	⋯	2.05	1.89
8	11	1	0	0.38	0.75	2.52	2.68	⋯	2.26	2.14
8	11	1	30	1.84	1.00	2.85	2.99	⋯	2.67	2.67
8	11	2	0	1.75	1.84	3.26	3.38	⋯	3.16	3.30
8	11	2	30	1.65	2.59	3.44	3.55	⋯	3.41	3.55
8	11	3	0	0.90	2.73	3.63	3.77	⋯	3.59	3.74
8	11	3	30	1.37	2.93	3.69	3.73	⋯	3.68	3.73
8	11	4	0	2.20	3.71	4.21	4.08	⋯	3.72	3.69
8	11	4	30	2.34	4.07	4.40	4.61	⋯	4.05	4.05
⋮	⋮	⋮	⋮	⋮	⋮	⋮	⋮	⋱	⋮	⋮
8	11	21	30	2.79	3.60	4.29	4.21	⋯	4.17	3.98
8	11	22	0	2.40	2.10	4.03	3.94	⋯	3.57	3.52
8	11	22	30	2.19	3.38	3.39	3.38	⋯	3.18	3.25
8	11	23	0	2.16	3.20	3.33	3.22	⋯	3.20	3.98
8	11	23	30	2.12	2.71	4.36	4.10	⋯	2.39	2.19

Since the historical wind speed measurements for the first day of the dataset were given, the new wind speed forecasts and Dr Wen's wind speed forecasts could be evaluated by comparing them with their corresponding measurements. For this purpose, various evaluation metrics summarised in Equations (3.9) to (3.14) were used to assess the predictive performance of the WRF models. More specifically, the MB, MAE, RMSE, IA, MAPE, and SMAPE were evaluated for each of the WRF model forecasts of the wind speed for the first day. A short version of the predictive performance assessment of the 1,335 WRF models by using six evaluation metrics is shown in Table 5.4. The first column represents the WRF model index. Particularly, Model 0, as a benchmark model in this study, referred to the WRF model previously created by Dr Wen. Models 1 to 1,334 represented the 1,334 individual WRF models based on different physical parameterisation scheme combinations. The values of the six evaluation metrics for each WRF model are shown in columns 2 to 7.

Table 5.4. Short version of the predictive performance assessment of the 1,335 WRF models for the first day of the dataset (the 11th of August 2015) by using six evaluation metrics.

Model index 1	MB (m/s)	MAE (m/s)	MAPE	SMAPE	RMSE (m/s)	IA
0	0.81	1.67	87.22%	58.74%	2.12	0.37
1	1.79	2.03	127.31%	62.33%	2.43	0.40
2	1.77	2.04	128.71%	63.07%	2.42	0.39
3	1.78	2.08	128.73%	63.65%	2.47	0.39
4	1.75	2.03	124.56%	62.65%	2.41	0.40
5	1.79	2.03	126.04%	62.76%	2.41	0.40
6	1.80	2.05	127.73%	62.80%	2.44	0.40
7	1.72	2.05	127.26%	63.37%	2.44	0.37
8	1.74	2.03	124.93%	62.87%	2.40	0.40
9	1.75	2.03	125.03%	62.82%	2.40	0.41
10	1.79	2.05	125.40%	62.91%	2.43	0.40
⋮	⋮	⋮	⋮	⋮	⋮	⋮
1,330	1.47	2.00	120.69%	62.54%	2.40	0.35
1,331	1.48	1.97	120.74%	61.49%	2.37	0.37
1,332	1.42	1.90	115.45%	60.34%	2.30	0.37
1,333	1.43	1.93	115.90%	61.15%	2.31	0.37
1,334	1.43	1.92	115.58%	60.66%	2.32	0.36

If there were only one specific metric, it would be straightforward to compare the 1,335 WRF model forecasts with the associated wind speed measurements using this metric and rank the individual forecasts from the best to the worst in predictive performance. However, in this case, six different metrics were employed, and the ranking of the 1,335 WRF model forecasts was different for each metric. For the purpose of finding the best-performing prediction among the various WRF model forecasts of the wind speed, the

TOPSIS scheme was applied to address this multi-metric decision making problem, and the process is carried out as follows:

(1) Step 1

Create a standardised evaluation matrix X consisting of 1,335 alternatives and six metrics:

$$X = \begin{bmatrix} 0.81 & 1.67 & 0.8722 & 0.5874 & 2.12 & 0.37 \\ 1.79 & 2.03 & 1.2731 & 0.6233 & 2.43 & 0.40 \\ 1.77 & 2.04 & 1.2871 & 0.6307 & 2.42 & 0.39 \\ 1.78 & 2.08 & 1.2873 & 0.6365 & 2.47 & 0.39 \\ 1.75 & 2.03 & 1.2456 & 0.6265 & 2.41 & 0.40 \\ 1.79 & 2.03 & 1.2604 & 0.6276 & 2.41 & 0.40 \\ 1.80 & 2.05 & 1.2773 & 0.6280 & 2.44 & 0.40 \\ 1.72 & 2.05 & 1.2726 & 0.6337 & 2.44 & 0.37 \\ 1.74 & 2.03 & 1.2493 & 0.6287 & 2.40 & 0.40 \\ 1.75 & 2.03 & 1.2503 & 0.6282 & 2.40 & 0.41 \\ 1.79 & 2.05 & 1.2540 & 0.6291 & 2.43 & 0.40 \\ \vdots & \vdots & \vdots & \vdots & \vdots & \vdots \\ 1.47 & 2.00 & 1.2069 & 0.6254 & 2.40 & 0.35 \\ 1.48 & 1.97 & 1.2074 & 0.6149 & 2.37 & 0.37 \\ 1.42 & 1.90 & 1.1545 & 0.6034 & 2.30 & 0.37 \\ 1.43 & 1.93 & 1.1590 & 0.6115 & 2.31 & 0.37 \\ 1.43 & 1.92 & 1.1558 & 0.6066 & 2.32 & 0.36 \end{bmatrix}. \tag{5.2}$$

(2) Step 2

Positivise the original matrix X, and use Y to represent the positivised matrix. Positivisation refers to the conversion of all non-benefit metrics into benefit ones. In this case, the MB was an intermediate metric since its optimal value was 0. Besides, the MAE, MAPE, SMAPE, and RMSE belonged to the cost metric. This is because, for all the errors, the lower is the better. Obviously, the last one, IA, was a benefit metric as the bigger was the better for it. Therefore, there were one intermediate and four cost metrics that needed to be converted to the benefit metrics. According to Equations (2.50) to (2.52), the positivised matrix was generated:

$$Y = P(X) = \begin{bmatrix} 1.90 & 1.10 & 0.7555 & 0.2507 & 1.24 & 0.37 \\ 0.91 & 0.75 & 0.3546 & 0.2149 & 0.93 & 0.40 \\ 0.93 & 0.73 & 0.3406 & 0.2075 & 0.94 & 0.39 \\ 0.93 & 0.69 & 0.3404 & 0.2016 & 0.89 & 0.39 \\ 0.95 & 0.75 & 0.3821 & 0.2117 & 0.95 & 0.40 \\ 0.92 & 0.74 & 0.3673 & 0.2105 & 0.95 & 0.40 \\ 0.90 & 0.73 & 0.3504 & 0.2102 & 0.92 & 0.40 \\ 0.99 & 0.72 & 0.3551 & 0.2045 & 0.93 & 0.37 \\ 0.97 & 0.74 & 0.3784 & 0.2095 & 0.97 & 0.40 \\ 0.96 & 0.74 & 0.3774 & 0.2099 & 0.96 & 0.41 \\ 0.92 & 0.73 & 0.3737 & 0.2090 & 0.93 & 0.40 \\ \vdots & \vdots & \vdots & \vdots & \vdots & \vdots \\ 1.23 & 0.78 & 0.4208 & 0.2128 & 0.97 & 0.35 \\ 1.23 & 0.81 & 0.4203 & 0.2232 & 0.99 & 0.37 \\ 1.29 & 0.87 & 0.4732 & 0.2347 & 1.06 & 0.37 \\ 1.27 & 0.85 & 0.4687 & 0.2267 & 1.06 & 0.37 \\ 1.28 & 0.86 & 0.4719 & 0.2316 & 1.04 & 0.36 \end{bmatrix}. \tag{5.3}$$

(3) Step 3

Normalise the positivised matrix Y, and use Z to represent the normalised matrix. The meaning of normalisation is to eliminate the influence of different metric dimensions. According to Equation (2.56), the normalised matrix was obtained:

$$Z = N(Y) = \begin{bmatrix} 0.0460 & 0.0378 & 0.0487 & 0.0321 & 0.0341 & 0.0263 \\ 0.0221 & 0.0256 & 0.0229 & 0.0275 & 0.0255 & 0.0287 \\ 0.0226 & 0.0250 & 0.0220 & 0.0266 & 0.0259 & 0.0280 \\ 0.0224 & 0.0237 & 0.0220 & 0.0258 & 0.0246 & 0.0273 \\ 0.0231 & 0.0256 & 0.0246 & 0.0271 & 0.0261 & 0.0285 \\ 0.0222 & 0.0255 & 0.0237 & 0.0270 & 0.0262 & 0.0286 \\ 0.0219 & 0.0250 & 0.0226 & 0.0269 & 0.0254 & 0.0284 \\ 0.0240 & 0.0249 & 0.0229 & 0.0262 & 0.0255 & 0.0262 \\ 0.0235 & 0.0256 & 0.0244 & 0.0268 & 0.0265 & 0.0286 \\ 0.0232 & 0.0255 & 0.0243 & 0.0269 & 0.0264 & 0.0288 \\ 0.0223 & 0.0250 & 0.0241 & 0.0268 & 0.0257 & 0.0286 \\ \vdots & \vdots & \vdots & \vdots & \vdots & \vdots \\ 0.0299 & 0.0267 & 0.0271 & 0.0273 & 0.0265 & 0.0247 \\ 0.0297 & 0.0277 & 0.0271 & 0.0286 & 0.0272 & 0.0266 \\ 0.0313 & 0.0298 & 0.0305 & 0.0301 & 0.0291 & 0.0263 \\ 0.0308 & 0.0291 & 0.0302 & 0.0290 & 0.0291 & 0.0260 \\ 0.0310 & 0.0294 & 0.0304 & 0.0297 & 0.0286 & 0.0259 \end{bmatrix} . \tag{5.4}$$

(4) Step 4

Determine the weights for the six model evaluation metrics. For this purpose, an entropy method was employed in this study rather than a customisation method (which is arbitrary). The results are shown in Table 5.5.

Table 5.5. Weights for the six model evaluation metrics determined by using an entropy method.

Metric	MB	MAE	MAPE	SMAPE	RMSE	IA
Weight	0.2105	0.2347	0.2268	0.1011	0.2036	0.0233

(5) Step 5

Define the positive ideal solution Z^+ and negative ideal solution Z^-. According to Equations (2.57) and (2.58), the positive and negative ideal solutions were acquired:

$$Z^+ = (0.0507, 0.0513, 0.0509, 0.0430, 0.0494, 0.0390) , \tag{5.5}$$

and

$$Z^- = (0, 0, 0, 0, 0, 0.0181) \ . \tag{5.6}$$

(6) Step 6

Calculate the distances between each alternative and the positive ideal solution D_i^+ and between each alternative and the negative ideal solution D_i^-. According to Equations (2.59) and (2.60), the distances for the first day of the dataset were calculated, and a short version of the results is shown in Table 5.6.

Table 5.6. Short version of the distances between each alternative and the positive ideal solution and between each alternative and the negative ideal solution for the first day of the dataset (the 11th of August 2015).

Positive ideal solution	Distance	Negative ideal solution	Distance
D_0^+	0.0106	D_0^-	0.0408
D_1^+	0.0255	D_1^-	0.0242
D_2^+	0.0257	D_2^-	0.0240
D_3^+	0.0264	D_3^-	0.0232
D_4^+	0.0247	D_4^-	0.0249
D_5^+	0.0252	D_5^-	0.0245
D_6^+	0.0258	D_6^-	0.0239
D_7^+	0.0253	D_7^-	0.0243
D_8^+	0.0246	D_8^-	0.0250
D_9^+	0.0247	D_9^-	0.0249
D_{10}^+	0.0253	D_{10}^-	0.0243
⋮	⋮	⋮	⋮
D_{1330}^+	0.0223	D_{1330}^-	0.0272
D_{1331}^+	0.0218	D_{1331}^-	0.0277
D_{1332}^+	0.0197	D_{1332}^-	0.0299
D_{1333}^+	0.0201	D_{1333}^-	0.0294
D_{1334}^+	0.0200	D_{1334}^-	0.0295

(7) Step 7

Calculate the similarity scores of all the alternatives to the positive ideal solution. According to Equation (2.61), the similarity scores for the first day of the dataset were calculated, and a short version of the results is shown in Table 5.7.

Table 5.7. Short version of the similarity scores of the alternatives to the positive ideal solution for the first day of the dataset (the 11th of August 2015).

Model	Similarity score
S_0	0.7938
S_1	0.4876
S_2	0.4825
S_3	0.4682
S_4	0.5018
S_5	0.4928
S_6	0.4807
S_7	0.4894
S_8	0.5032
S_9	0.5012
S_{10}	0.4905
⋮	⋮
S_{1330}	0.5495
S_{1331}	0.5593
S_{1332}	0.6030
S_{1333}	0.5942
S_{1334}	0.5965

(8) Step 8

Rank all the alternatives according to their similarity scores. Since the similarity scores of the 1,335 WRF models were obtained, these models could be ranked from the highest similarity score to the lowest one for the first day of the dataset. A short version of the result is shown in Table 5.8, from which it can be found that the similarity score of Model 210 was more than 10 times that of Model 682, indicating that for the first day, the wind speed predictive performance of Model 210 was much better than that

of Model 682.

Table 5.8. Short version of the model rankings for the first day of the dataset (the 11th of August 2015) according to the similarity scores.

Rank	Model index 1	Similarity score
1	210	0.9797
2	220	0.9679
3	211	0.9357
4	215	0.9256
5	256	0.9223
6	218	0.9207
7	217	0.9192
8	258	0.9173
9	230	0.9172
10	227	0.9139
11	222	0.9124
⋮	⋮	⋮
1,331	923	0.1002
1,332	692	0.1001
1,333	921	0.0965
1,334	664	0.0963
1,335	682	0.0921

As mentioned previously, it was not possible (computationally prohibitive) to compute 1,334 WRF model forecasts for each day of the 24-day dataset. The significance of testing the predictive performance of the 1,334 WRF models based only on the first day of the dataset was to provide the rational basis for picking a small number of the best-performing WRF models to be used in forecasting the wind speed for the remaining 23 days of the

dataset. The top 75 WRF models selected according to the similarity scores are shown in Table 5.9.

Table 5.9. Top 75 WRF models selected for the first day of the dataset (the 11th of August 2015) according to the similarity scores.

Rank	Model index 1	Similarity score
1	210	0.9797
2	220	0.9679
3	211	0.9357
4	215	0.9256
5	256	0.9223
6	218	0.9207
7	217	0.9192
8	258	0.9173
9	230	0.9172
10	227	0.9139
11	222	0.9124
12	223	0.9122
13	257	0.9122
14	237	0.9116
15	233	0.9108
16	225	0.9084
17	250	0.9062
18	228	0.9046
19	238	0.9035
20	209	0.9034
21	221	0.9032
22	247	0.9017

Rank	Model index 1	Similarity score
23	213	0.8987
24	216	0.8968
25	226	0.8959
26	236	0.8946
27	206	0.8940
28	224	0.8933
29	219	0.8833
30	207	0.8823
31	240	0.8817
32	246	0.8813
33	243	0.8780
34	252	0.8761
35	232	0.8734
36	825	0.8733
37	248	0.8715
38	251	0.8701
39	244	0.8700
40	200	0.8644
41	249	0.8591
42	253	0.8586
43	242	0.8570
44	214	0.8556
45	254	0.8507
46	212	0.8503
47	208	0.8482

Rank	Model index 1	Similarity score
48	231	0.8480
49	831	0.8464
50	234	0.8440
51	827	0.8437
52	255	0.8435
53	795	0.8410
54	830	0.8410
55	235	0.8397
56	241	0.8374
57	203	0.8362
58	828	0.8313
59	794	0.8294
60	229	0.8224
61	245	0.8183
62	829	0.8133
63	842	0.8096
64	205	0.8088
65	201	0.8063
66	832	0.8062
67	826	0.7971
68	204	0.7968
69	239	0.7954
70	1122	0.7940
71	0	0.7938
72	202	0.7933

Rank	Model index 1	Similarity score
73	844	0.7918
74	1126	0.7883
75	804	0.7869

From Table 5.9, it can be seen that the ranking of Model 0 was 71, indicating that there were 70 WRF models performing better than Dr Wen's WRF model in the wind speed forecasting for the first day. It should be noted that a certain number of these 70 WRF models (viz., Models 218, 223, 233, 238, 213, 243, 825, 248, 253, 208, 827, 203, and 832) failed to generate complete wind speed forecasts for the next 23 days and, as a consequence, had to be removed from the selection of the best-performing models. In accordance with the similarity scores and applicability, the top 50 WRF models for the first day of the dataset (see Table 5.10) were selected from the remaining WRF models and applied to provide the predictions of the wind speed for the remaining 23 days. For the purpose of convenience, the index of the 50 best-performing WRF models was renamed from model index 1 to model index 2. From Table 5.10, it can be seen that the similarity scores of these 50 WRF models were all greater than 0.8000 and higher than that of Model 0 (the benchmark).

Table 5.10. Top 50 WRF models selected for the first day of the dataset (the 11th of August 2015) according to the similarity scores and applicability.

Model index 2	Model index 1	Similarity score
1	210	0.9797
2	220	0.9679
3	211	0.9357
4	215	0.9256
5	256	0.9223
6	217	0.9192
7	258	0.9173
8	230	0.9172
9	227	0.9139

Model index 2	Model index 1	Similarity score
10	222	0.9124
11	257	0.9122
12	237	0.9116
13	225	0.9084
14	250	0.9062
15	228	0.9046
16	209	0.9034
17	221	0.9032
18	247	0.9017
19	216	0.8968
20	226	0.8959
21	236	0.8946
22	206	0.8940
23	224	0.8933
24	219	0.8833
25	207	0.8823
26	240	0.8817
27	246	0.8813
28	252	0.8761
29	232	0.8734
30	251	0.8701
31	244	0.8700
32	200	0.8644
33	249	0.8591
34	242	0.8570

Model index 2	Model index 1	Similarity score
35	214	0.8556
36	254	0.8507
37	212	0.8503
38	231	0.8480
39	831	0.8464
40	234	0.8440
41	255	0.8435
42	795	0.8410
43	830	0.8410
44	235	0.8397
45	241	0.8374
46	828	0.8313
47	794	0.8294
48	229	0.8224
49	245	0.8183
50	829	0.8133

Although the 50 WRF models selected above were few in number compared with the original 1,334 possible WRF models, this number of models was still too large for practical applications. The solution was to further reduce the number of WRF models based on the training dataset consisting of the wind speed measurements for the first 20 days. More specifically, the 50 best-performing WRF models selected above were applied to generate the wind speed forecasts for the first 20 days. The predictive performance of these 50 WRF models was evaluated by using six evaluation metrics, namely the MB, MAE, RMSE, IA, MAPE, and SMAPE. Following on from this evaluation, the TOPSIS scheme was used to rank the 50 WRF models over this 20-day wind speed forecast interval, and the ranking result is shown in Table 5.11. From Table 5.11, it can be seen that the similarity scores of these 50 best-performing WRF models were diverse. In particular, the highest similarity score among all the WRF models considered was 0.9770, while the lowest similarity score

was as low as 0.1015. Although all of these 50 WRF models outperformed Dr Wen's WRF model in the wind speed forecasting for the first day, there were only six WRF models superior to Model 0 in terms of the overall predictive performance over the period of 20 days.

Table 5.11. Model rankings for the 20 days of the training dataset according to the similarity scores.

Rank	Model index 2	Similarity score
1	39	0.9770
2	47	0.9141
3	46	0.8806
4	43	0.8755
5	42	0.8629
6	50	0.6100
7	0	0.5415
8	16	0.4277
9	45	0.3580
10	6	0.3530
11	10	0.3412
12	24	0.3368
13	28	0.3113
14	1	0.3010
15	3	0.3009
16	5	0.2932
17	26	0.2923
18	20	0.2829
19	19	0.2770
20	2	0.2699

Rank	Model index 2	Similarity score
21	27	0.2502
22	9	0.2496
23	4	0.2475
24	7	0.2470
25	23	0.2408
26	11	0.2379
27	30	0.2337
28	15	0.2282
29	49	0.2195
30	40	0.2152
31	25	0.2050
32	18	0.2035
33	29	0.2029
34	32	0.1943
35	14	0.1892
36	17	0.1875
37	37	0.1783
38	48	0.1727
39	22	0.1671
40	34	0.1626
41	12	0.1586
42	8	0.1566
43	35	0.1517
44	13	0.1450
45	41	0.1431

Rank	Model index 2	Similarity score
46	33	0.1427
47	38	0.1371
48	21	0.1298
49	44	0.1176
50	36	0.1065
51	31	0.1015

However, solely considering the overall predictive performance of a WRF model is insufficient. If a WRF model performs well under some conditions and poorly under other conditions, it cannot be regarded as a reliable and robust model. Consequently, the evaluation of the segmental predictive performance of the top six candidate WRF models was considered herein. Since the test dataset consisted of 4 days of wind speed data, it was useful to consider every group of wind data over a 4-day period to be a segment. From this perspective, the 20-day wind speed training dataset was split into five segments. After this split of the training dataset, the TOPSIS scheme was applied to each segment separately, and the rankings of the 51 WRF models for each segment were determined. The segmental and overall rankings of the top six candidate and Dr Wen's WRF models are displayed in Table 5.12.

Table 5.12. Segmental and overall rankings of the top six candidate and Dr Wen's WRF models as determined by using the 20-day training dataset.

Model index 2	1st 4-day	2nd 4-day	3rd 4-day	4th 4-day	5th 4-day	20-day
0	7	1	15	40	10	7
39	2	2	2	5	2	1
42	1	3	3	2	6	5
43	4	8	1	7	3	4
46	5	6	6	1	1	3
47	3	5	4	4	4	2
50	6	4	5	48	5	6

A careful examination of Table 5.12 shows that although Model 0 performed the best for the second segment, its predictive performance on the third segment was not very good, and its predictive performance on the fourth segment was poor. A similar finding applied to Model 50, which performed well for all the data segments except one: the predictive performance of Model 50 on the fourth segment (48th) was extremely terrible. In contrast, the segmental predictive performance of the other five WRF models, namely Models 39, 42, 43, 46, and 47, was generally good on all the data segments. Specifically, the rankings of these WRF models were in the top 10 for every segment and in the top five for the entire 20-day training dataset. Moreover, the predictive performance of Models 39 and 47 was consistently in the top five—resulting, as such, in their top two rankings for the overall wind speed predictive performance.

At this stage, the top five WRF models (viz., Models 39, 42, 43, 46, and 47) selected from the original 1,334 WRF models were optimal in the sense that they not only outperformed the other models but also performed consistently over all the data segments. The physical parameterisation scheme combinations of the top five WRF models are summarised in Table 5.13, from which it can be easily found that the planetary boundary-layer, surface-layer, and land-surface parameterisations were proved to be more sensitive than the microphysics and cumulus parameterisations. Specifically, the top five WRF models shared the same physical schemes for the planetary boundary-layer, surface-layer, and land-surface parameterisations, namely BouLac, revised MM5, and Noah-multi-physics, respectively. In addition, the selections for the microphysics and cumulus parameterisations were also very limited—three physical schemes (NSSL-LFO single-moment 6-class, NSSL single-moment 6-class, and Stony Brook University (Y. Lin)) for the former and two (new Tiedtke and Betts-Miller-Janjic) for the latter. By referring to Table 5.1, it can be categorised that three out of the 10 microphysics parameterisation schemes and two out of the eight cumulus parameterisation schemes contributed to the best-performing individual WRF models. In addition, one specific scheme combination for the planetary boundary-layer, surface-layer, and land-surface parameterisations from a number of possible choices was determined to outperform the other scheme combinations consistently.

Table 5.13. The physical parameterisation scheme combinations of the top five WRF models.

Rank	Model index 2	mp_physics	cu_physics	bl_pbl_physics	sf_sfclay_physics	sf_surface_physics
1	39	NSSL-LFO Single-Moment 6-Class	New Tiedtke	BouLac	Revised MM5	Noah-Multi-Physics
2	47	NSSL Single-Moment 6-Class	Betts-Miller-Janjic	BouLac	Revised MM5	Noah-Multi-Physics
3	46	Stony Brook University (Y. Lin)	New Tiedtke	BouLac	Revised MM5	Noah-Multi-Physics
4	43	NSSL Single-Moment 6-Class	New Tiedtke	BouLac	Revised MM5	Noah-Multi-Physics
5	42	NSSL-LFO Single-Moment 6-Class	Betts-Miller-Janjic	BouLac	Revised MM5	Noah-Multi-Physics

One possibility for the next step in the analysis was to simply apply Model 39 to forecast the wind speed for the last 4 days (the test dataset), as this was the best model based on the overall predictive performance on the training dataset. An alternative (perhaps more novel) possibility was proposed here: to create a 5-in-1 (ensemble) WRF model (referred to herein as Model 51) by combining the top five best-performing WRF models. As mentioned in Section 2.8.1, the TOPSIS can also be utilised as an approach to assigning weights for the various model alternatives. From this perspective, the proposed wind speed forecasts provided by the output of Model 51 were determined in accordance with the following schema:

$$M_{51} = w_{39}M_{39} + w_{42}M_{42} + w_{43}M_{43} + w_{46}M_{46} + w_{47}M_{47} \ , \tag{5.7}$$

in which

$$w_i = \frac{S_i}{S_{39} + S_{42} + S_{43} + S_{46} + S_{47}}, \quad i = 39,\ 42,\ 43,\ 46,\ 47 \ , \tag{5.8}$$

where M_{51}, M_{39}, M_{42}, M_{43}, M_{46}, and M_{47} are the wind speed forecasts provided by Models 51, 39, 42, 43, 46, and 47, respectively, w_i is the weight for Model i, and S_i is the similarity score of Model i (obtained from the TOPSIS scheme).

And then, Model 51 was compared with the top 50 and Dr Wen's WRF models, and these models were ranked by using the TOPSIS scheme again. The segmental and overall rankings of the 5-in-1 (ensemble), the top five, and Dr Wen's WRF models are summarised in Table 5.14. A careful perusal of this table shows that Model 51 was exceptional: in terms of predictive performance, this model either ranked first or second for every 4-day data segment and first for the entire 20-day wind speed training dataset.

Table 5.14. Segmental and overall rankings of the 5-in-1 (ensemble), the top five, and Dr Wen's WRF models as determined by using the 20-day training dataset.

Model index 2	1st 4-day	2nd 4-day	3rd 4-day	4th 4-day	5th 4-day	20-day
0	8	1	17	41	10	8
39	2	3	3	4	3	2
42	3	4	4	5	7	6
43	5	9	1	7	4	4
46	6	7	7	2	2	5
47	4	6	5	3	5	3
51	1	2	2	1	1	1

Finally, the test dataset was used to assess the wind speed predictive performance of the 5-in-1 (ensemble) WRF model as well as the top 50 and Dr Wen's WRF models. The model rankings, together with the similarity scores obtained by using the TOPSIS scheme, are presented in Table 5.15. An examination of this table indicates that Model 51

ranked second: this model exhibited excellent predictive performance and consistency in wind speed forecasting. Although the similarity score of Model 51 was slightly lower than that of Model 43, it was higher than Model 39, which was the best-performing individual model based on the training dataset. It is not surprising that Model 43 performed the best for the test dataset as the time interval for this dataset was only 4 days (a time interval that comprised only one data segment as defined previously). With reference to Table 5.14, Model 43 appeared to be the best-performing individual model because of its predictive performance on the third segment of the training dataset: indeed, Model 43 ranked first in the wind speed forecasting on this segment. Although the order of rankings changed, the top five and 5-in-1 (ensemble) WRF models selected in accordance with the evaluation metrics described above with reference to the training dataset remained, nevertheless, the top six best-performing forecasting models when evaluated on the test dataset. Furthermore, all these six WRF models outperformed Dr Wen's WRF model consistently.

Table 5.15. Model rankings for the 4 days of the test dataset according to the similarity scores.

Rank	Model index 2	Similarity score
1	43	0.9856
2	51	0.9641
3	46	0.9489
4	39	0.9447
5	47	0.7364
6	42	0.6197
7	5	0.5713
8	23	0.5037
9	0	0.4994
10	36	0.4843
11	50	0.4840
12	31	0.4571
13	11	0.4562
14	28	0.4512

Rank	Model index 2	Similarity score
15	18	0.4251
16	35	0.4245
17	27	0.4127
18	41	0.4090
19	33	0.3947
20	22	0.3905
21	21	0.3786
22	6	0.3691
23	40	0.3656
24	30	0.3655
25	12	0.3631
26	29	0.3618
27	14	0.3607
28	7	0.3432
29	49	0.3421
30	25	0.3340
31	34	0.3304
32	8	0.3247
33	37	0.3137
34	19	0.3042
35	20	0.2991
36	32	0.2831
37	26	0.2801
38	1	0.2792
39	9	0.2771

Rank	Model index 2	Similarity score
40	16	0.2560
41	45	0.2537
42	17	0.2481
43	38	0.2306
44	48	0.2303
45	4	0.1804
46	2	0.1792
47	10	0.1708
48	15	0.1641
49	44	0.1510
50	3	0.1304
51	13	0.1132
52	24	0.0984

The complete segmental rankings of the 5-in-1 (ensemble), the top five, and Dr Wen's WRF models are shown in Table 5.16, by which the consistency of the outstanding wind speed predictive performance of the 5-in-1 (ensemble) WRF model (Model 51) can be verified.

Table 5.16. Complete segmental rankings of the 5-in-1 (ensemble), the top five, and Dr Wen's WRF models as determined by using the 24-day dataset.

Model index 2	1st 4-day	2nd 4-day	3rd 4-day	4th 4-day	5th 4-day	6th 4-day
0	8	1	17	41	10	9
39	2	3	3	4	3	4
42	3	4	4	5	7	6
43	5	9	1	7	4	1
46	6	7	7	2	2	3
47	4	6	5	3	5	5
51	1	2	2	1	1	2

5.6 Wind Speed Forecasting Based on a 5-in-1 (Ensemble) WRF Model

As discussed in Section 5.5, a 5-in-1 (ensemble) WRF model was proposed for the wind speed forecasting in this study. A comparison of the 5-in-1 (ensemble) wind speed forecasts, the top 50 wind speed forecasts, Dr Wen's wind speed forecasts, and the historical wind speed measurements from the training dataset is shown in Figure 5.5, from which it can be seen that the 5-in-1 (ensemble) wind speed forecasts generally fit the historical wind speed measurements over the period of 20 days.

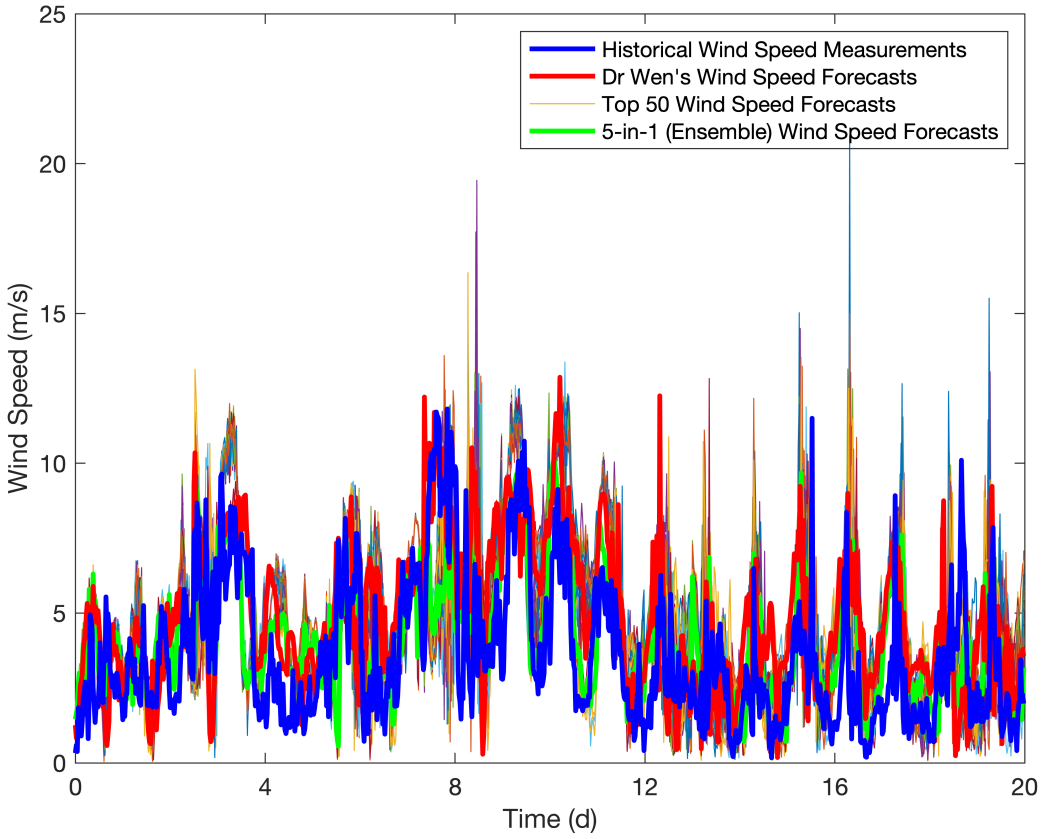

Figure 5.5. Comparison of the 5-in-1 (ensemble) wind speed forecasts, the top 50 wind speed forecasts, Dr Wen's wind speed forecasts, and the historical wind speed measurements from the 20-day training dataset.

In order to evaluate the predictive performance of the 5-in-1 (ensemble) WRF model on the 4-day test dataset, the MB, MAE, RMSE, IA, MAPE, and SMAPE for the wind speed forecasting for each day in the test dataset were calculated according to Equations (3.9) to (3.14). Besides, the 4-day average value of each evaluation metric was calculated as well. In addition, the metric values for the wind speed forecasting by using Dr Wen's WRF model were added for a comparative analysis. All the evaluation results are shown in Tables 5.17 to 5.22, from which it can be found that the 5-in-1 (ensemble) WRF model, with the 4-day average MB, MAE, RMSE, IA, MAPE, and SMAPE of 0.70 m/s, 1.29 m/s, 1.61 m/s, 0.83, 64.59%, and 42.15%, respectively, was superior to Dr Wen's WRF model not only in

the average predictive performance but also in the predictive performance on every single forecast day in terms of all the model evaluation metrics. Moreover, a comparison of the 5-in-1 (ensemble) wind speed forecasts, Dr Wen's wind speed forecasts, and the historical wind speed measurements from the test dataset is shown in Figure 5.6.

Table 5.17. MBs for the wind speed forecasting by using the 5-in-1 (ensemble) and Dr Wen's WRF models applied to the 4-day test dataset.

MB (m/s)		Forecast day				Average
		1	2	3	4	
Model	5-in-1 (ensemble) WRF model	1.58	0.12	0.61	0.48	0.70
	Dr Wen's WRF model	2.93	0.96	1.74	1.01	1.66

Table 5.18. MAEs for the wind speed forecasting by using the 5-in-1 (ensemble) and Dr Wen's WRF models applied to the 4-day test dataset.

MAE (m/s)		Forecast day				Average
		1	2	3	4	
Model	5-in-1 (ensemble) WRF model	1.79	1.23	1.08	1.05	1.29
	Dr Wen's WRF model	3.20	1.63	1.84	1.20	1.96

Table 5.19. RMSEs for the wind speed forecasting by using the 5-in-1 (ensemble) and Dr Wen's WRF models applied to the 4-day test dataset.

RMSE (m/s)		Forecast day				Average
		1	2	3	4	
Model	5-in-1 (ensemble) WRF model	2.18	1.53	1.30	1.44	1.61
	Dr Wen's WRF model	3.73	2.02	2.21	1.52	2.37

Table 5.20. IAs for the wind speed forecasting by using the 5-in-1 (ensemble) and Dr Wen's WRF models applied to the 4-day test dataset.

IA		Forecast day				Average
		1	2	3	4	
Model	5-in-1 (ensemble) WRF model	0.66	0.77	0.94	0.95	0.83
	Dr Wen's WRF model	-0.03	0.60	0.82	0.94	0.58

Table 5.21. MAPEs for the wind speed forecasting by using the 5-in-1 (ensemble) and Dr Wen's WRF models applied to the 4-day test dataset.

MAPE		Forecast day				Average
		1	2	3	4	
Model	5-in-1 (ensemble) WRF model	97.04%	74.85%	46.89%	39.59%	64.59%
	Dr Wen's WRF model	163.92%	112.20%	99.72%	43.06%	104.72%

Table 5.22. SMAPEs for the wind speed forecasting by using the 5-in-1 (ensemble) and Dr Wen's WRF models applied to the 4-day test dataset.

SMAPE		Forecast day				Average
		1	2	3	4	
Model	5-in-1 (ensemble) WRF model	56.31%	49.52%	33.07%	29.70%	42.15%
	Dr Wen's WRF model	79.66%	55.87%	50.14%	32.97%	54.66%

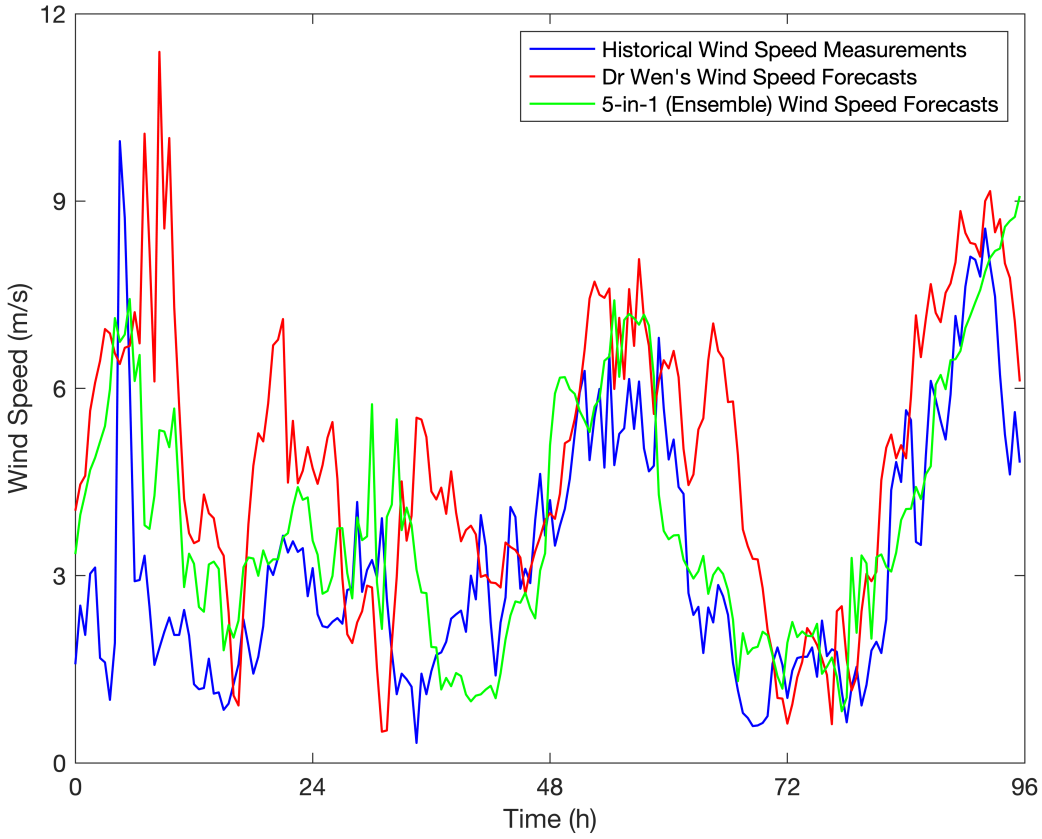

Figure 5.6. Comparison of the 5-in-1 (ensemble) wind speed forecasts, Dr Wen's wind speed forecasts, and the historical wind speed measurements from the 4-day test dataset.

5.7 Correcting Wind Speed Forecasts Based on an ANFIS Model

As discussed in Section 5.6, the wind speed forecasts provided by the 5-in-1 (ensemble) WRF model were obtained. Then, an ANFIS model was proposed here to correct these wind speed forecasts. For this application, the input of the ANFIS model was the wind speed forecasts provided by the 5-in-1 (ensemble) WRF model, and the output was the historical wind speed measurements. During the training process based on the first 20-day

wind speed data (the training and checking datasets), the ANFIS model learnt the implicit relationship between the wind speed forecasts and measurements, so the output of this model could provide corrected wind speed forecasts by inputting the wind speed forecasts generated by the 5-in-1 (ensemble) WRF model. Subsequently, the wind speed forecasts provided by the 5-in-1 (ensemble) WRF model for the test dataset were used as the inputs to the trained ANFIS model—which, in turn, permitted the quantitative assessment of the generalisation of the trained ANFIS model to the wind speed forecast data for which it had not been trained.

In order to evaluate the predictive performance of the corrected 5-in-1 (ensemble) WRF model on the test dataset, the MB, MAE, RMSE, IA, MAPE, and SMAPE for the wind speed forecasting for each day in the test dataset were calculated according to Equations (3.9) to (3.14). Besides, the 4-day average value of each evaluation metric was calculated as well. In addition, the metric values for the wind speed forecasting by using the original 5-in-1 (ensemble) WRF model were added for a comparative analysis. All the evaluation results are shown in Tables 5.23 to 5.28.

Table 5.23. MBs for the wind speed forecasting by using the corrected and original 5-in-1 (ensemble) WRF models applied to the 4-day test dataset.

MB (m/s)		Forecast day				Average
		1	2	3	4	
Model	Corrected 5-in-1 (ensemble) WRF model	0.93	0.02	0.03	-0.14	0.21
	Original 5-in-1 (ensemble) WRF model	1.58	0.12	0.61	0.48	0.70

Table 5.24. MAEs for the wind speed forecasting by using the corrected and original 5-in-1 (ensemble) WRF models applied to the 4-day test dataset.

MAE (m/s)		Forecast day				Average
		1	2	3	4	
Model	Corrected 5-in-1 (ensemble) WRF model	1.35	0.91	0.90	1.13	1.07
	Original 5-in-1 (ensemble) WRF model	1.79	1.23	1.08	1.05	1.29

Table 5.25. RMSEs for the wind speed forecasting by using the corrected and original 5-in-1 (ensemble) WRF models applied to the 4-day test dataset.

RMSE (m/s)		Forecast day				Average
		1	2	3	4	
Model	Corrected 5-in-1 (ensemble) WRF model	1.71	1.18	1.16	1.34	1.35
	Original 5-in-1 (ensemble) WRF model	2.18	1.53	1.30	1.44	1.61

Table 5.26. IAs for the wind speed forecasting by using the corrected and original 5-in-1 (ensemble) WRF models applied to the 4-day test dataset.

IA		Forecast day				Average
		1	2	3	4	
Model	Corrected 5-in-1 (ensemble) WRF model	0.79	0.87	0.95	0.95	0.89
	Original 5-in-1 (ensemble) WRF model	0.66	0.77	0.94	0.95	0.83

Table 5.27. MAPEs for the wind speed forecasting by using the corrected and original 5-in-1 (ensemble) WRF models applied to the 4-day test dataset.

MAPE		Forecast day				Average
		1	2	3	4	
Model	Corrected 5-in-1 (ensemble) WRF model	73.56%	56.39%	45.20%	39.69%	53.71%
	Original 5-in-1 (ensemble) WRF model	97.04%	74.85%	46.89%	39.59%	64.59%

Table 5.28. SMAPEs for the wind speed forecasting by using the corrected and original 5-in-1 (ensemble) WRF models applied to the 4-day test dataset.

SMAPE		Forecast day				Average
		1	2	3	4	
Model	Corrected 5-in-1 (ensemble) WRF model	47.08%	36.44%	31.03%	32.37%	36.73%
	Original 5-in-1 (ensemble) WRF model	56.31%	49.52%	33.07%	29.70%	42.15%

From Tables 5.23 to 5.28, it can be seen that the ANFIS-based wind speed correction model significantly improved the accuracy of the wind speed forecasts on the basis of the original 5-in-1 (ensemble) WRF model. In particular, the wind speed forecasting by using the corrected 5-in-1 (ensemble) WRF model, with the 4-day average MB, MAE, RMSE, IA, MAPE, and SMAPE of 0.21 m/s, 1.07 m/s, 1.35 m/s, 0.89, 53.71%, and 36.73%, respectively, was superior to that by using the original 5-in-1 (ensemble) WRF model in the average predictive performance in terms of all the model evaluation metrics. Besides, for every single forecast day, the wind speed forecasting by using the corrected 5-in-1 (ensemble) WRF model performed better than that by using the original 5-in-1 (ensemble) WRF model in all of the cases with three exceptions. Specifically, the MAE, MAPE, and SMAPE for the wind speed forecasting by using the corrected 5-in-1 (ensemble) WRF model were larger than those for the wind speed forecasting by using the original 5-in-1 (ensemble) WRF model on the fourth forecast day. Moreover, a comparison of the corrected 5-in-1 (ensemble) wind speed forecasts, the original 5-in-1 (ensemble) wind speed forecasts, Dr Wen's wind speed forecasts, and the historical wind speed measurements from the test dataset is shown in Figure 5.7.

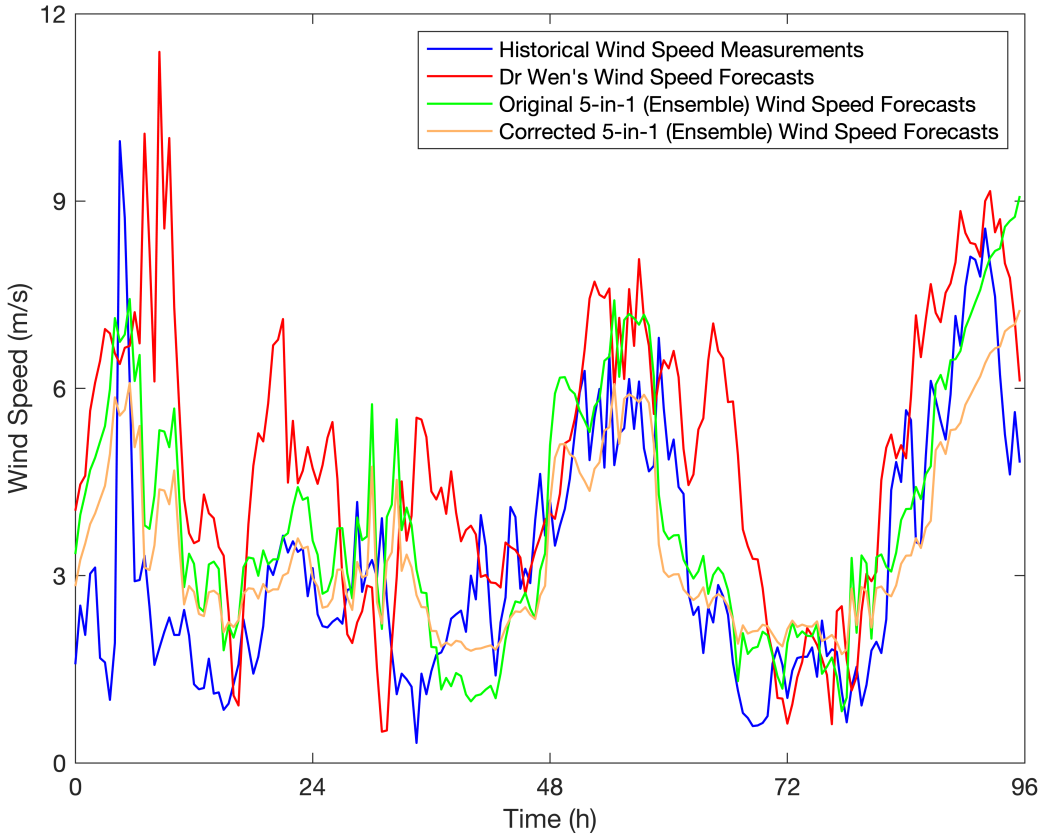

Figure 5.7. Comparison of the corrected 5-in-1 (ensemble) wind speed forecasts, the original 5-in-1 (ensemble) wind speed forecasts, Dr Wen's wind speed forecasts, and the historical wind speed measurements from the 4-day test dataset.

5.8 Wind Power Forecasting Based on a 5-in-1 (Ensemble) WRF Model

As discussed in Sections 5.6 and 5.7, the wind speed forecasts provided by the original 5-in-1 (ensemble) WRF model and the corresponding wind speed forecasts corrected by the ANFIS-based wind speed correction model were obtained. In this case, all the 4-day original and corrected wind speed forecasts for the test dataset were separately input to the

ANFIS-based power curve model created in Section 3.7, and then the corresponding wind power forecasts could be acquired as the outputs of the power curve model. According to Equations (3.9) to (3.12) and (3.15) to (3.18), the MBs, MAEs, RMSEs, IAs, accuracy rates, and qualification rates for the wind power forecasting by using the original and corrected 5-in-1 (ensemble) WRF models and their 4-day average values were calculated. In addition, the metric values for the wind power forecasting by using Dr Wen's WRF model were added for a comparative analysis. The corresponding results are shown in Tables 5.29 to 5.34.

Table 5.29. MBs for the wind power forecasting by using the corrected 5-in-1 (ensemble), the original 5-in-1 (ensemble), and Dr Wen's WRF models applied to the 4-day test dataset.

MB (kW)		Forecast day				Average
		1	2	3	4	
Model	Corrected 5-in-1 (ensemble) WRF model	22.0	-7.9	-30.9	-49.7	-16.6
	Original 5-in-1 (ensemble) WRF model	90.1	15.2	49.5	57.9	53.2
	Dr Wen's WRF model	268.8	64.6	168.2	146.7	162.1

Table 5.30. MAEs for the wind power forecasting by using the corrected 5-in-1 (ensemble), the original 5-in-1 (ensemble), and Dr Wen's WRF models applied to the 4-day test dataset.

MAE (kW)		Forecast day				Average
		1	2	3	4	
Model	Corrected 5-in-1 (ensemble) WRF model	91.1	38.5	72.9	108.6	77.8
	Original 5-in-1 (ensemble) WRF model	138.9	52.7	99.3	113.4	101.1
	Dr Wen's WRF model	321.5	98.2	172.1	150.5	185.6

Table 5.31. RMSEs for the wind power forecasting by using the corrected 5-in-1 (ensemble), the original 5-in-1 (ensemble), and Dr Wen's WRF models applied to the 4-day test dataset.

RMSE (kW)		Forecast day				Average
		1	2	3	4	
Model	Corrected 5-in-1 (ensemble) WRF model	184.9	59.2	111.0	164.1	129.8
	Original 5-in-1 (ensemble) WRF model	207.3	82.1	145.6	212.8	162.0
	Dr Wen's WRF model	431.3	126.4	221.3	220.8	250.0

Table 5.32. IAs for the wind power forecasting by using the corrected 5-in-1 (ensemble), the original 5-in-1 (ensemble), and Dr Wen's WRF models applied to the 4-day test dataset.

IA		Forecast day				Average
		1	2	3	4	
Model	Corrected 5-in-1 (ensemble) WRF model	0.60	0.37	0.82	0.83	0.66
	Original 5-in-1 (ensemble) WRF model	0.66	0.32	0.81	0.83	0.65
	Dr Wen's WRF model	0.28	0.12	0.68	0.86	0.48

Table 5.33. Accuracy rates for the wind power forecasting by using the corrected 5-in-1 (ensemble), the original 5-in-1 (ensemble), and Dr Wen's WRF models applied to the 4-day test dataset.

Accuracy rate		Forecast day				Average
		1	2	3	4	
Model	Corrected 5-in-1 (ensemble) WRF model	87.68%	96.05%	92.60%	89.06%	91.35%
	Original 5-in-1 (ensemble) WRF model	86.18%	94.52%	90.29%	85.82%	89.20%
	Dr Wen's WRF model	71.25%	91.57%	85.24%	85.28%	83.34%

Table 5.34. Qualification rates for the wind power forecasting by using the corrected 5-in-1 (ensemble), the original 5-in-1 (ensemble), and Dr Wen's WRF models applied to the 4-day test dataset.

Qualification rate		Forecast day				Average
		1	2	3	4	
Model	Corrected 5-in-1 (ensemble) WRF model	95.83%	100.00%	100.00%	95.83%	97.92%
	Original 5-in-1 (ensemble) WRF model	91.67%	100.00%	100.00%	89.58%	95.31%
	Dr Wen's WRF model	64.58%	100.00%	89.58%	87.50%	85.42%

From Tables 5.29 to 5.34, it can be seen that the ANFIS-based wind speed correction model significantly improved the accuracy of the wind power forecasts on the basis of the original 5-in-1 (ensemble) WRF model. In particular, the wind power forecasting by using the corrected 5-in-1 (ensemble) WRF model, with the 4-day average MB, MAE, RMSE, IA, accuracy rate, and qualification rate of -16.6 kW, 77.8 kW, 129.8 kW, 0.66, 91.35%, and 97.92%, respectively, was superior to that by using the original 5-in-1 (ensemble) and Dr Wen's WRF models in the average predictive performance in terms of all the model evaluation metrics. Besides, for every single forecast day, the wind power forecasting by using the corrected 5-in-1 (ensemble) WRF model performed better than or equal to that by using the original 5-in-1 (ensemble) and Dr Wen's WRF models in all of the cases with two exceptions. Specifically, the IAs for the wind power forecasting by using the corrected 5-in-1 (ensemble) WRF model were lower than those for the wind power forecasting by using the original 5-in-1 (ensemble) WRF model on the first forecast day and Dr Wen's WRF model on the fourth forecast day, respectively. Moreover, a comparison of the corrected 5-in-1 (ensemble) wind power forecasts, the original 5-in-1 (ensemble) wind power forecasts, Dr Wen's wind power forecasts, and the historical wind power measurements from the test dataset is shown in Figure 5.8. By comparing Figures 5.7 and 5.8, it can be found that the wind speed forecasting was less accurate than the wind power forecasting. This is mainly because the wind speed varied between the values of 0 and cut-in wind speed (typically 3 to 4 m/s); however, when the wind speed was in this range, the wind turbine did not work, and the corresponding wind power remained at 0, which significantly reduced the forecast

error.

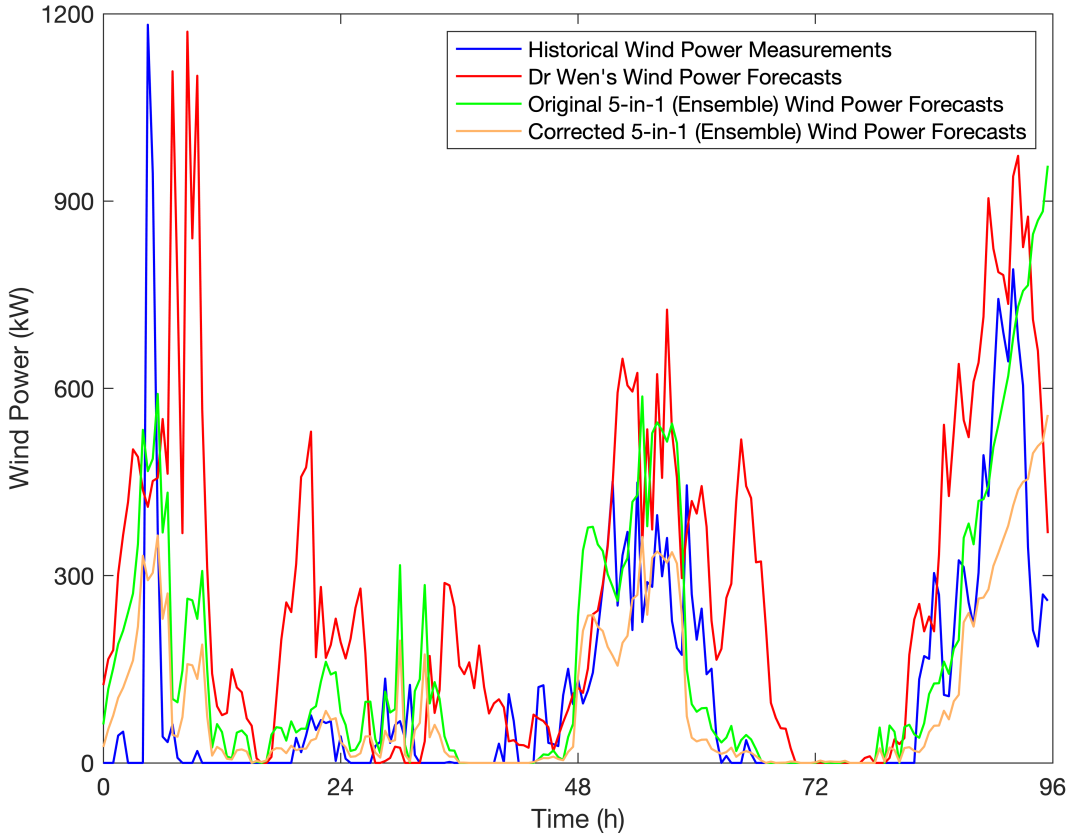

Figure 5.8. Comparison of the corrected 5-in-1 (ensemble) wind power forecasts, the original 5-in-1 (ensemble) wind power forecasts, Dr Wen's wind power forecasts, and the historical wind power measurements from the 4-day test dataset.

5.9 Summary

The WRF modelling, as a physical method for wind speed and wind power forecasting, is presented in Chapter 5. First of all, a WPS programme was set up by editing a *namelist.wps* file and completed by running three subprogrammes, namely *geogrid*, *ungrib*, and *metgrid*. Specifically, the *metgrid* programme interpolated the gridded meteorological fields

extracted by the *ungrib* programme to the model grids defined by the *geogrid* programme horizontally. Similarly, a WRF programme was set up by editing a *namelist.input* file and completed by running a *real* and a *wrf* programme. The *real* programme was an initialisation programme that took the 2D outputs created by the WPS programme and performed the vertical interpolation for 3D meteorological fields and sub-surface soil data. Then the boundary and initial condition files for each domain were produced and fed into the *wrf* programme, the output files of which contained all the meteorological data, including the wind speed forecasts needed in this research.

In the process of setting the parameters for the WRF model, it was found that some parameters had a number of optional values, implying that there were different candidate WRF models for the wind speed and wind power forecasting. The microphysics, cumulus, planetary boundary-layer, surface-layer, and land-surface parameterisations were selected as the critical physics options that needed to be determined. For each physics option, there were many parameterisation schemes available. Owing to the WRF model restrictions and applicability, the number of practical scheme combinations was 1,334, which was relatively small compared with that of possible scheme combinations in mathematics (10,800). The choices of the scheme combinations for the various physics options provide different WRF models that generate different wind speed forecasts. Nevertheless, there are no rules for selecting the parameterisation scheme for each physics option. Instead of an ad hoc method previously applied, a systematic approach was proposed to select the WRF models. To be precise, the entire set of 1,334 WRF models were applied to forecast the wind speeds for the first day. Then, the obtained wind speed forecasts were evaluated by comparing them with their corresponding historical wind speed measurements. Six evaluation metrics, namely the MB, MAE, MAPE, SMAPE, RMSE, and IA, were used to assess the predictive performance of the WRF models. For the purpose of finding the best-performing prediction among the various WRF model forecasts, a TOPSIS scheme was applied to address this multi-metric decision making problem. Finally, the top 50 WRF models were selected in accordance with the similarity scores and applicability. In addition, the wind speed forecasts provided by Dr Wen's WRF model were utilised as a benchmark.

After that, the 50 best-performing WRF models were applied to generate the wind speed forecasts for the remaining 23 days. By examining the overall and segmental predictive performance of the WRF models on the 20-day training dataset, Models 39, 42, 43, 46, and 47 were picked out as they not only outperformed the other models but also performed consistently over all the data segments. Besides, a novel 5-in-1 (ensemble) WRF model was constructed by combining the top five best-performing WRF models on the basis of the weights (similarity scores) provided by the TOPSIS scheme. It was demonstrated that the wind speed forecasts provided by the 5-in-1 (ensemble) WRF model outperformed those

obtained from the top five and Dr Wen's WRF models according to the overall predictive performance on the training dataset. Although the 5-in-1 (ensemble) WRF model ranked second for the test dataset, this model exhibited excellent predictive performance and consistency in the wind speed forecasting on the six data segments.

For the wind speed forecasting, the 5-in-1 (ensemble) WRF model, with the 4-day average MB, MAE, RMSE, IA, MAPE, and SMAPE of 0.70 m/s, 1.29 m/s, 1.61 m/s, 0.83, 64.59%, and 42.15%, respectively, was superior to Dr Wen's WRF model not only in the average predictive performance but also in the predictive performance on every single forecast day in terms of all the model evaluation metrics. Additionally, an ANFIS model was proposed to correct the wind speed forecasts provided by the 5-in-1 (ensemble) WRF model. The wind speed forecasting by using the corrected 5-in-1 (ensemble) WRF model, with the 4-day average MB, MAE, RMSE, IA, MAPE, and SMAPE of 0.21 m/s, 1.07 m/s, 1.35 m/s, 0.89, 53.71%, and 36.73%, respectively, was superior to that by using the original 5-in-1 (ensemble) WRF model in the average predictive performance in terms of all the model evaluation metrics. Besides, for every single forecast day, the wind speed forecasting by using the corrected 5-in-1 (ensemble) WRF model performed better than that by using the original 5-in-1 (ensemble) WRF model in all of the cases with three exceptions.

By using the ANFIS-based power curve model created in Section 3.7, the wind speed forecasts provided by the corrected 5-in-1 (ensemble), the original 5-in-1 (ensemble), and Dr Wen's WRF models were converted to the corresponding wind power forecasts. The wind power forecasting by using the corrected 5-in-1 (ensemble) WRF model, with the 4-day average MB, MAE, RMSE, IA, accuracy rate, and qualification rate of -16.6 kW, 77.8 kW, 129.8 kW, 0.66, 91.35%, and 97.92%, respectively, was superior to that by using the original 5-in-1 (ensemble) and Dr Wen's WRF models in the average predictive performance in terms of all the model evaluation metrics. Besides, for every single forecast day, the wind power forecasting by using the corrected 5-in-1 (ensemble) WRF model performed better than or equal to that by using the original 5-in-1 (ensemble) and Dr Wen's WRF models in all of the cases with two exceptions.

Chapter 6

Multi-Hour Ahead Wind Power Forecasting System

6.1 Comparison of Statistics-Based and Physics-Based Forecasting Models

As discussed in Chapters 4 and 5, the direct persistence, indirect persistence, ARIMA, and WRF-TOPSIS models were created for multi-hour ahead wind speed and wind power forecasting and evaluated based on a real case of an operational wind turbine. In those previous two chapters, the predictive performance of each wind power forecasting model for different forecast time horizons is compared and analysed. In contrast, these four wind power forecasting models will be compared with each other according to their predictive performance on different forecast time horizons in this section.

The first three models belong to the class of statistics-based forecasting models. Their characteristics can be summarised as simple models with low computational costs. Therefore, applying these statistics-based forecasting models for each forecast time horizon was computationally efficient. For example, for the 30-minute ahead wind power forecasting, the statistics-based forecasting models could assimilate the wind speed and wind power data at 00:00 and output the wind power forecasts at 00:30 and then assimilate the wind speed and wind power data at 00:30 to provide the wind power forecasts at 01:00, and so forth. In order to collect the wind power forecasts for a period of 1 day, each statistics-based forecasting model had to be run 48 times. Since the test dataset covers 4 days in total, each statistics-based forecasting model needed to be run 192 times in this case. For

another example of the 4-hour ahead wind power forecasting, the statistics-based forecasting models could assimilate the wind speed and wind power data at 00:00 and output the wind power forecasts for the next 4 hours and then assimilate the wind speed and wind power data at 04:00 to provide another set of wind power forecasts for 04:30 to 08:00, and so forth. For a period of 4 days, the statistics-based forecasting models had to be run 24 times.

For the 24-hour ahead wind power forecasting, the statistics-based forecasting models generated 48 wind power forecasts (at 30-minute intervals) for the next 24 hours at one time. In consequence, this process needed to be repeated three more times in order to provide all the wind power forecasts for the next 4 days. Similarly, the WRF-TOPSIS model was applied in exactly the same way to provide the 24-hour ahead wind power forecasts for the next 4 days. In particular, the WRF-TOPSIS model was run at 18:00 one day before the forecast day and was used to provide the wind power forecasts for 24 hours of the next day at one time. After three more repetitions of this process, all the wind power forecasts could be obtained for the next 4 days. With respect to the other forecast time horizons, it was impractical to re-run the WRF-TOPSIS model as in the case of the statistics-based forecasting models simply because the computational costs associated with the WRF-TOPSIS model runs were prohibitive. For instance, for the 6-hour ahead wind power forecasting, the most rigorous way is to re-run the WRF-TOPSIS model every 6 hours, which means running the WRF-TOPSIS model four times a day or 16 times for the 4 days. Unfortunately, it was computationally prohibitive to run the WRF-TOPSIS model multiple times a day.

In view of this, for any forecast time horizon in this study, the same wind power forecasts were used to represent the predictive performance of the WRF-TOPSIS model. Once the WRF-TOPSIS model generated the 48 wind power forecasts for 24 hours of the next day, its daily mission was accomplished. For the 30-minute ahead wind power forecasting, the statistics-based forecasting models updated their wind power forecasts every 30 minutes within the 24-hour forecast period. However, this was not practical for the WRF-TOPSIS model. Because this model had already provided the 48 wind power forecasts before the next day, the wind power forecasts could be reported based on this information every 30 minutes without model re-runs. Similarly, for the other forecast time horizons, there was no need for the WRF-TOPSIS model to be re-run in order to update its wind power forecasts for 24 hours of the next day.

In addition, the NEA requires wind farms to forecast the wind power for 24 hours of the next day with a minimum accuracy rate of 80% [100]. However, in reality, it is acceptable if the forecast accuracy rate for a wind farm is lower than 80% for a day or a couple of days because the forecasting performance of a wind farm is evaluated based on 1 month,

and the monthly accuracy rate is the arithmetic mean of the daily accuracy rates for that month. It is not statistically significant to evaluate the model performance based on 1 day. This requirement of averaging the evaluation metrics over multiple days was employed in the current study.

In order to compare the overall predictive performance of the proposed wind power forecasting models, the 4-day average MBs, MAEs, RMSEs, IAs, accuracy rates, and qualification rates for the multi-hour ahead wind power forecasting calculated in Chapters 4 and 5 are summarised in Tables 6.1 to 6.6, respectively.

Table 6.1. Four-day average MBs for the wind power forecasting by using the direct persistence, indirect persistence, ARIMA, and WRF-TOPSIS models applied to the 4-day test dataset.

4-day average MB (kW)		Direct persistence model	Indirect persistence model	ARIMA model	WRF-TOPSIS model
Forecast time horizon	30 minutes	-1.4	-0.5	-24.0	-16.6
	1 hour	-2.8	-2.0	-33.3	-16.6
	1.5 hours	-3.7	-3.0	-45.7	-16.6
	2 hours	-4.7	-4.0	-49.5	-16.6
	3 hours	-9.6	-9.1	-49.7	-16.6
	4 hours	-17.3	-17.1	-63.6	-16.6
	6 hours	-31.2	-31.5	-64.7	-16.6
	8 hours	-38.7	-39.7	-89.6	-16.6
	12 hours	-48.5	-49.7	-87.1	-16.6
	24 hours	-38.7	-40.0	-104.6	-16.6

Table 6.2. Four-day average MAEs for the wind power forecasting by using the direct persistence, indirect persistence, ARIMA, and WRF-TOPSIS models applied to the 4-day test dataset.

4-day average MAE (kW)		Direct persistence model	Indirect persistence model	ARIMA model	WRF-TOPSIS model
Forecast time horizon	30 minutes	48.6	50.8	49.0	77.8
	1 hour	69.1	68.4	57.2	77.8
	1.5 hours	80.3	79.8	68.9	77.8
	2 hours	87.5	87.6	74.0	77.8
	3 hours	95.5	95.1	78.3	77.8
	4 hours	107.4	105.7	77.1	77.8
	6 hours	116.4	115.4	100.5	77.8
	8 hours	129.1	126.7	98.6	77.8
	12 hours	157.3	155.2	111.8	77.8
	24 hours	161.4	159.5	110.2	77.8

Table 6.3. Four-day average RMSEs for the wind power forecasting by using the direct persistence, indirect persistence, ARIMA, and WRF-TOPSIS models applied to the 4-day test dataset.

4-day average RMSE (kW)		Direct persistence model	Indirect persistence model	ARIMA model	WRF-TOPSIS model
Forecast time horizon	30 minutes	104.7	104.7	104.4	129.8
	1 hour	139.8	138.9	115.0	129.8
	1.5 hours	158.2	157.6	137.0	129.8
	2 hours	167.7	166.7	142.8	129.8
	3 hours	178.7	177.5	150.5	129.8
	4 hours	191.7	189.5	154.4	129.8
	6 hours	197.9	194.9	169.6	129.8
	8 hours	214.6	210.5	179.0	129.8
	12 hours	242.2	237.7	193.4	129.8
	24 hours	259.1	254.0	195.6	129.8

Table 6.4. Four-day average IAs for the wind power forecasting by using the direct persistence, indirect persistence, ARIMA, and WRF-TOPSIS models applied to the 4-day test dataset.

4-day average IA		Direct persistence model	Indirect persistence model	ARIMA model	WRF-TOPSIS model
Forecast time horizon	30 minutes	0.82	0.82	0.78	0.66
	1 hour	0.66	0.65	0.73	0.66
	1.5 hours	0.56	0.55	0.54	0.66
	2 hours	0.53	0.53	0.53	0.66
	3 hours	0.54	0.54	0.52	0.66
	4 hours	0.41	0.41	0.50	0.66
	6 hours	0.42	0.42	0.40	0.66
	8 hours	0.33	0.34	0.40	0.66
	12 hours	0.18	0.18	0.34	0.66
	24 hours	0.21	0.21	0.38	0.66

Table 6.5. Four-day average accuracy rates for the wind power forecasting by using the direct persistence, indirect persistence, ARIMA, and WRF-TOPSIS models applied to the 4-day test dataset.

4-day average accuracy rate		Direct persistence model	Indirect persistence model	ARIMA model	WRF-TOPSIS model
Forecast time horizon	30 minutes	93.02%	93.02%	93.04%	91.35%
	1 hour	90.68%	90.74%	92.33%	91.35%
	1.5 hours	89.45%	89.49%	90.86%	91.35%
	2 hours	88.82%	88.89%	90.48%	91.35%
	3 hours	88.09%	88.17%	89.96%	91.35%
	4 hours	87.22%	87.37%	89.71%	91.35%
	6 hours	86.81%	87.01%	88.69%	91.35%
	8 hours	85.69%	85.97%	88.06%	91.35%
	12 hours	83.85%	84.15%	87.11%	91.35%
	24 hours	82.73%	83.07%	86.96%	91.35%

Table 6.6. Four-day average qualification rates for the wind power forecasting by using the direct persistence, indirect persistence, ARIMA, and WRF-TOPSIS models applied to the 4-day test dataset.

4-day average qualification rate		Direct persistence model	Indirect persistence model	ARIMA model	WRF-TOPSIS model
Forecast time horizon	30 minutes	98.96%	98.96%	99.48%	97.92%
	1 hour	97.40%	97.40%	98.96%	97.92%
	1.5 hours	96.35%	96.35%	97.92%	97.92%
	2 hours	96.35%	96.35%	96.88%	97.92%
	3 hours	93.75%	93.23%	96.35%	97.92%
	4 hours	92.19%	93.75%	96.35%	97.92%
	6 hours	94.79%	94.79%	93.75%	97.92%
	8 hours	90.62%	91.15%	94.27%	97.92%
	12 hours	90.10%	90.62%	92.19%	97.92%
	24 hours	88.54%	89.06%	92.19%	97.92%

From Table 6.1, it can be found that for each forecast time horizon, the 4-day average MB for the wind power forecasting by using the direct persistence model was extremely close to that by using the indirect persistence model, and the 4-day average MB absolute value for the ARIMA model was the largest one compared with those for the direct persistence, indirect persistence, and WRF-TOPSIS models. Besides, the direct and indirect persistence and WRF-TOPSIS models had the smallest 4-day average MB absolute values for the forecast time horizons ranging from 30 minutes to 3 hours and 4 to 24 hours, respectively.

From Table 6.2, it can be found that the 4-day average MAE for the wind power forecasting by using the direct persistence model was extremely close to that by using the indirect persistence model for each forecast time horizon. Besides, the direct persistence model had the smallest 4-day average MAE for the forecast time horizon of 30 minutes, and the 4-day average MAEs for the direct and indirect persistence models were consistently larger than those for the ARIMA and WRF-TOPSIS models starting from the forecast time horizon of 1.5 hours. Moreover, the ARIMA and WRF-TOPSIS models had the smallest

4-day average MAEs for the forecast time horizons of 1, 1.5, 2, and 4 hours and 3, 6, 8, 12, and 24 hours, respectively.

From Table 6.3, it can be found that the 4-day average RMSE for the wind power forecasting by using the direct persistence model was extremely close or equal to that by using the indirect persistence model for each forecast time horizon. Besides, the 4-day average RMSEs for the direct and indirect persistence models were consistently larger than those for the ARIMA and WRF-TOPSIS models starting from the forecast time horizon of 1 hour. Moreover, the ARIMA and WRF-TOPSIS models had the smallest 4-day average RMSEs for the forecast time horizons ranging from 30 minutes to 1 hour and 1.5 to 24 hours, respectively.

From Table 6.4, it can be found that the 4-day average IA for the wind power forecasting by using the direct persistence model was equal or extremely close to that by using the indirect persistence model for each forecast time horizon. Besides, the direct and indirect persistence and ARIMA models had the highest 4-day average IAs for the forecast time horizons of 30 minutes and 1 hour, respectively. Moreover, the 4-day average IAs for the WRF-TOPSIS model were consistently higher than those for the direct persistence, indirect persistence, and ARIMA models starting from the forecast time horizon of 1.5 hours.

From Table 6.5, it can be found that the 4-day average accuracy rate for the wind power forecasting by using the direct persistence model was extremely close or equal to that by using the indirect persistence model for each forecast time horizon. Besides, the 4-day average accuracy rates for the direct and indirect persistence models were consistently lower than those for the ARIMA and WRF-TOPSIS models starting from the forecast time horizon of 1 hour. Moreover, the ARIMA and WRF-TOPSIS models had the highest 4-day average accuracy rates for the forecast time horizons ranging from 30 minutes to 1 hour and 1.5 to 24 hours, respectively.

From Table 6.6, it can be found that the 4-day average qualification rate for the wind power forecasting by using the direct persistence model was equal or extremely close to that by using the indirect persistence model for each forecast time horizon. Besides, the 4-day average qualification rates for the direct and indirect persistence models were consistently lower than those of the ARIMA and WRF-TOPSIS models starting from the forecast time horizon of 1 hour (except the forecast time horizon of 6 hours). Moreover, the ARIMA and WRF-TOPSIS models had the highest 4-day average qualification rates for the forecast time horizons ranging from 30 minutes to 1.5 hours and 1.5 to 24 hours, respectively.

A careful examination of Tables 6.1 to 6.6 shows that initially, the statistics-based forecasting models performed very well and even better than the physics-based forecasting model. Nevertheless, as the forecast time horizon increased, the predictive performance

of the statistics-based forecasting models decreased significantly, and this was especially so for the direct and indirect persistence models. As discussed above, the WRF-TOPSIS model provided the same wind power forecasts for every forecast time horizon. The values in the last column of each table (see Tables 6.1 to 6.6) kept unchanged as these values were based on a single 24-hour ahead forecast only (viz., the WRF-TOPSIS model was run once every day to provide a 24-hour ahead forecast). Nevertheless, the predictive performance of the WRF-TOPSIS model (the physics-based forecasting model) was significantly better than that of the statistics-based forecasting models as the forecast time horizon increased.

6.2 Model Determination for Each Forecast Time Horizon

From the findings summarised in Section 6.1, it can be seen that the statistics-based forecasting models outperformed the physics-based forecasting model in terms of shorter-term wind power forecasting. In contrast, the physics-based forecasting model had more advantages over longer forecast time horizons. For the purpose of determining the specific model to be used for each forecast time horizon, the TOPSIS scheme was utilised to rank the direct persistence, indirect persistence, ARIMA, and WRF-TOPSIS models with respect to their predictive performance as evaluated by six metrics, namely the MB, MAE, RMSE, IA, accuracy rate, and qualification rate, described in Section 3.5. The ranking results are summarised in Table 6.7.

Table 6.7. Model rankings for each forecast time horizon according to the similarity scores.

Similarity score		Rank 1	Rank 2	Rank 3	Rank 4
Forecast time horizon	30 minutes	Direct persistence model (0.9727)	Indirect persistence model (0.9617)	ARIMA model (0.5034)	WRF-TOPSIS model (0.2039)
	1 hour	ARIMA model (0.7086)	Indirect persistence model (0.3620)	Direct persistence model (0.3433)	WRF-TOPSIS model (0.3414)

Similarity score		Ranking 1	Ranking 2	Ranking 3	Ranking 4
	1.5 hours	ARIMA model (0.7177)	WRF-TOPSIS model (0.5111)	Indirect persistence model (0.2546)	Direct persistence model (0.2435)
	2 hours	WRF-TOPSIS model (0.8042)	ARIMA model (0.6587)	Indirect persistence model (0.2701)	Direct persistence model (0.2649)
	3 hours	WRF-TOPSIS model (0.9391)	ARIMA model (0.6067)	Indirect persistence model (0.2732)	Direct persistence model (0.2656)
	4 hours	WRF-TOPSIS model (0.9865)	ARIMA model (0.6230)	Indirect persistence model (0.2713)	Direct persistence model (0.2602)
	6 hours	WRF-TOPSIS model (1.0000)	ARIMA model (0.3744)	Indirect persistence model (0.2071)	Direct persistence model (0.2013)
	8 hours	WRF-TOPSIS model (1.0000)	ARIMA model (0.4394)	Indirect persistence model (0.2206)	Direct persistence model (0.2133)
	12 hours	WRF-TOPSIS model (1.0000)	ARIMA model (0.4237)	Indirect persistence model (0.1911)	Direct persistence model (0.1898)
	24 hours	WRF-TOPSIS model (1.0000)	ARIMA model (0.4805)	Indirect persistence model (0.2191)	Direct persistence model (0.2163)

According to Table 6.7, it is evident that for the shortest forecast time horizons of 30 minutes and 1 hour, the statistics-based forecasting models performed better than the physics-based forecasting model. The similarity scores of the direct and indirect persistence models were comparable (indeed practically indistinguishable) for the 30-minute ahead wind power forecasting: the direct persistence model ranked first. With reference to Tables 6.1 to 6.6, the predictive performance of the direct persistence model for the 30-minute forecast time horizon was precisely the same as that of the indirect persistence model in terms of the RMSE, IA, accuracy rate, and qualification rate. Moreover, the indirect persistence model had a lower MB absolute value, while the direct persistence model had a lower value of the MAE. As a consequence, it was difficult to determine which one of these two statistics-based models was better in terms of their predictive performance of the wind power for very short forecast time horizons. Nevertheless, it is clear that the persistence models performed better than the ARIMA (time series) and WRF-TOPSIS (physics-based) models. As a result, the persistence models should be used for 30-minute ahead wind power forecasting (viz., for very short forecast time horizons).

For the 1-hour ahead wind power forecasting, the ARIMA model exhibited the best predictive performance: the similarity score of this model was twice as large (approximately or better) as those of the other models. Indeed, with reference to Tables 6.1 to 6.6, the ARIMA model for the 1-hour forecast time horizon had the lowest MAE and RMSE and the highest IA, accuracy rate, and qualification rate compared with the other models. The only disadvantage was that this model had the largest MB absolute value. In other words, the ARIMA model ranked first in five of the six evaluation metrics. In view of this, the ARIMA model should be applied for 1-hour ahead wind power forecasting.

For the forecast time horizon of 1.5 hours, although the ARIMA model achieved the highest similarity score among all the models, the similarity score of it was not much higher than that of the WRF-TOPSIS model. With reference to Tables 6.1 to 6.6, the ARIMA model for the 1.5-hour forecast time horizon had a larger MB absolute value and RMSE and a lower MAE, IA, and accuracy rate in comparison with the WRF-TOPSIS model. Both models had the same qualification rate. From these considerations, the only advantage of the ARIMA model relative to the WRF-TOPSIS model for the 1.5-hour forecast time horizon was that it had a lower MAE. Nevertheless, the WRF-TOPSIS model performed better on all the other evaluation metrics. The only reason for the ARIMA model ranking first is that the MAE was given too high a weighting as determined by the entropy method used by the ranking process of the TOPSIS scheme. Therefore, it is recommended that the WRF-TOPSIS model should be utilised for 1.5-hour ahead wind power forecasting.

For the forecast time horizons of 2, 3, 4, 6, 8, 12, and 24 hours, the ranking order of the various forecasting models was the same. More specifically, the order of the ranking in

terms of the similarity scores from best to worst is as follows: the WRF-TOPSIS, ARIMA, indirect persistence, and direct persistence models. In particular, with the increasing forecast time horizon, the similarity score of the WRF-TOPSIS model rose monotonically until it reached a maximum value. For the wind power forecast time horizons greater than or equal to 6 hours, the similarity score of the WRF-TOPSIS model attained a value of 1.0000—implying that the WRF-TOPSIS model outperformed the ARIMA, direct persistence, and indirect persistence models in terms of every single evaluation metric for the predictive performance on the wind power forecasting 6, 8, 12, and 24 hours in advance. In addition, for the forecast time horizons between 2 and 24 hours, the ARIMA model consistently held the second place with the intermediate similarity scores, meaning that the ARIMA model performed worse than the WRF-TOPSIS model but better than the direct and indirect persistence models which remained at the bottom with pretty low similarity scores, and the indirect persistence model consistently outperformed the direct persistence model, although their similarity scores for each forecast time horizon were extremely close to each other. Consequently, the WRF-TOPSIS model is the most appropriate model to be employed for wind power forecasting with time horizons greater than or equal to 2 hours.

An examination of Tables 6.1 to 6.6 shows that the 4-day average MBs, MAEs, RMSEs, IAs, accuracy rates, and qualification rates for the direct persistence, indirect persistence, and ARIMA models progressively deteriorated with the increasing values of the forecast time horizon—a result that is consistent with intuition. By taking the 4-day average accuracy rate (see Table 6.5) as an example, a decreasing trend of predictive performance with an increasing forecast time horizon should also be seen for the WRF-TOPSIS model. This does not arise from the fact that all the values for the accuracy rate reported in Table 6.5 for the WRF-TOPSIS model correspond only to the 24-hour ahead wind power forecast (recall that the WRF-TOPSIS model was run only once each day to provide the 24-hour ahead wind power forecast). In fact, if the WRF-TOPSIS model is re-run every 6 hours to give a true 6-hour ahead wind power forecast, the 4-day average accuracy rate calculated will be expected to be higher than that of the 24-hour ahead wind power forecast (viz., the 4-day average accuracy rate for the 24-hour ahead wind power forecast corresponds to a lower bound for that of the 6-hour ahead wind power forecast). A similar conclusion can be made with respect to the 4-day average MB, MAE, RMSE, IA, and qualification rate for the 6-hour ahead wind power forecast compared with those for the 24-hour ahead wind power forecast. Even so, it is essential to note that the WRF-TOPSIS model based on the 24-hour ahead wind power forecast still outperformed the statistics-based forecasting models for the 1.5-hour to 12-hour ahead wind power forecasts (even though the WRF-TOPSIS predictive performance for the 24-hour ahead wind power forecast corresponds to only the lower bound on the actual predictive performance for these smaller forecast time

horizons). This result is even more compelling as it suggests that for wind power forecast time horizons longer than 1 hour, the WRF-TOPSIS model is expected to provide the best predictive performance of all the forecasting models.

6.3 Analysis of Statistics-Based and Physics-Based Forecasting Models

The persistence model is the simplest model to be used for wind speed or wind power forecasting. This model has no adjustable parameters and requires the smallest computational effort of all the wind speed and wind power forecasting models considered herein. However, the persistence model is only useful for very short forecast time horizons (no more than 30 minutes). Indeed, the results presented above suggested that the direct and indirect persistence models outperformed the ARIMA and WRF-TOPSIS models only for the 30-minute ahead wind speed and wind power forecasting. Basically, the persistence model relies on a naive assumption that the wind speed or wind power does not change between the current and future times.

The ARIMA model is a classical statistics-based (time series) forecasting model that is more sophisticated than the persistence model but still much simpler than the physics-based forecasting model. The complexity and computational effort of the ARIMA model are intermediate between those of the persistence and WRF-TOPSIS models. This study demonstrated that the ARIMA model gave better predictive performance than the direct persistence, indirect persistence, and WRF-TOPSIS models for the 1-hour ahead wind power forecasting. Unlike the persistence model, the ARIMA model takes into account the temporal correlation structure of the wind speed or wind power: as a result, it is expected to provide better wind speed or wind power forecasts compared with the direct and indirect persistence models for forecast time horizons longer than 30 minutes. Nevertheless, once the forecast time horizon reached or exceeded 1.5 hours, the predictive performance of the ARIMA model was worse than that of the WRF-TOPSIS (physics-based) model.

The physics-based WRF-TOPSIS model is the most sophisticated wind speed and wind power forecasting model considered in the current study. This model has the largest number of adjustable parameters of all the forecasting models studied herein and, moreover, incurs the highest computational cost. The physics-based model uses the mathematical models of the atmosphere to predict the weather (including wind velocity, temperature, humidity, etc.) and, as such, incorporates the complete information of the spatial-temporal structure of the atmospheric motions. As a consequence, the wind speed and wind power forecasts

provided by the physics-based forecasting model were more reliable than those obtained from the statistics-based forecasting models when the forecast time horizon was longer than or equal to 1.5 hours (viz., the longer forecast time horizons).

6.4 Creation of a Multi-Hour Ahead Wind Power Forecasting System

As discussed in Section 6.2, the components of a multi-hour ahead wind power forecasting system for each forecast time horizon were determined according to the results of the case study. A complete architecture diagram of the multi-hour ahead wind power forecasting system is shown in Figure 6.1. This wind power forecasting system consisted of a collection of statistical, physical, and AI models. In particular, historical wind power measurements were the only input data required for the direct persistence model, which could directly provide 30-minute ahead wind power forecasts. Historical wind speed and wind power measurements formed a training dataset that was used to train the ANFIS-based power curve model, which provided a mapping for converting wind speed forecasts to wind power forecasts. Moreover, historical wind speed measurements were the only input data for the indirect persistence model, which could produce 30-minute ahead wind speed forecasts that were then converted to 30-minute ahead wind power forecasts by using the ANFIS-based power curve model. Similarly, historical wind speed measurements were the only input data for the ARIMA model, which could generate 1-hour ahead wind speed forecasts that were then converted to 1-hour ahead wind power forecasts by using the ANFIS-based power curve model. Furthermore, static geographical and GFS gridded meteorological data were the input data for the WRF-TOPSIS model, which could be employed to provide 1.5-hour to 24-hour ahead wind speed forecasts with a temporal resolution of 30 minutes. These forecasts together with the corresponding historical wind speed measurements formed a training dataset that was used to train the ANFIS-based wind speed correction model, which was designed explicitly to correct the original wind speed forecasts provided by the WRF-TOPSIS model. Finally, the corrected 1.5-hour to 24-hour ahead wind speed forecasts were converted to 1.5-hour to 24-hour ahead wind power forecasts with a temporal resolution of 30 minutes by using the ANFIS-based power curve model.

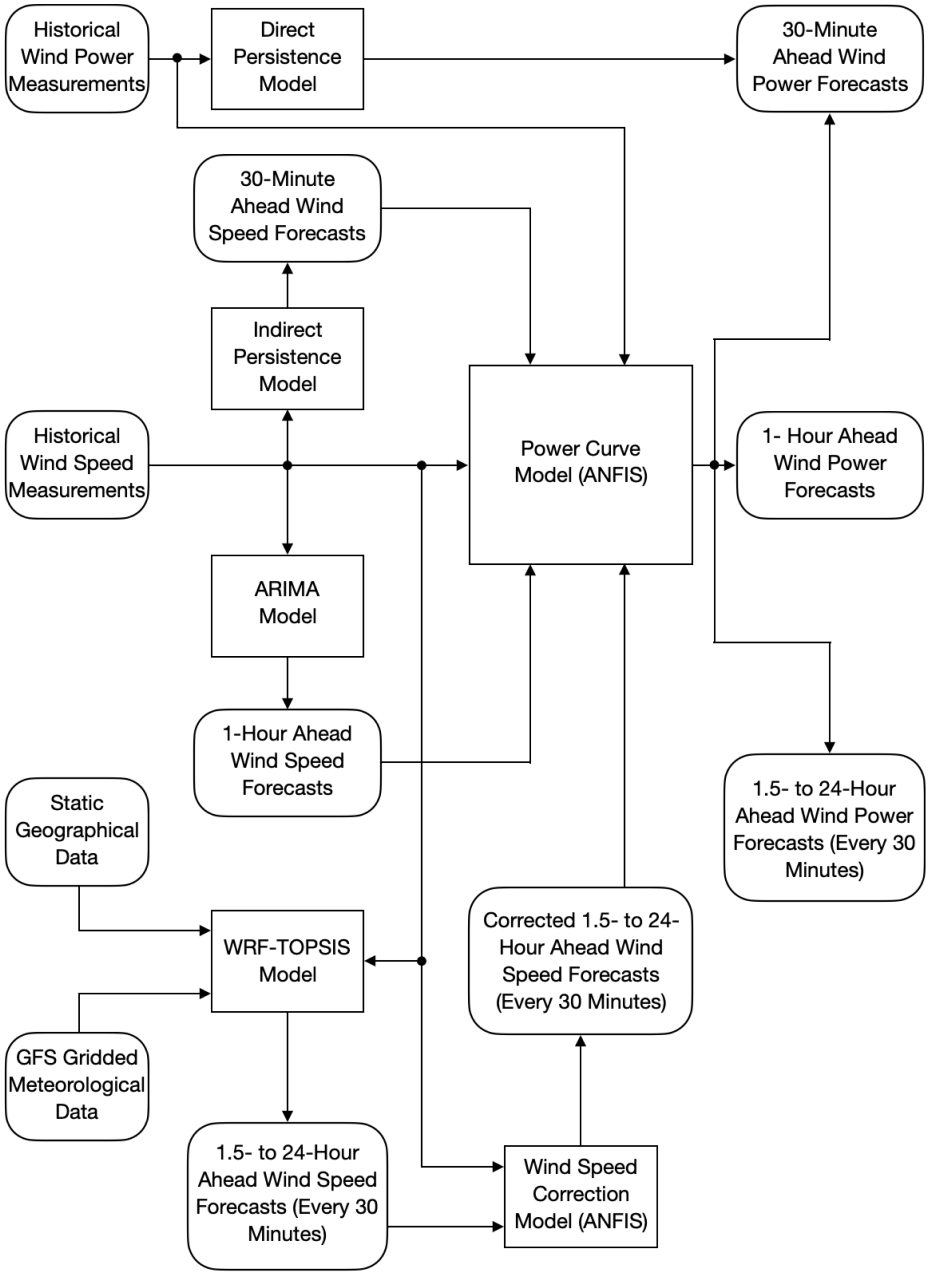

Figure 6.1. Architecture diagram of the multi-hour ahead wind power forecasting system.

6.5 Evaluation of the Multi-Hour Ahead Wind Power Forecasting System

In accordance with the architecture of the multi-hour ahead wind power forecasting system shown in Figure 6.1, the system's overall predictive performance was a combination of the individual predictive performance of the direct persistence, indirect persistence, ARIMA, and WRF-TOPSIS models. The MBs, MAEs, RMSEs, IAs, accuracy rates, and qualification rates for the multi-hour ahead wind power forecasting system applied to the test dataset and their 4-day average values are summarised in Tables 6.8 to 6.13, respectively. An examination of these tables shows that for each evaluation metric, the multi-hour ahead wind power forecasting system performed well. The accuracy rate is the only metric clearly specified in the official document released by the NEA. Specifically, the accuracy rate for 4-hour ahead wind power forecasting needs to be no lower than 85%, and it should be at least 80% for 24-hour ahead wind power forecasting. For the wind power forecasting 4 and 24 hours in advance in this study, the single-day accuracy rate for the proposed multi-hour ahead wind power forecasting system ranged from 87.68% to 96.05%, and the overall accuracy rate for the forecasting system was 91.35%. The multi-hour ahead wind power forecasting system exceeded the predictive performance standards stipulated by the NEA. Additionally, a comparison of the multi-hour ahead wind power forecasts provided by the proposed forecasting system and the historical wind power measurements from the test dataset is shown in Figure 6.2. A serious perusal of this figure reveals that the multi-hour ahead wind power forecasts provided by the proposed forecasting system successfully captured the changing trends of the actual wind power values. All of these study results verified the reliability and accuracy of the multi-hour ahead wind power forecasting system.

Table 6.8. MBs for the multi-hour ahead wind power forecasting system applied to the 4-day test dataset.

MB (kW)		Forecast day				Average
		1	2	3	4	
Forecast time horizon	30 minutes	-0.1/ -2.1	-1.9/ -0.4	2.0/ -4.6	-5.4/ 5.1	-1.4/ -0.5
	1 hour	-21.9	-10.2	-44.5	-56.8	-33.3
	1.5 hours to 24 hours (every 30 minutes)	22.0	-7.9	-30.9	-49.7	-16.6

Table 6.9. MAEs for the multi-hour ahead wind power forecasting system applied to the 4-day test dataset.

MAE (kW)		Forecast day				Average
		1	2	3	4	
Forecast time horizon	30 minutes	58.2/ 54.7	26.6/ 28.3	59.0/ 64.2	50.7/ 56.2	48.6/ 50.8
	1 hour	53.2	27.5	66.8	81.2	57.2
	1.5 hours to 24 hours (every 30 minutes)	91.1	38.5	72.9	108.6	77.8

Table 6.10. RMSEs for the multi-hour ahead wind power forecasting system applied to the 4-day test dataset.

RMSE (kW)		Forecast day				Average
		1	2	3	4	
Forecast time horizon	30 minutes	199.4/ 193.6	46.0/ 45.9	90.9/ 93.8	82.7/ 85.4	104.7/ 104.7
	1 hour	186.5	44.3	101.6	127.7	115.0
	1.5 hours to 24 hours (every 30 minutes)	184.9	59.2	111.0	164.1	129.8

Table 6.11. IAs for the multi-hour ahead wind power forecasting system applied to the 4-day test dataset.

IA		Forecast day				Average
		1	2	3	4	
Forecast time horizon	30 minutes	0.74/ 0.74	0.68/ 0.68	0.90/ 0.88	0.97/ 0.97	0.82/ 0.82
	1 hour	0.64	0.57	0.82	0.90	0.73
	1.5 hours to 24 hours (every 30 minutes)	0.60	0.37	0.82	0.83	0.66

Table 6.12. Accuracy rates for the multi-hour ahead wind power forecasting system applied to the 4-day test dataset.

Accuracy rate		Forecast day				Average
		1	2	3	4	
Forecast time horizon	30 minutes	86.71%/ 87.09%	96.94%/ 96.94%	93.94%/ 93.74%	94.49%/ 94.31%	93.02%/ 93.02%
	1 hour	87.57%	97.04%	93.23%	91.49%	92.33%
	1.5 hours to 24 hours (every 30 minutes)	87.68%	96.05%	92.60%	89.06%	91.35%

Table 6.13. Qualification rates for the multi-hour ahead wind power forecasting system applied to the 4-day test dataset.

Qualification rate		Forecast day				Average
		1	2	3	4	
Forecast time horizon	30 minutes	95.83%/ 95.83%	100.00%/ 100.00%	100.00%/ 100.00%	100.00%/ 100.00%	98.96%/ 98.96%
	1 hour	97.92%	100.00%	100.00%	97.92%	98.96%
	1.5 hours to 24 hours (every 30 minutes)	95.83%	100.00%	100.00%	95.83%	97.92%

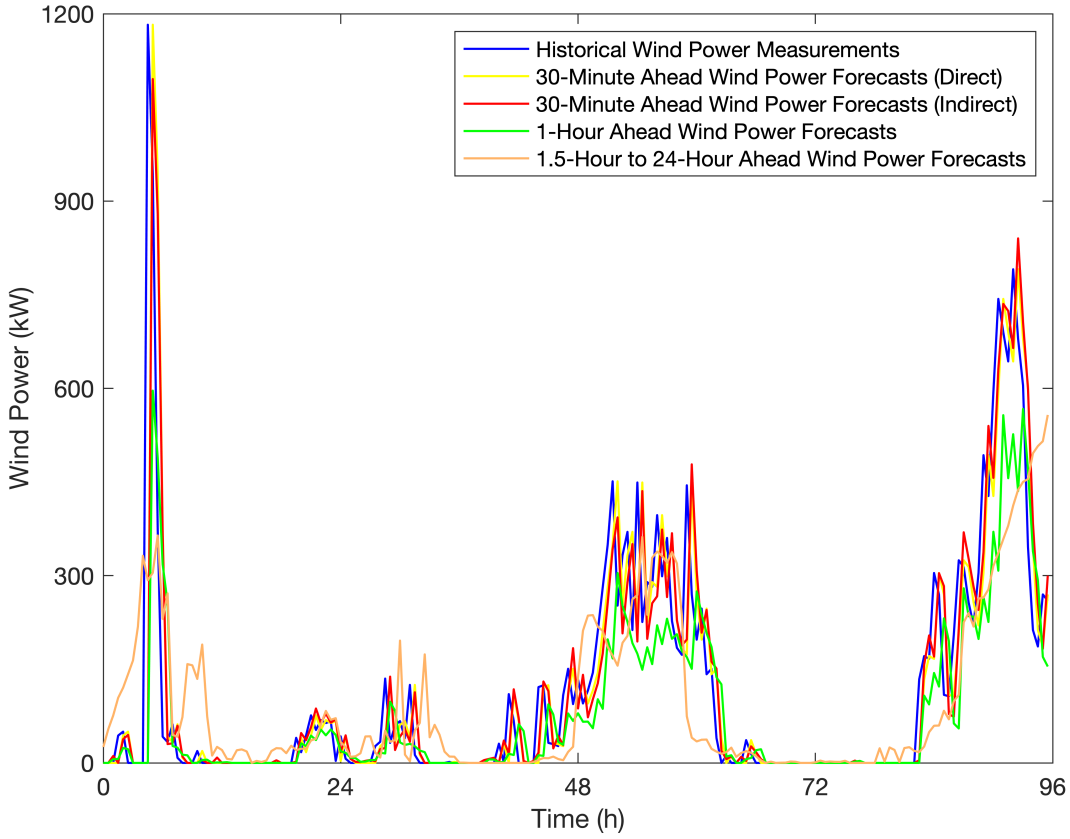

Figure 6.2. Comparison of the multi-hour ahead wind power forecasts provided by the proposed forecasting system and the historical wind power measurements from the 4-day test dataset. The 30-minute ahead wind power forecasts are obtained by using the direct and indirect persistence (statistical + AI) models, the 1-hour ahead wind power forecasts are obtained by using the ARIMA (statistical + AI) model, and the 1.5-hour to 24-hour ahead wind power forecasts are obtained by using the ANFIS-corrected (ensemble) WRF-TOPSIS (physical + AI) model.

6.6 Summary

A multi-hour ahead wind power forecasting system consisting of an optimal combination of statistical, physical, and AI models is created in Chapter 6. The statistics-based and physics-based wind power forecasting models (viz., the direct persistence, indirect persis-

tence, ARIMA, and WRF-TOPSIS models) generated in Chapters 4 and 5, respectively, were compared with each other according to their predictive performance on different forecast time horizons. For the purpose of determining the specific model to be used for each forecast time horizon, the TOPSIS scheme was utilised to rank these statistical/AI and physical/AI forecasting models with respect to their predictive performance as evaluated by six metrics, namely the MB, MAE, RMSE, IA, accuracy rate, and qualification rate. After a comparative analysis of these forecasting models, the direct and indirect persistence models were shown to provide the best predictive performance for the very short forecast time horizon of 30 minutes. The ARIMA model was demonstrated to provide the best predictive performance for the 1-hour ahead wind power forecasting. However, for the forecast time horizons ranging from 1.5 to 24 hours (with a 30-minute temporal resolution), the corrected WRF-TOPSIS model performed the best among all the wind power forecasting models. Finally, the construction of the multi-hour ahead wind power forecasting system was completed, and the system architecture diagram is shown in Figure 6.1. A perusal of Tables 6.8 to 6.13 indicates that the multi-hour ahead wind power forecasting system performed well for each evaluation metric, and it exceeded the predictive performance standards stipulated by the NEA. Additionally, from the comparison of the multi-hour ahead wind power forecasts and historical wind power measurements from the test dataset (see Figure 6.2), it can be found that the multi-hour ahead wind power forecasts provided by the proposed forecasting system successfully captured the changing trends of the actual wind power values. All of these study results verified the reliability and accuracy of the multi-hour ahead wind power forecasting system.

Chapter 7

Conclusions and Future Work

In order to meet the requirements of the wind power industry, a novel multi-hour ahead wind power forecasting system consisting of an optimal combination of statistical, physical, and AI models was proposed in this research. The historical wind speed and wind power measurements acquired from an operational wind turbine in a real wind farm located in North China were used to train and evaluate the forecasting system.

First of all, an ANFIS was utilised to construct a power curve model that played the role of mapping wind speed forecasts to wind power forecasts. Through a comparative analysis, three key ANFIS model parameters, namely the type of membership functions, number of membership functions, and number of training epochs, were determined to be generalised bell-shaped, 3, and 10, respectively. The effectiveness of the selected ANFIS model was verified as the model IA, accuracy rate, and qualification rate were 1.00, 98.87%, and 100.00%, respectively. The 1.13% wind power prediction error, as characterised by the accuracy rate, mainly resulted from the systematic errors, model errors, and neglect of other variables that affected the wind power. The established power curve was sufficient in this research.

Second, the persistence (statistics-based) modelling was presented for multi-hour ahead wind speed and wind power forecasting. There are two ways of forecasting wind power based on a persistence model. One is called direct forecasting. In this method, historical wind power measurements are the only necessary data and are simply regarded as future wind power forecasts. The other is indirect forecasting, in which historical wind speed measurements are considered future wind speed forecasts that can be converted to wind power forecasts by utilising the ANFIS-based power curve model. Both the direct and indirect wind power forecasting were tested for 10 different forecast time horizons ranging

from 30 minutes to 24 hours. The results revealed that the direct and indirect persistence models performed quite well for the 30-minute ahead wind power forecasting. However, with the rise in the forecast time horizon, the MB, MAE, RMSE, IA, accuracy rate, and qualification rate for the wind power forecasting by using the direct and indirect persistence models deteriorated.

Third, the ARIMA time series (statistics-based) modelling was applied for multi-hour ahead wind speed and wind power forecasting. Through an exploratory and a confirmatory data analysis of the historical wind speed measurements, the ARIMA $(2, 1, 1)$ model was selected as the most appropriate model for the wind speed forecasting. The wind speed forecasts provided by the ARIMA $(2, 1, 1)$ model were converted to the wind power forecasts by using the ANFIS-based power curve model. The wind power forecasting was tested for 10 different forecast time horizons ranging from 30 minutes to 24 hours. It was concluded that the ARIMA $(2, 1, 1)$ model performed well for the 30-minute ahead wind power forecasting. However, with the rise in the forecast time horizon, the 4-day average MB absolute value, MAE, and RMSE for the wind power forecasting by using the ARIMA $(2, 1, 1)$ model increased gradually, while the corresponding 4-day average IA, accuracy rate, and qualification rate went down.

Fourth, the WRF (physics-based) modelling was employed for multi-hour ahead wind speed and wind power forecasting. The numerical weather forecasts provided by the WRF model depended critically on the choice of a number of physical process subgrid-scale parameterisation schemes that played a significant role in determining the model behaviour and, as a result, offered a large initial ensemble of different possible WRF models that gave various wind speed forecasts. A systematic approach was proposed to determine the critical subgrid-scale parameterisation options that impacted the quality of the model predictions, namely the amount of energy that reached the Earth's surface, the subgrid-scale cumulus cloud and convective development, the evolution of the planetary boundary layer and surface layer, and the subgrid-scale orography. More specifically, the TOPSIS scheme was employed to select the 50 best-performing WRF models from the 1,334 possibilities (arising from the different physical parameterisation scheme combinations) according to their predictive performance based on the first day of the training dataset. Following this analysis, these 50 candidates were applied to the entire training dataset of the 20-day wind speed measurements, and the top five WRF models were selected from them in accordance with their similarity scores provided by the TOPSIS scheme. Subsequently, a novel 5-in-1 (ensemble) WRF model was constructed by combining the top five WRF models on the basis of the weights (similarity scores) provided by the TOPSIS scheme. Furthermore, another ANFIS was utilised to build a wind speed correction model exclusively for further improving the wind speed forecasts obtained from the 5-in-1 (ensemble) WRF model. A

comparative analysis demonstrated that the wind speed forecasts provided by the corrected 5-in-1 (ensemble) WRF model were superior to those obtained from the original 5-in-1 (ensemble) and Dr Wen's (the benchmark) WRF models—assessed in terms of the average performance of a number of evaluation metrics on the test dataset. Finally, the wind speed forecasts provided by the corrected 5-in-1 (ensemble) WRF model were converted to the wind power forecasts by using the ANFIS-based power curve model. As a result, the superiority of the wind power forecasting by using the corrected WRF-TOPSIS model was verified.

For the purpose of comprehensively evaluating the wind power predictive performance of the statistical/AI and physical/AI forecasting models and determining the specific model to be used for each forecast time horizon, the TOPSIS scheme was utilised to rank these forecasting models with respect to their predictive performance for 10 different forecast time horizons ranging from 30 minutes to 24 hours on the test dataset. After a comparative analysis of these forecasting models, the direct and indirect persistence models were shown to provide the best predictive performance for the very short forecast time horizon of 30 minutes. The ARIMA model was demonstrated to provide the best predictive performance for the 1-hour ahead wind power forecasting. However, for the forecast time horizons ranging from 1.5 to 24 hours (with a 30-minute temporal resolution), the corrected WRF-TOPSIS model performed the best among all the wind power forecasting models.

Finally, the construction of the multi-hour ahead wind power forecasting system consisting of all these model components was completed (see Figure 6.1). The multi-hour ahead wind power forecasts provided by the proposed forecasting system successfully captured the changing trends of the actual wind power values. It was demonstrated that the forecasting system was reliable and exceeded the predictive performance standards stipulated by the NEA. Moreover, the impacts of using the forecasting system for real-world applications are obvious. Specifically, very short-term (30 minutes ahead) wind power forecasting is helpful for wind turbine control, regulation actions, real-time grid operations, electricity market clearing, and so on; short-term (1 to 24 hours ahead) wind power forecasting is beneficial to power dispatch schedules, load smart decisions, operational security in electricity markets, and so on. In addition, the forecasting system with an accuracy rate greater than 80% can keep wind farms in China free of penalties. All of these benefits reveal that the proposed forecasting system is of great practical relevance.

The primary contribution of this research is the novel WRF-TOPSIS ensemble model strategy used to select and combine the best-performing WRF models from a vast ensemble of possible models. Meteorological conditions and land use features can vary significantly from one season to the next over the course of a year. Since these various factors affect the predictive performance of WRF models based on various physical parameterisation scheme

combinations, the final selection of WRF models may exhibit a seasonal variation—which will be reflected in distinct WRF models and even the number of WRF models that need to be combined. In other words, the same setup of the WRF-TOPSIS ensemble model may not be optimal for the wind farm in a different season or another wind farm at a different geographical location. In spite of this, the critical point herein is the systematic methodology proposed to select and combine the various WRF models for producing the most reliable and accurate wind speed and wind power forecasts. Some suggestions for the future work on the enhancement of the current multi-hour ahead wind power forecasting system are summarised as follows:

(1) Inputting 6-hourly GFS meteorological data to the WRF-TOPSIS model and examining whether the predictive performance is better than that of the direct persistence, indirect persistence, and ARIMA models in terms of 30-minute and 1-hour ahead wind power forecasting;

(2) Testing the proposed wind power forecasting system based on a set of four-season data from the wind farm in China and investigating the necessity of seasonal forecasting models;

(3) Applying the proposed methodology for multi-hour ahead wind power forecasting to other wind farms at diverse (including offshore) locations and verifying the adaptability of the methodology and necessity of ocean models for offshore wind farms;

(4) Comparing the predictive performance of high-resolution and coarse-resolution WRF models and discussing the feasibility of coarse-resolution WRF models;

(5) Adding more types of meteorological data (such as wind direction, temperature, humidity, and pressure) as the additional input variables to the proposed wind power forecasting system;

(6) Integrating the proposed wind power forecasting system with a higher-resolution computational fluid dynamics (CFD) model to model the terrain effects explicitly.

References

[1] Ajith Abraham. Adaptation of fuzzy inference system using neural learning. In Nadia Nedjah and Luiza de Macedo Mourelle, editors, *Fuzzy Systems Engineering: Theory and Practice*, Studies in Fuzziness and Soft Computing, pages 53–83. Springer, Berlin, July 2005.

[2] Dave Anderson and George McNeill. Artificial neural networks technology. Technical report, Kaman Sciences Corporation, Utica, August 1992.

[3] Temitope Raphael Ayodele, Adiasa A. Jimoh, Josial L. Munda, and Agee J. Tehile. Challenges of grid integration of wind power on power system grid integrity: A review. *International Journal of Renewable Energy Research*, 2(4):618–626, August 2012.

[4] Bruce Bailey, Michael C. Brower, and John Zack. Short-term wind forecasting: Development and application of a mesoscale model. In *Proceedings of the European Wind Energy Conference & Exhibition 1999*, pages 1062–1065, Nice, March 1999. EWEA.

[5] Vasiliki Balioti, Christos Tzimopoulos, and Christos Evangelides. Multi-criteria decision making using TOPSIS method under fuzzy environment. application in spillway selection. *Proceedings*, 2(11):637, July 2018.

[6] David Barbosa de Alencar, Carolina De Mattos Affonso, Roberto Célio Limão de Oliveira, Jorge Laureano Moya Rodriguez, Jandecy Cabral Leite, and José Carlos Reston Filho. Different models for forecasting wind power generation: Case study. *Energies*, 10(12):1976, November 2017.

[7] Radian Belu. *Fundamentals and Source Characteristics of Renewable Energy Systems*. Nano and Energy. CRC Press, Boca Raton, September 2019.

[8] Hans Georg Beyer, Detlev Heinemann, Harald Mellinghoff, Kai Mönnich, and Hans-Peter Waldl. Forecast of regional power output of wind turbines. In *Proceedings of the European Wind Energy Conference & Exhibition 1999*, pages 1070–1073, Nice, March 1999. EWEA.

[9] Hassen Bouzgou and Nabil Benoudjit. Multiple architecture system for wind speed prediction. *Applied Energy*, 88(7):2463–2471, July 2011.

[10] George E.P. Box, Gwilym M. Jenkins, Gregory C. Reinsel, and Greta M. Ljung. *Time Series Analysis: Forecasting and Control*. Wiley Series in Probability and Statistics. Wiley, Hoboken, fifth edition, May 2015.

[11] BP. Statistical review of world energy 2021. Technical report, British Petroleum, London, 2021.

[12] Erasmo Cadenas and Wilfrido Rivera. Wind speed forecasting in the south coast of Oaxaca, México. *Renewable Energy*, 32(12):2116–2128, October 2007.

[13] Erasmo Cadenas and Wilfrido Rivera. Short term wind speed forecasting in La Venta, Oaxaca, México, using artificial neural networks. *Renewable Energy*, 34(1):274–278, January 2009.

[14] Erasmo Cadenas and Wilfrido Rivera. Wind speed forecasting in three different regions of Mexico, using a hybrid ARIMA–ANN model. *Renewable Energy*, 35(12):2732–2738, December 2010.

[15] CanWEA. A wind energy vision for Canada. Technical report, Canadian Wind Energy Association, Ottawa, 2019.

[16] CanWEA. Wind energy in Canada. Technical report, Canadian Wind Energy Association, Ottawa, 2020.

[17] J.P.S. Catalão, H.M.I. Pousinho, and V.M.F Mendes. Hybrid intelligent approach for short-term wind power forecasting in Portugal. *IET Renewable Power Generation*, 5(3):251–257, May 2011.

[18] J.P.S. Catalão, H.M.I. Pousinho, and V.M.F Mendes. Hybrid wavelet-PSO-ANFIS approach for short-term wind power forecasting in Portugal. *IEEE Transactions on Sustainable Energy*, 2(1):50–59, January 2011.

[19] J.P.S. Catalão, H.M.I. Pousinho, and V.M.F Mendes. Short-term wind power forecasting in Portugal by neural networks and wavelet transform. *Renewable Energy*, 36(4):1245–1251, April 2011.

[20] Wen-Yeau Chang. Application of back propagation neural network for wind power generation forecasting. *International Journal of Digital Content Technology and its Applications*, 7(4):502–509, February 2013.

[21] Wen-Yeau Chang. Short-term wind power forecasting using the enhanced particle swarm optimization based hybrid method. *Energies*, 6(9):4879–4896, September 2013.

[22] Wen-Yeau Chang. A literature review of wind forecasting methods. *Journal of Power and Energy Engineering*, 2(4):161–168, April 2014.

[23] Mei-Fang Chen and Gwo-Hshiung Tzeng. Combining grey relation and TOPSIS concepts for selecting an expatriate host country. *Mathematical and Computer Modelling*, 40(13):1473–1490, December 2004.

[24] Q. Chen and K.A. Folly. Wind power forecasting. *IFAC-PapersOnLine*, 51(28):414–419, December 2018.

[25] Vijay Dahiya. Analysis of Lagrange interpolation formula. *International Journal of Innovative Science, Engineering & Technology*, 1(10):619–624, December 2014.

[26] A.D. Dongare, R.R. Kharde, and Amit D. Kachare. Introduction to artificial neural network. *International Journal of Engineering and Innovative Technology*, 2(1):189–194, July 2012.

[27] Jimy Dudhia. WRF modeling system overview. In *WRF-ARW Tutorials*. National Center for Atmospheric Research, 2014.

[28] Peter Enevoldsen, Scott Victor Valentine, and Benjamin K. Sovacool. Insights into wind sites: Critically assessing the innovation, cost, and performance dynamics of global wind energy development. *Energy Policy*, 120:1–7, September 2018.

[29] Ergin Erdem and Jing Shi. ARMA based approaches for forecasting the tuple of wind speed and direction. *Applied Energy*, 88(4):1405–1414, April 2011.

[30] Bernhard Ernst, Kurt Rohrig, and René Jursa. Online-monitoring and prediction of wind power in German transmission system operation centres. In *Proceedings of the*

First IEA Joint Action Symposium on Wind Forecasting Techniques, pages 125–145, Norrköping, December 2002. Swedish Defence Research Agency.

[31] İrfan Ertuğrul and Nilsen Karakaşoğlu. Performance evaluation of Turkish cement firms with fuzzy analytic hierarchy process and TOPSIS methods. *Expert Systems with Applications*, 36(1):702–715, January 2009.

[32] Ulrich Focken, Matthias Lange, and Hans-Peter Waldl. Previento - A wind power prediction system with an innovative upscaling algorithm. In *Proceedings of the European Wind Energy Conference & Exhibition 2001*, volume 276, pages 826–829, Copenhagen, July 2001. EWEA.

[33] Aoife M. Foley, Paul G. Leahy, Antonino Marvuglia, and Eamon J. McKeogh. Current methods and advances in forecasting of wind power generation. *Renewable Energy*, 37(1):1–8, January 2012.

[34] Robert Fullér. *Introduction to Neuro-Fuzzy Systems*, volume 2 of *Advances in Soft Computing*. Springer, Heidelberg, January 2000.

[35] Wayne A. Fuller. *Introduction to Statistical Time Series*. Wiley Series in Probability and Statistics. Wiley, New York, second edition, April 1996.

[36] C. Gallego, P. Pinson, H. Madsen, A. Costa, and A. Cuerva. Influence of local wind speed and direction on wind power dynamics – Application to offshore very short-term forecasting. *Applied Energy*, 88(11):4087–4096, November 2011.

[37] G. Giebel, L. Landberg, and T.S. Nielsen. The ZEPHYR project: The next generation prediction tool. In *Proceedings of the European Wind Energy Conference & Exhibition 2001*, volume 1, pages 777–781, Copenhagen, July 2001. EWEA.

[38] Gregor Giebel, Richard Brownsword, Georges Kariniotakis, Michael Denhard, and Caroline Draxl. The state-of-the-art in short-term prediction of wind power. A literature overview, January 2011.

[39] Gregor Giebel, Georges Kariniotakis, and Richard Brownsword. The state-of-the-art in short term prediction of wind power from a Danish perspective. In *Proceedings of the 4th International Workshop on Large-Scale Integration of Wind Power and Transmission Networks for Offshore Wind Farms*, Billund, October 2003. Energynautics GmbH.

[40] G. Gow. Short term wind forecasting in the UK. In *Proceedings of the First IEA Joint Action Symposium on Wind Forecasting Techniques*, pages 3–10, Norrköping, December 2002. Swedish Defence Research Agency.

[41] Steve R. Gunn. Support vector machines for classification and regression. Technical report, University of Southampton, Southampton, May 1998.

[42] Zhenhai Guo, Jing Zhao, Wenyu Zhang, and Jianzhou Wang. A corrected hybrid approach for wind speed prediction in Hexi Corridor of China. *Energy*, 36(3):1668–1679, March 2011.

[43] Zhenhai Guo, Weigang Zhao, Haiyan Lu, and Jianzhou Wang. Multi-step forecasting for wind speed using a modified EMD-based artificial neural network model. *Renewable Energy*, 37(1):241–249, January 2012.

[44] Dinesh Kumar Gupta. A review on wireless sensor networks. *Network and Complex Systems*, 3(1):18–23, 2013.

[45] GWEC. Global wind 2008 report. Technical report, Global Wind Energy Council, Brussels, February 2009.

[46] GWEC. Annual market update 2017: Global wind report. Technical report, Global Wind Energy Council, Brussels, April 2018.

[47] GWEC. GWEC | Global wind report 2018. Technical report, Global Wind Energy Council, Brussels, April 2019.

[48] GWEC. GWEC | Global wind report 2019. Technical report, Global Wind Energy Council, Brussels, March 2020.

[49] GWEC. GWEC | Global wind report 2021. Technical report, Global Wind Energy Council, Brussels, March 2021.

[50] James D. Hamilton. *Time Series Analysis*. Princeton University Press, Princeton, January 1994.

[51] Shahram Hanifi, Xiaolei Liu, Zi Lin, and Saeid Lotfian. A critical review of wind power forecasting methods—Past, present and future. *Energies*, 13(15):3764, July 2020.

[52] E.J. Hannan. Stationary time series. In John Eatwell, Murray Milgate, and Peter Newman, editors, *Time Series and Statistics*, The New Palgrave, pages 271–276. Palgrave Macmillan, London, July 1990.

[53] Michèle Hibon and Theodoros Evgeniou. To combine or not to combine: Selecting among forecasts and their combinations. *International Journal of Forecasting*, 21(1):15–24, January–March 2005.

[54] Ying-Yi Hong and Christian Lian Paulo P. Rioflorido. A hybrid deep learning-based neural network for 24-h ahead wind power forecasting. *Applied Energy*, 250:530–539, September 2019.

[55] Mikael Höök and Xu Tang. Depletion of fossil fuels and anthropogenic climate change—A review. *Energy Policy*, 52:797–809, January 2013.

[56] Z. Huang and Z.S. Chalabi. Use of time-series analysis to model and forecast wind speed. *Journal of Wind Engineering and Industrial Aerodynamics*, 56(2-3):311–322, May 1995.

[57] Ching-Lai Hwang, Young-Jou Lai, and Ting-Yun Liu. A new approach for multiple objective decision making. *Computers & Operations Research*, 20(8):889–899, October 1993.

[58] Ching-Lai Hwang and Kwangsun Yoon. Methods for multiple attribute decision making. In M. Beckmann and H.P. Künzi, editors, *Multiple Attribute Decision Making: Methods and Applications A State-of-the-Art Survey*, volume 186 of *Lecture Notes in Economics and Mathematical Systems*, pages 58–191. Springer, Berlin, February 1981.

[59] IRENA. Renewable power generation costs in 2020. Technical report, International Renewable Energy Agency, Abu Dhabi, 2021.

[60] J.-S.R. Jang. ANFIS: Adaptive-network-based fuzzy inference system. *IEEE Transactions on Systems, Man, and Cybernetics*, 23(3):665–685, May–June 1993.

[61] André Jones, Arnold Kaufmann, and Hans-Jürgen Zimmermann, editors. *Fuzzy Sets Theory and Applications*, volume 177 of *NATO ASI Series C: Mathematical and Physical Sciences*. Springer, Berlin, December 2012.

[62] Christopher Jung and Dirk Schindler. The role of the power law exponent in wind energy assessment: A global analysis. *International Journal of Energy Research*, 45(6):8484–8496, May 2021.

[63] Jaesung Jung and Robert P. Broadwater. Current status and future advances for wind speed and power forecasting. *Renewable and Sustainable Energy Reviews*, 31:762–777, March 2014.

[64] René Jursa and Kurt Rohrig. Short-term wind power forecasting using evolutionary algorithms for the automated specification of artificial intelligence models. *International Journal of Forecasting*, 24(4):694–709, October–December 2008.

[65] Lalarukh Kamal and Yasmin Zahra Jafri. Time series models to simulate and forecast hourly averaged wind speed in Quetta, Pakistan. *Solar Energy*, 61(1):23–32, July 1997.

[66] Georges Kariniotakis, Pierre Pinson, Nils Siebert, Gregor Giebel, and Rebecca Barthelmie. The state of the art in short-term prediction of wind power - From an offshore perspective. In *Proceedings of the 2004 SeaTech Week-Ocean Energy Conference*, Brest, October 2004. ADEME-IFREMER.

[67] Rajesh G. Kavasseri and Krithika Seetharaman. Day-ahead wind speed forecasting using f-ARIMA models. *Renewable Energy*, 34(5):1388–1393, May 2009.

[68] George J. Klir and Bo Yuan. *Fuzzy Sets and Fuzzy Logic: Theory and Applications*. Prentice Hall, Upper Saddle River, May 1995.

[69] S.P.T. Krishnan, Bharadwaj Veeravalli, Vetharenian Hari Krishna, and Wu Chia Sheng. Performance characterisation and evaluation of WRF model on cloud and HPC architectures. In *2014 IEEE Intl Conf on High Performance Computing and Communications, 2014 IEEE 6th Intl Symp on Cyberspace Safety and Security, 2014 IEEE 11th Intl Conf on Embedded Software and Syst (HPCC, CSS, ICESS)*, pages 1280–1287, Paris, August 2014. IEEE.

[70] Ben Kröse and Patrick van der Smagt. *An Introduction to Neural Networks*. University of Amsterdam, Amsterdam, eighth edition, November 1996.

[71] Harsh Kukreja, N. Bharath, C.S. Siddesh, and S. Kuldeep. An introduction to artificial neural network. *International Journal of Advance Research and Innovative Ideas in Education*, 1(5):27–30, 2016.

[72] Lars Landberg. Short-term prediction of the power production from wind farms. *Journal of Wind Engineering and Industrial Aerodynamics*, 80(1-2):207–220, March 1999.

[73] Lars Landberg, Lisbeth Myllerup, Ole Rathmann, Erik Lundtang Petersen, Bo Hoffmann Jørgensen, Jake Badger, and Niels Gylling Mortensen. Wind resource estimation—An overview. *Wind Energy*, 6(3):261–271, June 2003.

[74] Matthias Lange and Ulrich Focken. *Physical Approach to Short-Term Wind Power Prediction*. Springer, Berlin, January 2006.

[75] Matthias Lange and Ulrich Focken. *State-of-the-Art in Wind Power Prediction in Germany and International Developments*. energy & Meteorological systems GmbH, Oldenburg, 2006.

[76] Matthias Lange, Ulrich Focken, and Detlev Heinemann. Previento: Regional wind power prediction with risk control. In *Proceedings of the World Wind Energy Conference 2002*, Berlin, July 2002. WWEC.

[77] Gong Li and Jing Shi. On comparing three artificial neural networks for wind speed forecasting. *Applied Energy*, 87(7):2313–2320, July 2010.

[78] Gong Li, Jing Shi, and Junyi Zhou. Bayesian adaptive combination of short-term wind speed forecasts from neural network models. *Renewable Energy*, 36(1):352–359, Nanuary 2011.

[79] Zi Lin, Xiaolei Liu, and Maurizio Collu. Wind power prediction based on high-frequency SCADA data along with isolation forest and deep learning neural networks. *International Journal of Electrical Power & Energy Systems*, 118:105835, June 2020.

[80] Fang Liu, Ranran Li, and Aliona Dreglea. Wind speed and power ultra short-term robust forecasting based on Takagi–Sugeno fuzzy model. *Energies*, 12(18):3551, September 2019.

[81] Hui Liu, Hong-Qi Tian, Chao Chen, and Yan-fei Li. A hybrid statistical method to predict wind speed and wind power. *Renewable Energy*, 35(8):1857–1861, August 2010.

[82] Hui Liu, Hong-qi Tian, and Yan-fei Li. Comparison of two new ARIMA-ANN and ARIMA-Kalman hybrid methods for wind speed prediction. *Applied Energy*, 98:415–424, October 2012.

[83] Jinqiang Liu, Xiaoru Wang, and Yun Lu. A novel hybrid methodology for short-term wind power forecasting based on adaptive neuro-fuzzy inference system. *Renewable Energy*, 103:620–629, April 2017.

[84] Wenyi Liu, Baoping Tang, and Yonghua Jiang. Status and problems of wind turbine structural health monitoring techniques in China. *Renewable Energy*, 35(7):1414–1418, July 2010.

[85] David J. Livingstone. *Artificial Neural Networks: Methods and Applications*, volume 458 of *Methods in Molecular Biology*. Humana Press, Totowa, October 2008.

[86] Lei Ma, Shiyan Luan, Chuanwen Jiang, Hongling Liu, and Yan Zhang. A review on the forecasting of wind speed and generated power. *Renewable and sustainable energy reviews*, 13(4):915–920, May 2009.

[87] M. Carolin Mabel and Eugene Fernandez. Analysis of wind power generation and prediction using ANN: A case study. *Renewable Energy*, 33(5):986–992, May 2008.

[88] Henrik Madsen, Henrik Aalborg Nielsen, and Torben Skov Nielsen. A tool for predicting the wind power production of off-shore wind plants. In *Proceedings of the European Offshore Wind Conference & Exhibition 2005*, Copenhagen, October 2005. EWEA.

[89] I. Martí. Wind forecasting activities. In *Proceedings of the First IEA Joint Action Symposium on Wind Forecasting Techniques*, pages 11–20, Norrköping, December 2002. Swedish Defence Research Agency.

[90] Ignacio Martí, Daniel Cabezón, Javier Villanueva, Maria Jesús Sanisidro, Yolanda Loureiro, Elena Cantero, and Javier Sanz. LocalPred and RegioPred. Advanced tools for wind energy prediction in complex terrain. In *Proceedings of the European Wind Energy Conference & Exhibition 2003*, pages 16–19, Madrid, June 2003. EWEA.

[91] Zhongxian Men, Eugene Yee, Fue-Sang Lien, Deyong Wen, and Yongsheng Chen. Short-term wind speed and power forecasting using an ensemble of mixture density neural networks. *Renewable Energy*, 87:203–211, October 2016.

[92] Terence C. Mills. *Applied Time Series Analysis: A Practical Guide to Modeling and Forecasting*. Academic Press, London, January 2019.

[93] Ali Mohammadi, Abolfazl Mohammadi, and Hossain Aryaeefar. Introducing a new method to expand TOPSIS decision making model to fuzzy TOPSIS. *The Journal of Mathematics and Computer Science*, 2(1):150–159, January 2011.

[94] Mohamed A. Mohandes, Shafiqur Rehman, and Talal O. Halawani. A neural networks approach for wind speed prediction. *Renewable Energy*, 13(3):345–354, March 1998.

[95] Mohammad A. Mohandes, Talal O. Halawani, Shafiqur Rehman, and Ahmed A. Hussain. Support vector machines for wind speed prediction. *Renewable Energy*, 29(6):939–947, May 2004.

[96] C. Monteiro, R. Bessa, V. Miranda, A. Botterud, J. Wang, and G. Conzelmann. Wind power forecasting: State-of-the-art 2009. Technical report, Argonne National Laboratory, Lemont, November 2009.

[97] Anurag More and M.C. Deo. Forecasting wind with neural networks. *Marine Structures*, 16(1):35–49, January–February 2003.

[98] Peter Musgrove. *Wind Power*. Cambridge University Press, Cambridge, January 2010.

[99] Detlef Nauck, Frank Klawonn, and Rudolf Kruse. *Foundations of Neuro-Fuzzy Systems*. Wiley, Chichester, September 1997.

[100] NEA. 风电场功率预测预报管理暂行办法 [Interim Regulations for the Wind Farm Power Prediction and Forecast Management]. National Energy Administration, Beijing, June 2011.

[101] Giovanni Nicoletti, Natale Arcuri, Gerardo Nicoletti, and Roberto Bruno. A technical and environmental comparison between hydrogen and some fossil fuels. *Energy Conversion and Management*, 89:205–213, January 2015.

[102] Mariusz Niemiec. *Fuzzy Inference System - Theory and Applications*. Scitus Academics LLC, Wilmington, January 2017.

[103] Vilém Novák, Irina Perfilieva, and Jiří Močkoř. *Mathematical Principles of Fuzzy Logic*, volume 517 of *The Springer International Series in Engineering and Computer Science*. Kluwer Academic Publishers, Boston, August 1999.

[104] G.J. Osório, J.C.O. Matias, and J.P.S. Catalão. Short-term wind power forecasting using adaptive neuro-fuzzy inference system combined with evolutionary particle swarm optimization, wavelet transform and mutual information. *Renewable Energy*, 75:301–307, March 2015.

[105] Xiaoduo Pan, Xin Li, Xiaokang Shi, Xujun Han, Lihui Luo, and Liangxu Wang. Dynamic downscaling of near-surface air temperature at the basin scale using WRF-a case study in the Heihe River Basin, China. *Frontiers of Earth Science*, 6(3):314–323, May 2012.

[106] J. Parkes, A. Tindal, S.V.S. Works, and S. Lane. Forecasting short term wind farm production in complex terrain. In *Proceedings of the European Wind Energy Conference & Exhibition 2004*, pages 22–25, London, November 2004. EWEA.

[107] S. Gopal Krishna Patro and Kishore Kumar Sahu. Normalization: A preprocessing stage. *arXiv:1503.06462 [cs.OH]*, March 2015.

[108] Sujata Pattanayak and U.C. Mohanty. Development of extended WRF variational data assimilation system (WRFDA) for WRF non-hydrostatic mesoscale model. *Journal of Earth System Science*, 127(4):1–24, May 2018.

[109] Jonas C. Pelajo, Luiz E.T. Brandão, Leonardo L. Gomes, and Marcelo C. Klotzle. Wind farm generation forecast and optimal maintenance schedule model. *Wind Energy*, 22(12):1872–1890, September 2019.

[110] Cameron W. Potter and Michael Negnevitsky. Very short-term wind forecasting for Tasmanian power generation. *IEEE Transactions on Power Systems*, 21(2):965–972, May 2006.

[111] Amirali Pourahmadi, Taghi Ebadi, and Manouchehr Nikazar. Industrial wastes risk ranking with TOPSIS, multi criteria decision making method. *Civil Engineering Journal*, 3(6):372–381, June 2017.

[112] Jordan G. Powers, Joseph B. Klemp, William C. Skamarock, Christopher A. Davis, Jimy Dudhia, David O. Gill, Janice L. Coen, David J. Gochis, Ravan Ahmadov, Steven E. Peckham, Georg A. Grell, John Michalakes, Samuel Trahan, Stanley G. Benjamin, Curtis R. Alexander, Geoffrey J. Dimego, Wei Wang, Craig S. Schwartz, Glen S. Romine, Zhiquan Liu, Snyder Chris, Fei Chen, Michael J. Barlage, Wei Yu, and Michael G. Duda. The weather research and forecasting model: Overview, system efforts, and future directions. *Bulletin of the American Meteorological Society*, 98(8):1717–1737, August 2017.

[113] Alfonso Quarati, Emanuele Danovaro, Antonella Galizia, Andrea Clematis, Daniele D'Agostino, and Antonio Parodi. Scheduling strategies for enabling meteorological simulation on hybrid clouds. *Journal of Computational and Applied Mathematics*, 273:438–451, January 2015.

[114] Ashok Rao. *Sustainable Energy Conversion for Electricity and Coproducts: Principles, Technologies, and Equipment*. Wiley, Hoboken, April 2015.

[115] Cristian Rodríguez Rivero, Julián Pucheta, Efrén Gorrostieta, H. Daniel Patiño, Sergio Laboret, and Víctor Sauchelli. Bayesian enhanced modified forecasting approach: Application to wind power series. In *Proceedings of the 25° Congreso Argentino de Control Automático*, Buenos Aires, November 2016. AADECA.

[116] A. Rodrigues, J.A. Lopes, P. Miranda, J. Palma, C. Monteiro, J.N. Sousa, R.J. Bessa, C. Rodrigues, and J. Matos. EPREV - A wind power forecasting tool for Portugal. In *Proceedings of the European Wind Energy Conference & Exhibition 2007*, volume 7, Milan, May 2007. EWEA.

[117] K. Rohrig, B. Ernst, M. Hoppe-Kilpper, and F. Schlögl. Online-monitoring and prediction of wind power in German transmission system operation centres. In *Proceedings of the World Wind Energy Conference 2003*, Cape Town, November 2003. WWEC.

[118] Leszek Rutkowski. *Flexible Neuro-Fuzzy Systems: Structures, Learning and Performance Evaluation*. Kluwer Academic Publishers, Boston, May 2004.

[119] Bikash Kumar Sahu. Wind energy developments and policies in China: A short review. *Renewable and Sustainable Energy Reviews*, 81:1393–1405, January 2018.

[120] I. Sánchez, J. Usaola, O. Ravelo, C. Velasco, J. Domínguez, M.G. Lobo, G. González, F. Soto, B. Diaz-Guerra, and M. Alonso. Sipreólico - A wind power prediction system based on flexible combination of dynamic models. Application to the Spanish power system. In *Poster on the 2002 World Wind Energy Conference*, Berlin, July 2002.

[121] A. Sfetsos. A novel approach for the forecasting of mean hourly wind speed time series. *Renewable Energy*, 27(2):163–174, October 2002.

[122] Rahul Sharma and Diksha Singh. A review of wind power and wind speed forecasting. *Journal of Engineering Research and Application*, 8(7):1–9, July 2018.

[123] Jing Shi, Jinmei Guo, and Songtao Zheng. Evaluation of hybrid forecasting approaches for wind speed and power generation time series. *Renewable and Sustainable Energy Reviews*, 16(5):3471–3480, June 2012.

[124] Nils Siebert. *Development of Methods for Regional Wind Power Forecasting*. PhD thesis, MINES ParisTech, Paris, March 2008.

[125] Jolanta Siewert and Krzysztof Kroszczynski. GIS data as a valuable source of information for increasing resolution of the WRF model for Warsaw. *Remote Sensing*, 12(11):1881, June 2020.

[126] William C. Skamarock, Joseph B. Klemp, Jimy Dudhia, David O. Gill, Zhiquan Liu, Judith Berner, Wei Wang, Jordan G. Powers, Michael G. Duda, Dale M. Barker, and Xiang-Yu Huang. A description of the advanced research WRF model version 4. Technical report, National Center for Atmospheric Research, Boulder, March 2019.

[127] Richard E. Smalley. Future global energy prosperity: The terawatt challenge. *MRS Bulletin*, 30(6):412–417, June 2005.

[128] Saurabh S. Soman, Hamidreza Zareipour, Om Malik, and Paras Mandal. A review of wind power and wind speed forecasting methods with different time horizons. In *Proceedings of the North American Power Symposium 2010*, Arlington, September 2010. IEEE.

[129] Wadim Strielkowski. *Social Impacts of Smart Grids: The Future of Smart Grids and Energy Market Design*, chapter Renewable energy sources, power markets, and smart grids, pages 97–151. Elsevier, Cambridge, October 2019.

[130] Tomohiro Takagi and Michio Sugeno. Fuzzy identification of systems and its applications to modeling and control. *IEEE Transactions on Systems, Man, and Cybernetics*, SMC-15(1):116–132, January–February 1985.

[131] Jose Luis Torres, Almudena Garcia, Marian De Blas, and Adolfo De Francisco. Forecast of hourly average wind speed with ARMA models in Navarre (Spain). *Solar Energy*, 79(1):65–77, July 2005.

[132] I. Troen and L. Landberg. Short term prediction of local wind conditions. In *Proceedings of the 1990 European Community Wind Energy Conference*, volume EUR-13251, pages 76–78, Madrid, September 1990. H.S. Stephens and Associates.

[133] Abhisek Ukil. *Intelligent Systems and Signal Processing in Power Engineering*, chapter Support vector machine, pages 161–226. Power Systems. Springer, Berlin, September 2007.

[134] Navneet Walia, Harsukhpreet Singh, and Anurag Sharma. ANFIS: Adaptive neuro-fuzzy inference system- A survey. *International Journal of Computer Applications*, 123(13), August 2015.

[135] Hailong Wang, William C. Skamarock, and Graham Feingold. Evaluation of scalar advection schemes in the advanced research WRF model using large-eddy simulations of aerosol–cloud interactions. *Monthly Weather Review*, 137(8):2547–2558, August 2009.

[136] Jianzhou Wang, Haiyan Jiang, Qingping Zhou, Jie Wu, and Shanshan Qin. China's natural gas production and consumption analysis based on the multicycle Hubbert model and rolling Grey model. *Renewable and Sustainable Energy Reviews*, 53:1149–1167, January 2016.

[137] Qin Wang, Carlo Brancucci Martinez-Anido, Hongyu Wu, Anthony R. Florita, and Bri-Mathias Hodge. Quantifying the economic and grid reliability impacts of improved wind power forecasting. *IEEE Transactions on Sustainable Energy*, 7(4):1525–1537, October 2016.

[138] Wei Wang, Cindy Bruyère, Michael Duda, Jimy Dudhia, Dave Gill, Michael Kavulich, Kelly Werner, Ming Chen, Hui-Chuan Lin, John Michalakes, Syed Rizvi, Xin Zhang, Judith Berner, Domingo Munoz-Esparza, Brian Reen, Soyoung Ha, and Kate Fossell. *Weather Research & Forecasting Model ARW Version 4 Modeling System User's Guide*. National Center for Atmospheric Research, Boulder, January 2019.

[139] Xiaochen Wang, Peng Guo, and Xiaobin Huang. A review of wind power forecasting models. *Energy Procedia*, 12:770–778, December 2011.

[140] Ying-Ming Wang and Taha M.S. Elhag. Fuzzy TOPSIS method based on alpha level sets with an application to bridge risk assessment. *Expert Systems with Applications*, 31(2):309–319, August 2006.

[141] Yu-Jie Wang. Applying FMCDM to evaluate financial performance of domestic airlines in Taiwan. *Expert Systems with Applications*, 34(3):1837–1845, April 2008.

[142] Helen J. Wearing. Spectral analysis in R, June 2010.

[143] Frank West. *Fuzzy Inference System*. NY Research Press, New York, March 2015.

[144] Yu-chen Wu and Jun-wen Feng. Development and application of artificial neural network. *Wireless Personal Communications*, 102(2):1645–1656, September 2018.

[145] Yuan-Kang Wu and Jing-Shan Hong. A literature review of wind forecasting technology in the world. In *Proceedings of the 2007 IEEE Lausanne Power Tech*, pages 504–509, Lausanne, July 2007. IEEE.

[146] Zhongyou Xing. Study on the application of TOPSIS method to the introduction of foreign players in CBA games. *Physics Procedia*, 33:2034–2039, June 2012.

[147] Beibei Xu, Diyi Chen, M. Venkateshkumar, Yu Xiao, Yan Yue, Yanqiu Xing, and Peiquan Li. Modeling a pumped storage hydropower integrated to a hybrid power system with solar-wind power and its stability analysis. *Applied Energy*, 248:446–462, August 2019.

[148] Hongming Yang, Jing Qiu, Ke Meng, Jun Hua Zhao, Zhao Yang Dong, and Mingyong Lai. Insurance strategy for mitigating power system operational risk introduced by wind power forecasting uncertainty. *Renewable Energy*, 89:606–615, April 2016.

[149] Kwangsun Yoon. A reconciliation among discrete compromise solutions. *Journal of the Operational Research Society*, 38(3):277–286, March 1987.

[150] Jiajun Zeng, Guangsi Lin, and Guoru Huang. Evaluation of the cost-effectiveness of Green Infrastructure in climate change scenarios using TOPSIS. *Urban Forestry & Urban Greening*, 64:127287, September 2021.

[151] Shijie Zhang, Jing Wei, Xi Chen, and Yuhao Zhao. China in global wind power development: Role, status and impact. *Renewable and Sustainable Energy Reviews*, 127:109881, July 2020.

[152] Wenyu Zhang, Jujie Wang, Jianzhou Wang, Zengbao Zhao, and Meng Tian. Short-term wind speed forecasting based on a hybrid model. *Applied Soft Computing*, 13(7):3225–3233, July 2013.

[153] Xian-Da Zhang. *A Matrix Algebra Approach to Artificial Intelligence*, chapter Support vector machines, pages 617–679. Springer Nature, Singapore, May 2020.

[154] Chunyu Zhao, Yan Cui, Xiaoyu Zhou, and Ying Wang. Evaluation of performance of different methods in detecting abrupt climate changes. *Discrete Dynamics in Nature and Society*, 2016, May 2016.

[155] Pan Zhao, Jiangfeng Wang, Junrong Xia, Yiping Dai, Yingxin Sheng, and Jie Yue. Performance evaluation and accuracy enhancement of a day-ahead wind power forecasting system in China. *Renewable Energy*, 43:234–241, July 2012.

[156] Xin Zhao, Shuangxin Wang, and Tao Li. Review of evaluation criteria and main methods of wind power forecasting. *Energy Procedia*, 12:761–769, December 2011.

[157] Yongning Zhao, Lin Ye, Zhi Li, Xuri Song, Yansheng Lang, and Jian Su. A novel bidirectional mechanism based on time series model for wind power forecasting. *Applied Energy*, 177:793–803, September 2016.

[158] Junyi Zhou, Jing Shi, and Gong Li. Fine tuning support vector machines for short-term wind speed forecasting. *Energy Conversion and Management*, 52(4):1990–1998, April 2011.

[159] Bo Zhu, Min-you Chen, Neal Wade, and Li Ran. A prediction model for wind farm power generation based on fuzzy modeling. *Procedia Environmental Sciences*, 12(A):122–129, April 2012.